Republic of Iraq
Ministry of Higher Education
and Scientific Research
University of Babylon
College of Engineering
Department of Mechanical Engineering

Magneto-hydrodynamic Natural Convection in I-Shaped Wavy Walls Enclosure Partially Inserted with Nano Fluid-Porous Media

A Thesis

Submitted to the College of Engineering, University of Babylon in Partial Fulfillment of the Requirements of the Degree of Doctorate of Philosophy in Engineering / Mechanical Engineering / Power

By

Ammar Abdulkadhim Fathi Saeed

Supervised by

Prof. Dr. Isam Mejbel Abed **Prof. Dr. Nejla Mahjoub saïd**

2022 A.D **1444 A.H**

A B S T R A C T

The present study examines the magnetohydrodynamics natural convection within a novel I-shaped wavy-walled enclosure considering different thermal managements. The enclosure is vertically filled by Al_2O_3 – water nanofluid layer and the other layer is containing the same nanofluid saturated with the porous media considering thermal equilibrium model between the nanofluid and porous media. The dimensionless parameters are involved the influence of Rayleigh number $(10^4 \leq Ra \leq 10^6)$, Darcy number $(10^{-5} \leq Da \leq 0.1)$, Hartmann number $(0 \leq Ha \leq 60)$, Nanofluid loading $(0 \leq \phi \leq 0.06)$, Magnetic field inclination angle $(0° \leq \gamma \leq 90°)$, Trapezoidal heater length $(0.4 \leq B \leq 1.4)$, Location of the trapezoidal heater $(0.2 \leq E \leq 0.8)$, Position of the circular cylinder $(0.3 \leq \delta \leq 1.3)$ on fluid flow and heat transfer.

The first part of the study is the CFD numerical work that it been built based upon homogeneous flow model for treating the nanofluid and Darcy-Brinkmann model for treating the porous media through the usage of COMSOL V 6.0. Four different numerical thermal works had been presented. The first work is on the examination of MHD within the enclosure considering multi-inner circular bodies with three different thermal management of them. The second CFD work is an extension of the first mentioned above CFD study considering the influence of different inner bodies shapes (circle, square, rhombus and triangle) on magnetohydrodynamics natural convection within the enclosure. The third CFD work is an insight view to the influence of trapezoidal heater along with inner circular body on natural convection within the novel enclosure considering different location and length of trapezoidal heater. Finally, a detail CFD study is on full-examination to the shape of the wavy walls considering four different patterns including the existence of inner elliptical body.

The second part is the experimental work that includes fabrication novel shape of enclosure takes the I-shaped with wavy-walled with inner circular rod. The left layer

is filled by nanofluid while the right layer is filled with nanofluid/porous media. The nanofluid thermophysical properties had been measured experimentally. Two cores of magnetic field had been installed with magnetic intensity of 20 mT.

The results show that regarding the first proposed numerical CFD investigation that at low Rayleigh number (Ra = 10^4) there is no noticeable influence of the inner hot body locations for all of the selected three cases on the fluid flow strength while at high Rayleigh number (Ra = 10^6), the fluid flow strength increases for Case 1 by 84.16% in a comparison with Case 3. Additionally, it can be seen that Case 3 reveals the lowest heat transfer augmentation. Additionally, Applied the magnetic field in the vertical direction leads to intensify the fluid flow strength of Case one by approximately three times that for case three. Regarding the second CFD model, for various values of Ra, Da, Ha, γ_{MHD}, ϕ, Case 1 which represent the circular shapes reveals the highest augmentation in Nusselt number followed by Case 3 (rhombus), Case 2 (square) and Case 4 (triangular) reveals the lowest improving in heat transfer rate. Additionally, for the third CFD model as Hartmann number increases, the magnetic field inclination angle be more effect on the heat transfer behavior as it is noted that applied the magnetic field in the vertical direction at γ=90° enhance Nusselt number by 20% in a comparison with applied the magnetic field in the horizontal direction. Finally, for the CFD model of different wavy patterns, it had been proved that Case 4 along with locating the inner elliptical body in the bottom of the enclosure reveals the best strength in the fluid flow. Also, increasing Hartmann number from $Ha = 0$ to $Ha = 60$ leads to an obvious reduction in the fluid flow by 48.95%.

In Experimental study, it can be seen that there is slight increasing in the temperature with the existence of the magnetic field. Additionally, it proved that increasing the hot side wavy wall temperature leads to increase the temperature difference which increases the temperature level in the nanofluid-porous region and the nanofluid region. Finally, there is an excellent agreement of the experimental and numerical results of the present work in addition there is quite good agreements in the

trends and values of the numerical results of the present work with those obtained by significant researchers.


بسم الله الرحمن الرحيم
الله لا إله إلا هو الحي القيوم لا تأخذه سنة
ولا نوم له ما في السموات وما في الأرض من ذا الذي
يشفع عنده إلا بإذنه يعلم ما بين أيديهم وما
خلفهم ولا يحيطون بشيء من علمه إلا بما شاء وسع
كرسيه السموات والأرض ولا يؤوده حفظهما
وهو العلي العظيم صدق الله العظيم

DEDICATION

TO

My Father, Mother and Sisters

TO

My Supervisors

TO

Researchers of Heat Transfer

With Respect and Love

Supervisors Certificate

*We certify that this Ph. D. thesis entitled "**Magneto-hydrodynamic Natural Convection in I-shaped Wavy Walls Enclosure Partially Inserted with Nano Fluid-Porous Media**" has been prepared under our supervision at the Mechanical Engineering Department, University of Babylon – Iraq, as a partial fulfillment of the requirements for the Philosophy Degree in Mechanical Engineering.*

We recommend that this thesis be forwarded for examination in accordance with the regulation of the University of Babylon.

Prof. Dr. Isam Mejbel Abed

Date: - - 2022

Prof. Dr. Nejla Mahjoub Said

Date: - - 2022

Examination Committee Certification

We certify the we have read thesis entitled "Magneto-hydrodynamic Natural Convection in I-shaped Wavy Walls Enclosure Partially Inserted with Nano Fluid-Porous Media" and as an examining committee, examined the student "Ammar Abdulkadhim Fathi", in its content and that in our opinion it meets the standard of thesis for the degree of Doctorate of Philosophy in Mechanical Engineering

Prof. Dr. Esam Mejbel Abed
Supervisor
Date:

Prof. Dr. Nejla Mahjoub Said
Supervisor
Date:

Asst. Prof. Dr. Mohammad Wahhab Aljibory
Member
Date:

Prof. Dr. Qusay Rasheed Al-Amir
Member
Date:

Prof. Dr. Riyadh S. Al-Turaihi
Member
Date:

Prof. Dr. Ahmed Kadhim Hussein
Member
Date:

Prof. Dr. Karima E. Amori
Chairman
Date:

Approval of Mechanical Engineering Department

Asst. Prof. Dr. Samer Abdulhaleem

Date:

Approval of the College of Engineering

Prof. Dr. Hatem Hadi Obeid

Date:

ACKNOWLEDGMENTS

*First of all, I would like to praise and thank **GOD** for helping me to complete this thesis.*

*I wish to express my gratefulness to my supervisors, **Prof. Dr. Isam Mejbel Abed** and **Prof. Dr. Nejla Mahjoub Said** for their continuous supervision, positive discussions and important ideas through this research work.*

*Also, very extraordinary deepest thanks to **Prof. Dr. Hameed Kadhem Hamzah** for his special contribution and help in completing this work.*

*I would like to thank Al-Mustaqbal University College representing by **Prof. Dr. Hasan Sh. Majdi** and **Asst. Prof. Dr. Azher M. Abed** for helping me throughout my study.*

*I would like also to thank the Dean of College of Engineering, University of Babylon **Prof. Dr. Hatem Hadi Obeid** and the Head of Mechanical Engineering Department **Asst. Prof. Dr. Samer Mohammad Abdulhaleem** and all of the staff of Mechanical Engineering Department, University of Babylon.*

*My deepest thanks, love and gratitude for all of **My Father, Mother and Sisters**. This work would not have been completed without their love and continuous support.*

Ammar Abdulkadhim

2022

Table of Contents

Nomenclature

Symbol	Description
Cp	Specific heat at constant pressure (kJ/kg. K)
B	Length trapezoidal heater
E	Position of the trapezoidal heater
Da	Darcy number
g	Gravitational acceleration (m/s^2)
Gr	Grashof number
Ha	Hartmann number
k	Thermal conductivity (W/m. K)
P	Dimensionless pressure
p	Pressure (Pa)
Pr	Prandtl number
Ra	Rayleigh number
T	Temperature (K)
Nu	Local Nusselt number on the hot inner cylinder
N	Number of undulations
No	Number of hot bodies
U	Dimensionless velocity component in x-direction
u	Velocity component in x-direction (m/s)
V	Dimensionless velocity component in y-direction
v	Velocity component in y-direction (m/s)
X	Dimensionless coordinate in horizontal direction
x	Cartesian coordinates in horizontal direction (m)
Y	Dimensionless coordinate in vertical direction
y	Cartesian coordinate in vertical direction (m)
Greek symbols	

α	Thermal diffusivity (m^2/s)
β	Volumetric coefficient of thermal expansion (K^{-1})
γ	MHD angle
ε	Porosity
θ	Dimensionless temperature (T-Tc/ΔT)
σ	Electrical conductivity
ψ	Dimensional stream function (m2/s)
Ψ	Dimensionless stream function
ϕ	Nanofluid volume fraction
μ	Dynamic viscosity (kg.s/m)
ν	Kinematic viscosity (μ /ρ) (Pa. s)
ρ	Density (kg/m3)
k	Thermal conductivity
ϕ	Nanofluid loading
λ	Amplitude
Subscripts	
c	Cold
f	Fluid (pure)
h	hot
na	Nanofluid
np	Nanoparticle
bf	Base fluid (water)
Abbreviations	
HX	Heat Exchanger
MHD	Magnetohydrodynamics
FVS	Finite Volume Scheme
FDS	Finite Difference Scheme

FES	Finite Element Scheme
CVFEM	Control Volume Finite Element Method
CFD	Computational Fluid Dynamics
LBM	Lattice Boltzmann method

Chapter One

Introduction

Chapter One

Introduction

Convective heat transfer is a promising mode in the thermal energy systems. Basically, there are two types of the convection heat transfer which are the natural (buoyancy driven flow), forced as well as the mixed convection heat transfer which is the combination of natural and forced. The forced convection required a fan or blower for driven the fluid flow leads to more cost is required. Unlike, the natural convection type which depends upon the temperature difference which is the driven force of the flow without any mechanical equipment. This makes the natural convection has the ability to drive the flow with lower cost. Based upon the application of each device, there is devices required to dissipate the heat because of the agglomeration of the heat leads to error in the equipment. On the other hands, there is component required to receive heat to work properly like the solar collectors. In both cases, there should be a fluid in order to control the heat transfer considering the absorbing or dissipate it. The working fluid may be traditional fluids such as air, water, ethylene glycol or untraditional fluids such as nanofluids.

The magnetic field had important contribution on controlling on the heat transfer as increasing the strength of the magnetic field (B_o) leads to increment of Hartmann number leading to an obvious reduction in the fluid flow strength. Hartmann number increasing leads to make the conduction heat transfer is the dominant mode. In this way, Rayleigh number and Hartmann number had inverse relations on the heat transfer. Mathematically, Hartmann number may be calculated as indicated below;

$$Ha = B_o H \sqrt{\frac{\sigma_{na}}{\rho_{na} \nu_{na}}} \tag{1.1}$$

Buoyancy driven flow considering multi-layers thermal systems of porous media and nanofluid within enclosures under magnetic field had been taken a lot

of interest by numerous researchers, as their applications in industrial engineering projects can be summarized as below [1-4];

- Heat exchangers industry
- Solar thermal collectors
- cooling systems of nuclear reactor
- Geothermal systems
- Fuel cell
- Crude oil production
- Storage of nuclear waste materials

In this way, the natural convection within different shapes of enclosures took a lot of attention. The shapes of enclosures can be classified into two major categories; simples enclosures shapes and complex enclosure shape. The simple shapes of enclosures such as (square, rectangular, triangular). The complex shapes of enclosures such as rhombus, parallelogrammic, trapezoidal, elliptical, wavy. It is shown in Figure (1.1).

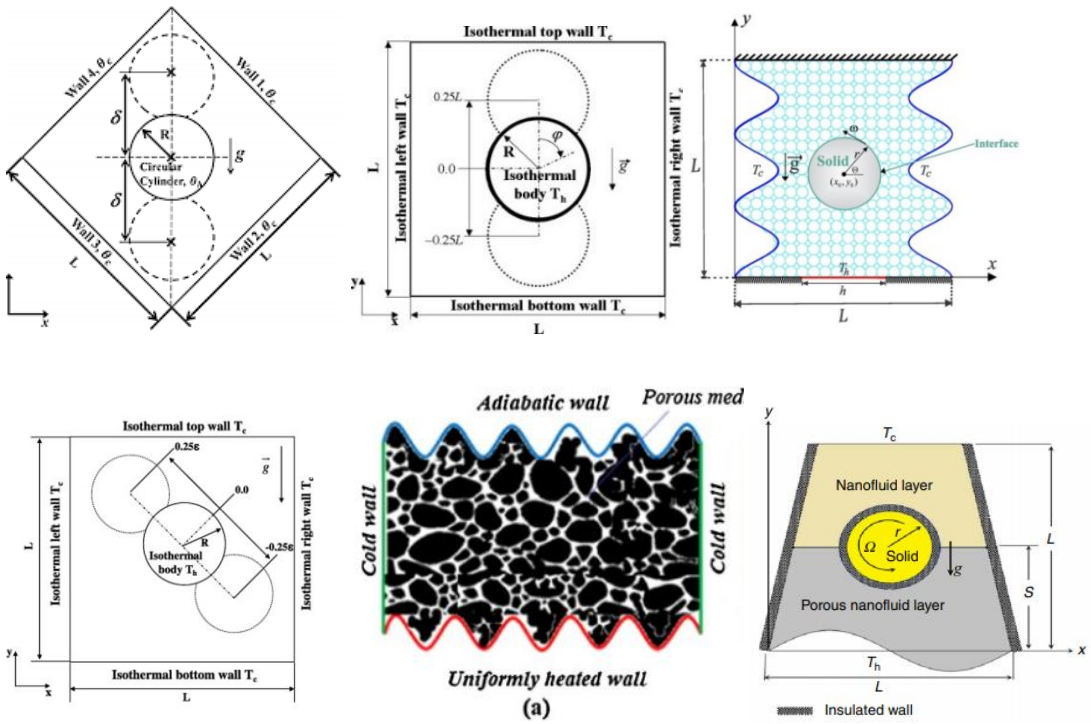

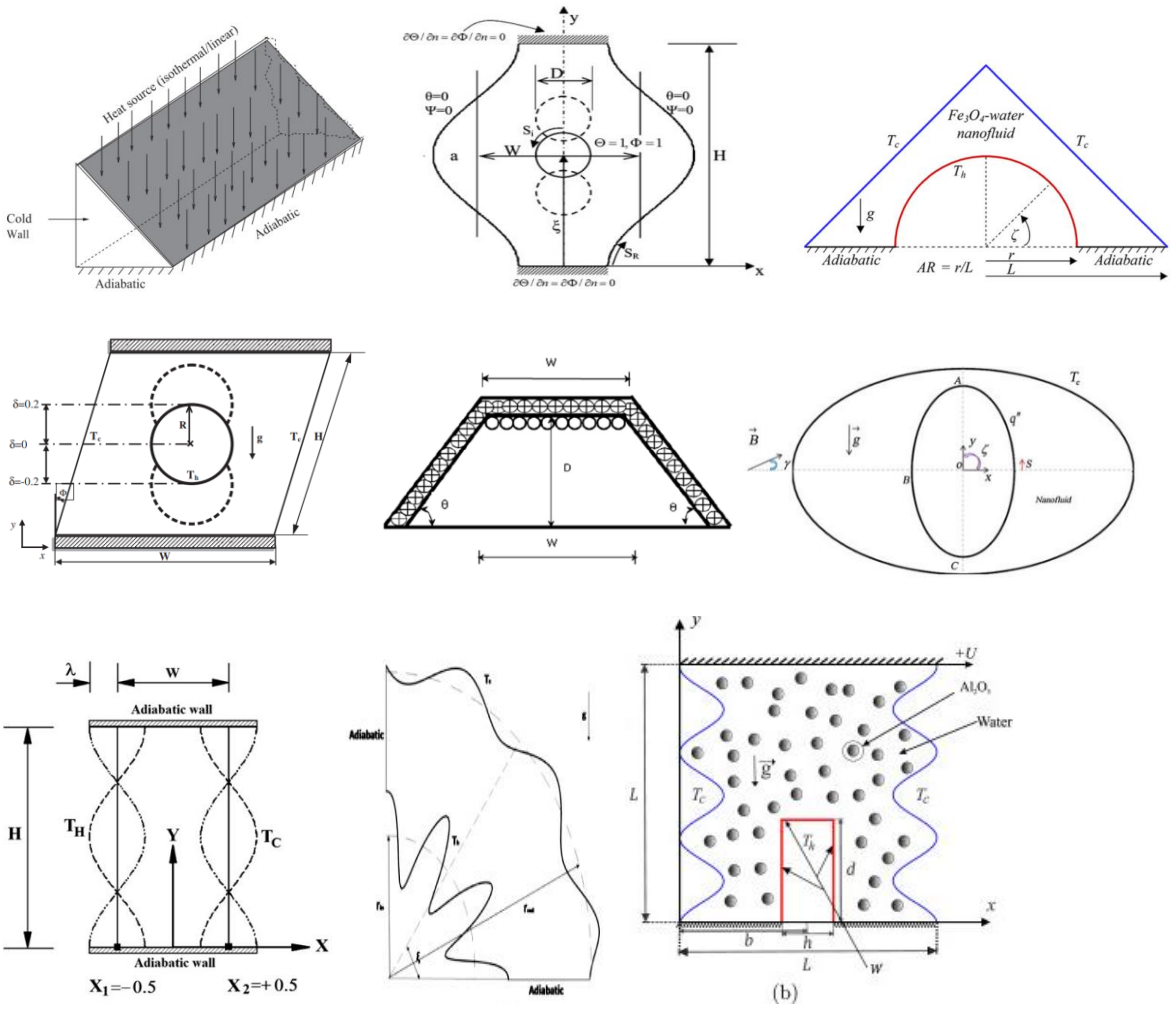

Figure (1.1) selected shapes of enclosures taken from Refs [5, 6]

In this way, the present chapter reveals a general introduction of natural convection within enclosure. Additionally, there is various techniques in receiving the heat or dissipate it such as porous media and enhancing the heat transfer such as utilizing of the nanofluid. Lastly, manipulation in the geometry of the enclosure itself leads to control the heat transfer.

1.1. Porous media role in heat transfer

The porous media filled enclosure had been studied a lot for its important role in heat transfer field. Simply, the porous media is commonly to be defined as a substance or material that containing pores or voids through them the fluid which may be liquid or gas are filled. The general structure is called matrix [7]. There are various important specifications such as its capability in dissipation large amount of heat in a comparison with that from fins or baffles. Besides, it

helps the fluid that penetrate through the voids of the porous media which contribute in absorbing a lot of heat by the fluid. However, the physics of penetration of the fluid is so complex and it actually depends based upon many thermophysical properties of the porous media like the size as well as the shape of the porous media in addition to the permeability which is the ability of the porous media to allow to the fluid to flow through it easily at a higher flow rate which help in absorbing the heat from the porous media and transfer it. However, the porous material usually used as an insulation material that reduce the heat transfer from the hot component as it resists the fluid flow. The porous media that had been used in the present thesis is made of glass bead it will be discussed in-full details in Chapter Four.

1.2. Nanofluid role in heat transfer

There is another problem which is related to traditional working fluids such as water, oil, ethylene glycol. The major problem is related to the thermophysical properties of these conventional fluids which have low thermal conductivity, which is a real limitation in improving and increasing the rate of heat transfer [8]. This problem has motivated many researchers to find a solution to this problem, which is now a new science of engineering and physics known as nanofluid. It is simply a matter of adding tiny, solid nanoparticles such as Cu, Zn, and Ag at the nanoscale, with high thermal conductivity, to the traditional (conventional) fluid that is the host fluid such as water as indicated below in Table (1.1). The resulting fluid has exceptional thermophysical properties that contribute to improving the heat transfer rate of industrial and medical engineering systems.

Table (1.1) Thermophysical properties of nanoparticle and the selected base fluid in this study [9]

Properties	Cp (J/kg. K)	k (W/m. K)	ρ (kg/m^3)	β (1/K)
Water	4180	0.614	997	$2.1*10^{-4}$
Al_2O_3	765	40	3970	$0.85*10^{-5}$

1.3. Wavy (Corrugated) wall role in heat transfer

As mentioned before, there is different shapes of enclosures. However, there is another enclosure geometry, called wavy, which is considered a little more complex in comparison to the shapes mentioned previously. The wavy shapes of the enclosure walls have played an important role in saving energy and improving heat exchange within thermal systems. Figure (1.3) shows the number of the previous publications for the period 2010 – 2020 based upon Elsevier data. The consideration in selecting the wavy enclosure is based on its applications in industrial projects especially its shape, number of undulations influence on the fluid flow and heat transfer.

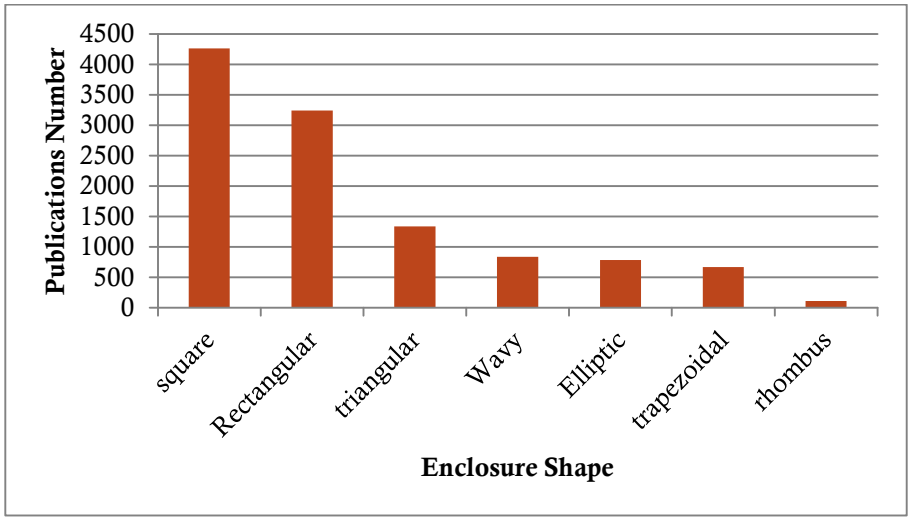

Figure (1.2) The total publications with respect to the enclosure shapes based upon sciencedirect data.

1.4. Aim of the Present Work

There are various techniques in controlling on the heat transfer such as nanofluid, porous media and corrugated wall which had been studied a lot under various and wide range of conditions like isotherm and non-isotherm applied thermal conditions, various types of nanofluid, applied magnetic field, inner body position and its size and their impact on receiving or removing the heat transfer.

Besides, the influence of nanofluid, porous media in addition to the multi-layers systems (porous media saturated with nanofluid) filled the simple shapes

of enclosure like square, rectangular, triangle and circular in addition to the complex one like trapezoidal, parallelogrammic, elliptical and wavy considering the existence or the absence of the inner body under various conditions had been investigated by researchers.

The material point in the present work is by utilizing new category of the more complex enclosure which formally known as the combined enclosure like U-shaped, E-shaped, F-shaped and I-shaped. There are serious limitations of the combined shapes of enclosures which are consist of numbers of interconnected enclosures making them had more applications than those of the simpler enclosure's shapes especially in the I-shaped enclosure as indicated in Figure (1.4). Additionally, the influence of magnetic field had received many attentions by researchers to draw its impact on the heat transfer rate.

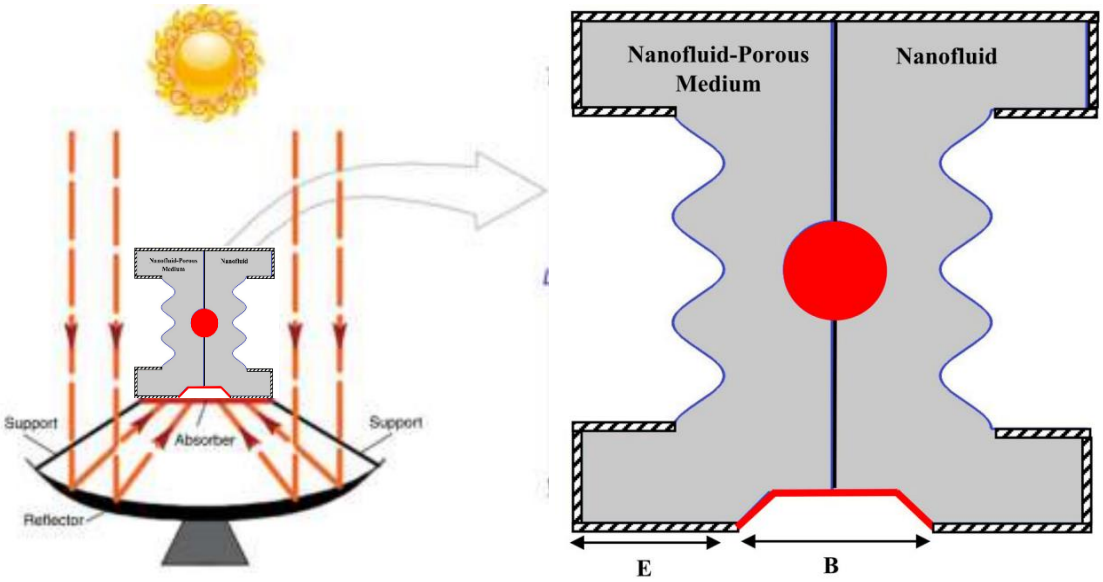

Nonetheless, these investigations had been the corner stone of the present Ph.D. work that leads to build a mathematical model, applied thermal conditions of porous media saturated with nanofluid filled novel shape that combine the I-shaped enclosure with wavy (corrugated) walls to form the novel I-shaped wavy-walled enclosure.

The computational fluid dynamics (CFD) has been developed under wide range of Rayleigh number, Darcy number, Hartmann number, inner body shapes, numbers, and position in addition to the magnetic field angle. The selected complex I-wavy shaped along with the boundary conditions will be helpful in the next modern generation of technology especially the present work predictions for the fluid flow and heat transfer is completely different to what is found in the previous work.

In this way, the present work is dividing into two major parts (CFD and experimental work);

Firstly, with respect to the numerical CFD work there will be four thermal different cases had been selected that can be summarized as indicated below;

- The first case involves multi-circular bodies located in complex novel I-shaped - wavy walled enclosure filled with nanofluid and porous media. The influence of Rayleigh number, Darcy number, Hartmann number, number of undulations, porous layer thickness and MHD inclination angle had been examined under three different locations of inner hot bodies.
- The second case indicate four different types of inner body (circle, square, rhombus and triangle) along with the numbers, position of the inner hot inner body under wide range of dimensionless parameters like Rayleigh number, Darcy number, Hartmann number and magnetic field angle.
- The third case involves to attach a trapezoidal heater to the novel enclosure to its bottom wall with the existence of inner hot circular cylinder considering wide range of dimensionless parameters such as the trapezoidal heater length and position.
- The fourth case focuses on utilizing four different cases of wavy wall patterns with inner hot elliptical body.

Secondly, the experimental part reveals the problem and with the help of the measurement instruments, there will be visualization to the nanofluid-porous media filled the designated novel enclosure.

In this way, the objective of the present work can be summarized in the following materials points;

- Examining the influence of wide range of dimensionless parameters such as the most well-known dimensionless parameters Rayleigh number, Darcy number, Hartmann number in addition to the influence of the nanofluid.
- Examining the influence of various geometrical parameters such as number of undulations, shape of the inner body, the locations and the number of the inner hot body.
- Investigating numerically the impact of porous layer thickness on the fluid flow strength and the heat transfer rate.
- To better understanding the role of magnetohydrdynamics thermogravitional heat transfer within such a complex and novel enclosure shape filled partially by nanofluid and partially by porous media saturated with the same nanofluid.

Chapter Two
Literature Review

Chapter Two

Literature Review

The present chapter demonstrates the previous studies for the subject of natural convection within different shapes of enclosure considering wide range of dimensionless parameters. The researchers investigated the influence of wide range of physical and geometrical parameters such as various thermal boundary conditions considering changing of the heat source locations and its shape, or heated uniformly or/and non-uniformly, applied heat flux and internal heat generation/absorption along with the magnetic field. Also, the researchers investigated the impact of catalysts like nanofluid or/and porous media and by changing the geometry of the enclosure wall into the corrugated (wavy) shape which is contribute in the augmentation of heat transfer.

2.1. Simple Shaped Enclosure

There are three types of the simple shapes of enclosures such as square, rectangle in addition to the triangular.

2.1.1. Previous studies related to the square enclosure

The square enclosures may be considered one of the simplest geometries to study one of the hardest physics phenomenon that it is called natural convection. It had many applications in industry. Different thermal cases studies in the subject of natural convection had been examined like the problems of conjugate, Newtonian as well as non-Newtonian fluids. For example, Osman et al. **[10]** demonstrated impact of Bingham fluid and Newtonian fluids upon momentum and heat transfer numerically using FLUENT package under varied Rayleigh, Bingham as well as Prandtl numbers. It does reflect that Nusselt number for Newtonian fluid was higher in a comparison with that of Bingham fluid under the same Rayleigh number. Also, rising Bingham number causes to obvious reduction in Nusselt number till it reaches unity which means that the conduction heat transfer will be dominated. The natural flow of non-Newtonian fluids based up on

power- law approach as Osman et al. [11]. New correlation of Nusselt number for power-law and Newtonian fluids had been developed. Pishkar et al. **[12]** examined the transient free convection for both the Newtonian along with the Non-Newtonian fluids in a partially oscillating square enclosure heated from bottom using SIMPLIC algorithm and the deduced that the oscillation of the heat source effects on the fluid flow behavior. It had been shown non – Newtonian fluids gives better enhancement in heat transfer than Newtonian fluids.

Biswal et al. **[13]** investigated the problem under various inclination angles for two cases of different heating (isotherm and non – isotherm) conditions of the bottom wall of tilted square enclosure filled with porous media. Finite element scheme was used to solve the problem via heatlines along with entropy generation. The results were crucial and it was obtained that case 1 showed higher average Nusselt and Bejan numbers as well as higher total entropy generation along with that due to friction in a comparison with case 2. Roy et al. **[14]** studied the square porous media filled lid – driven enclosure modeled using Darcy-Brinkman-Forchheimer model and solved numerically using finite element scheme. It was obtained that maximum thermal rate in the heat transfer was at its maximum value on the bottom wall for all selected cases

There was a serious limitation by using the traditional heat transfer fluids like oil and water which was its low thermal conductivity and this is make limitations in the augmentations of heat transfer rate. So that the researchers found that additions tiny solid particles to the base fluid (oil or water) promote to increase the thermal conductivity of the resultant fluids and this called nanofluid technology. Various researchers investigated the nanofluids like Ho et al. **[15]** which deduced experimentally that addition of nanoparticle to the base fluid in order to intensify the thermal rate and transfer the heat. Al_2O_3 used filled three different constructions and dimensions of square enclosure. The results indicated that only the increasing in the thermal conductivity leads to enhancement in the heat transfer beneficially while there is no obvious augmentation in the case of

increasing other thermophysical properties of nanofluid like thermal expansion, specific heat and viscosity. The same nanofluid which is Al_2O_3 had been chosen in a numerical work suggested by Hsiang et al. **[16]** using scheme of the Lattice Boltzmann. The results indicated that increasing nanofluid loading as well as Rayleigh number leads to augmentation in Nusselt number. Besides that, it found that the nanofluid thermophysical model for finding the dynamics viscosity was highly affected on the average Nusselt accuracy. Corcione **[17]** proved that the classical models of nanofluid properties like dynamics viscosity and thermal conductivity were inaccurate. These models considered the impact of nanofluid loading and neglecting the influence of temperature, size of nanoparticle and Brownian motion. Sheikhzadeh et al. **[18]** used the non – homogenous flow model (transport model) considering both the Brownian and thermophoresis diffusions. The previous works illustrates that homogenous flow model was not competent. A comparison of the results of transport model with homogenous model and experimental data had been made to examine the prediction accuracy for the thermal driven flow within Al_2O_3 nanofluid square enclosure. A Corcione **[17]** correlations for predicting nanofluid properties had been used. It was obtained that transport models give better predictions and closed to the experimental data from predictions of homogenous model

The magnetic field had took a lot of interest and studied wildly by designs, engineers and researchers like Ghasemi et al. **[19]** studied the action of magnetic field on a square enclosure filled with Al_2O_3 nanofluid using control volume method modeled using FORTRAN. The results indicate that increasing Hartmann number reduces the heat transfer while Rayleigh number leads to obvious enhancement in the heat transfer. While the influence of nanofluid may be augment or reduce the heat transfer based on the values of the two – dimensionless numbers Rayleigh and Hartmann.

Ahmed et al. **[20]** investigated using finite difference line method the influence of inclined uniform magnetic field along with viscous dissipation as

well as thermal radiation on the natural convection within differentially heated square enclosure. It was admitted that the magnetic distribution leads to deceleration of the fluid flow strength. Also, increasing the radiation leads to augmentation in Nu along the isotherm warm and cold vertical walls while the increasing of viscous dissipation reduces the hot wall's local Nusselt number and improves it for the cold one. Bourantas and Loukopoulos **[21]** used Moving Least Squares scheme for the examination of heat transfer in a micropolar-nanofluid square enclosure and it was obtained that the existence the magnetic field attends to reduction in the strength of flow while increasing Rayleigh numbers and nanofluid loading leads to enhance the heat transfer. It was worthy to mention that Nusselt number of pure nanofluid was better than that of micropolar nanofluid.

2.1.2. Previous Studies related to Rectangular Enclosures

Hong et al. **[22]** used conjugate problem scheme to find out the temperature of the bottom wall of partially heated enclosure under the influence of radiation and buoyancy driven flow. Sivasankaran et al. **[23]** investigated numerically using finite difference scheme the discrete heating within a rectangular enclosure filled by porous media. The cavity was partially heated from its left side vertical wall with two heat sources while the rest parts of this wall as well as the top and bottom wall are adiabatic. The right vertical wall was kept at isotherm cold temperature. The authors examined the significance of modified number of Rayleigh along with that of Darcy, geometric aspect ratio and the two discrete heating. The results express that rising both of modified Rayleigh and Darcy number attends to an obvious augmentation of the heat transfer while increasing aspect ratio reduces the heat transfer. The findings of discrete heating walls were crucial as it was obtained that the bottom's Nu number is higher in a comparison with that of the top heat source except when the ratio of the heat source is 0.5. On the other hand that highest value of temperature will be at the top heater except when the ratio of the heat source is 0.5. Alam et al. **[24]** examined numerically the impact basis on the thermal approach under various Rayleigh number and aspect ratio in the

natural convection heat transfer within a partially heated rectangular enclosure. The enclosure heated in the bottom part of left vertical side wall partially while cooled from its top part of the right vertical side wall. The rest parts of the vertical walls as well as the others walls are thermally adiabatic. The results indicate that increasing Rayleigh number leads to augmentation of heat transfer. While increasing aspect ratio from 0.5 into 1 (square enclosure case) leads to strengthen the rate of heat transfer due to thermal driven flow while growing up the value of the aspect ratio beyond 1 leads to reduction in the heat transfer

Hossain et al. **[25]** studied numerically the transfer of the heat in a rectangular enclosure that it was open to the ambient fluid temperature from its left side wall. The right vertical wall was hot while the two horizontal walls were at ambient fluid temperature. Up – wind finite discretization scheme together with the successive over relaxation method had been used. The findings reveal that the fluid flow strength increases. Al-Badawi and Duwairi **[26]** studied using Forchheimer extension of Darcy model to solve the thermal buoyancy driven flow filled with the porous media. The authors used finite difference approach to discretize the governing equations and solving them numerically. The output of their research indicates that viscous as well as joule heating impacts attends for the reduction in thermal performance. Wu et al. **[27]** utilized local thermal non-equilibrium model to simulate the natural convection in a rectangular enclosure considering internal heat generation. The right and left vertical walls were heated and cooled partially using sinusoidal temperature. The top as well as bottom wall are kept adiabatic. The results indicate that increasing of thermal conductivity ratio as well as inter – phase coefficient of heat transfer leads to augmentation in the heat transfer.

Rahimi et al. **[28]** investigated numerically through the usage of the finite volume discretization the influence of ultra-fine metallic– water nanofluid in a rectangular enclosure on the free convective flow. Their mathematical model was based upon non – Boussinesq model.

Ilyas et al. **[29]** studied experimentally the utilizing functionalization scheme. It was found that the nanofluid had a higher heat transfer coefficient and exhibit better heat transfer characterisitcs in a comparison with the pure oil. Salari et al. **[30]** utilized the FVM to study the influence of aspect ratio, location and the length of the partially heat source numerically on heat transfer.

Teamah et al. [31] examined the heat transfer problem in a tilted rectangular enclosure along with the magnetic field in a laminar nature with heat absorption or generation. The cavity was adiabatic from its top and bottom walls while the vertical right walls was heated and had the higher concentration while the left walls is cooled and at low concentration. The hydrodynamics magnetic field was applied normally to the vertical walls. The governing equations solved numerically using finite volume scheme. The results indicate that as the magnetic field increases, the Hartmann number increases and this reduces the flow intensity changing the heat transfer mode into conduction which reduces the average Nu

2.1.3. Previous Studies related to Triangular Enclosure

Kaluri et al. **[32]** examined using finite element method the buoyancy driven flow in right angled cavity for various angles via heatlines flow under different discrete types of uniform (isotherm) and linear heating of boundary conditions. The influence of various parameters such as diverse range of dimensionless numbers such as ($Pr = 7.2, 1000, 0.015$) and ($Ra = 10^3 - 10^5$) on distribution of heat flow had been discussed. Four different cases of thermal boundary conditions were selected where "case 1: hot isothermal left wall and cold isothermal right wall, case 2: linearly heated left wall and cold isothermal right wall, case 3: cold isothermal left wall and hot isothermal right wall and case 4: cold isothermal left wall and linearly heated right wall".

The results indicated that isothermal heating exhibited exponential reduction profile in Nusselt number while linear heating showed intermediate maximum. Finally, the authors developed correlations of Nusselt number for various angles and Prandtl number.

Bhardwaj and Dalal **[33]** examined the thermal driven flow as well as the generation of the entropy in a porous triangular enclosure filled by air which was wavy from its left wall that kept at cold temperature. The influence of Rayleigh number ($Ra = 10^3 - 10^6$) and Darcy number ($Da = 10^{-4} - 10^{-2}$) had been studied. The inclined wall of triangular enclosure was cooled also, on the other hand, hot conditions had been considered for the bottom wall. It was solved the problem of porous media using finite difference method along with Darcy – Forcheimer model to simulate the porous media in the momentum equation. The results found that increasing Rayleigh and Darcy number helped in augmentation of the heat transfer rate. Mansour and Ahmed **[34]** used implicit finite difference scheme to study the natural convection heat transfer in an inclined triangular cavity filled with copper water nanofluid and porous media in the presence of heat generation. The results indicated that nanoparticle attended for an obvious augmentation in the heat transfer rate. It proved that Nusselt number reduced as the parameter of the heat generation increased.

Ghasemi and Aminossadati **[35, 36]** studied the natural convection in a right – angled triangular cavity filled with copper – water nanofluid. The enclosure was supplied with a partially heated source on its left wall. The authors used (FVS) to illustrate the impact of Rayleigh number, nanofluid loading, location of the heat source, aspect ratio of the cavity and the Brownian motion. The results indicated that for any values of nanofluid volume fraction, an increasing of Rayleigh number augmented the strength of the fluid flow strength.

Mahmoudi et al. **[37]** investigated numerically using (FVS) to study the problem in a partially heated triangular enclosure. The influence of Hartman number $(0 < Ha < 100)$, Rayleigh number $(10^4 < Ra < 10^7)$ in addition to the nanofluid volume fraction $(0 < \phi < 0.05)$ had been considered. The triangular enclosure was heated from below partially while the tilted wall was cold and the vertical wall was insulated. The results showed that nanoparticles are more effective at lower dimensionless values of Rayleigh number.

Rashad et al. **[38]** demonstrated numerically the impact of MHD and internal heat generation in a triangular enclosure loaded with hybrid nanofluid using finite difference scheme. The tilted wall was cold and had low temperature, heated partially from its bottom wall by uniform heat flux, while the rest lengths were insulated. It was worthy to illustrated that magnetic field was applied uniformly in the horizontal. The results indicated that increasing heat generation parameter led to enhance the heat transfer due to conduction and reduced the mode of convection. Increasing of Hartmann number reduced Nusselt number at high Rayleigh number. With respect to the partially heated source, it was obtained that when it moved closer to the tilted wall of the triangular enclosure there will be increasing in the Nusselt number value. Besides that, Nusselt number enhanced as there was a reduction in the size of the heat source.

2.2. Complex Shaped Enclosures

2.2.1. Previous Studies related to Trapezoidal Enclosure

Basak et al. **[39]** studied the heatlines in a trapezoidal enclosure using (FES). It was examined impact of thermal heating under both cases; uniform as well as non – uniform from its bottom wall. They concluded that the Nusselt number will be at its maximum value close to the bottom's corner wall in the case of uniformly heated walls for any value of angle of inclination regardless the value of Prandtl and Darcy numbers. While, Nusselt number would be minimum close to the corners in the case of non – uniformly heating. Also the behavior of local Nusselt number was found to be in a sinusoidal distribution with respect to the length of the wall for any angles of inclination at high Darcy number. Basak et al. **[40]** examined the natural convection in trapezoidal enclosure for two different cases : (i) both of the side walls are heated in a linear manner, (ii) the left side wall was linearly heated while the cold temperature applied to the right wall. Both cases were including adiabatic conditions for horizontal top and bottom walls. The authors examined also the influence of Prandtl and Rayleigh numbers as well as

angle of inclination. The findings revealed that the heat was augmented better for the case two regardless the angle of inclination

Natarajan et al. **[41]** illustrated the radiation and natural convection within an absorber of the solar trapezoidal enclosure of linear Fresnel reflector that inserted below. FLUENT 6.3 under steady, laminar nature to solve the problem had been utilized. The authors examined the influence of a lot of parameters like Grashof number, angles of the trapezoidal absorber, emissivity of the surface, aspect ratio as well as ratio of temperature and radiation – conduction number. It was developed a correlation of average Nusselt in terms of the above-mentioned parameters.

UI Haq et al. **[42]** utilized FES to study Single Wall Carbon Nanotubes trapezoidal enclosure. The results reveal that heat transfer was slow and the strength of fluid flow was stronger when the viscous effects were low. Besides that, the presence of nanofluid leads to better augmentation in the rate of heat. Gowda et al. **[43]** studied a five different thermal cases of a building geometry using finite volume method. The selected parameters are $(Ra = 10^3 - 10^7)$ and the orientation of the heated wall are $60°$ and $120°$. The results showed that case 2 had the minimum Nusselt number and the case 3 record the maximum rate of heat.

Saleh et al. **[44]** considered two types of nanofluid had been selected CuO and Al_2O_3.The authors developed correlation for mean value of Nusselt number in terms of sloping wall angle in addition to influence of Grashof number, viscosity of the working fluid along with the thermal conductivity. It had been concluded that increasing nanofluid volume fractions led to an augmentation in average Nu.

Al sabery et al. **[45]** used FDS to model the natural convection in trapezoidal – shaped enclosure. It was consisted of two layers, the left layer is filled with nanofluid / porous media, while the right layer was filled with non-Newtonian fluid. The influence of Rayleigh and Darcy numbers, volume fraction of nanofluid, power-law index, porous layer thickness, and angle of inclination had

been studied. The results indicated that as the Rayleigh and Darcy numbers, volume fraction of nanofluid increased, the heat transfer will improved. Besides that, as the power index dimensionless value intensify, then there would be an obvious cutback on the dimensionless average value of Nusselt number. While, it was improved as the angle of an inclined wall increases. Shermet et al. **[46]** used FDS with Buongiorno's model to study the natural convection nanofluid/porous filled trapezoidal cavity .It had been found that addition of solid nanoparticles may be lead to an enhancement or a reduction in the thermal performance of heat transfer based on Brownian and thermophoresis parameters and aspect ratio

Saleh et al. **[47]** examined of inclined magnetic field in a porous trapezoidal enclosure subjected to an inclined magnetic field by FDS. The authors found that increasing Hartmann number attends for an obvious increment in the rate of heat transfer. Rising of the inclination angle of magnetic field, slopping wall angle and Rayleigh number attends to an augmentation of heat transfer rate

2.2.2. Previous Studies related to Parallelogrammic and Rhombic Enclosures

Garcia et al. **[48]** studied the problem in an inclined Parallelogrammic enclosure filled by air within the ranges Rayleigh numbers $5 \times 10^3 \leq Ra \leq 3 \times 10^9$ in addition to the inclination angle of the enclosure within $-60° \leq \alpha \leq +60°$. The top and bottom wall were insulated. New correlation of average Nusselt number had been proposed that can be applied for real engineering systems like solar energy sector. Bairi **[49]** developed a correlation in a Parallelogrammic enclosure for real building under wide range of Rayleigh number $1.84 \times 10^5 \leq Ra \leq 1.70 \times 10^9$. It had been used FVS to simulate the phenomenon within the enclosure. Hussein **[50]** used FVS to study the natural convection heat transfer between hot internal circular cylinder located in a parallelogrammic enclosure. The gap between the inner body and the enclosure was filled by air. The author examined the influence of Rayleigh number as well as the influence of geometrical parameters like position of the circular cylinder, angle of inclination

of two vertical walls on the fluid flow behavior. It had been indicated that for better heat transfer, it was recommended to move the inner cylinder downward.

Bairi et al. **[51]** presented an important review on the previous studies regarding the natural convection heat transfer in a parallelogrammic enclosure. It was reviewed the influence of various parameter like Rayleigh number, aspect ratio, radiation discrete heating, turbulence, distinct thermal applied conditions along with the parallelogrammic's inclination angles. Hussein and Mustafa **[52]** used (FVM) to demonstrate numerically the natural convection in an enclosure with Parallelogrammic shape open from its top wall and heated partially from the bottom wall. The enclosure was filled by copper – water nanofluid. The influence of the impact of physical dimensionless parameters like Rayleigh number and nanofluid volume fraction had been examined. It was included also influence of geometrical parameters like the position of the heater length along the bottom wall and the angle of inclination. The results indicated that for better heat transfer characteristics, it was recommended to move the heater position close to the vertical left wall. Besides that, growing up and rising the dimensionless value of Rayleigh number and nanofluid solid volume fraction leading to enhance and augment as well as improve the rate of heat transfer

Anandalakshmi and Basak **[53]** studied natural convection with the entropy generation within rhombic cavity filled by porous media. It was utilized local thermal non – equilibrium model along with non – Darcy generalized model to treat with the porous media and the whole equations had been solved numerically utilizing FES. The results showed that at low Darcy number, Nusselt number was higher when the inclination angle was 30°. Choi et al. **[54]** studied the influence of circular cylinder position located within a rhombic enclosure on the natural convection under transient conditions. The range of selected dimensionless parameters were $10^3 \leq Ra \leq 10^7$ in addition to the vertical position of the inner circular body $-0.4 \leq \delta \leq +0.4$. The authors deduced that the heat transfer rate

will be at its maximum value when the internal cylinder moved up and become close to the bottom part of the enclosure

Hosseinjani and Nikfar **[55]** used iterative direct immersed boundary scheme to examine the buoyancy driven flow within a rhombus cavity filled with two heated isothermally circular body. The space between them was filled by copper nanofluid. The influence of diameter of the inner body, loading of nanoparticle $0 \leq \phi \leq 0.02$ and the distance between the two internal cylinders as well as Rayleigh number $10^4 \leq Ra \leq 10^6$ had been demonstrated. The results indicate that as the distance that separate both of the cylinders increases, the central upward flow will be strong. Lee and Kim **[56]** studied the natural convection within a ferrofluid filled square enclosure containing internal source of heat with different configuration (circle, rhombus and square). The authors used COMSOL software which was based upon finite element scheme to simulate and solve numerically the influence of magnetic hydrodynamics along with the ferrofluids. The authors found that the inner body with the shape of rhombus gives better rate of heat transfer. The results also indicate the strength of magnetic field in the bettering of heat transfer.

2.2.3. Previous Studies related to Elliptical Enclosure

The annulus elliptical enclosure had been studied a lot by numerous researchers using different numerical methods like Mahfouz **[57]** used Fourier spectral scheme to simulate the natural convection between two annulus elliptical enclosure. The outer enclosure was cold while two different thermal boundary conditions had been applied for the internal elliptical body, uniform wall hot temperature and applied heat flux. The results indicated that in the case for the uniformly distribution of the temperature along the wall, the average Nusselt increases as the angle of inclination increased which attends to an obvious enhancement in the rate of heat. Ghasemi et al. **[58]** showed that as the space between the hot inner elliptical internal body and outer cold circular enclosure

increased, the average Nusselt number increased while the fluid flow strength reduces as this space increases

Hu et al. **[59]** utilized FVS to study the thermal driven buoyancy flow within an elliptical – shaped enclosure for various dimensionless parameters like Ra, parameter of density inversion as well as aspect ratio, elliptical ratio and angle of inclination. It was developed an empirical correlation of heat transfer. The results indicate that reducing the aspect ratio and increasing the elliptical ratio led to an augmentation of heat transfer rate.

Ravnik et al. **[60]** studied the free convection between two different shapes of inner body (ellipse and circle) within a cubical cavity numerically using boundary layer scheme. The spaces filled by nanofluid (Cu, TiO_2 and Al_2O_3). The results reveal that both of the loading of the nanofluid in addition to the dimensionless Rayleigh number improve the thermal rate for the heat transfer. Also, the internal body with elliptical shape showed better rate of heat transfer compared with the circular body. Cho et al. **[61]** used immersed boundary scheme to study the effect of aspect ratio as well as the location of the internal body with the shape of ellipse on the thermal performance within a square enclosure containing elliptical and cylindrical body. Two different cases of location of the internal bodies had been examined. In case one, the elliptical body had been installed once on the upper part of the enclosure while the cylindrical body to the bottom side. Case two, the elliptical body had been located on the bottom while the circular body to the top. The results indicate at higher Ra for the case two in which the elliptical body was located in the lower side of the square enclosure at aspect ratio equals to 4 and having higher average Nusselt number in a compared with the case of two cylindrical cylinders of circular shapes.

Magnetic field researches had been examined by numerous researchers like Sheikholeslami et al. **[62]** demonstrated numerically using CVFEM to study the magnetohydrodynamic nanofluid buoyancy driven flow and radiation between two elliptical annulus enclosure. The nanofluid was ferrofluid Fe_3O_4 filled the

space between them. The authors investigated the influence of Hartmann and Rayleigh number, angle of inclination, nanofluid loading and Radiation parameter. The findings indicate that increasing parameter of radiation, angle of inclination and buoyancy ratio augments the heat transfer. Besides that, rising up Rayleigh number along with reducing Hartmann number attends to an obvious and a clear improvement of the thermal rate in heat transfer. Hashemi et al. **[63]** illustrated the inclined MHD on heat transfer between internal hot elliptical cylinder located within a square – shaped nanofluid enclosure and porous media using FES. The authors used Koo-Kleinstreuer-Li to simulate the nanofluid fluid flow. With respect to the modeling of porous media, Local thermal non-equilibrium model along with Darcy model had been utilized. The researchers of this article displayed the influence of Radiative parameter, Hartmann in addition to Rayleigh numbers, ratio of thermal conductivity, porosity, loading of nanofluid and interface heat transfer coefficient. It was found that increasing porosity of the porous media and the magnetic field force attends the heat transfer to be reduced while it enhances as the interface of heat transfer, nanofluid concentration and radiative parameter increases. Aghakhani et al. **[64]** showed effect of the magnetic and radiation influence on the rate free convection heat transfer along with entropy generation within an inclined nanofluid of squared – shaped cavity with elliptical heater applied to its bottom wall. The results reveal that there will be an increasing maximum entropy generation along with an enrichment to the heat transfer rate with Ra goes up. At the same time magnetic field rising up leads to an obvious depression in both entropy generation and rate of heat transfer.

2.2.4. Previous Studies related to Wavy Enclosure

The wavy shape of enclosure had critical challenge which is due to its complexity in a comparison with the square enclosure for example. This is the material point that motivate various researchers to study the wavy enclosure. Additionally, there is a second motivation that it had been took a lot of interest also due to its applications. Various numerical methods had been used to solve the heat transfer PDEs like finite volume, element and difference.

For example, finite volume methods had been used a lot by many researchers like; Oztop et al. **[65]** used FVS to examine the influence of volumetric heat source on the buoyancy driven flow within wavy enclosure. The enclosure was wavy from its top as well as bottom wall and both of them were adiabatic. The vertical left and right walls kept at uniform hot and cold temperature, respectively. The results indicate that increasing the number of amplitudes of the wavy wall attends to an augmentation in the rate of heat transfer. Esmaeilpour and Abdollahzadeh **[66]** studied by finite volume method to examine the natural convection in addition to the generation of the entropy inside different shapes of wavy enclosure. The enclosure was filled by CuO nanofluid. The outputs of this study reveal that increasing Grashof number and concentration of nanofluid loading lead to lowering the of heat. Also, the nanofluid helps in reducing the entropy generation. Cho et al. **[67]** used FVS to solve a similar work to the previous published work by **[66]** in a wavy cavity. The top and bottom were adiabatic. Three types of nanofluid had been selected $TiO_2 – H_2O$, $Cu – H_2O$ and $Al_2O_3 – H_2O$. The authors examined the affect of dimensionless well – known Rayleigh number, nanofluid loading and three different cases of wavy surface on the average Nusselt number. The results indicate that copper – water nanofluid exhibit the better characteristics of heat transfer and lowest of entropy generation. Tang et al. **[68]** studied the natural convection in complex wavy enclosure filled with nanofluid using both FVM and response surface method. The influence of amplitude of outer wavy wall as well as deviation of phase and different types of nanofluids like $Ag – H_2O$, $Al_2O_3 – H_2O$ and $TiO_2 – H_2O$ on the heat transfer had been investigated numerically. The output of this study reveals that the heat transfer coefficient of Ag solid nanoparticle was higher than the other types. Besides that, the wavy enclosure at the outer surface of the cavity gives better average Nusselt number in a comparison with the circular wall at the cavity.

Besides that finite difference method had been utilized also for example by Bhardwaj et al. **[69]** studied the physical phenomenon of generation of entropy in addition to the natural convection and within a cavity corrugated from the left.

The base of the cavity was kept at non – uniformly hot temperature while the inclined wall was adiabatic. It was found that the presence of the wavy wall makes the generation of entropy in addition to the Nusselt number higher than the flat wall. Gibanov et al. **[70]** used finite difference method to study the free convection in a wavy enclosure filled with micropolar Newtonian fluid. The cavity was wavy from its left wall heated uniformly at hot temperature while the right flat wall was kept at cold temperature. The top and bottom walls were adiabatic. The influence of Prandtl and Rayleigh numbers, parameter of vortex viscosity and number of undulation in the left wall had displayed. The results proved that as the number of undulation increases, there will be a reduction to rate of heat of the right wavy wall. Sheremet et al. **[71]** utilized finite difference method to study the impact of inclined magnetic field on the natural flow within an inclined partially heated wavy enclosure. Copper – water nanofluid wad filling the cavity. It was heated partially from the corner of the left bottom wall. It was demonstrated that the influence of Hartmann number, MHD angle, undulation number, cavity inclination angle, nanofluid loading and time. The results were crucial and indicate increasing the Hartmann number reduces the rate of heat transfer. With respect to the influence of angle of magnetic field, it was obtained that when it increases from 0 to $\pi/2$ leads to a reduction of heat transfer rate, while when it goes up from $\pi/2$ into π leads to an improvement in the rate of heat transfer. Beside, a reduction in the thermal rate of heat transfer was achieved when there was an increasing in the number of undulations. Sheremet et al. **[72]** examined the buoyancy driven flow in a nanofluid / porous wavy enclosure utilizing finite difference method. The wavy enclosure was partially heated from its right flat vertical wall with corrugated from the left wall and kept at isotherm cold temperature. The adiabatic conditions had been applied to the top and bottom wall. Darcy – Boussenisq model had been used to simulate the porous media while the two – phase model had been used to simulate the nanofluid flow taking into the account the influence of thermophoresis and Brownian diffusion. The influence of Rayleigh number, undulation number and heat source size had been

illustrated. The results showed that mean value of Nusselt number was decreasing function for the size of the heater. Sheremet et al. **[73]** studied it in triangular-wavy enclosure using finite difference. The influence of Prandtl number, dimensionless time in addition to the viscosity parameter had been examined. The results showed that Nusselt number is a decreasing function of the number of undulations.

Finite element method had been involved in the numerical analysis for example; Hatami and Safari **[74]** used finite element method to study the natural convection between circular cylinder located within a wavy enclosure. The gap between the internal body and the enclosure was filled by nanofluid. The influence of internal body location horizontally and vertically on the average Nusselt number had been investigated. It was found that the center location of the cylinder gives better performance of heat transfer. Hatami **[75]** used finite element method to study natural convection between cylinder located within wavy enclosure to find out the best wavy profile in the enhancement of heat transfer rate considering nine different wavy patterns. The results indicate that among the nine cases of wavy walls profiles, the case 7 and case 9 reveals better average Nusselt number while the lowest profile of Nusselt number was for case 4. Besides, it was found that for all cases, the average Nusselt number measured along the wavy wall was higher than that along the cylinder.

2.3. Summary

It can be seen from the previous publications that there are many investigation on the natural convection within different shapes of enclosures filled with traditional fluids, nanofluid, porous media that had been solved using different numerical method such as finite difference, finite element and finite volume formulation. It can be noted increasing Rayleigh number, Darcy number, nanofluid loading and reducing the Hartmann number leads to enhance the convection heat transfer.

Based upon the comprehensive review and according to the best author's knowledge there is many works on wavy enclosure as indicated in Figure 2.1 especially in I-shaped enclosure despite the limitations in the latter enclosure but there is no single study that combine between the I-shaped enclosure with two wavy walls filled partially by nanofluid and partially by porous media saturated with nanofluid considering different inner body shapes. Besides, the influence of the inner hot body locations and numbers will be studied for the first time considering the influence of inclined magnetic field in such enclosure which fill the gap in the previous publications. Also, there is no experimental work on this shape of enclosure which can leads to illustrate the complex phenomenon in full-details.

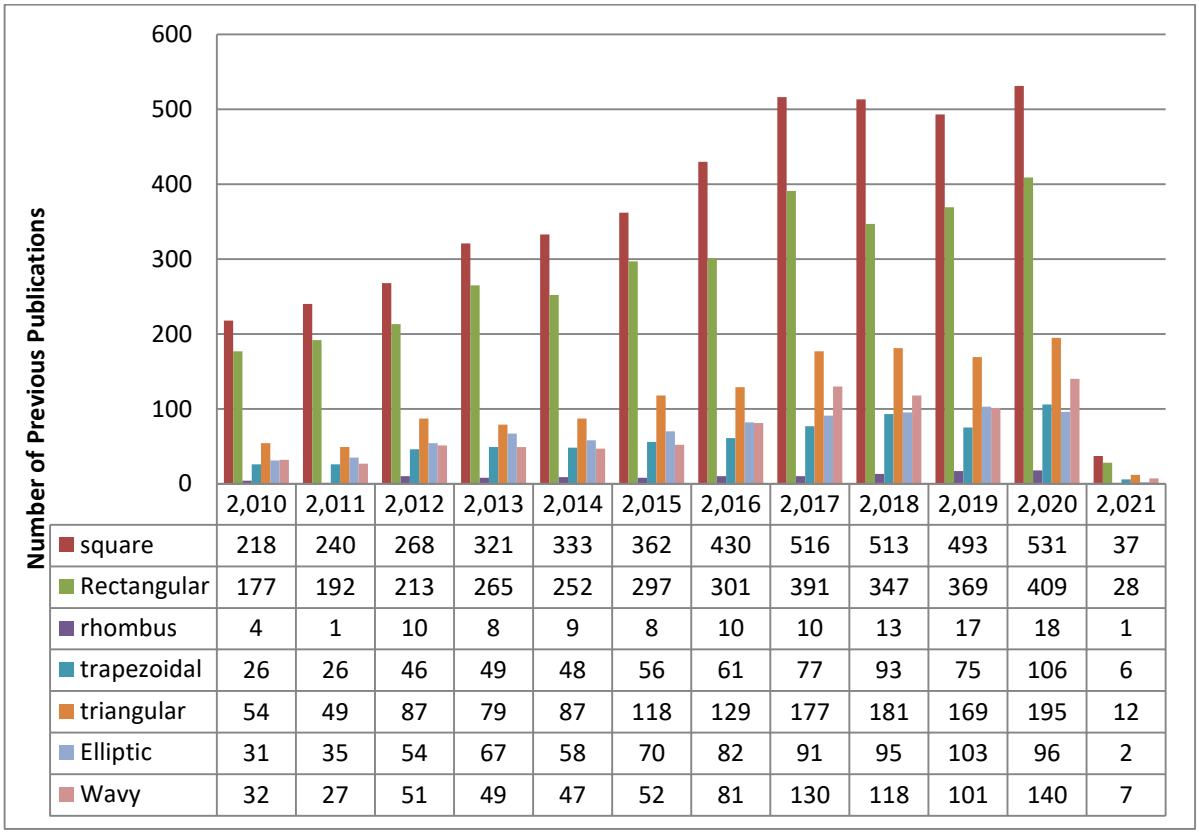

	2,010	2,011	2,012	2,013	2,014	2,015	2,016	2,017	2,018	2,019	2,020	2,021
square	218	240	268	321	333	362	430	516	513	493	531	37
Rectangular	177	192	213	265	252	297	301	391	347	369	409	28
rhombus	4	1	10	8	9	8	10	10	13	17	18	1
trapezoidal	26	26	46	49	48	56	61	77	93	75	106	6
triangular	54	49	87	79	87	118	129	177	181	169	195	12
Elliptic	31	35	54	67	58	70	82	91	95	103	96	2
Wavy	32	27	51	49	47	52	81	130	118	101	140	7

Figure (2.1) Previous studies based upon Sciencedirect data

Table 2.1 Selected Complex shapes of enclosures

Reference	Case Study/Problem	Method	Major Findings
[39]	Influence of uniform and non-uniform heating in trapezoidal enclosure filled by porous media	Finite element method	Increasing Darcy number leads to increase the Nusselt number. Additionally, sinusoidal profile for Nusselt number was noted.
[41]	Natural convection and radiation in a solar trapezoidal absorber enclosure of Compact Linear Fresnel Reflector	FLUENT 6.3	They develop a correlation for Nusselt number. Also, they deduced that heat loss can be minimized if the trapezoidal geometric aspect ratio was higher than 2.5 and the ratio of temperature was greater than 0.6.
[42]	Natural convection within trapezoidal enclosure filled by carbon nanotube heated partially from bottom	Finite element method	Increasing Rayleigh number and nanofluid loading leads to enhance the thermal rate of heat transfer.
[44]	The influence of Cu and Al_2O_3 nanoparticle on heat transfer augmentation within trapezoidal enclosure	Finite difference method	The results indicate that Cu was better in heat transfer augmentation than Al_2O_3. Additionally, increasing the slopping wall angle leads to enhance the Nusselt number. However, the angle of sloping had ignorance effect at high Grashof number.
[45]	Heatline study within inclined trapezoidal enclosure filled by multi-layers of nanofluid/porous media layer and non-Newtonian fluid layer	Finite volume method	Nusselt number improves with increasing of inclination angle of the trapezoidal enclosure
[46]	Utilizing of Buongiorno's model to study the natural convection within right-angle trapezoidal	Finite difference method	Reducing the Lewis number and aspect ratio decreases Nusselt number

	enclosure filled by porous media and		
[50]	The influence of inner circular cylinder position within parallelogrammic enclosure	Finite volume method	It is obtained that movement of the inner cylinder downwards with inclination angle of Parallelogrammic enclosure wall 15^{o} for better heat transfer rate
[52]	Study the influence of heater on Natural convection in an open Parallelogrammic enclosure	Finite volume method	Location of the heater closed to the left side inclined wall reveals better heat transfer
[53]	Natural convection along with entropy generation within rhombic enclosure filled by porous media	finite element method	Maximum heat transfer rate was when the angle of inclination of the enclosure was 30^{o}
[54]	Impact of position of inner circular cylinder on heat transfer	immersed boundary method	The position of inner body in addition to Rayleigh number highly effect on the contours of fluid flow and heat transfer
[55]	Transient natural convection within rhombus enclosure with two inner cylinders	immersed boundary method	Increasing of the distance between two cylinders leads to transient asymmetric fluid flow
[56]	Non-uniform magnetic field along with different shape of inner bodies (circle, rhombus, square) in a square enclosure	COMSOL software	The results indicate that the rhombus as in inner body had the highest Nusselt number
[76]	The influence of position of elliptical body within square enclosure on natural convection	Lattice Boltzmann method	It is better to move the elliptical body downwards for better heat transfer rate
[58]	The size of inner elliptical body in a circular enclosure	CVFEM	Increasing the size of inner elliptical body increases Nusselt number
[59]	The inner circular body size along with different orientation of elliptical enclosure	Finite volume method	It was obtained that increasing the inner body reduces the fluid flow strength

[60]	Comparison between the inner circular and elliptical body in a 3-D cubical enclosure	Finite element method	Elliptical body had high better heat transfer rate than the circular body
[61]	The influence of one inner elliptical and cylinder within square enclosure	Finite volume method	The position of elliptical inner body as well as the aspect ratio highly effect on heat transfer rate
[63]	Inclined Magnetic field on natural convection between inner elliptical body inside square enclosure filled by nanofluid and porous media	Finite element method	Increasing the porosity of the porous media and Hartmann number augment Nusselt number
[77]	MHD around a 3-D elliptical inner body within cubic enclosure	Lattice Boltzmann method	Increasing of Darcy as well as Reynolds number enhance Nusselt number
[64]	Natural convection along with MHD within an elliptic fin in an inclined square enclosure filled by nanofluid	Finite volume method	Increasing Hartmann number minimizes the total entropy generation and also decreases Nusselt number
[65]	Volumetric heat source within wavy enclosure	Finite volume method	The amplitude of wavy wall influence on heat transfer rate highly
[66]	The influence of wavy patterns on natural convection heat transfer and entropy generation within nanofluid wavy enclosure	Finite volume method	It was obtained that by increasing of nanofluid loading, there would be reduction in entropy generation as well as heat transfer
[67]	Different types of nanofluid filled complex shape of wavy enclosure	Finite volume method	The good tuning of wavy surfaces can be used to increase the heat transfer and reduces the entropy generation. In this regards, Cu-water nanofluid is the best choice
[68]	Sinusoidal wavy inner body within wavy enclosure filled with different types of nanofluids	Finite volume method	Ag-water nanofluid had the highest heat transfer rate
[69]	The influence of wavy wall on entropy generation	Finite difference method	The flat surface is favorite than the wavy surface in the case of minimization

			of entropy generation due to fluid friction
[70]	The influence of wavy wall on heat transfer	Finite difference method	Heat transfer at the hot wall reduces with increasing of undulations numbers
[71]	Inclined magnetic field on inclined wavy nanofluid enclosure	Finite difference method	The magnetic field angle highly effect on heat transfer reduction or improving
[74]	Comparison between circular and wavy wall on natural convection	Finite element method	Wavy wall enhance the heat transfer than circular wall

Chapter Three
Mathematical Modelling and Numerical Work

Chapter Three

Mathematical Modelling and Numerical Work

This chapter illustrates the CFD part of the study representing by introducing the mathematical modelling of the I-shaped enclosure with wavy walls considering the explanation of the boundary conditions. The governing equations of heat transfer and fluid dynamics considering the three low of physics (mass, momentum of fluid and energy) had been presenting for the nanofluid and porous media. The numerical solution is presenting through using of the powerful CFD tools called COMSOL Version 6.0

The physical domain is presented in this paragraph as presented in Figure (3.1) which had been designated via SOLIDWORKS 2020. Since many different thermal case studies are taken into account, each case will be presented separately. The physical model of the I-shaped with wavy walls enclosure along with its dimensions in (mm) is inserted in Figure (3.2). The enclosure had been filled partially by Al_2O_3 – water nanofluid and the other vertical layer filled by porous media saturated with the same nanofluid.

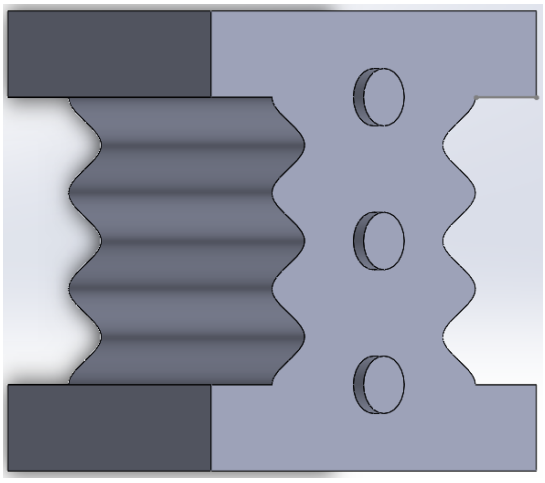

Figure (3. 1) I-shaped with wavy walls enclosure with inner bodies

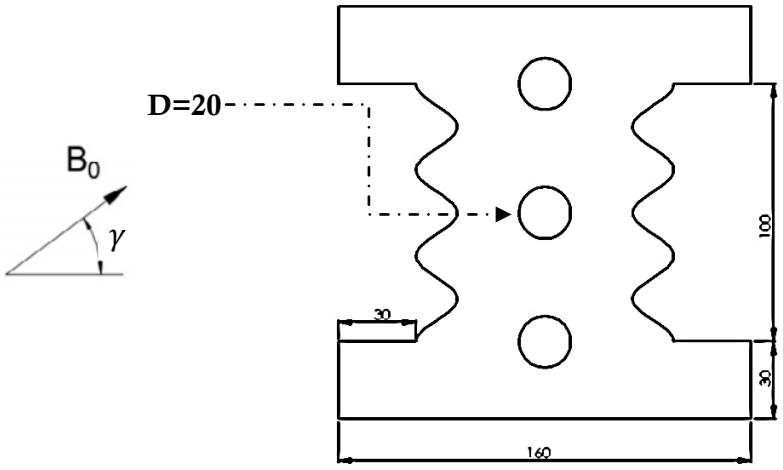

Figure (3. 2) Schematic diagram of CFD model of the present work

3.1. Governing Equations

The fluid flows and heat transfer problems are based upon the three laws of physics which are conservation of mass, momentum of the fluid along with the energy equations. It is solved numerically in the present application using finite element formulation. Numerous hypotheses are taken into account:

- Steady flow, two-dimensional, laminar and incompressible flow.
- There is no internal heat generation or absorption.
- Radiation effects are negligible.
- No – slip conditions had been applied at the walls.
- Darcy – Brinkmann model is used to model the porous media taking into account the local thermal equilibrium with the nanofluid and the porous media.
- It is assumed that the thermophysical properties are constant but that the density is related to temperature and processed by Boussinesq approximation.
- The interface between two layers (nanofluid and porous media saturated with the same nanofluid) is considered permeable.

Based upon the above-mentioned assumptions, the governing equation in the dimensional form may be written as indicated below **[78]**

Continuity Equation

$$\frac{\partial u}{\partial x}+\frac{\partial v}{\partial y}=0 \tag{3.1}$$

X – direction Momentum Equation

$$\rho_{nf}\left(u\frac{\partial u}{\partial x}+v\frac{\partial v}{\partial y}\right)=-C_1\frac{\partial p}{\partial x}+C_2\mu_{nf}\left(\frac{\partial^2 u}{\partial x^2}+\frac{\partial^2 u}{\partial y^2}\right)-C_3\mu_{nf}\frac{u}{K}+$$
$$C_1{B_o}^2\sigma_{nf}\left(Vsin(\gamma)cos(\gamma)-Usin^2(\gamma)\right) \tag{3.2}$$

Y – direction Momentum Equation

$$\rho_{nf}\left(u\frac{\partial v}{\partial x}+v\frac{\partial v}{\partial y}\right)=-C_1\frac{\partial p}{\partial y}+C_2\mu_{nf}\left(\frac{\partial^2 v}{\partial x^2}+\frac{\partial^2 v}{\partial y^2}\right)-C_3\mu_{nf}\frac{v}{K}+$$
$$C_1\rho_{nf}\beta_{nf}\,g\,(T-T_c)+C_1{B_o}^2\sigma_{nf}\left(Usin(\gamma)cos(\gamma)-Vcos^2(\gamma)\right) \tag{3.3}$$

Energy Equation

$$u\frac{\partial T}{\partial x}+v\frac{\partial T}{\partial y}=C_4\left(\frac{\partial^2 T}{\partial x^2}+\frac{\partial^2 T}{\partial y^2}\right) \tag{3.4}$$

By utilizing the dimensionless parameters, the dimensionless form of the governing equations may be written as indicated below;

$$X=\frac{x}{H};\ Y=\frac{y}{H};\ U=\frac{uH}{\alpha_{bf}};\ V=\frac{vH}{\alpha_{bf}};\ \theta=\frac{T-T_c}{(T_h-T_c)};\ P=\frac{pH^2}{\rho_{na}\alpha_{bf}^2};\ Pr=$$
$$\frac{\nu_{bf}}{\alpha_{bf}};\quad Ra=\frac{g\beta_{bf}(T_h-T_c)H^3}{\alpha_{bf}\nu_{bf}};\ Da=\frac{K}{H^2};\ Ha=B_oH\sqrt{\frac{\sigma_{na}}{\rho_{na}\nu_{na}}} \tag{3.5}$$

This makes the dimensionless form of the governing equations as indiacted below;

$$\frac{\partial U}{\partial X}+\frac{\partial V}{\partial Y}=0 \tag{3.6}$$

$$U\frac{\partial U}{\partial X}+V\frac{\partial V}{\partial Y}=-C_1\frac{\partial P}{\partial X}+C_2\frac{\mu_{nf}}{\rho_{nf}\alpha_f}\left(\frac{\partial^2 U}{\partial X^2}+\frac{\partial^2 U}{\partial Y^2}\right)-C_3\frac{\mu_{nf}}{\rho_{nf}\alpha_f}\frac{U}{Da}+$$
$$C_1PrHa^2\left(Vsin(\gamma)cos(\gamma)-Usin^2(\gamma)\right) \tag{3.7}$$

$$U\frac{\partial V}{\partial X}+V\frac{\partial V}{\partial Y}=-C_1\frac{\partial P}{\partial Y}+C_2\frac{\mu_{nf}}{\rho_{nf}\alpha_f}\left(\frac{\partial^2 V}{\partial X^2}+\frac{\partial^2 V}{\partial Y^2}\right)-C_3\frac{\mu_{nf}}{\rho_{nf}\alpha_f}\frac{V}{Da}+C_1\frac{(\rho\beta)_{nf}}{\rho_f\beta_{nf}}Ra\theta+$$
$$C_1Ha^2Pr\left(Usin(\gamma)cos(\gamma)-Vcos^2(\gamma)\right) \tag{3.8}$$

$$U\frac{\partial\theta}{\partial X}+V\frac{\partial\theta}{\partial Y}=C_4\left(\frac{\partial^2\theta}{\partial X^2}+\frac{\partial^2\theta}{\partial Y^2}\right) \tag{3.9}$$

The coefficients in the equations (3.7) to (3.9) are as indicated below;

Right Layer (Nanofluid Layer): $C_1=1, C_2=1, C_3=0\ and\ C_4=\alpha_{nf}/\alpha_f$

Left Layer (Nano – Porous Layer): $C_1=\varepsilon^2, C_2=\varepsilon, C_3=\varepsilon^2\ and\ C_4=\alpha_{eff}/\alpha_f$

The conditions that had been applied at the interface between the nanofluid layer and the porous media layer saturated with the same nanofluid are as indicated below;

$\theta_{po}=\theta_{na},\ \frac{\partial\theta_{na}}{\partial X}=\frac{K_{eff}}{K_{na}}\frac{\partial\theta_{po}}{\partial X},\quad \Psi_{po}=\Psi_{na},\quad \frac{\partial\Psi_{na}}{\partial X}=\frac{\partial\Psi_{po}}{\partial X},\quad \Omega_{po}=\Omega_{na},$

$\frac{\partial\Omega_{na}}{\partial X}=\frac{\partial\Omega_{po}}{\partial X}, \mu_{po}\left(\frac{\partial U_{po}}{\partial Y}+\frac{\partial V_{po}}{\partial X}\right)=\mu_{na}\left(\frac{\partial U_{na}}{\partial Y}+\frac{\partial V_{na}}{\partial X}\right),\ P_{po}=P_{na},\ \frac{\partial P_{po}}{\partial X}=\frac{\partial P_{na}}{\partial Y}$

The thermophysical properties of nanofluids are inserted below [79]

$$\alpha_{na}=\frac{k_{na}}{(\rho c_p)_{na}} \tag{3.10}$$

$$\rho_{na}=(1-\phi)\rho_{bf}+\phi\rho_{sp} \tag{3.11}$$

$$\rho c_p=(1-\phi)(\rho c_p)_{bf}+\phi(\rho c_p)_{sp} \tag{3.12}$$

$$(\rho\beta)_{na}=(1-\phi)(\rho\beta)_{bf}+\phi(\rho\beta)_{sp} \tag{3.13}$$

The dynamics viscosity of the nanofluid had been estimated via Brinkman model

$$\mu_{na}=\frac{\mu_{bf}}{(1-\phi)^{2.5}} \tag{3.14}$$

The thermal conductivity of the nanofluid had been obtained via Maxwell approach

$$\frac{k_{na}}{k_{bf}}=\frac{k_{sp}+2k_{bf}-2\phi(k_{bf}-k_{sp})}{k_{sp}+2k_{bf}+2\phi(k_{bf}-k_{sp})} \tag{3.15}$$

The effective thermal conductivity of the porous media can be calculated from

$$k_{eff}=(1-\varepsilon)k_{sp}+\varepsilon k_{na} \tag{3.16}$$

The effective diffusivity of the porous media is calculated based upon the formula inserted below;

$$\alpha_{eff} = \frac{k_{eff}}{(\rho c_p)_{na}} \tag{3.17}$$

The electrical conductivity of the nanofluid can be estimated from **[80]**

$$\frac{\sigma_{na}}{\sigma_{bf}} = 1 + \frac{3\left(\frac{\sigma_{sp}}{\sigma_{bf}} - 1\right)\phi}{\left(\frac{\sigma_{sp}}{\sigma_{bf}} + 2\right) - \left(\frac{\sigma_{sp}}{\sigma_{bf}} - 1\right)\phi} \tag{3.18}$$

The CFD contours of streamlines for the fields of the fluid flow within the enclosure had been represented and defined as indicated below **[81]**

$$U = \frac{\partial \Psi}{\partial Y}, V = -\frac{\partial \Psi}{\partial X} \tag{3.19}$$

The stream function in its dimensionless formula can be written as follow;

$$\frac{\partial^2 \Psi}{\partial X^2} + \frac{\partial^2 \Psi}{\partial Y^2} = \frac{\partial U}{\partial Y} - \frac{\partial V}{\partial X} \tag{3.20}$$

Since the Nusselt number is an important indicator in heat transfer enhancement, it had been determined on the inner hot body from the equation inserted below;

$$Nu_L = \frac{k_{nf}}{k_f}\frac{\partial \theta}{\partial n}\ , \overline{Nu} = \frac{1}{l}\int_0^l Nu_L\,(\varphi) d\varphi \tag{3.21}$$

3.2. Thermal Case Studies Utilizing CFD Code

Many thermal cases had been considered in the CFD part of the present work considering wide range of selected parameters and geometrical parameters such as; Rayleigh number, Darcy number, Hartmann number, MHD angle along with the number of undulations in addition to the position, shape and number of the inner hot bodies. So, different thermally boundary conditions which is better to examine them by dividing the study into many cases as indicated in the following;

3.2.1. MHD Thermogravitional within Novel Enclosure

This section of the numerical simulation is presented in Figure (3.5) which shows Novel I-Shaped enclosure with two corrugated walls considering the existence of multi-circular bodies of heat exchanger for three different shapes of inner hot body locations. The gap is filled partially by nanofluid in the left layer and partially by porous media saturated with the same nanofluid in the right layer. Three different cases of the thermal boundary conditions of the inner hot bodies had been investigated in order to obtain the best case in terms of augmentation of the heat transfer as presented via Figure (3.3).

The boundary conditions for the first CFD case can be written as below;

- $\theta = 0$, At $X = 0$ and $Y = 0$ to 1.6
- $\theta = 0$, At $X = 1$ and $Y = 0$ to 1.6
- The top and bottom of the horizontal walls of the enclosure; $\frac{\partial \theta}{\partial Y} = 0$
- Two Inner bodies are cold $(\theta = 0)$, and the third body is hot $(\theta = 1)$.
- No-slip boundary conditions for all walls and bodies

The selected dimensionless parameters for this case study are;

- Rayleigh number $(10^4 \leq Ra \leq 10^6)$
- Darcy number $(10^{-5} \leq Da \leq 0.1)$
- Hartmann number$(0 \leq Ha \leq 60)$
- MHD angle $(0° \leq \gamma \leq 90°)$
- Number of undulations $(1 \leq N \leq 5)$
- Position of the inner body $(0.3 \leq X_P \leq 1.3)$

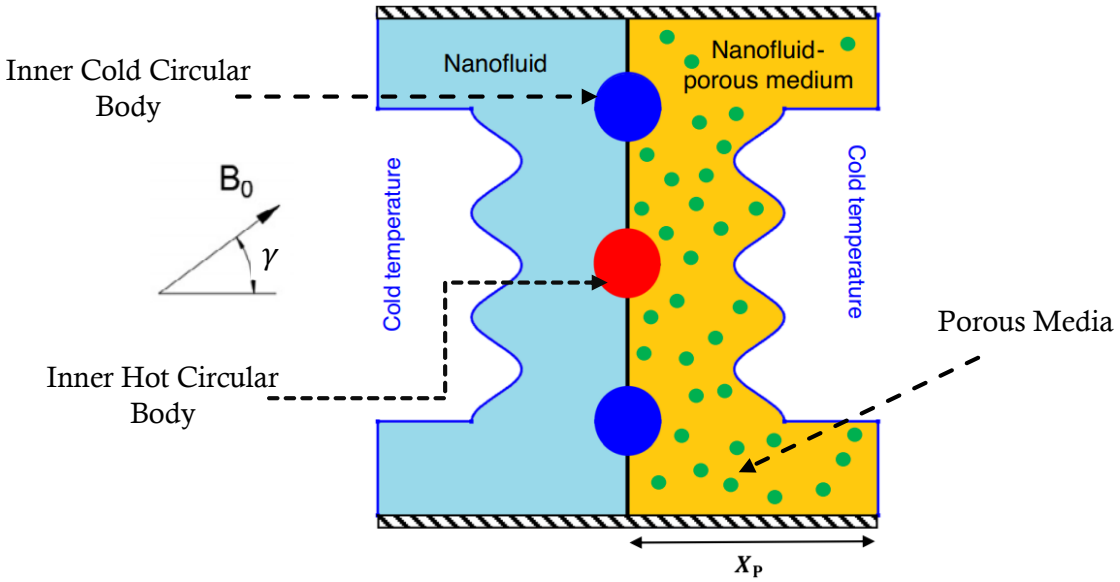

Figure (3. 3) Schematic Representation of the Proposed Model

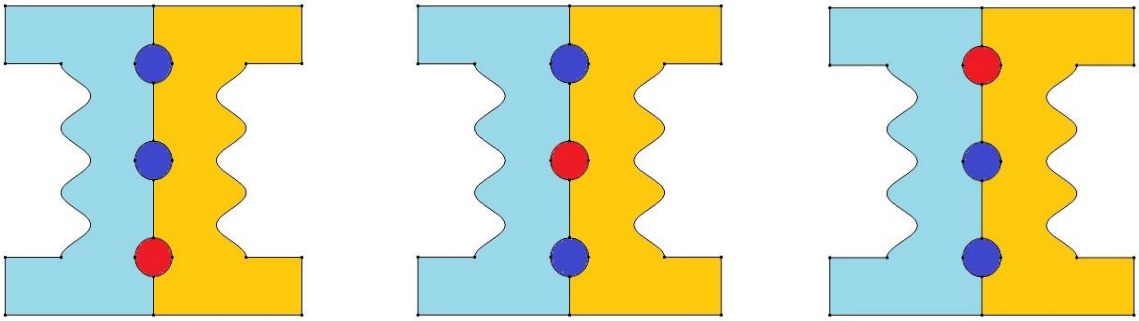

Figure (3. 4) three different thermal cases of inner HX bodies

3.2.2. Inner Bodies Shapes Within the Novel Enclosure

The second CFD case as shown in Figure (3.5) explains more details on the influence of four different cases of inner body shape. Four different shapes had been selected (circular, square, rhombus, triangular) on the fluid flow and heat transfer as shown in Figure (3.6) considering the influence of the following dimensionless parameters;

The boundary conditions for the first CFD case can be written as below;

- $\theta = 1$, At $X = 0$ and $Y = 0$ to 1.6
- $\theta = 0$, At $X = 1$ and $Y = 0$ to 1.6
- The top and bottom of the horizontal walls of the enclosure; $\frac{\partial \theta}{\partial Y} = 0$

- Two Inner bodies are cold $(\theta = 0)$, and the third body is hot $(\theta = 1)$.
- No-slip boundary conditions for all walls and bodies

The selected dimensionless parameters of the second CFD case are;

- Rayleigh number $(10^4 \leq Ra \leq 10^6)$
- Darcy number $(10^{-5} \leq Da \leq 0.1)$
- Hartmann number$(0 \leq Ha \leq 60)$
- MHD angle $(0° \leq \gamma \leq 90°)$
- Number of the hot body $(1 \leq No \leq 3)$
- Position of the inner body $(0.3 \leq \delta \leq 1.3)$

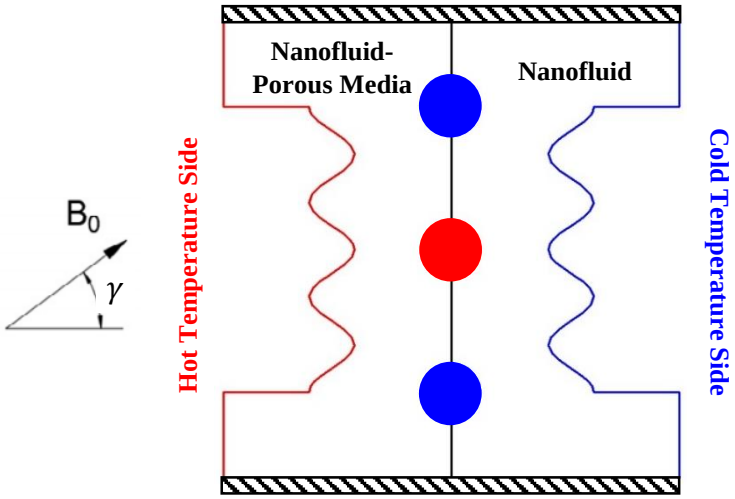

Figure (3. 5) schematic representation of the second CFD case

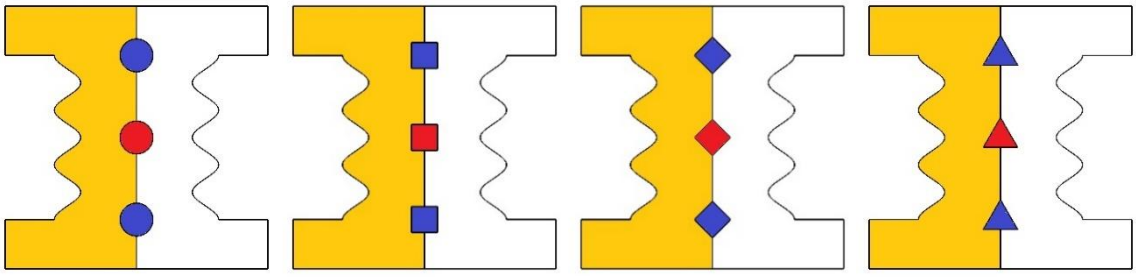

case 1 case 2 case 3 case 4

Figure (3. 6) schematic representation for the computational domain

3.2.3. Trapezoidal Heater at the base of Novel Enclosure

The third selected CFD case was on more details about the influence of magnetic field angle considering trapezoidal heater and inner heated circular cylinder as shown in Figure (3.7).

The boundary conditions for the first CFD case can be written as below;

- $\theta = 0$, At $X = 0.3, Y = 0.3$ to $X = 0.3, Y = 1.3$
- $\theta = 0$, At $X = 1.3, Y = 0.3$ to $X = 1.3, Y = 1.3$
- The trapezoidal heater and the inner circular body: $\theta = 1$
- The rest walls of the enclosure; $\frac{\partial \theta}{\partial Y} = 0$
- No-slip boundary conditions for all walls and bodies
- The boundary conditions are applied to the permeable surfaces between the porous partition and the nanofluid and can be defined as below:

$$\theta_{po} = \theta_{na}, \quad \frac{\partial \theta_{na}}{\partial X} = \frac{K_{eff}}{K_{na}} \frac{\partial \theta_{po}}{\partial X}, \quad \Psi_{po} = \Psi_{na}, \quad \frac{\partial \Psi_{na}}{\partial X} = \frac{\partial \Psi_{po}}{\partial X}, \quad \Omega_{po} = \Omega_{na}, \quad \frac{\partial \Omega_{na}}{\partial X} = \frac{\partial \Omega_{po}}{\partial X}, \quad \mu_{po}\left(\frac{\partial U_{po}}{\partial Y} + \frac{\partial V_{po}}{\partial X}\right) = \mu_{na}\left(\frac{\partial U_{na}}{\partial Y} + \frac{\partial V_{na}}{\partial X}\right), \quad P_{po} = P_{na}, \quad \frac{\partial P_{po}}{\partial X} = \frac{\partial P_{na}}{\partial Y}$$

The selected dimensionless parameters are inserted below;

- Rayleigh number $10^4 \leq Ra \leq 10^6$
- Darcy number $10^{-5} \leq Da \leq 0.1$
- Hartmann number $0 \leq Ha \leq 60$
- Nanofluid loading $0 \leq \phi \leq 0.05$
- Magnetic field inclination angle $0° \leq \gamma \leq 90°$
- Trapezoidal heater length $0.4 \leq B \leq 1.4$
- Location of the trapezoidal heater $0.2 \leq E \leq 0.8$
- Position of the circular cylinder $0.3 \leq \delta \leq 1.3$

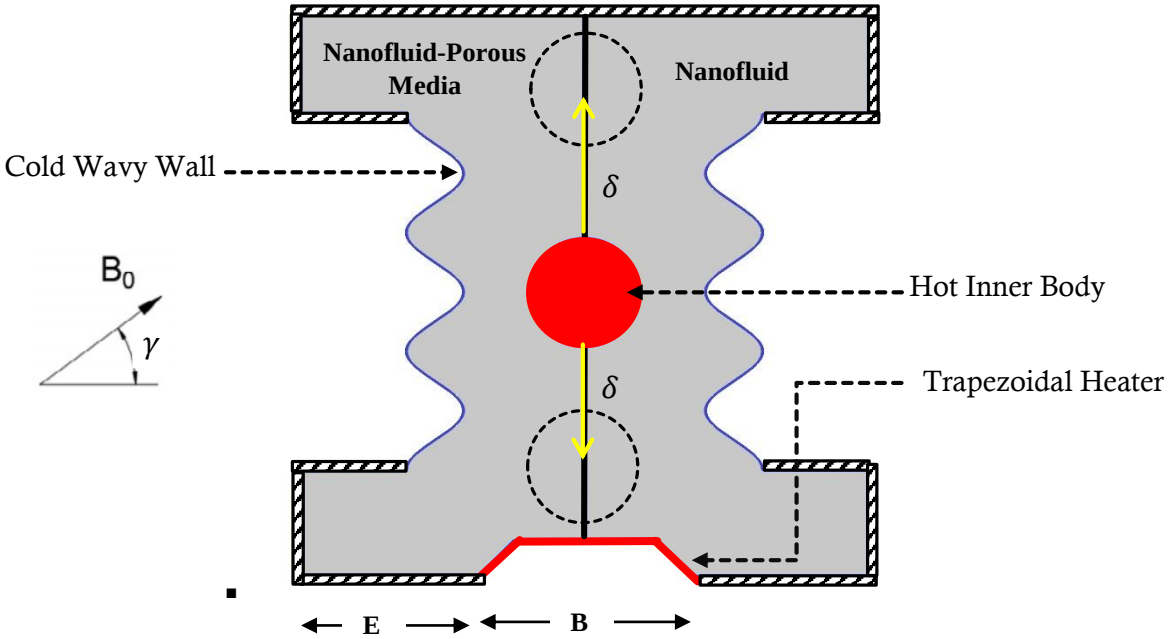

Figure (3. 7) schematic representation for computational domain

3.2.4. Wavy Patterns of Novel Enclosure

The influence of various parameters such as number of undulations, the distance between the wavy walls, and the inner elliptical body position for four different cases of wavy walls patterns with and without magnetic field on fluid flow and heat transfer had been drawn in terms of streamlines, isotherms and Nusselt number as it would be illustrated in full-details in Chapter five. It can be seen from Figure (3.8) that case 1 represents (In-In), case 2 represents (In-Out), Case 3 represents (Out-In), Case 4 represents (Out-Out). This idea of wavy patterns is created based upon the published original researches as there is serious limitations in these four wavy patterns [66, 82].

The boundary conditions had been as indicated below;

- $\theta = 1$, At $X = 0, Y = 0$ *to* $X = 0, Y = 1.6$
- $\theta = 1$ at the inner elliptical body
- $\theta = 0$, At $X = 1.6, Y = 0$ *to* $X = 1.6, Y = 1.6$
- The top and bottom walls are adiabatic $\frac{\partial \theta}{\partial Y} = 0$

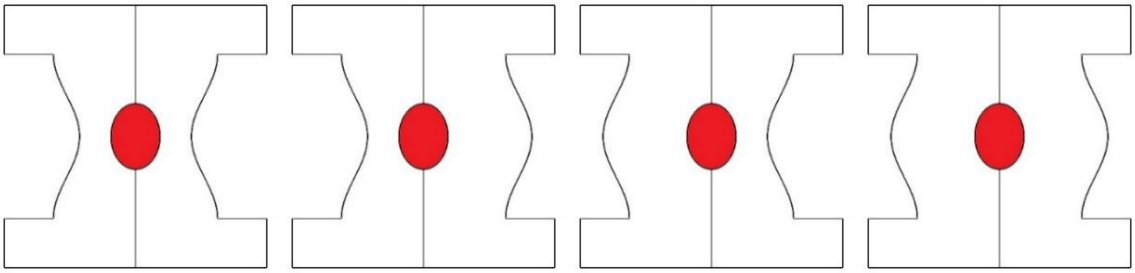

Case 1 (In-In) | Case 2 (In-Out) | Case 3 (Out-In) | Case 4 (Out-Out)

Figure (3. 8) Selected CFD cases of the Present Problem

3.2.5. I-shaped wavy walls enclosure: Experimental Model

The natural convection heat transfer within I-shaped wavy walls enclosure considering inner heater had been discussed in this section. This case had been considered for the comparison purposes between the numerical and experimental results. The left layer is partly filled by Al_2O_3 – water nanofluid while partly filled by porous media saturated with the same nanofluid. The left wall of the enclosure is kept at cold temperature while the right walls and the inner heater are kept to hot temperature.

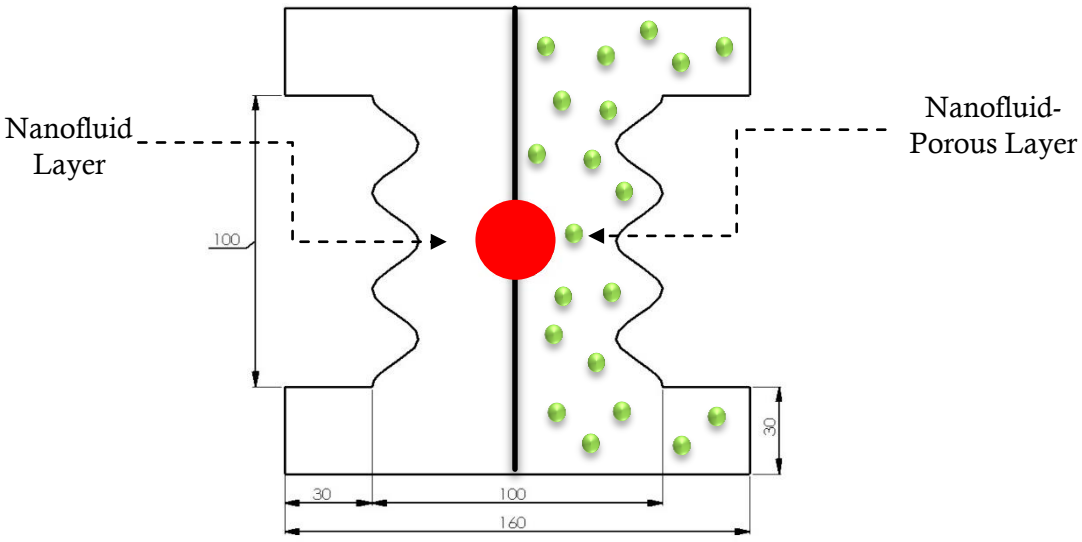

Figure 3. 9 Exp-CFD case

It is important to write the equation that had been used to represent the wavy walls;

$$Y = \lambda \cos(Ny) \tag{3.22}$$

Where, λ is the amplitude

N is the number of undulations

3.3. Numerical Work

3.3.1. CFD Convergence Criteria

The present work for the whole of the CFD simulation is done based upon finite element formulation. The computational domain is divided into small elements. The governing equations that mentioned before had been solved by COMSOL CFD software for computing the fluid flow characteristics in terms of streamlines along with the isotherms and the heat transfer characteristics in terms of Nusselt number. The convergence criteria had been considered is less than 10^{-7}. CFD COMSOL solver uses an iterative process to solve the equations of mass, momentum along with the energy equation and in order to judge the convergence, there is three major parameters which they are residual plot, creating monitor and finally check the fluid flow patterns. The monitor is a physical quantity that it is important in the numerical results which is Nusselt number in this study as it will be explained later in this chapter in the section of mesh independent study. The flow chart of the numerical solution is inserted in Appendix A.

The governing equations were solved numerically using a finite element scheme under steady state conditions. The generation of the numerical grid has been tested many times and the convergence error criterion has been set to 10^{-5} as shown in the equations below:

$$\sum \left| \xi_{i,j}^{n+1} - \xi_{i,j}^{n} \right| \Big/ \left| \xi_{i,j}^{n+1} \right| \leq 10^{-7} \tag{3.23}$$

3.3.2. Mesh generation

The numerical gird generation is an important step in CFD work especially it consume the time of numerical solution as well as selecting the appropriate number of elements is highly influences on the accuracy of the obtained CFD numerical results. In this way, triangular shape of numerical points (mesh) had been chosen in this study because this mesh type is simple and quick in order to cover all of the enclosure. An explanation for the number of elements for different inner bodies within the proposed Novel I-shaped wavy-walled enclosure with different numerical CFD cases that had been illustrated in section (3.2) as shown in Figure (3.10).

Since the number of selected elements highly effected on the time of numerical solution, so mesh independent study had been done for all of the entire CFD work. When the increasing numbers of element had no powerful impact of the accuracy of the results. The numerical work of the existence of inner circular body in the I-shaped wavy-walled enclosure along with the existence of trapezoidal heater attached to the bottom wall of it had been selected to present the mesh independent study as shown in Figure (3.11). Also, Table (3.1) shows the influence of number of elements on the accuracy of the numerical grid generation for different inner bodies. It can be seen that required number of elements is highlighted in order to depend on this number of elements for the whole simulation. Further increments of number of elements, had no influence on the accuracy of Nusselt number which in turn not necessary to increases the number of elements.

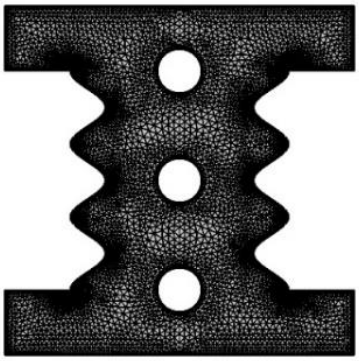

Mesh of Case in 3.2.1.

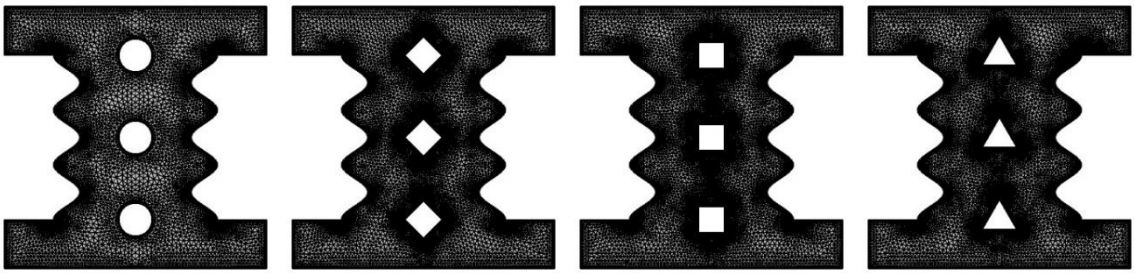

Mesh of Case in 3.2.2.

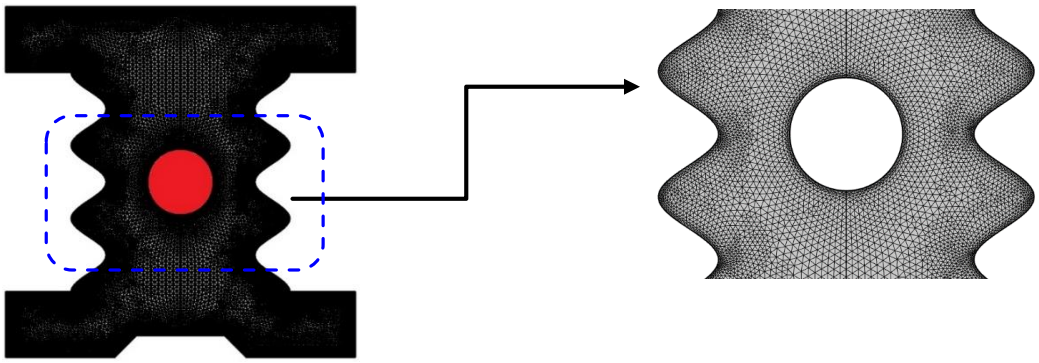

Mesh of Case in 3.2.3.

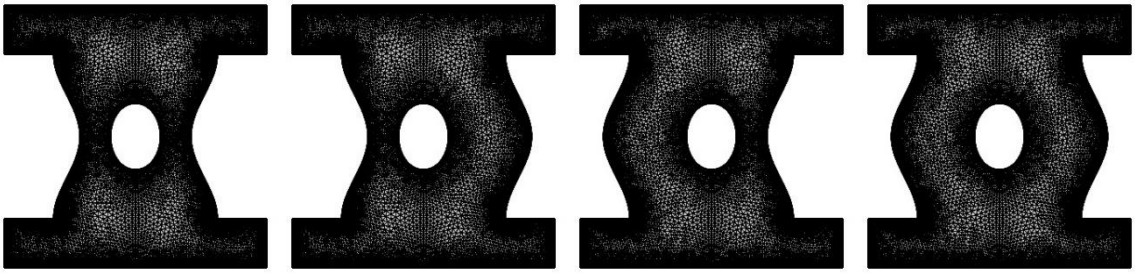

Mesh of Case 3.2.4.

Figure 3. 10 mesh generation for the proposed novel I-shaped wavy-walled enclosure with different inner bodies at $Ra = 10^6, Da = 0.001, Ha = 60, \gamma = 45, \Phi = 0.02$

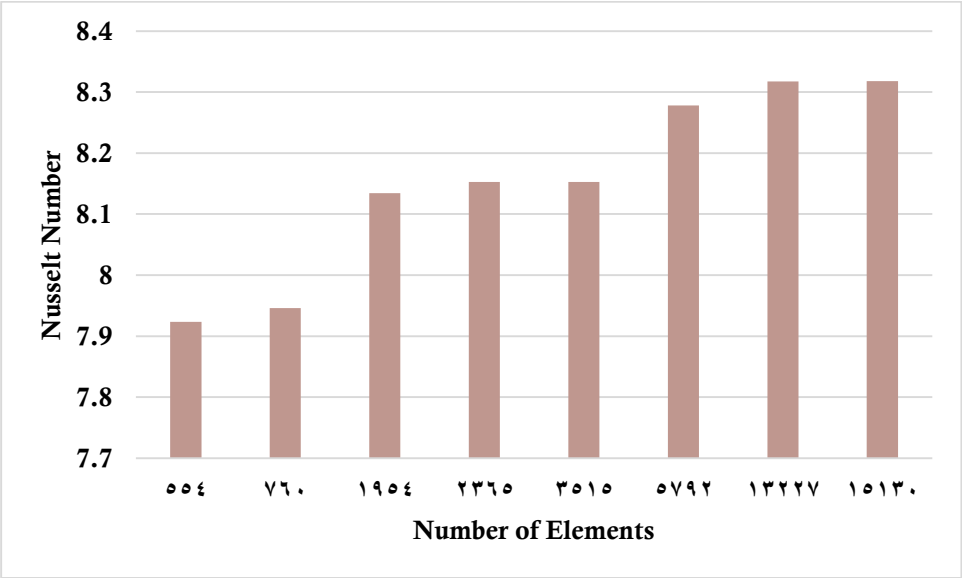

Figure 3. 11 Mesh independent study in terms of Nusselt number for the third CFD case [3.2.3] considering the trapezoidal heater at the base of the novel enclosure

Table (3.1) the influence of number of elements on the dimensionless value of Nusselt number considering different inner bodies shapes (circle, rhombus, square and triangle)

Grid Size	Circle	$\Delta = \frac{Nu_{new} - Nu_{old}}{Nu_{new}}$	Grid Size	Rhombus	$\Delta = \frac{Nu_{new} - Nu_{old}}{Nu_{new}}$	Grid Size	Square	$\Delta = \frac{Nu_{new} - Nu_{old}}{Nu_{new}}$	Grid Size	Triangle	$\Delta = \frac{Nu_{new} - Nu_{old}}{Nu_{new}}$
1212	6.7986	----	1443	5.7121	----	1488	5.0595	----	8905	3.8138	----
1862	6.9059	0.015537	2074	6.1378	0.074526	2068	5.3381	0.052191	9379	3.9895	0.044041
2974	7.0314	0.017849	3314	6.2893	0.024683	3426	5.7014	0.063721	13195	4.9453	0.193274
4786	7.1201	0.012458	5198	6.518	0.036363	5354	5.9863	0.047592	16959	5.377	0.080286
5594	7.0934	-0.00376	6756	6.603	0.013041	7018	6.1613	0.028403	21946	5.5939	0.038774
8250	7.1328	0.005524	10206	6.6742	0.010783	10598	6.2721	0.017666	32235	5.733	0.024263
12506	7.1595	0.003729	19366	6.8583	0.027584	19644	6.5535	0.042939	57337	6.0448	0.051582
28146	7.2577	0.01353	44938	6.9392	0.011796	45048	6.7201	0.024791	107239	6.2323	0.030085
32234	7.2564	-0.00018	51878	6.9395	4.32E-05	52176	6.723	0.000431	142832	6.2323	0

Chapter Four
Experimental Work

Chapter Four

Experimental Work

The present chapter focuses on the experimental heat transfer point of view to the novel I-Shaped-Wavy-walled enclosure considering inner heater. The left layer is filled by Al_2O_3 – water nanofluid while the right layer had been filled by porous media saturated with the same nanofluid.

4.1. Experimental rig

The experimental model that had been utilized in this study is presented schematically in Figure (4.1a) and photograph to the real system is shown in Figure (4.1b) which consists the enclosure along with the mechanical equipments that had been used to applied the required thermally boundary conditions such the intensity of the magnetic field, temperature difference and fluid flow strength. The experimental setup had the following parts;

1. I-shaped wavy-walled Enclosure
2. Right hot wavy wall
3. Left cold wavy wall
4. Magnetic Field Core
5. Heating System Controller
6. Water – Cooled Chiller
7. Magnetic Field Controller
8. 24-Type-K Thermocouples
9. Temperature Data Logger
10. Inner hot body

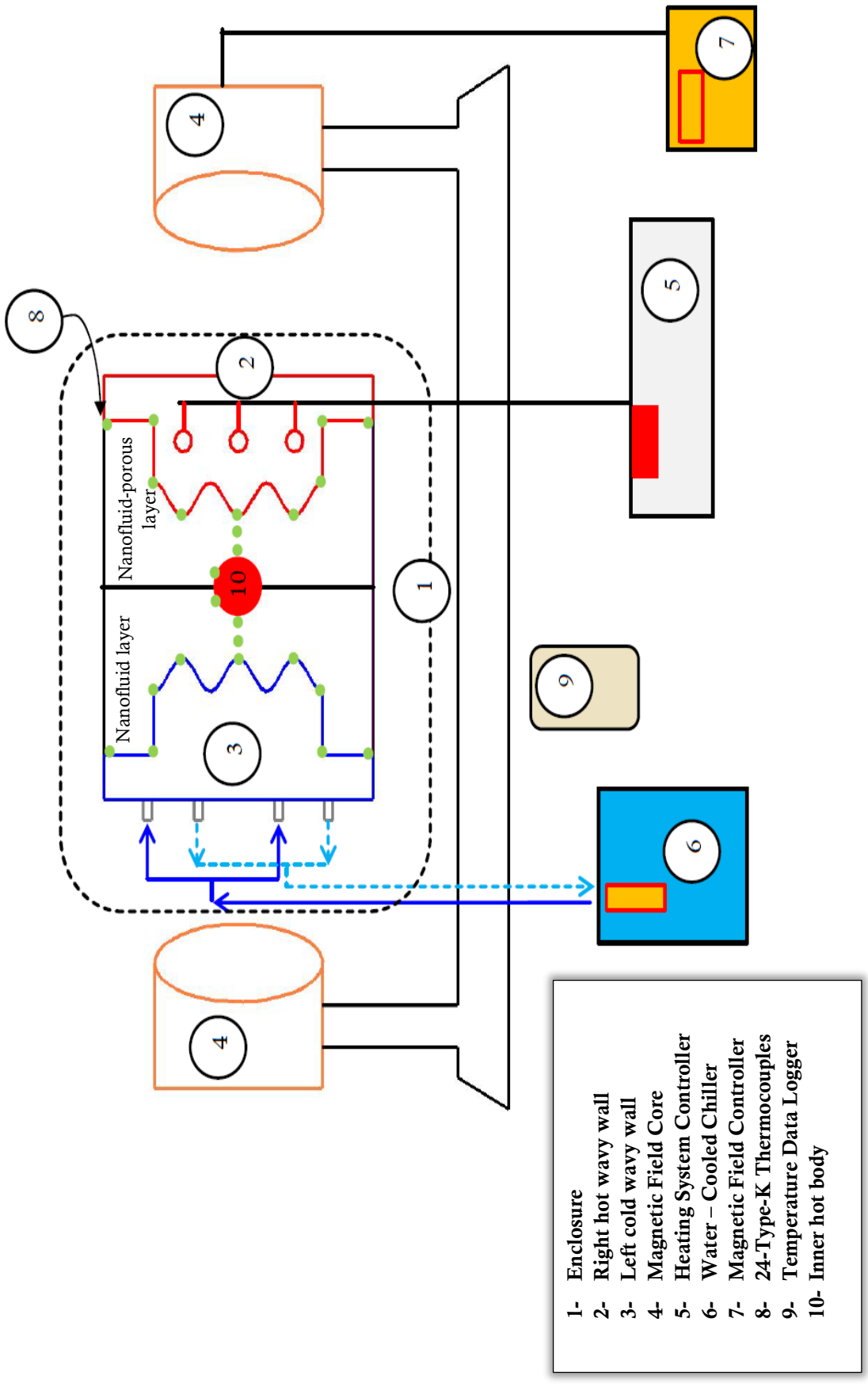

Figure (4. 1 a) Schematic representation of the experimental setup

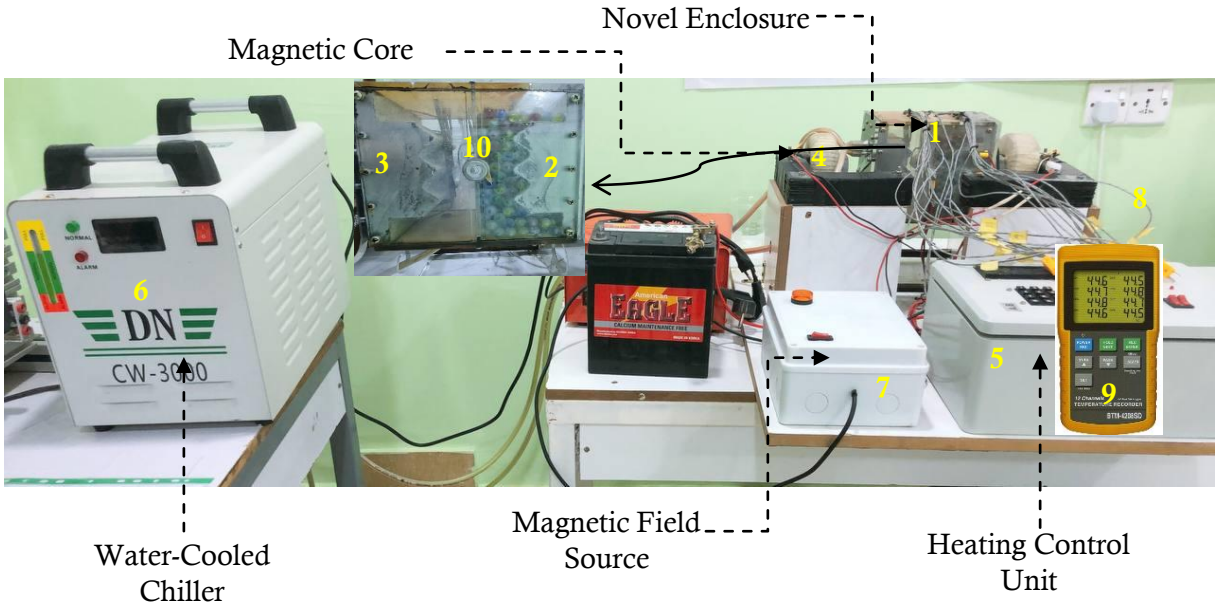

Figure (4.1 b) Photograph of the experimental rig

4.1.1. Novel Enclosure

The enclosure which is the major part of the present rig represents the designated novel I-shaped wavy walled enclosure. A pure aluminum plate had been utilized in the present work in order to make the right and left walls of the enclosure. SOLIDWORKS software had been utilized to design the enclosure and then with a CNC machine had been used to fabricate the required I – shaped including the wavy walls enclosure with the required dimensions.

Since the natural convection is takes place due to temperature differences, so the isotherms hot conditions are made with the help of a drilling machine. Three holes had been made within the front side of the right wavy walls in order to supply the required uniform hot temperature. The inner hot circular body is made of the same Aluminum alloy located at the center of the enclosure and it had been supplied with the heater. On the other hands, grooves had been implemented within the left cold wall in order to make counter flow heat exchanger and keep the entire wall at the cold room temperature with the help of water – cooled chiller as it will be indicated later through this chapter.

The others walls (top, bottom, front and back) is formed from an acrylic glass sheet within the enclosure. Additionally, the acrylic had good insulation properties, low cost, durability and easy handling.

Finally, the stages of design for each part of the experimental prototype of the enclosure is shown in figure (4.2).

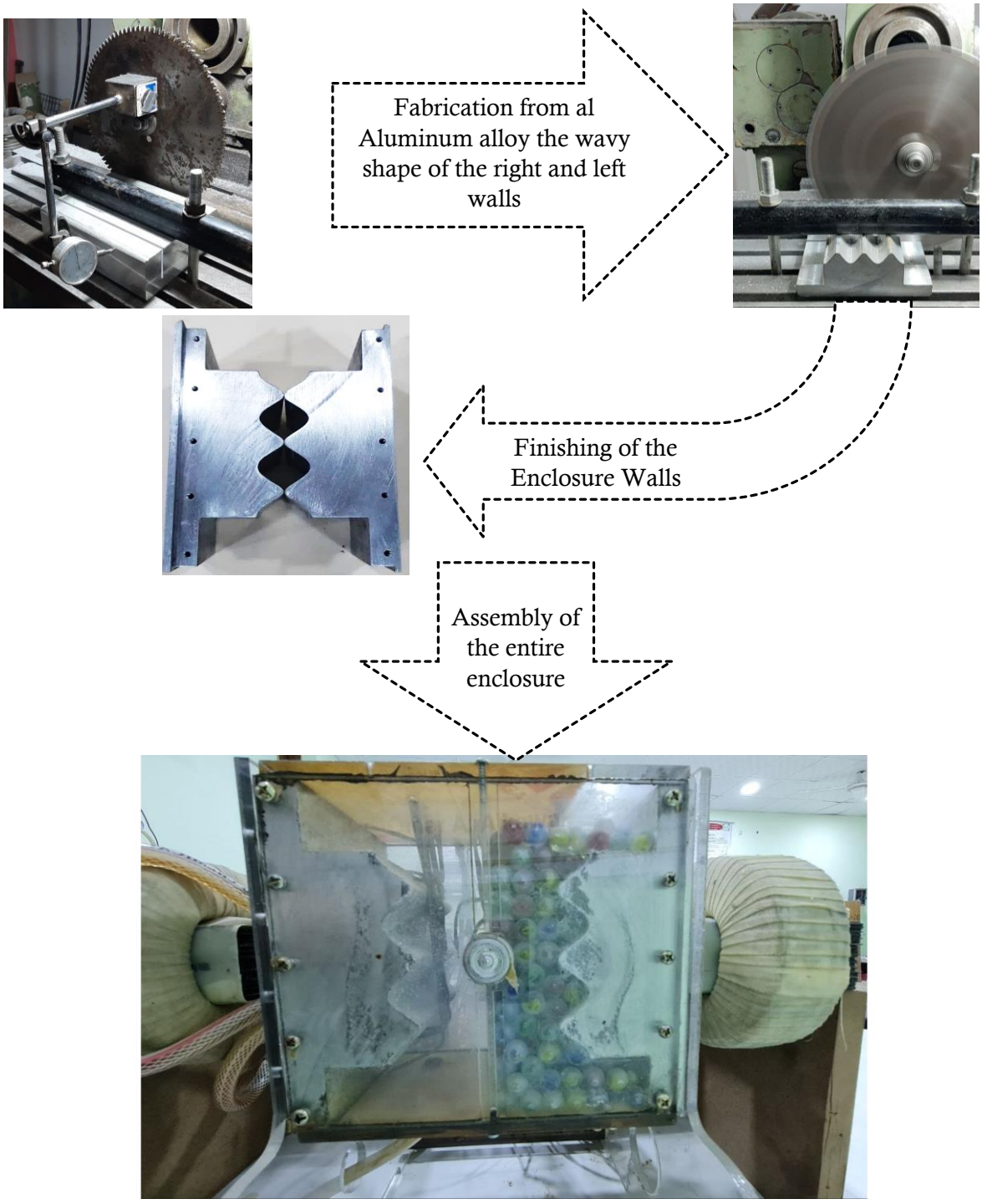

Figure (4. 2) stages of design the novel I-shaped wavy-walled enclosure

4.1.2. Heating unit

The electrical heaters are used for heating the water with four numbers, three of them that had been installed in the right wall as a point source to get the required hot temperature. The inner hot rode had been attached with the fourth heater that located inside it. A control heating unit had been prepared in order to get the required hot temperature. It is worthy to mention, that the heater located within the inner body as well as the right wavy wall are controlled to have the same hot temperature. The supplied current is 7 Amps and the voltage is 12 V. Thus, the power of the heater is 90 W. Additionally, the temperature ranges that had been used in the experimental work are from 30 – 40 Celsius. The heating control unit and the heaters are shown in Figure (4.3).

(a) Control unit

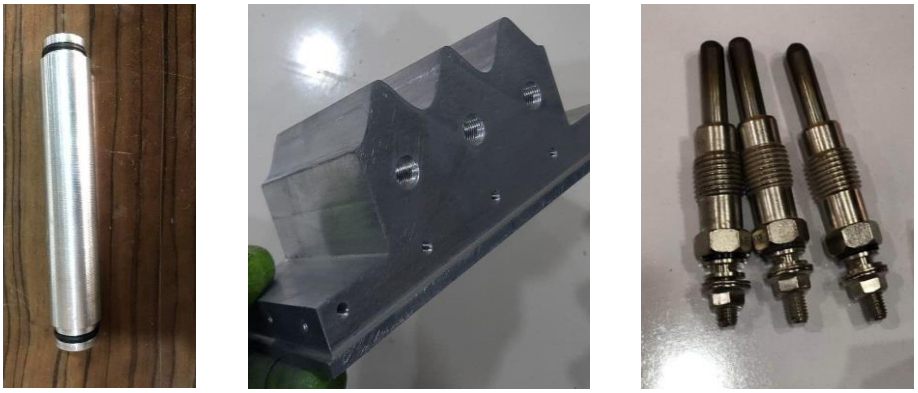

(b) Heaters

Figure (4. 3) Thermal Heating System

4.1.3. Water-Cooled Chiller

For the purpose of maintaining the left wall of the enclosure at cold temperature, CW-3000DG Thermolysis Type Industrial water-cooled chiller had been implemented. Its specification is indicated in Table (4.1). The capacity of the chiller is 8.5 Liter that can be used for long time and dissipating a lot of heat. It is used for small cooling devices and provide a stable condition during its working. Its sensitive parts can be easily protected with the help of Alarm.

Table (4.1) specification of water-cooled chiller

Power supply	220 V AC / 50 Hz
Capacity	8.5 L
System of cooling	Air cooling fan
Maximum water pumping lift	6 m
Wight	16 kg

The methodology of keeping the left wall of the enclosure is achieved by making a groove within the aluminum left wall to form a cross flow heat exchanger within the back of the wall as shown in Figure (4.4). The reason behind this is to ensure a uniform temperature along the wall.

The cooling water machine unit as shown in Figure (4.5) contains of temperature controller, fan, water tank, air inlet, cooling water inlet and exit. The forced air-cooled radiator that with the help of fan, the water will cool and then goes into the left side of the enclosure. photograph of the water-cooled chiller with its construction inserted in Figure (4.4).

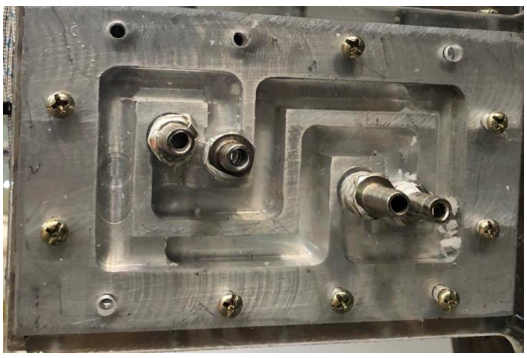

Figure (4. 4) grooves within the back of the left wavy wall

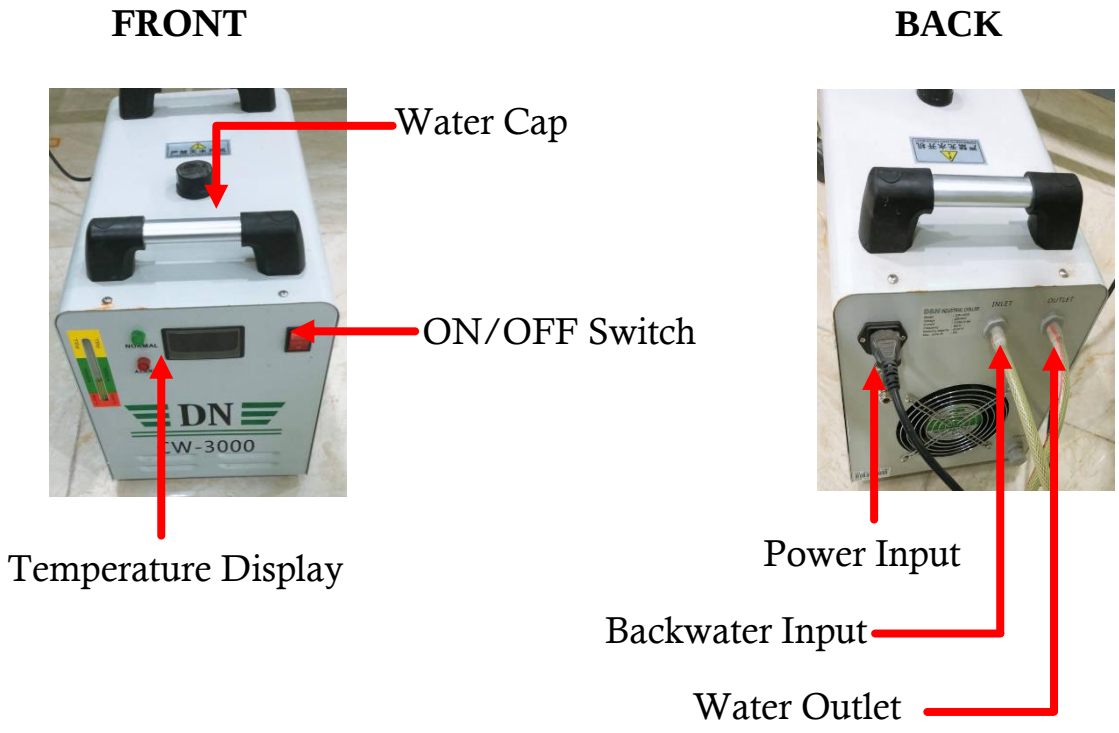

Figure (4. 5) water-cooled chiller

4.1.4. The Magnetic Field Machine

The electromagnetic field is made of 110 mm horseshoe with two windings along with AC voltage source having 3500 turns of wire made of copper with 0.87 mm diameter. The basic dimensions of the electromagnet are presented in the figure (4.6). The magnetic field intensity was kept at constant of 20 mT.

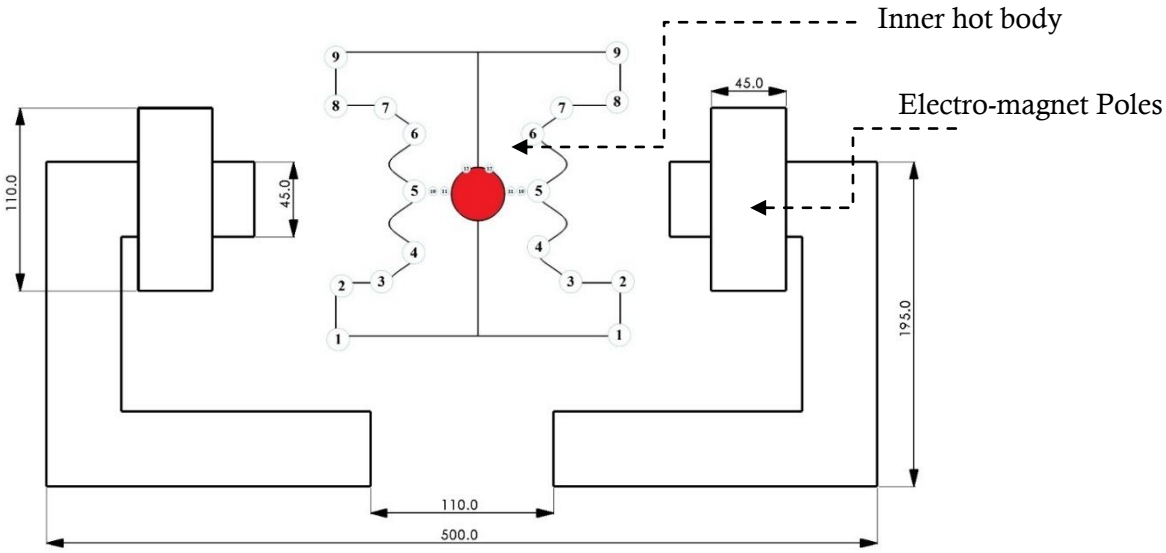

Figure (4. 6) schematic representation of the magnet system

The process of the magnetic field system is starting by CNC machine in order to cut the mild steel into many sections to takes the shapes of horseshoe and then tighten all of them together. After that, two cores had been located on the horseshoe and an electrical current equal to 2 Amps passes through them. A control system allows to the current and passed through the entire magnetic system. The details of magnetic field construction are inserted in figure (4.7).

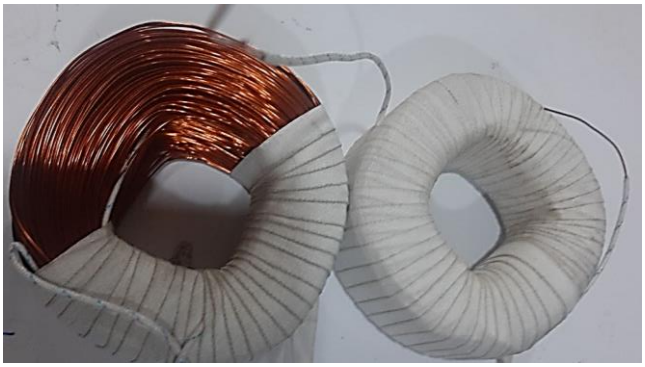

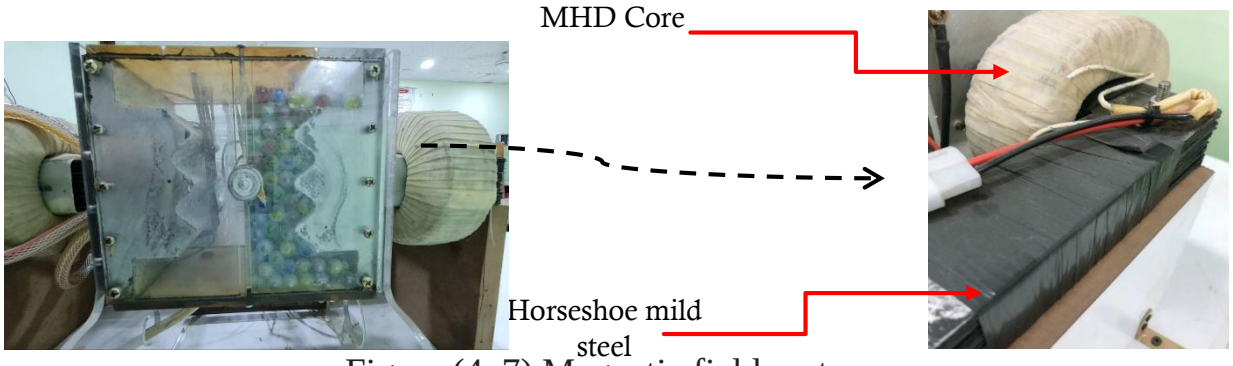

Figure (4. 7) Magnetic field system

4.2. Temperature Measurements

The measurements of temperature are very important especially when the comparison between the experimental and CFD work is made. The twenty-four thermocouples (Type K of measuring range of 0 to 800 ^{o}C) were installed within the enclosure in the required position as shown in Figure (4.8). The reason for these locations is to find out the temperature of the right hot wall and the temperature of left cold walls as well as the temperature in the nano-porous mid-region. A schematic representation of the thermocouples positions is shown in Figure (4.9). These positions and numbers of thermocouples are based upon many experimental heat transfer articles [83, 84]. The measurements of the temperature are made utilizing by two temperature data logger each of them with 12 channels. This is commonly known as BTM-4208SD as indicated in Figure (4.10).

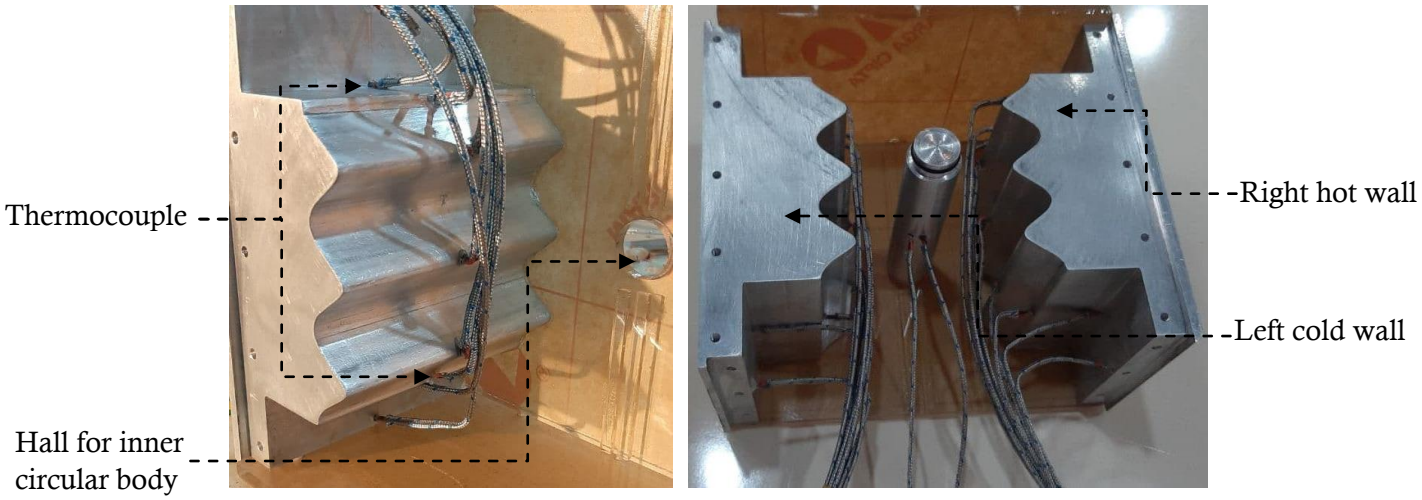

Figure (4. 8) positions of thermocouples types K within the enclosure

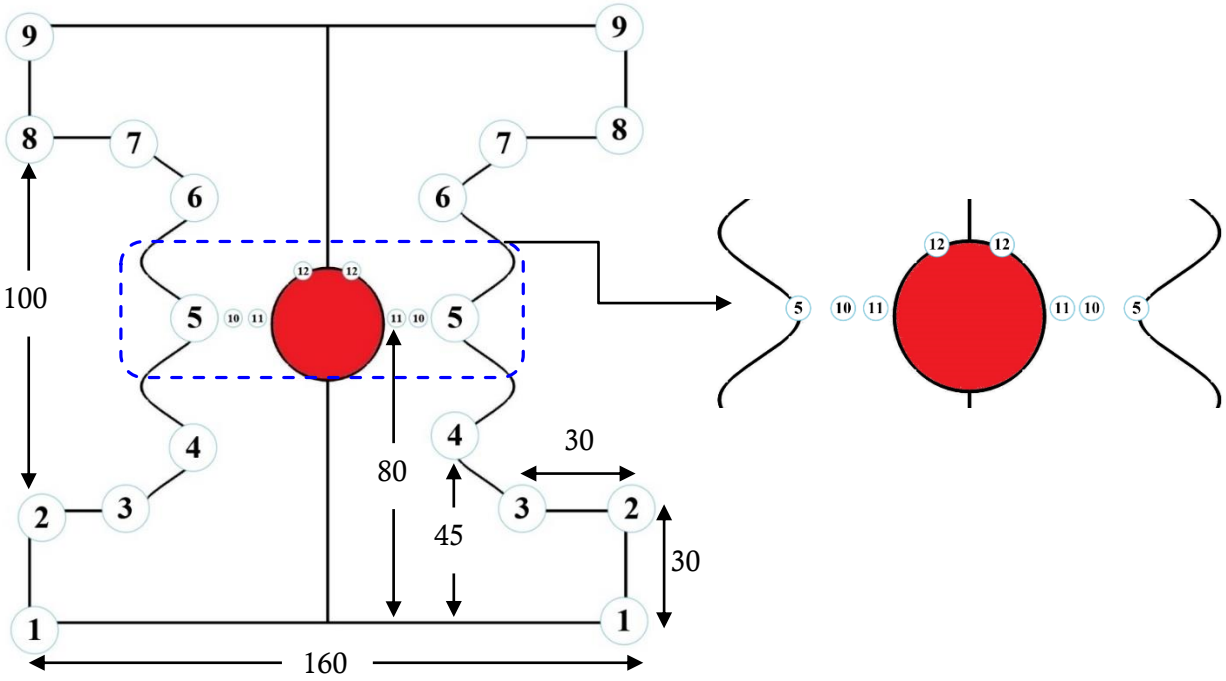

Figure (4. 9) schematic representation of the thermocouples position on the experimental prototype

Figure (4. 10) Temperature data logger

4.3. Porous media

It is commonly to define the porous media as a solid matrix contains empty spaces and filled with the fluid. In the present work, small glass ball of 11.28 mm diameter had been utilized as the porous matrix. The specifications of the porous media had been illustrated in full-details as below with the following points **[85]**:

- Porosity ε which is estimated based upon the formula inserted below;

$$\varepsilon = \frac{V_{void}}{V_{total}} \quad (4.1a)$$

$$\varepsilon = 0.3454 + 11.6985\, d_p \quad (4.1b)$$

The porosity is $\varepsilon = 0.47$ (4.2)

- Permeability had been calculated based upon Blake-Kozeny equation;

$$K = \frac{{d_p}^2 \varepsilon^3}{150(1-\varepsilon)^2} \quad (4.3)$$

The permeability was $K = 3.135 * 10^{-7} m^2$

- The effective thermal conductivity is depending on both of the thermal conductivity as well as the porosity of the nanofluid in addition to the solid porous matrix. It can be calculated as indicated below;

$$k_{eff} = (1-\varepsilon)\, k_s + \varepsilon\, k_{na} \quad (4.4)$$

- Effective diffusivity is depending based upon the effective thermal conductivity in addition to the thermophysical properties of the fluid as shown below;

$$\alpha_{eff} = \frac{K_{eff}}{(\rho C_p)_{nf}} \quad (4.5)$$

The thermophysical properties of some porous materials are tabulated in Table (4.2)

Table (4.2) Thermophysical properties of small glass ball as a porous media

Material Property	Value
ρ_s[kg/m^3]	2507
C_{ps}[J/kg. K]	670
k_s[W/m. K]	0.78

4.4. Nanofluid preparation

The nanofluids had been prepared within the laboratories of University of Babylon. Alumina nanoparticles (Al_2O_3) had been selected in the present work having a BT-9300Z particle size less than 45 nm and purity of provided by 99.99%. The selected nano-powder had been tested using x-ray diffractometer (XRD) and its size had been measured using particle size analyzer as indicated in Figure 4. 11 and 4. 12, respectively. Additionally, Scanning Electron Microscopy (SEM) TESCAN VEGA had been used to visualize the nanofluid as illustrated in Figure (4. 13).

Figure 4. 11 XRD diffractometer

Figure 4. 12 BT-9300Z particle size analyzer

Figure 4. 13 SEM

The structure of the nanofluid had been illustrated based upon SEM and it looks like as indicated in Figure (4. 14).

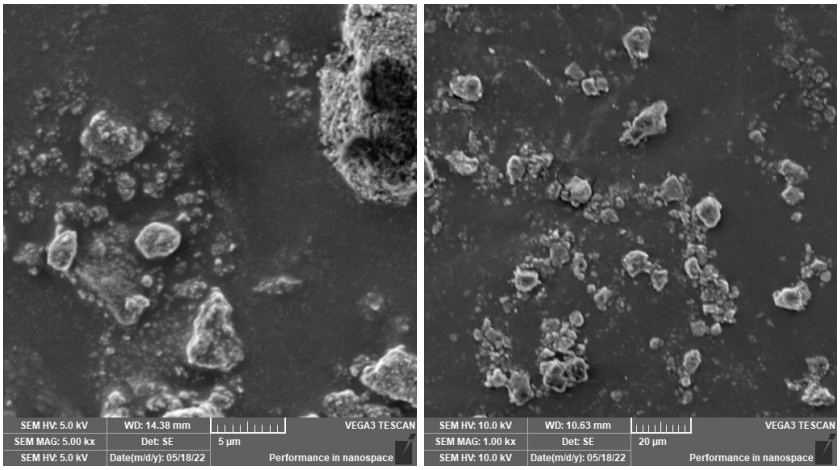

Figure (4. 14) SEM photograph of Al_2O_3

The experimental procedure of nanofluid preparation is summarized as indicated below;

1. The mass of base fluid and nanoparticle is measured using sensitive balance XPR106DUHQ as this one inserted below;

Figure (4. 15) XPR106DUHQ sensitive balance device

2. The measured nanoparticles of nanopowder had been dispersed in 1.5 liter of the base fluid which is the distilled water in order to get the required volume fraction of the nanofluids as tabulated in Table (4.3).

$$\phi = \frac{[m_{np}/\rho_{np}\,]}{[m_{np}/\rho_{np}\,]+[m_{bf}/\rho_{bf}\,]} \qquad (4.6)$$

Table (4.3) theoretical calculation of required nanofluid volume fraction

Concentration percent of Al_2O_3 nanoparticles	Mass of Al_2O_3 nanoparticles (g)
0.02	1.191238248
0.04	2.382953181
0.06	3.575145087

3. In the present work, the two-steps preparation method had been used as it enhanced technique for the preparation of metal or metal oxide nanofluid the steps of this method is indicated via Figure (4. 16). This method has the

advantage of reduced agglomeration. In order to get homogenous dispersed solution of nanopowder-water mixture, a mechanical stirrer GGT – 121 model had been used for one hour. This method had been used by [86].

4. After that, the resulted solution had been subjected to an ultrasonic wave's apparatus SJIA – 1200 W Model for at 30 minutes.
5. The obtained nanofluid had been fills up the enclosure in order to examine its role in heat transfer.

Photograph of mechanical stirrer along with ultrasonic device is inserted in Figure (4. 17) and Figure (4. 18), respectively.

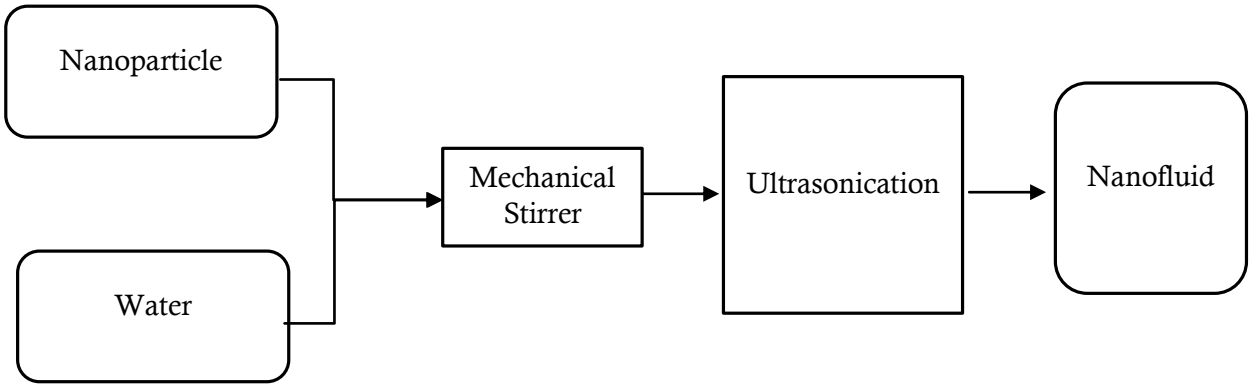

Figure (4. 16) Two-step method in nanofluid preparation

Figure (4. 17) Mechanical Stirrer device

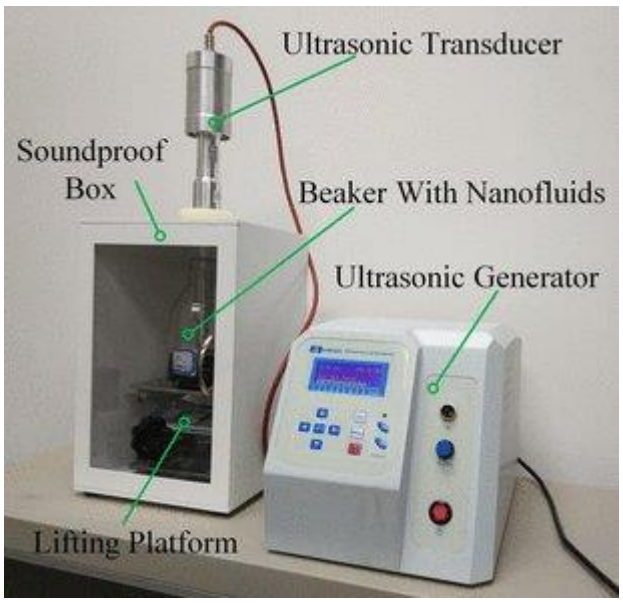

Figure (4. 18) Ultrasonic device SJIA – 1200 W Model

4.5. Measurement of the thermophysical properties

In the energy engineering problems related to the fluid flow and heat transfer, the nanofluids play an important role in bettering the thermal rate of heat transfer. In this section, the details regarding the measurment related to the base fluid (water) along with the nanofluid thermophysical properties such as (density, dynamics viscosity and the thermal conductivity) had been examined.

The thermophysical properties of the base fluid a proposed correlations for estimation the thermo-physical propeties based upon the based fluid temperture which had been used in the present work. These empirical correlations within a range of $(5 \leq T_w \leq 70)$ as below [87];

$$\rho_{bf} = 1000 * \left\{1 - \frac{(T_f - 4)^2}{119000 + 1365\,T_f - 4{T_f}^2}\right\} \quad (4.7)$$

$$k_{bf} = 0.56112 + 0.00193\,T_f - 2.60152749\,e^{-6\,{T_f}^2} - 6.08803\,e^{-8\,{T_f}^3} \quad (4.8)$$

$$\mu_{bf} = 0.00169 - 4.25263\,e^{-5\,T_f} + 4.9255\,e^{-7\,{T_f}^2} - 2.0993504\,e^{-9\,{T_f}^3} \quad (4.9)$$

The theoretical calculations reagaring the nanofluid thermophysical properties, following empirical correlations had been utilized [79];

$$\rho_{na} = (\phi)\rho_{sp} + (1-\phi)\rho_{bf} \quad (4.10)$$

Brinkman Model of dynamics viscosity had been implementated

$$\mu_{na} = \frac{\mu_{bf}}{(1-\phi)^{2.5}} \quad (4.11)$$

The thermal conductivity of the nanofluid had been predicted via Maxwell model

$$k_{na} = k_f \frac{(k_{sp}+2k_{bf})-2\phi(k_{bf}-k_{sp})}{(k_{sp}+2k_{bf})+\phi(k_{bf}-k_{sp})} \quad (4.12)$$

The theoretical calcualtions of the density, dynamics viscosity as well as the thermal conductivity under different nanofluid volume fraction is indicated in Table (4.4).

Table (4.4) nanofluid measurements based upon theoretical models

No	Nanofluid Concentration	Density	Dynamics viscosity	Thermal conductivity
1	0.00	997	0.001003	0.613
2	0.02	1056.46	0.001054959	0.648823843
3	0.04	1115.92	0.001111	0.686071
4	0.06	1175.38	0.001171	0.724828

Additionally, measurement instruments had been used in order to measure the thermophysical properties of nanofluid such as the density, viscosity and thermal conductivity had been measured within the laboratories of Material Engineering – University of Babylon, Iraq.

The density of nanofluid had been measured experimentally using Densitometer device as indicated in Figure (4. 19). On the other hand, commercial Brookfield DV-I prime viscometer had been used to measure the nanofluid dynamics viscosity which is shown in Figure (4. 20). The transient hot-wire technique had been used to experimentally measure the thermal conductivity of the nanofluids as demonstrated in Figure (4. 21).

Specifications of nanofluid thermophysical properties are illustrated in Table (4.5), (4.6) and (4.7)

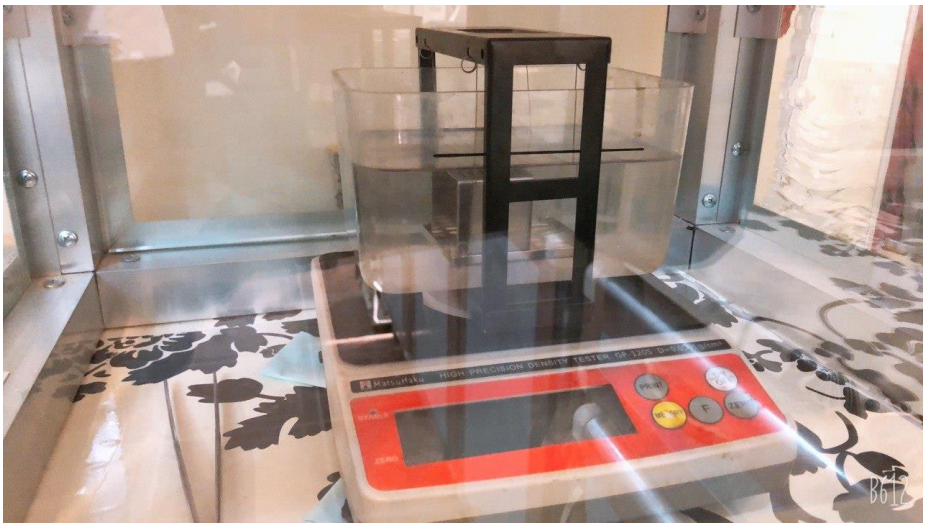

Figure 4. 19 densitometer device for measurment of nanofluid density

Figure 4. 20 Brookfield DV-I prime viscometer

Figure 4. 21 thermal conductivity device

Table (4.5) specification of Densitometer device

Measuring range	0-1200 - g
Accuracy	0.001
Power supply	220

Table (4.6) Specification of Brookfield DV-I prime viscometer

Speed	0-100 RPM
Operating Environment	0 – 40 ^{o}C
Analog Torque Output	0 - 1 Volt DC (0 - 100% Torque)

Table (4.7) specification of KD2 Pro

Accuracy	±5 to ±10%
Operating Environment of Sensors	-50 to 150°C
Compliance to Standards	IEEE Standard

4.6. Uncertainty Analysis

The error analysis in experimental measurements is important. So, the measured data by the temperature sensors for 10 experiments is presented in Table (4.8).

Table (4.8) repeatability analysis of the experimental measured data

Sensor ID	Iteration No. 1	Iteration No. 2	Iteration No. 3	Iteration No. 4	Iteration No. 5	Iteration No. 6	Iteration No. 7	Iteration No. 8	Iteration No. 9	Iteration No. 10
T1	28.6	28.9	28.3	28	28.2	28.7	28.8	28.4	28.5	28.8
T2	28.7	28.8	28.5	28.2	28.3	28.5	28.8	28.6	28.6	28.9
T3	29.3	29.4	29.5	29.2	29.6	29.4	29.3	29.9	30	29.6
T4	29.6	29.1	29.3	28.8	28.9	28.9	28.8	28.8	29.6	29.4
T5	30	30	30	30	30	30	30	30	30	30
T6	29.5	29.5	29.8	29.4	29.5	29.4	29.4	29.4	29.9	29.9
T7	29.9	29.6	29.7	29.2	29.3	29.2	29.2	29.2	29.9	29.7
T8	29.6	29.6	30	29.6	29.6	29.6	29.6	29.5	30.1	30.1
T9	29.8	29.2	29.7	29.4	29.4	29.3	29.2	29.2	29.6	29.7

Based upon these experimental data, the mean value ($\overline{X_m}$) can be estimated as indicated below [88];

$$\overline{X_m} = \frac{\sum_1^n x_i}{n} \tag{4.13}$$

Where, n is the readings and x_i represents the measured temperature

The standard deviation can be obtained from the equation inserted below;

$$\sigma = \sqrt{\frac{\sum_1^n (x_i - \overline{X_m})^2}{n-1}} \tag{4.14}$$

Thus, the standard error can be calculated as;

$$\sigma_m = \frac{\sigma}{\sqrt{n}} = \frac{\sqrt{\frac{\sum_1^n (x_i - \overline{X_m})^2}{n-1}}}{\sqrt{n}} \tag{4.15}$$

The uncertainty deviation may be obtained as follow;

$$X = \overline{X_m} + \sigma_m = \overline{X_m} + \frac{\sigma}{\sqrt{n}} \tag{4.16}$$

After applying the above-mentioned equations to the measured data listed in Table (4.8), the mean (average value, standard deviation and the standard error will be obtained as tabulated in Table (4.9).

Table (4.9) Uncertainty Analysis

Sensor ID	Average Value	Standard Deviation	Standard Error
T1	28.52	0.293636207	0.092856
T2	28.59	0.223358208	0.070632
T3	29.52	0.261618892	0.082731
T4	29.12	0.329309041	0.104137
T6	29.57	0.211081869	0.06675
T7	29.49	0.299814758	0.09481
T8	29.73	0.235937845	0.07461
T9	29.45	0.232139805	0.073409

4.7. Calibration

The thermocouples that installed within the novel-I-shaped-wavy-walled enclosure had been calibrated with thermometer. The temperature recorder named as [BTM-4208SD] had been used in order to be calibrated with the thermometer as shown in Figure (4.20) that related as a polynomial function as indicated below;

$$T_{Calibrated} = -0.0009\,T^2 + 1.0587\,T - 0.8863 \qquad R^2 = 0.9997$$

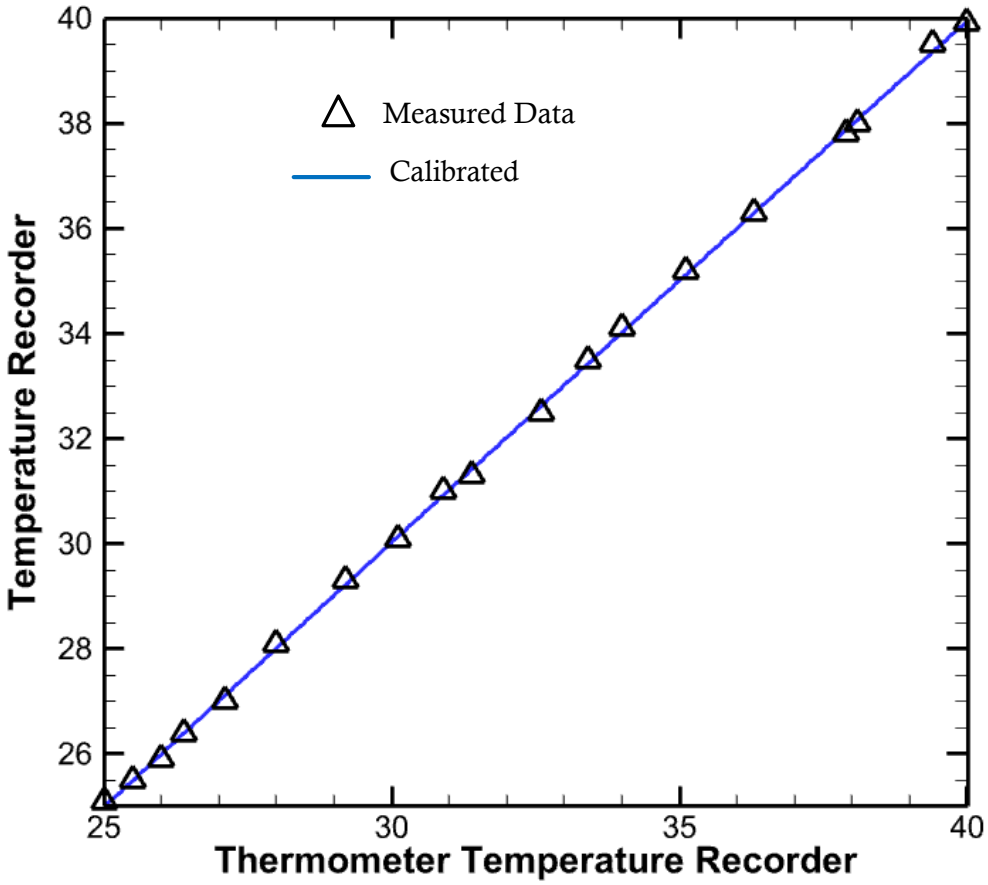

Figure 4. 22 Calibration curve

4.8. Design Consideration

This section illustrates the design consideration including the time schedule of the experimental model, Redundancy and Reliability Requirements, cost of the construction and the details of the calculations.

- One of the important consideration parameters is the magnetic field strength. As a starting point, the magnetic coils that the lines of the magnetic field pass through them is inserted in Figure (4.23).

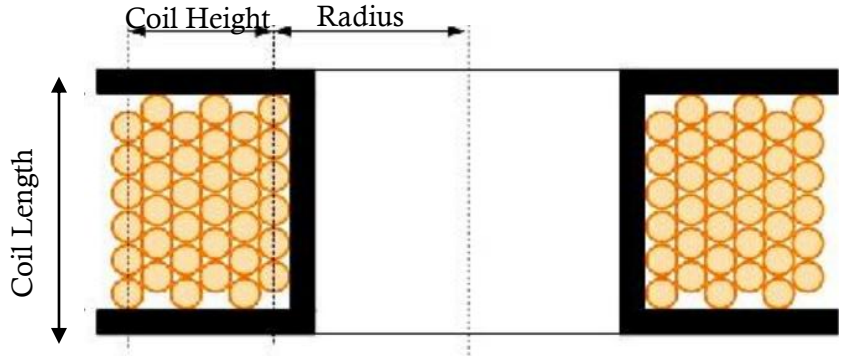

Figure 4. 23 Cross sectional view of the magnetic coil

The magnetic field produced by a current-carrying solenoid had been used in the experimental work. The selected solenoid is a long coil of wire (with 3500 turns. The magnetic field direction had been controlled due to the solenoid shape. One of the advantages of the magnetic field inside a solenoid is very uniform as well as it is strong. The direction of magnetic field had been given by Right-hand role as examined in Figure (4.24).

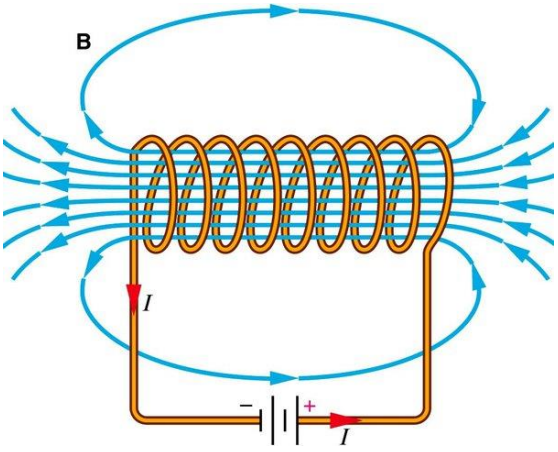

Figure 4. 24 schematic representation of the magnetic field direction

- On the other hand, the design of the I-shaped enclosure that made of Aluminum plate had been taken into consideration especially the heated plate of the right wall as it taken 2 hours for achieving the steady state conditions.
- For achieving cold temperature and uniform temperature distribution as much as possible in the back of the left wall with two inlet and outlet of the hot and cold water
- Four of the Thermocouples positioned on the mid of the enclosure to measure the temperature. This number is quite enough to understand the physical behavior considering the existence of the magnetic field.
- The total cost of the entire system is 3000 USD including the construction of the enclosure, heating unit, water – cooled chiller and the magnetic field unit in addition to the preparation of the nanofluid and its measurements.

Chapter Five
Results and Discussion

Chapter Five

Results and Discussion

5.1. Validation of the numerical results

The validation of the numerical CFD based results is an important work as it reveals the accuracy of the software. So numerous validations had been done with significant researchers in terms of streamlines, isotherms and Nusselt number in order to be sure that the results of fluid flows along with the obtained data of heat transfer can be considered in this study.

5.1.1. First Validation

This validation had been done with Al-Zamily and Amin [89] study about the natural convection within square enclosure utilizing finite element formulation. The enclosure is filled by two horizontal layers. The bottom layer consists of porous media saturated with nanofluid while the top layer is filled by the same nanofluid. The validation is presented in Figure (5.1) in terms of streamlines was made under $Ra = 10^4, Da = 0.1, Ha = 60$.

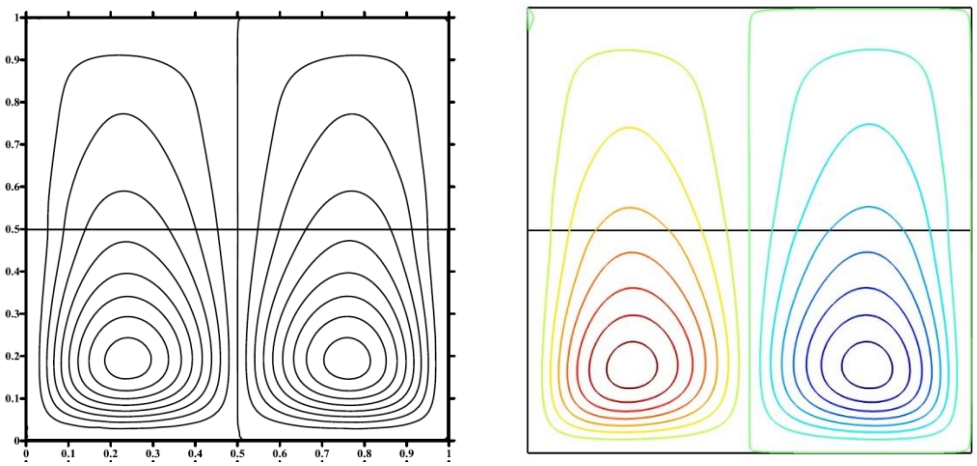

Al-Zamily and Amin [89] Present Work

Figure (5. 1) Validation in terms of streamlines of the present work CFD results with the numerical results obtained by Al-Zamily and Amin [89]

5.1.2. Second Validation

This validation had been done with Hussain and Rahomey [90] that studied numerically the natural convection within square enclosure considering the existence of inner heated cylinder. The gap had been filled by two vertical layers. The right layer is nanofluid layer while the left layer is filled by saturated porous media within the same nanofluid. The validation is presented via Figure (5.2) in terms of streamlines for various porous layer thickness at $Ra = 10^6, Da = 10^{-3}, \phi = 0.05$. The top streamlines contours are obtained by Hussain and Rahomey [90] while the bottom image are obtained based upon the present CFD code.

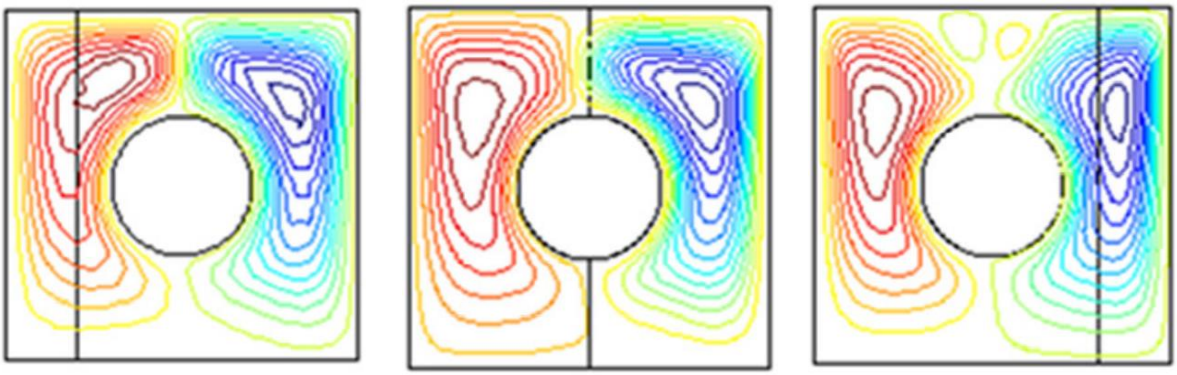

Hussain and Rahomey [90]

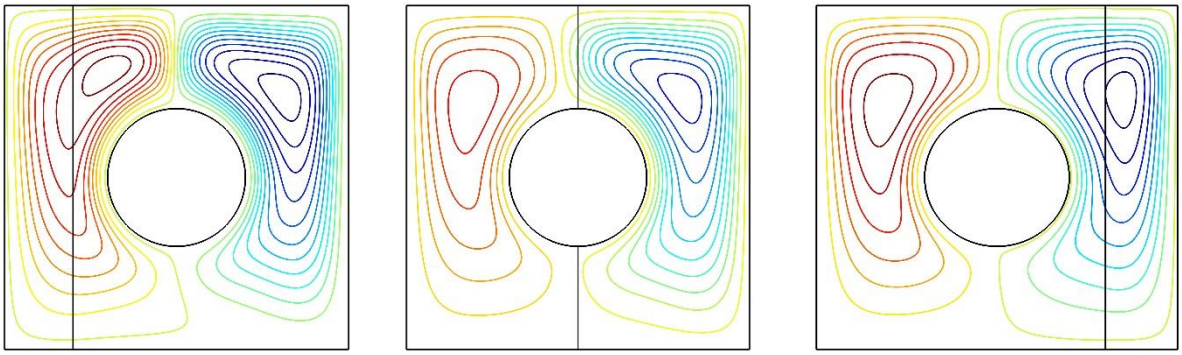

Present Work

Figure (5. 2) Validation in terms of streamlines of the present work CFD results with the numerical results obtained by Hussain and Rahomey [90]

5.1.3. Third Validation

This validation is done with the streamlines and isotherms of Malekpour et al. [91] that utilized a similar enclosure to the enclosure of the present selected shape filled by nanofluid considering the existence of the magnetic field as inserted in Figure (5.3).

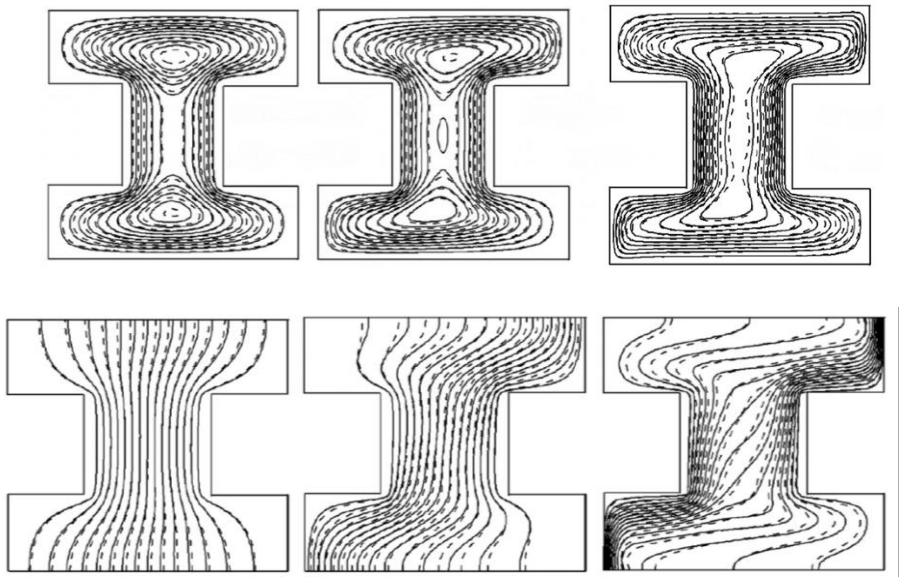

Malekpour et al. [91]

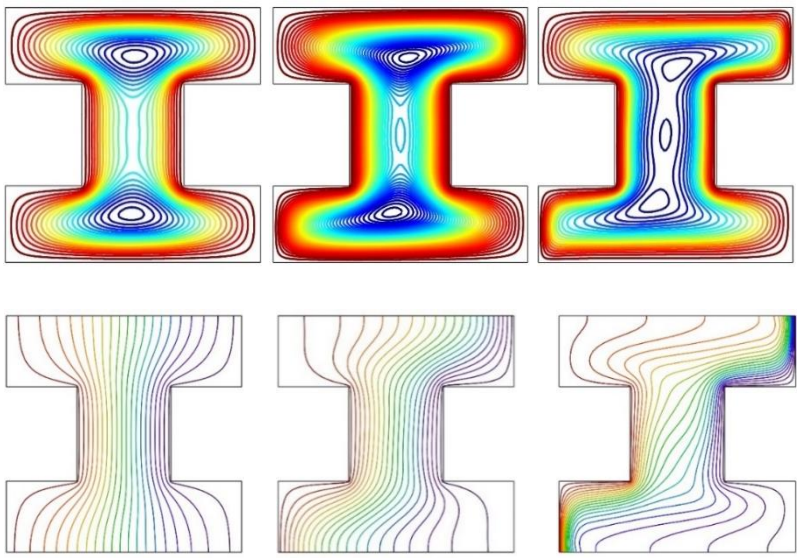

Present Work

Figure (5. 3) Validation in terms of streamlines and isotherms of the present work CFD results with the numerical results obtained by Malekpour et al. [91] at $Ha = 40, \gamma_{MHD} = 0\ , \phi = 0.04$

5.1.4. Fourth Validation

This section illustrates the validation with Ma et al. [92] that studied numerically the natural convection within I-shaped enclosure with multi-inner hot and cold bodies along with magnetic field. The space had been filled by nanofluid using Lattice – Boltzmann method for simulating the problems. The results had been demonstrated as inserted below in Figure (5.4) in terms of streamlines when $Ra = 10^6, \phi = 0.02, Ha = 0$.

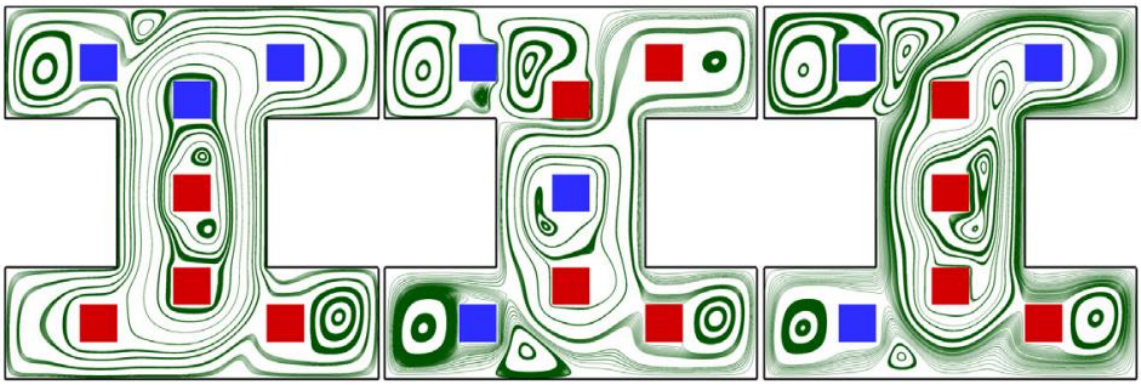

Ma et al. [92]

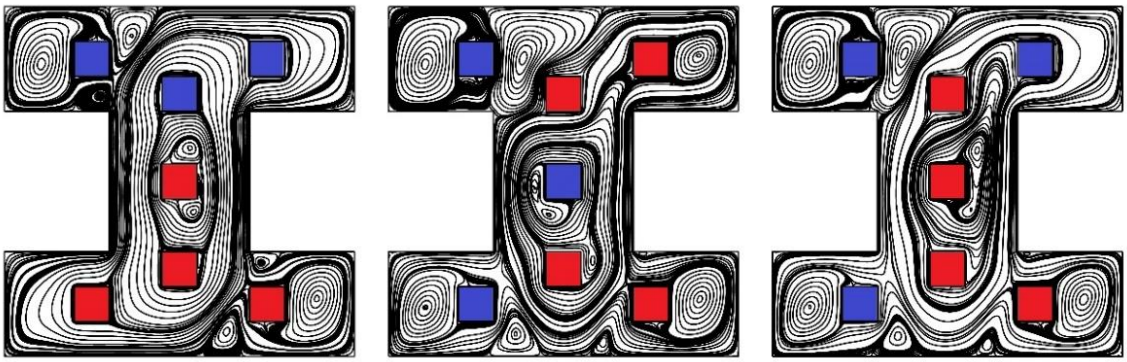

Present Work

Figure (5. 4) Validation in terms of streamlines of the present work CFD results with the numerical results obtained by Ma et al. [92] at $Ra = 10^6, \phi = 0.02, Ha = 0$

The validation in terms of Nusselt number had been presented in Figure (5.5) versus different dimensionless values of Rayleigh numbers. It can be seen that there is an excellence agreement in terms of Nusselt number, too. This validation of I-shaped enclosure is important as in related and similar to the proposed novel enclosure of this study.

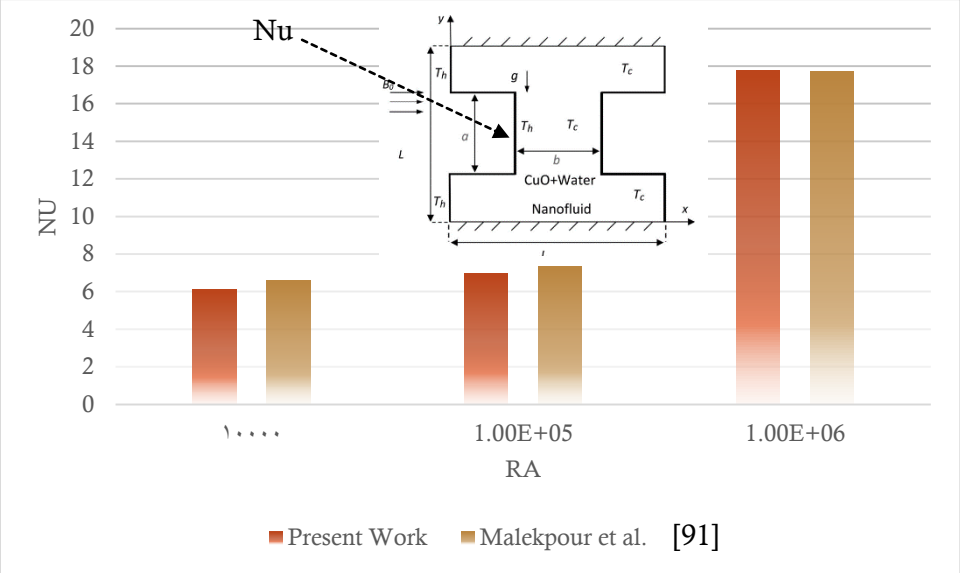

Figure (5. 5) Validation of the present work with Malekpour et al. [91] in terms of Nusselt number at $\varphi = 0.04, Ha = 80$

Finally, additional validation in term of Nusselt number with significant researchers as shown in Figure (5.6) like (Khanafer et al. [93] , Fusegi et al. [94] , Davis et al. [95] , Barakos et al. [96]) under wide range of Rayleigh numbers.

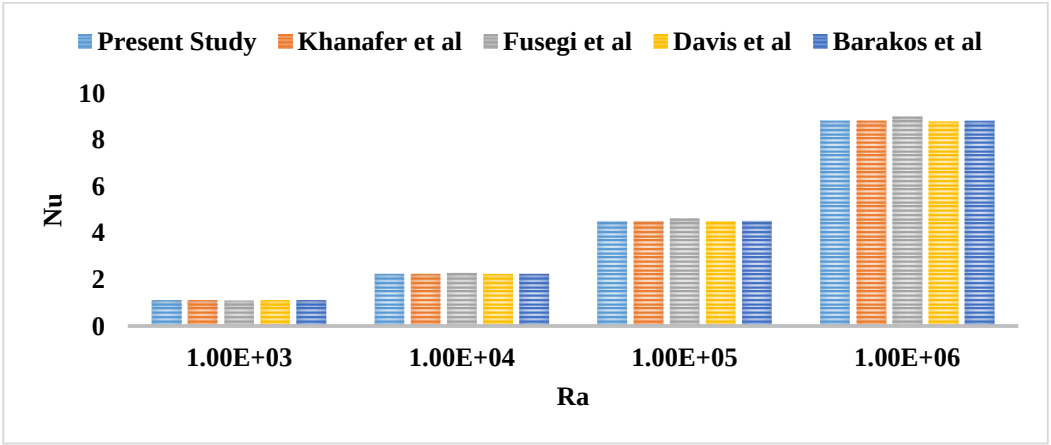

Figure (5. 6) Validation with significant researchers in terms of Nusselt number

5.2. Numerical CFD Results

5.2.1. MHD Thermogravitional within Novel Enclosure

This paragraph illustrates the influence of various selected dimensionless parameters such as Rayleigh numbers, Darcy numbers, Hartmann numbers, magnetohydrodynamic inclination angle, porous layer thickness and undulation number. It is done for description of fluid dynamics characteristics and heat transfer rate properties for three different cases of heat source location in terms of streamlines, isotherms and mean Nusselt number.

5.2.1.1. The influence of Rayleigh number

First of all, the influence of Rayleigh number on the fluid flow in terms of streamlines and isotherms contours had been presented in Figures (5.7, 5.8 and 5.9), respectively for three cases at $Da = 0.001,\ Ha = 0,\ \gamma = 45,\ \phi = 0.02$. Its noted that for the three selected cases, the increase in Rayleigh number leads to an increase in the strength of the fluid flow as shown in Figures (5.7 and 5.8), which is evident in the dimensionless value of the maximum stream function. However, the location of the heated source influences and contributes strongly to the strengthening of the fluid flow. For example, at a low Rayleigh number ($Ra = 10^4$), the influence of the inner body has a negligible impact on the strength of the fluid flow. Indeed, it noted that for case 1 in which the inner body is closed at the bottom wall, the maximum stream function is $|\Psi_{max}| = 0.87320$ while this value does not change so much when the inner body moves upwards and closes at the top of the enclosure (case 3) in which the maximum stream function $|\Psi_{max}| = 0.8373$ which is approximately for case 1. However, it decreases a slightly for case 2 that had the maximum stream function $|\Psi_{max}| = 0.6327$. The physical reason for this situation is that in case 1, the internal hot body at the bottom of the enclosure will exchange heat transfer with the wavy wall enclosure and the shape of the circular body with the internal wavy wall will be similar to that of the nozzle. The same happens when the inner body is located at the top of the enclosure (case 3). In case 2, it can be seen that the space between the inner

body and the wavy wall will break the inner cell into two inner cells, reducing the flow strength of the fluid. As the Rayleigh number increases ($Ra = 10^5$), the fluid flow strength increases for all cases because the convection heat transfer mode will be the dominant mode. As can be seen, $|\Psi_{max}| = 0.87320$ at ($Ra = 10^3$) while it increase to $|\Psi_{max}| = 5.1330$ at ($Ra = 10^5$). At the high value of the Rayleigh number ($Ra = 10^6$), the influence of the heated body will be clearer. For example, case 2 has the highest fluid flow strength followed by case 1 while case 3 has the lowest fluid flow strength. For example, $|\Psi_{max}| = 23.890, 21.350, 11.593$ for case 2, case 1, case 3, respectively. The physical reason for higher strength for case 2 is because of there is no higher number in breaking of the vortices as recorded for case 1 especially at higher Rayleigh number. Generally, the geometry undulations and the position of the heater have major role in the fluid flow strength.

The contours of the isotherms are shown in Figure (5.9). It's noted that the increase in Rayleigh number and the location of the internal hot body have a large impact on the spatial isothermal patterns. It can be noted that at low Rayleigh numbers, the isotherms do not cover the entire space and their shape is controlled by the thermal conditions of the undulated cold wall of the enclosure and the adjacent cold body. This is due to the fact that conduction heat transfer is dominant at low Rayleigh numbers. As the Rayleigh number increases, so does the flow strength of the fluid and this increase is due to the increased collision between the particles of the nanofluid/porous media molecules which leads and reflects to the increase of the internal thermal energy of the fluids. So, this will overcome the effect of the cold wavy walls and other cold bodies which resist the penetration of the hot fluid from the hot body due to the buoyancy force.

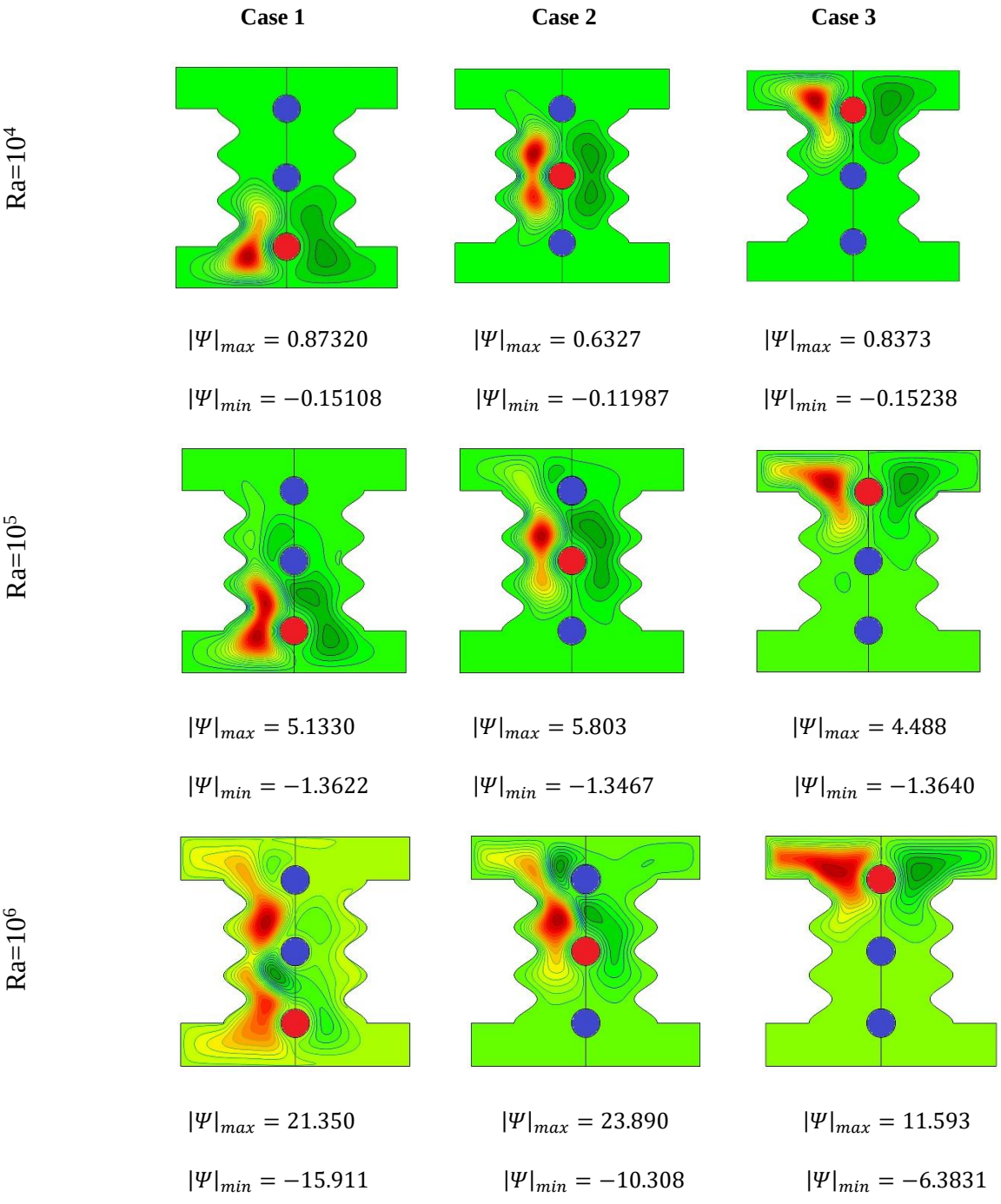

Figure (5. 7) Streamlines under distinct values of Rayleigh number at $Da = 0.001, Ha = 0, \gamma = 45, \phi = 0.02$

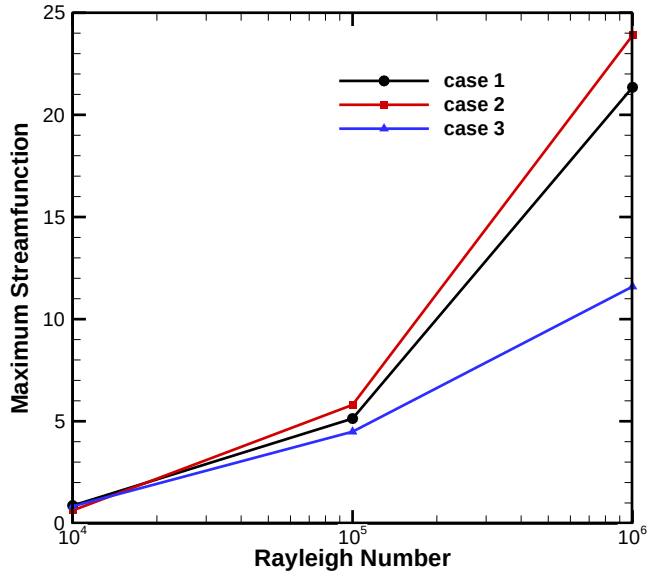

Figure (5. 8) The fluid flow strength in terms of maximum streamfunction with Rayleigh number for three thermal selected cases of inner hot body location

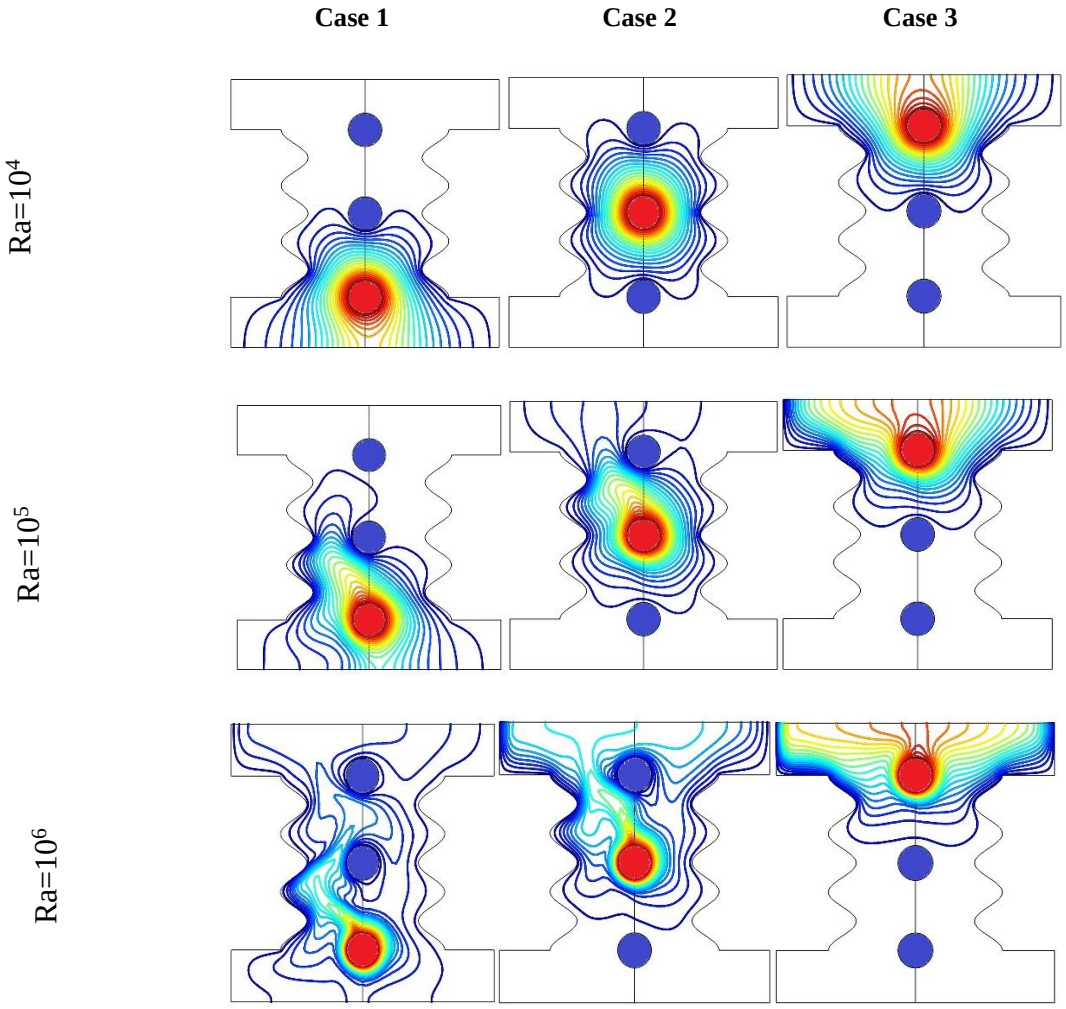

Figure (5. 9) Isotherms under distinct values of Rayleigh number at $Da = 0.001, Ha = 0, \gamma = 45, \phi = 0.02$

5.2.1.2. The influence of Hartmann number

The influence of Hartmann number on the fluid flow in terms of streamlines and isotherms contours had been presented in Figures (5.10, 5.11 and 5.12), respectively for three cases at ($Da = 0.001, Ra = 10^6, \gamma = 45, \phi = 0.02$). From the first point of view of Figures (5.10 and 5.11), which reveal the streamlines contours, it can be deduced that the increase in the Hartmann number reduces the maximum stream function by reducing the fluid flow strength for the three cases because it may be noted that $|\Psi_{max}| = 21.350$, $|\Psi_{max}| = 23.890$, $|\Psi_{max}| = 11.593$ at $Ha = 0$ while it reduces to $|\Psi_{max}| = 13.370$, $|\Psi_{max}| = 11.317$, $|\Psi_{max}| = 5.0900$ at $Ha = 60$ for cases 1, 2 and 3, respectively. It should be mentioned that the position of the internally heated body is strongly affected by the strength of the fluid flow as well as the Hartmann number. For example, it can be seen that case 3 had the lowest fluid flow strength. The reason is due to the position of the inner heater at the top of the enclosure and it can't cover all of the enclosure space. The other cases, i.e., cases 1 and 2, show an interesting behavior of the fluid flow strength and the Hartmann number. This behavior illustrates the fact that there is a critical value of the Hartmann number which is $Ha = 26$ and that the influence of the inner body on the fluid flow strength is completely reversed. For example, when the value of the Hartmann number is lower than the critical value, it may be noted that the fluid flow strength for case 2 is better than that of case 1. As the Hartmann number value increases and becomes higher than its critical value, case 1 gives a better fluid flow strength than case 2.

The influence of Hartmann number on isotherms contours is shown in Figure (5.12). It can be seen that in case 1, when the Hartmann number is below its critical value, the red isotherms lines are distributed on the left layer which contains only the nanofluid layer. Whereas when the Hartmann number increases above its critical value, the red isothermal lines are distributed and change direction in the right layer that contains a porous media saturated with the same nanofluid. This is due to increasing the conduction heat transfer with increasing of Hartmann number and since there is porous media in the right layer that it

absorb the heat emitted from the heater so that more heat flow towards the right layer. It can be seen that in case 1, the isothermal lines cover most of the area of the enclosure between the inner bodies and the enclosure. A similar behavior is observed for case 2, but the distribution of isotherms does not cover the whole area. Whereas in case 3, the distribution of isothermal lines over the space between the bodies and the enclosure wall is the lowest.

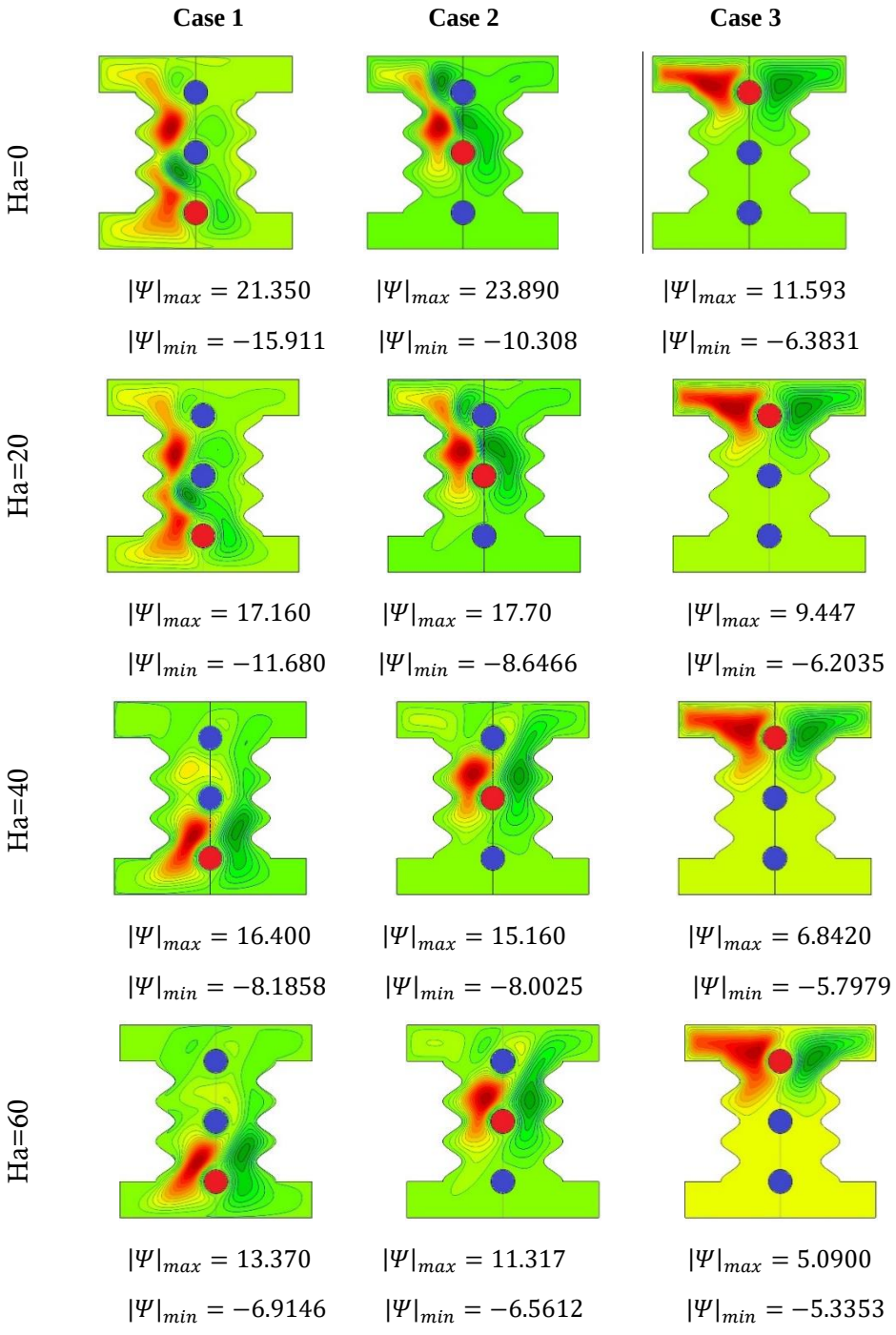

Figure (5. 10) Streamlines under distinct values of Hartmann number at $Da = 0.001, Ra = 10^6, \gamma = 45, \phi = 0.02, N = 3$

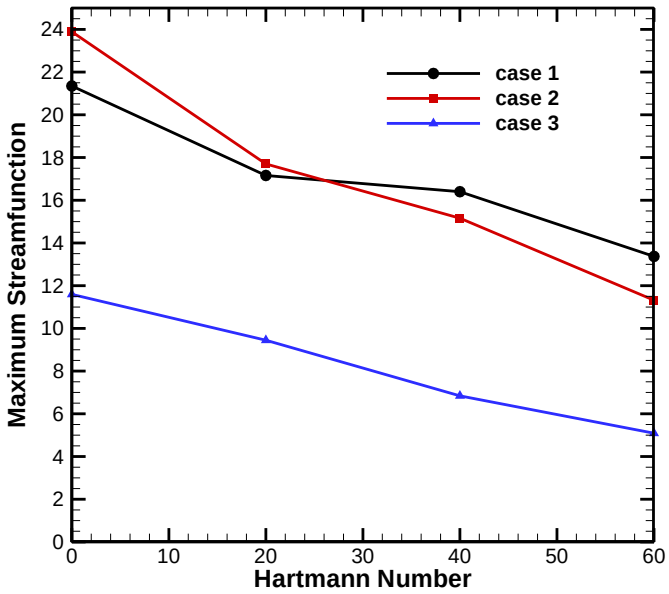

Figure (5. 11) The fluid flow strength in terms of maximum stream function with Hartmann number for three thermal selected cases of inner hot body location

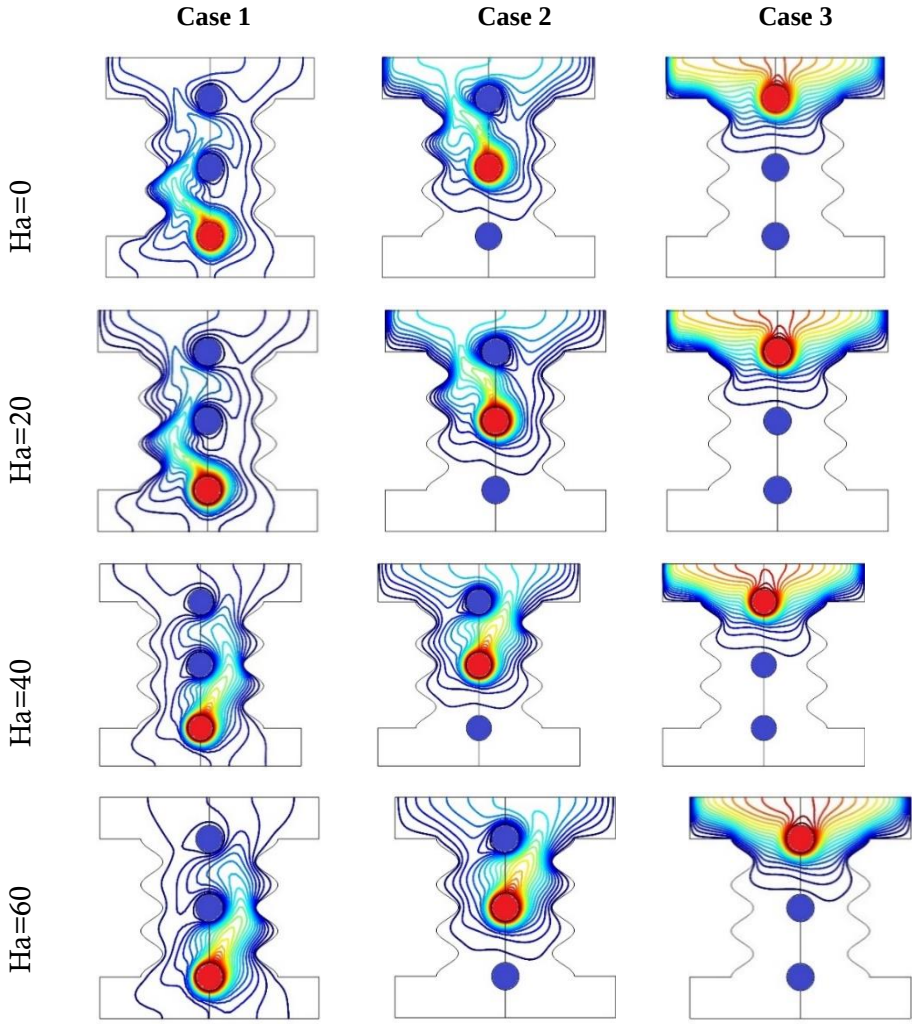

Figure (5. 12) Isotherms under distinct values of Hartmann number at $Da = 0.001, Ra = 10^6, \gamma = 45, \phi = 0.02$

5.2.1.3. The influence of Darcy number

The influence of the Darcy number on the fluid flow in terms of streamlines and isotherms contours was presented in Figures (5.13, 5.14 and 5.15), respectively for three cases at $Ha = 60, Ra = 10^6, \gamma = 45, \phi = 0.04$. It can be seen that increasing the Darcy number leads to an obvious increase in the fluid flow strength by increasing the minimum stream function for all of the three selected cases as shown in Figures (5.13 and 5.14). For example, increasing the Darcy number by $Da = 1e-5$ to $Da = 1e-1$, with the absolute minimum stream function increasing by $|\Psi_{min}| = 0.2890$, $|\Psi_{min}| = 0.91572$, $|\Psi_{min}| = 0.26785$ into $|\Psi_{min}| = 9.5445, |\Psi_{min}| = 8.4630, |\Psi_{min}| = 6.8424$ for case 1, 2 and 3, respectively. At the low value of Darcy number $Da = 1e-5$, where conduction heat transfer is dominated, there is not much influence of the location of the inner body on the improving of the fluid flow strength. While at the high dimensionless value of the Darcy number ($Da = 1e-1$), it can be seen that case 1 reveals the best case of improvement of the fluid flow strength followed by case 2 while the case 3 is the lowest case of improvement of the fluid flow strength.

Regarding the contours of the isotherms, as shown in Figure (5.15), it can be seen that at the low value of Darcy number $Da = 1e-1$, the distribution of isotherms does not cover and fills the entire area of the enclosure. It can be seen that there is not much change for case 3 at the low and high value of the Darcy number while the contribution of the Darcy number is very large for case 1 as shown by the fact that the increase of its value at $Da = 1e-1$, leads to the isothermal lines filling most of the surface of the enclosure. However, for case 2, it covers the area of the enclosure from the inner body in the middle of the enclosure.

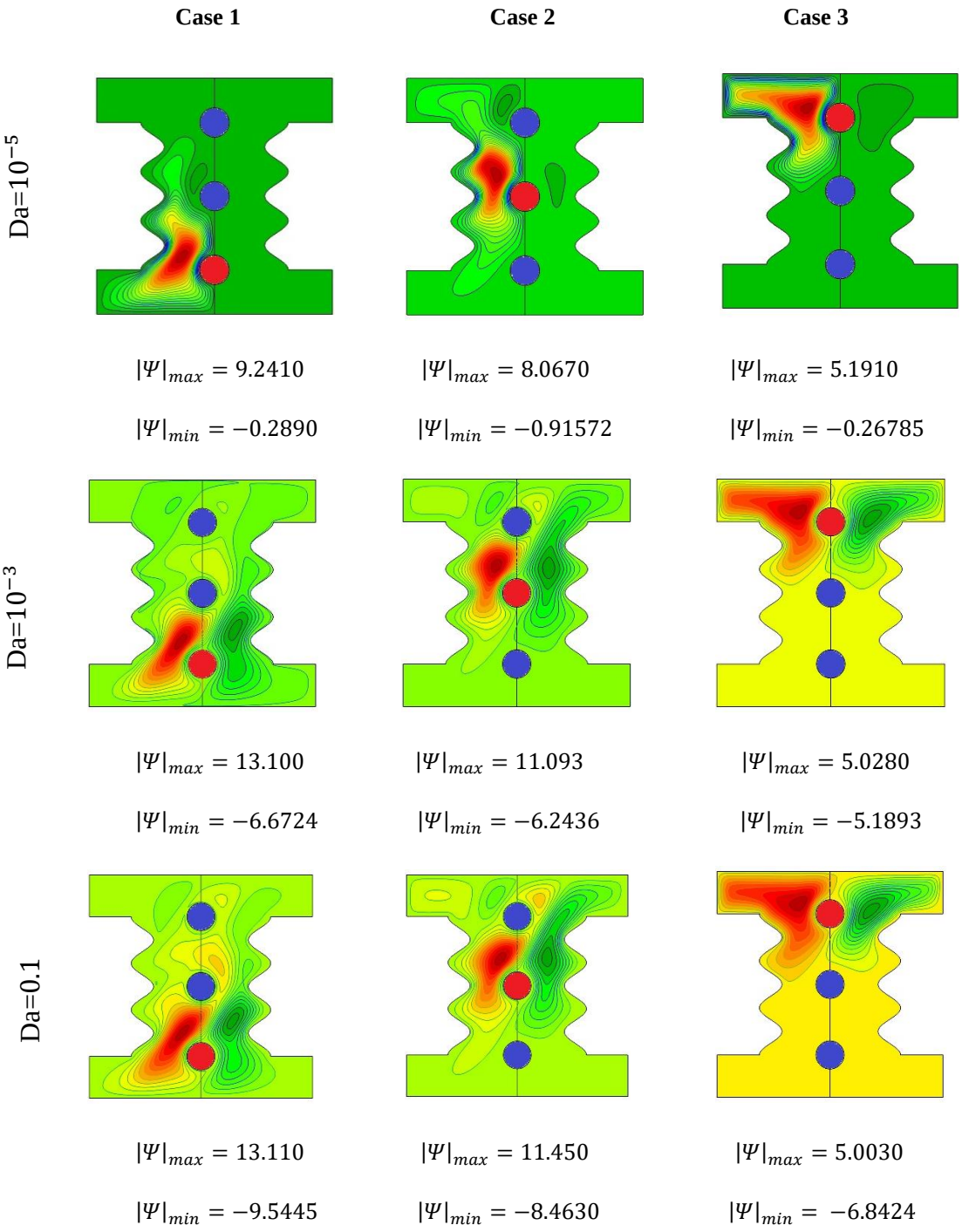

Figure (5. 13) Streamlines under distinct values of Darcy number at $Ha = 60, Ra = 10^6, \gamma = 45, \phi = 0.04$

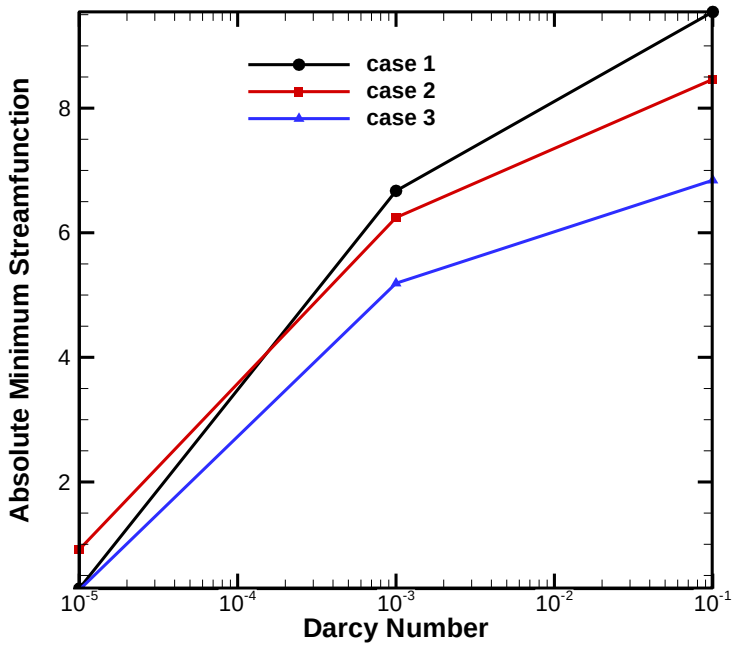

Figure (5. 14) The fluid flow strength in terms of minimum stream function with Darcy number for three thermal selected cases of inner hot body location

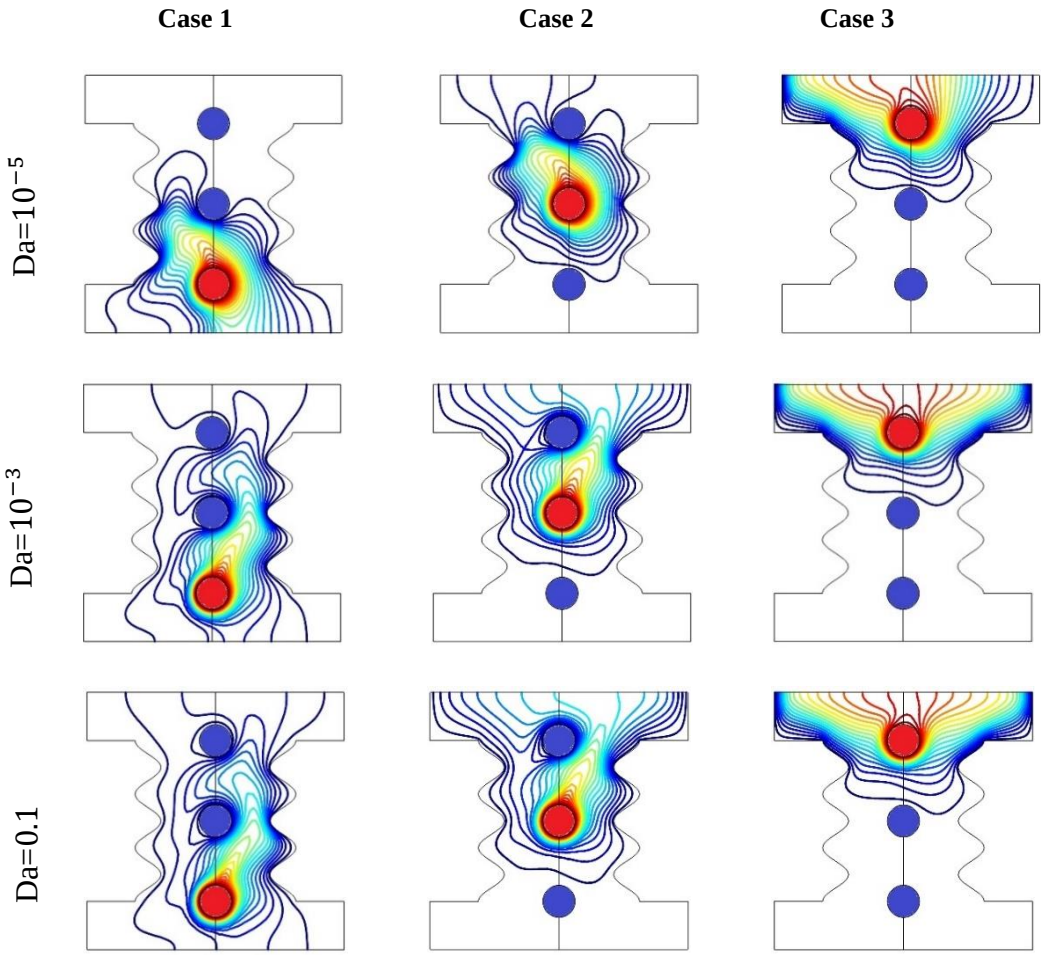

Figure (5. 15) Isotherms under distinct values of Darcy number at $Ha = 60, Ra = 10^6, \gamma = 45, \phi = 0.04, N = 3$

5.2.1.4. The influence of MHD Inclination angle

The influence of the MHD inclination angle on the fluid flow in terms of streamlines and isotherms contours had been presented in Figures (5.16, 5.17 and 5.18), respectively for three cases at $\mathrm{Ha} = 60,\ \mathrm{Ra} = 10^6,\ \mathrm{Da} = 0.1,\ \phi = 0.04$. With respect to the streamlines contours, it can be seen that the location of the inner body again plays an important role in the fluid flow strength. For example, from the first point of view on Figures (5.16, 5.17), it can be noted that for case 3, the increase of the MHD inclination angle leads to a reduction of the stream function which, in turn, reduces the strength of the fluid flow. For example, the maximum stream function decreases by $|\Psi_{max}| = 6.8910, 5.0030$ when the inclination angle increases by $\gamma = 0, 45$, respectively. However, when the inclination angle of MHD is $\gamma = 0$, there is a slight increase in the fluid flow strength for case 3 which is a little better than case 2 while case 1 was the lowest case in the increase of fluid flow strength. For example, $|\Psi_{max}| = 5.532,\ 6.564,\ 6.891$ for cases 1, 2 and 3, respectively. On the other hand, by increasing the angle of inclination in $\gamma = 45$, the influence of angle of inclination becomes more noticeable as case 1 will have the highest stream function followed by case 2 and case 3 was the lowest case. For example, $|\Psi_{max}| = 13.110, 11.450\ and\ 5.0030$ for case 1, 2 and 3, respectively. When the inclination angle increases up to $\gamma = 90$, the influence on the fluid flow strength is not taken into account for case 3. On the other hand, the stream function improves slightly for case 2, while the fluid flow strength improves again clearly and significantly for case 1. The reason behind increasing the fluid flow strength of case 1 and case 2 is that applying the magnetic field in the horizontal direction $\gamma = 0$, the magnetic field is normal to the natural convection current while as it starts to tilted till reaching the normal direction, it would be in same direction as the hot fluid rises up. However, regarding case 3, the heater is located in the top region and the corrugated (wavy) walls contribute in the fluid flow strength.

With respect to Figure (5.18), which illustrates the contours of the isotherms, it can be seen that the angle of inclination of the MHD has an important

effect on the lines of the isotherms. For example, increasing the MHD angle for case 1, leads the isotherms cover the area inside the enclosure. It can be seen that for case 1, when the γ = 0, the hot red line of the isotherms goes into the left layer, then penetrates into the right layer at γ = 45, and finally moves into the left layer at γ = 90. The same distribution of isotherms is observed for case 2, but it did not cover the lower area of the enclosure. In case 3, the coverage of the enclosure by the isothermal distribution lines is the lowest.

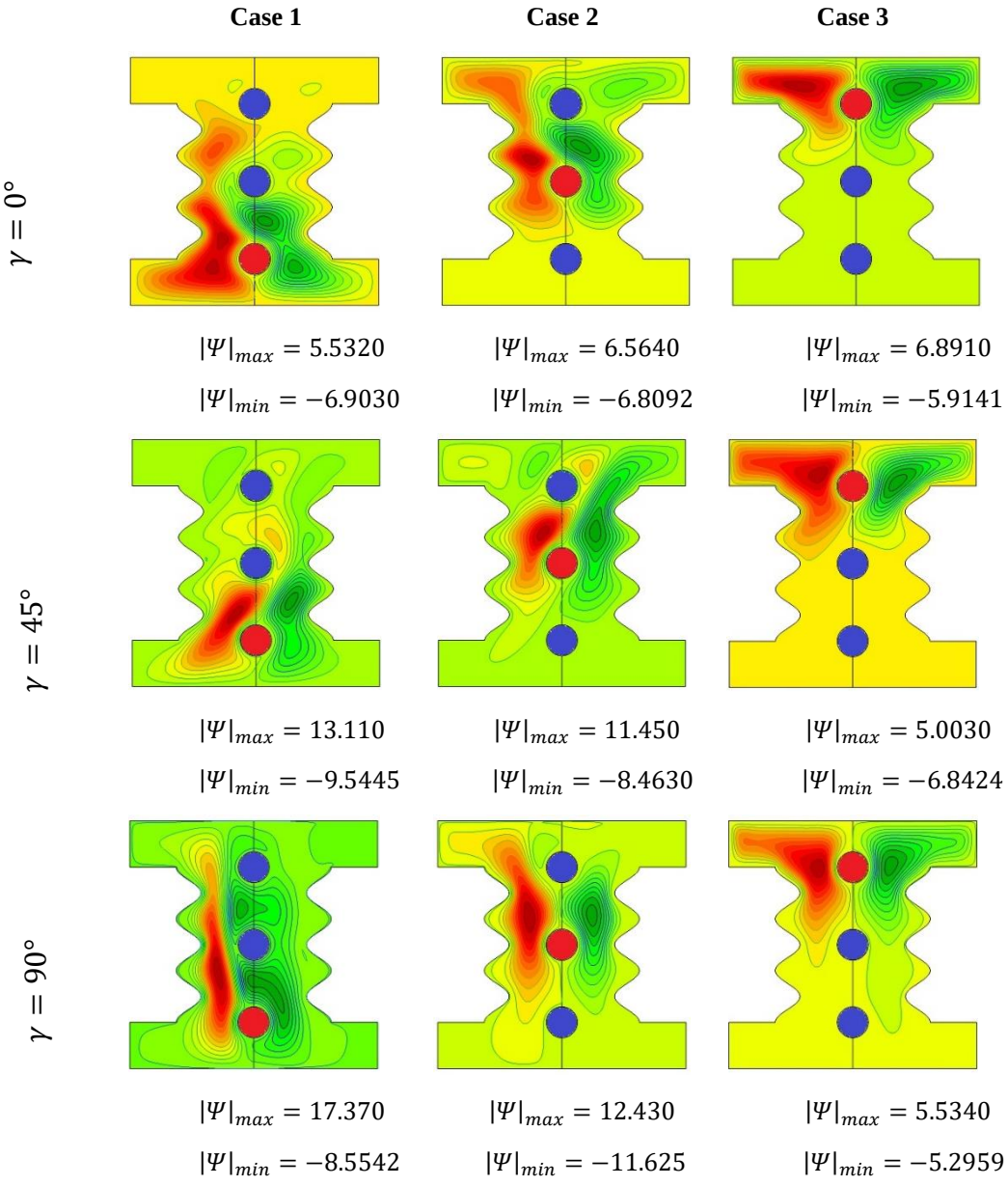

Figure (5. 16) Streamlines under distinct values of Magnetic field angle at $Ha = 60, Ra = 10^6, Da = 0.1, \phi = 0.04, N = 3$

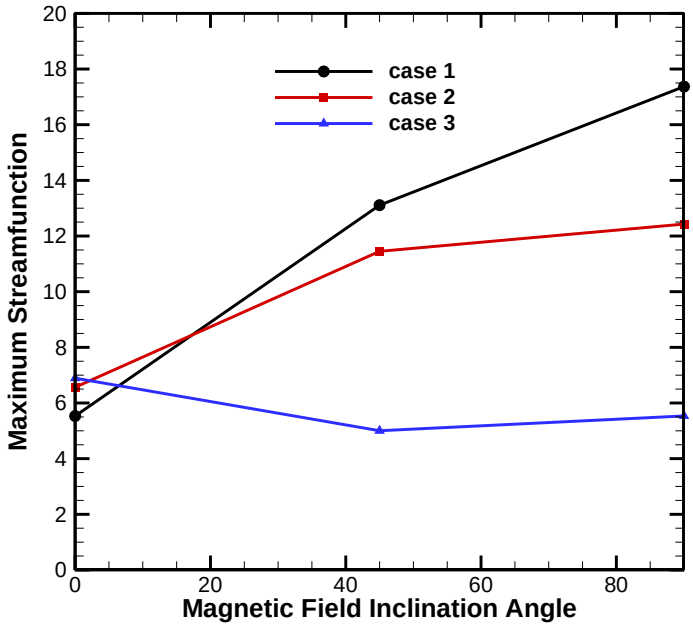

Figure (5. 17) The fluid flow strength in terms of maximum stream function with MHD inclination angle for three thermal selected cases of inner hot body location

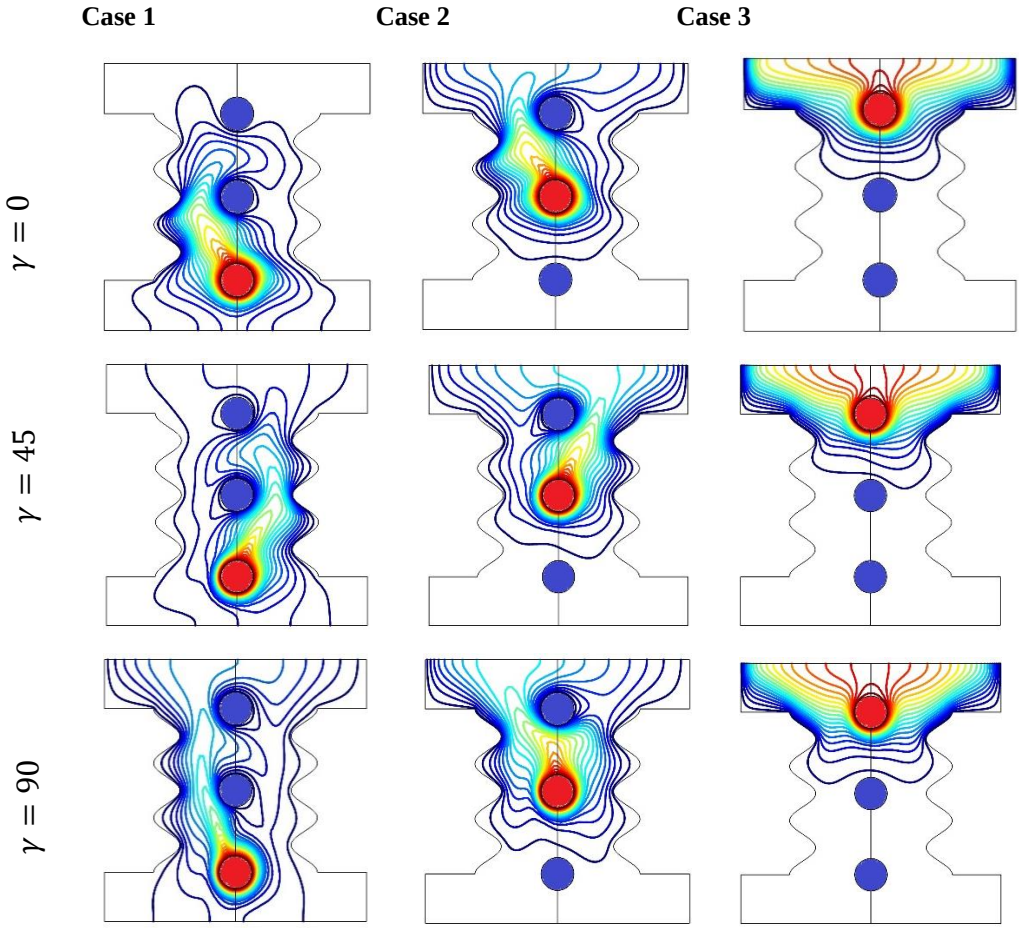

Figure (5. 18) Isotherms under distinct values of Magnetic field angle at $Ha = 60, Ra = 10^6, Da = 0.1, \phi = 0.04$

5.2.1.5. Number of undulations

The influence of the number of undulations on the fluid flow in terms of streamlines and isotherms contours had been presented in Figures (5.19, 5.20 and 5.21), respectively for three cases at $Ha = 40, Ra = 10^6, Da = 0.001, \phi = 0.04$. According to the first observation in Figures (5.19, 5.20), for case 3 in which the internal hot body is at the top of the enclosure, the influence of the increase in the number of undulations is ignored. When the number of undulations is N=1, case 1 reveals a better stream function which leads to a better strength of the fluid flow, followed by case 2, while case 3 is the lowest case. For example, maximum stream function is $|\Psi_{max}| = 18.340, 13.870\ and\ 6.8350$ for cases 1, 2 and 3, respectively. This is due to the position of the heater as when it located at the bottom, more heat emitted reflecting on more impact on the molecular basis occurred and this leading to highest fluid flow strength. When the number of undulations increases from $N = 1$ into $N = 2$, the maximum stream function for case 1 decreases from $|\Psi_{max}| = 18.340$ into $|\Psi_{max}| = 10.402$, respectively. In case 2, it goes from $|\Psi_{max}| = 13.871$ to $|\Psi_{max}| = 15.660$ when the number of undulations goes from $N = 1$ to $N = 2$. It should be mentioned here, for case 2, that the number of undulations is a critical number as it was obtained on the basis of numerical simulation according to which the influence of the increase of the number of undulations beyond this number is ignored. Similarly, for case 1, stream function still decreases when the number of undulation increases until it reaches $N = 5$, where the stream function closes at the value of case 2. As general conclusion, the position of the heated body and the number of undulations are the responsible for increasing/decreasing the fluid flow strength as the two vortices are located at the top region.

With respect to the Figure (5.21), which shows the isotherms lines for various numbers of undulations. Here again, the isotherms line does not cover the whole area of the enclosure for case 3. It is also worth mentioning that for case 1, the isothermal lines fill the largest part of the enclosure, whereas if the number of undulations increase beyond this, it increases the surface area of the wavy walls

that absorb part of the internal energy of the fluid by conduction, which limits the isothermal lines to the closed area, in particular the isothermal lines cannot reach and fill the upper area of the enclosure. In case 2, the isothermal lines do not cover the lower zone.

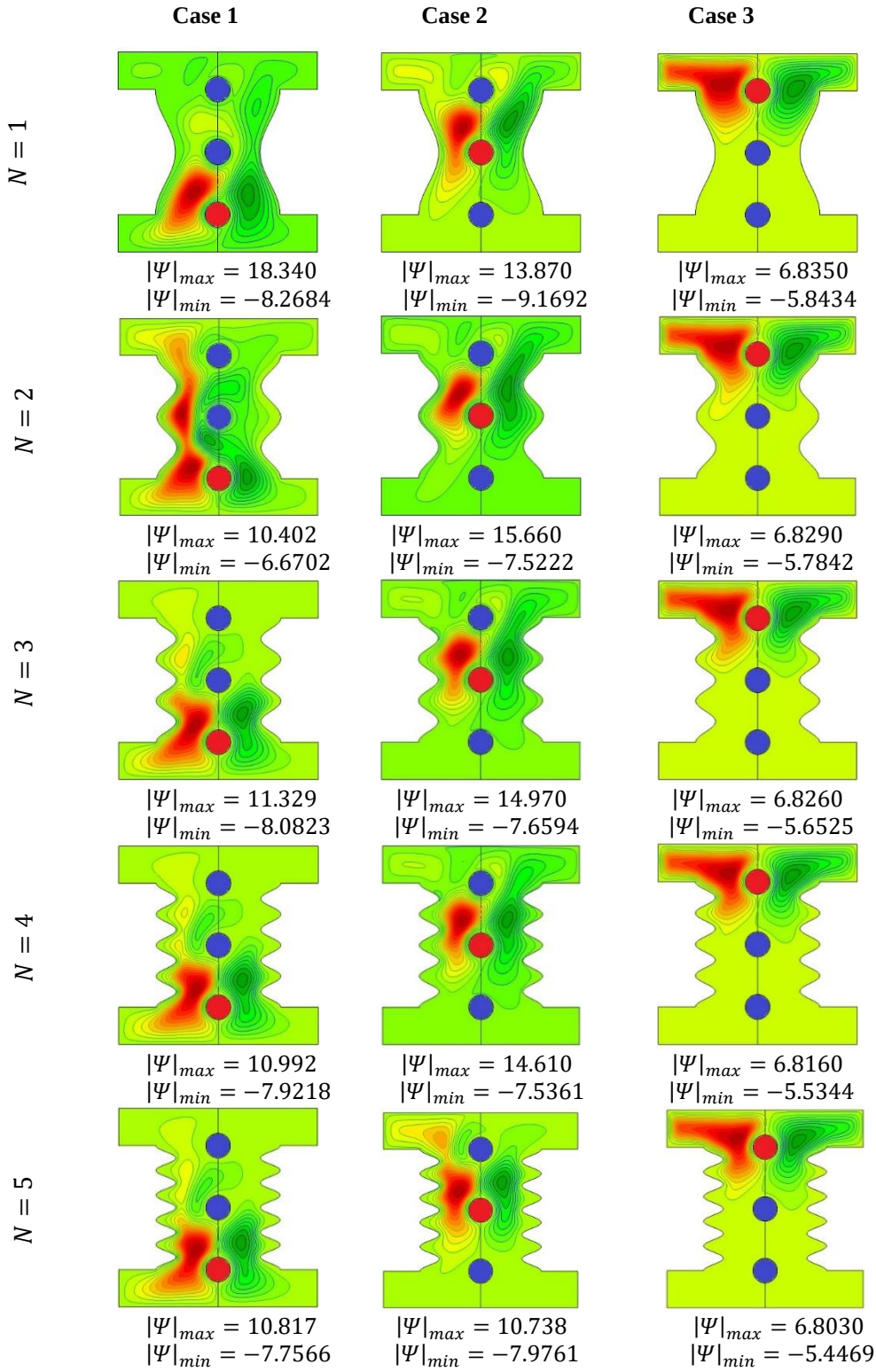

Figure (5. 19) Streamlines under distinct values of number of undulations at $Ha = 40, Ra = 10^6, Da = 0.001, \phi = 0.04, \gamma = 45$

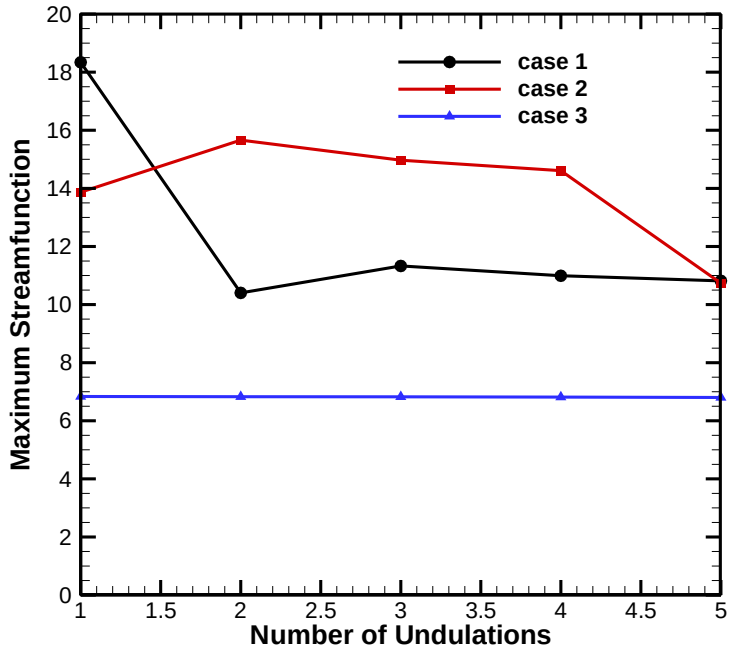

Figure (5. 20) The fluid flow strength in terms of maximum stream function with number of undulations for three thermal selected cases of inner hot body location

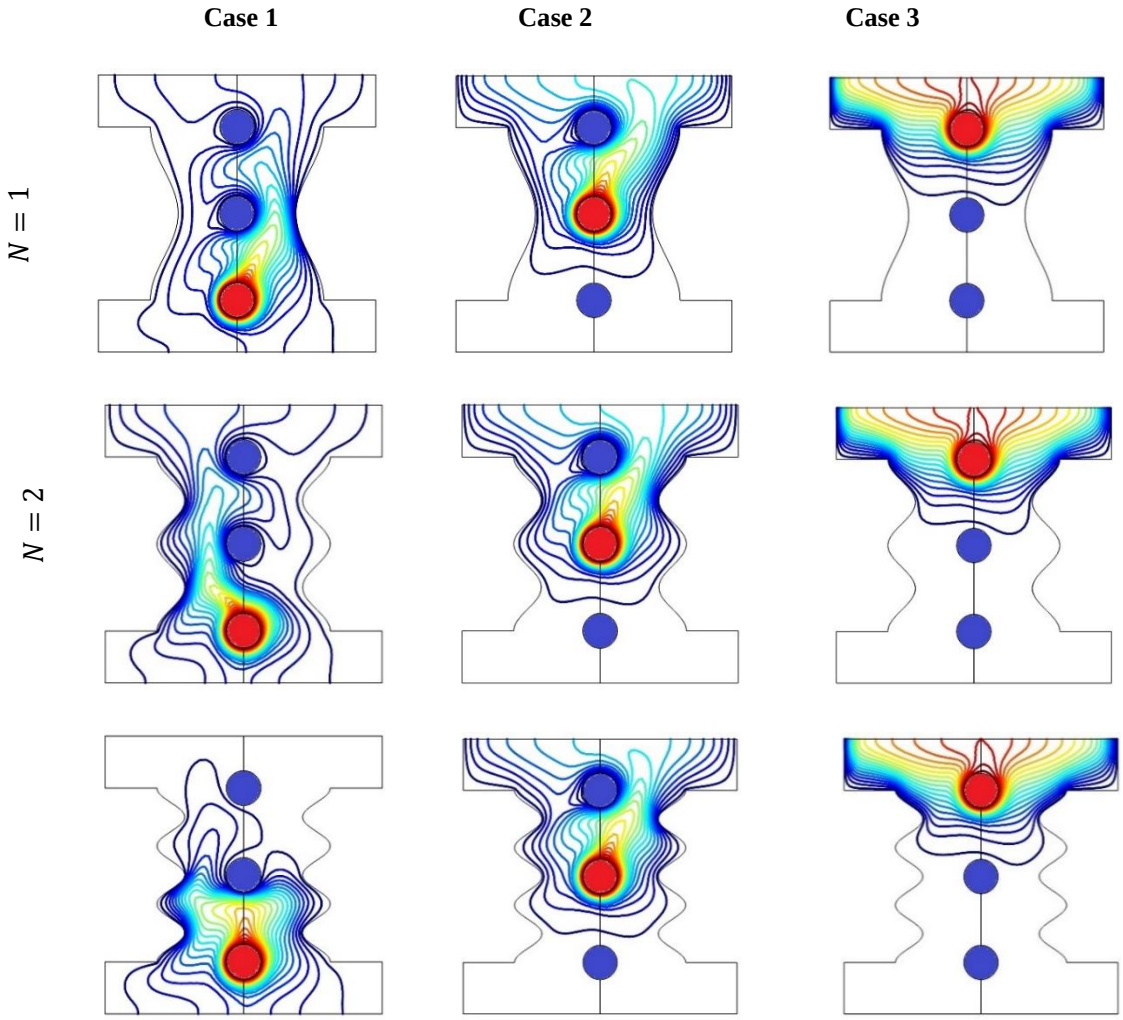

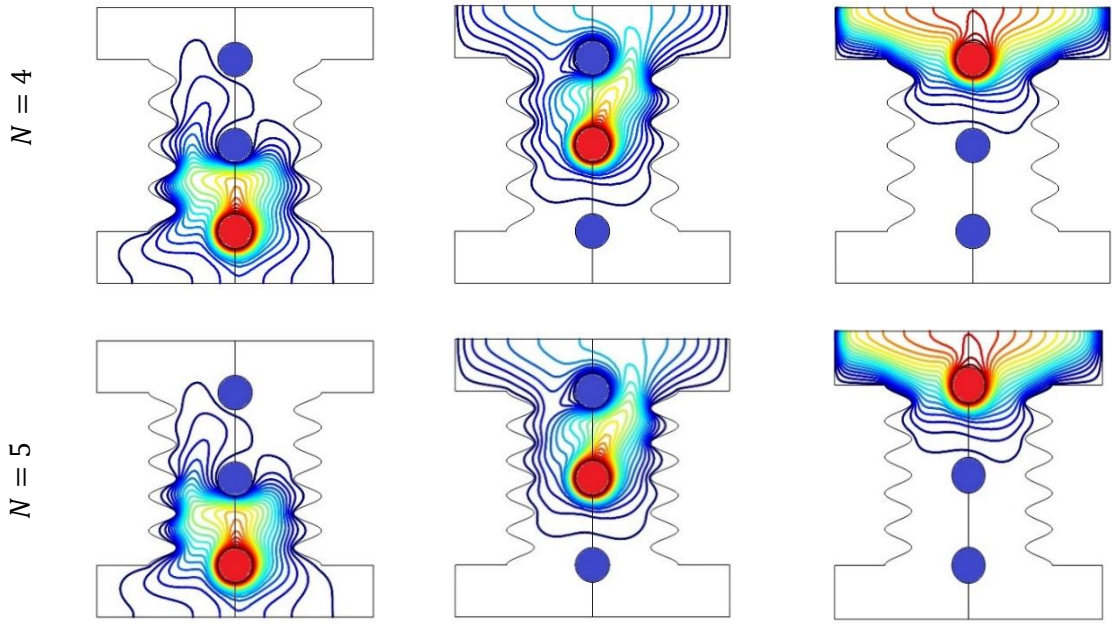

Figure (5. 21) Isotherms under distinct values of number of undulations at $Ha = 40, Ra = 10^6, Da = 0.001, \phi = 0.04, \gamma = 45$

5.2.1.6. Porous layer thickness

The influence of the porous layer thickness on the fluid flow in terms of streamlines and isotherms contours had been presented in Figures (5.22, 5.23 and 5.24), respectively for three cases at $Ha = 60$, $Ra = 10^6$, $Da = 0.001$, $\phi = 0.02$, $\gamma = 45$. With respect to the streamlines that presented in Figures (5.22, 5.23), it can be seen that the increase in the thickness of the porous layer leads to an obvious reduction in the flow function which, in turn, reduces the fluid flow strength for the three cases of location of the internal body. The influence of the location of the internal hot body as well as the value of the thickness of the porous layer affects the fluid flow strength. For example, when the internal hot body is located in the top of the enclosure (case 3), the influence of the thickness of the porous layer is very small and can be negligible. Whereas for cases 1 and 2, the impact of the thickness of the porous layer is very strong as it is obviously reducing the flow strength of the fluid. For example, the increase in the thickness of the porous layer when the internal hot body is located in the middle of the enclosure (case 2) from $X_P = 0.6$ to $X_P = 1$, resulting in an obvious reduction of the fluid flow strength from $|\Psi_{max}| = 12.16$ to $|\Psi_{max}| = 8.839$, respectively.

The same reduction is observed, but to a lesser extent for case 1 compared to case 2. Thus, case 1 in which the internal hot body shows a better resistance to fluid flow, followed by case 2 and the lowest was for case 3, again.

With respect to Figure (5.24), which shows the influence of the thickness of the porous layer and the location of the hot body on the isotherms, it can be seen that the increase in the thickness of the porous layer larded to increase the mode of heat transfer by conduction because the lines appear horizontal at a high value of the thickness of the porous layer.

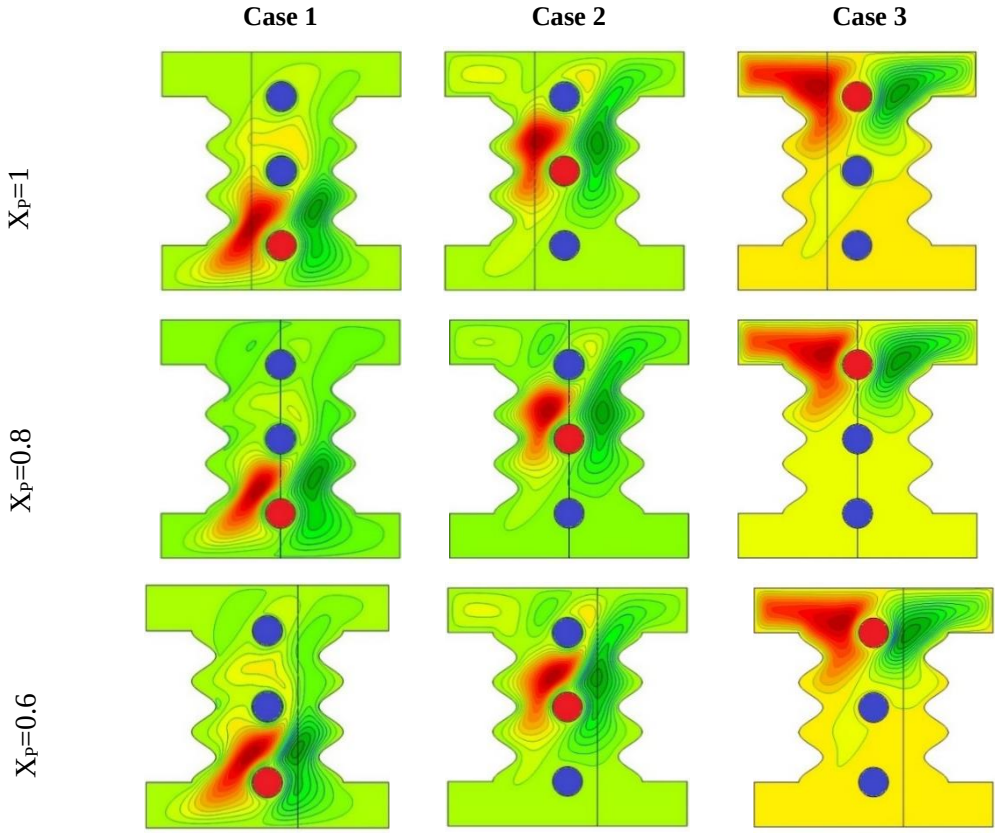

Figure (5. 22) Stream function contours under distinct values of Darcy numbers

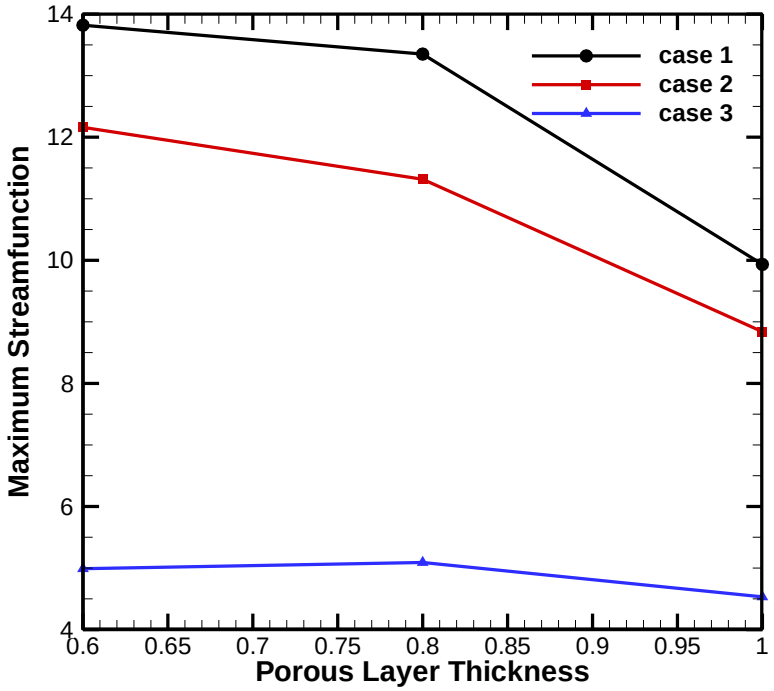

Figure (5. 23) The fluid flow strength in terms of maximum streamfunction with porous layer thickness for three thermal selected cases of inner hot body location

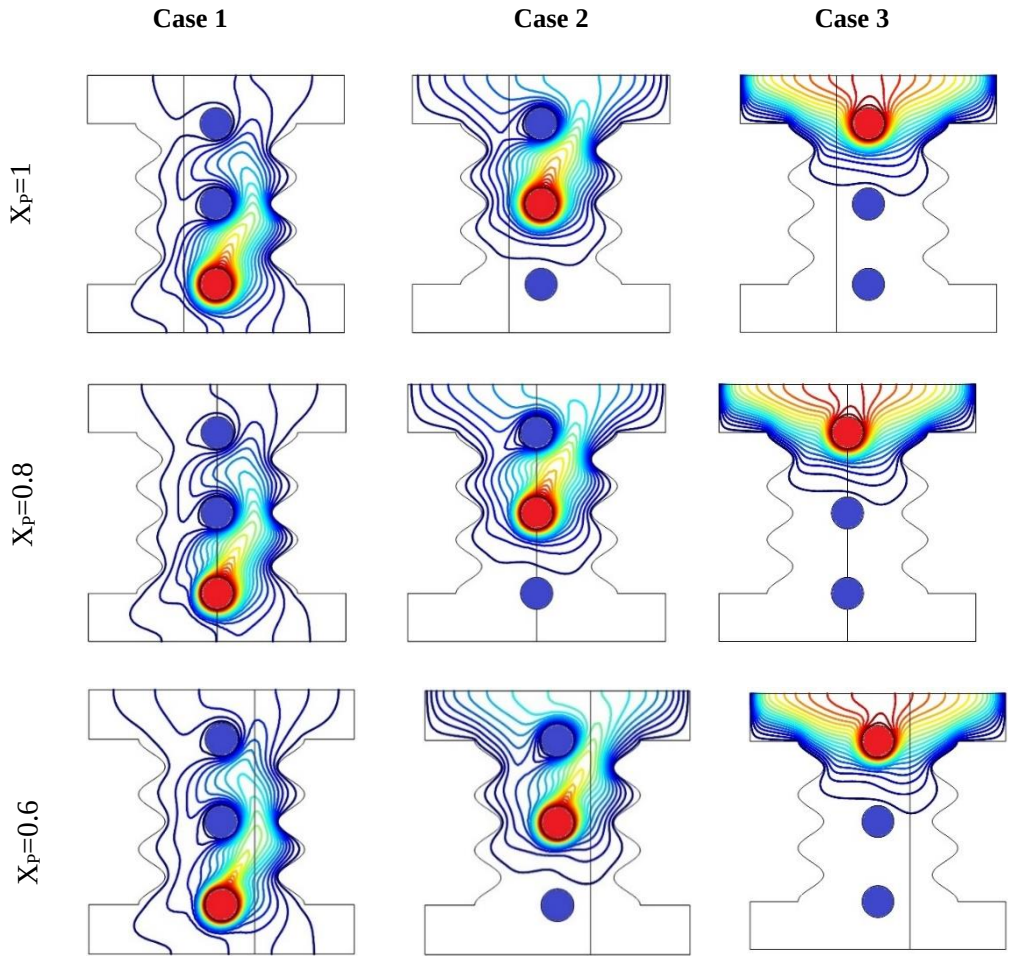

Figure (5. 24) Isotherm distributions for various porous layer thickness

5.2.1.7. Nusselt Number Results

Since the Nusselt number is the indicator of the increase in heat transfer, this section shows the influences of various selected parameters such as Ra, Ha, Da, MHD inclination angle, number of undulations and thickness of the porous layer considering three different localization cases for the inner hot body. First of all, regarding the influence of Ra and Ha, presented in Figure (5.25). It can be seen that the impact of Ra and Ha on the mean Nusselt number is inversely related. As can be seen, the increase in Ra leads to an enhancement, improvement and increase in the average number of Nusselt, which contributes to an improvement in the rate of heat transfer. While the increase in Hartmann's number leads to an obvious reduction in heat transfer. The influence of the angle of inclination of the MHD is shown in Figure (5.26), it may be noted that case 3 has the lowest average Nusselt number in comparison with the other two cases. The influence of the MHD angle on Nu along the hot body for cases 1 and 2 is strongly influenced by the MHD angle. For example, when $\gamma=0$ the Nu for case 2 where the hop body in the middle of the enclosure is higher than the Nu for case 1. By increasing the MHD angle in $\gamma=45$, case 1 has a slightly higher Nu than case 2. Finally, Nu for case 2 is higher than Nu for case 1 at $\gamma=90$. The influence of Darcy number on Nu and its impact on heat transfer for three different cases is also shown in Figure (5.27). For the three selected cases, it can be seen that increasing the Darcy number increases Nu. For the other cases 1 and 2, the influence of the location of the hot body has a significant effect on the Nu. For example, at a low Darcy number Da=1e-5, where conduction heat transfer is the dominant mode, it can be seen that case 2 has a higher Nu than case 1. As soon as the Darcy number increases, the Nu of case 1 will be higher than that of case 2.

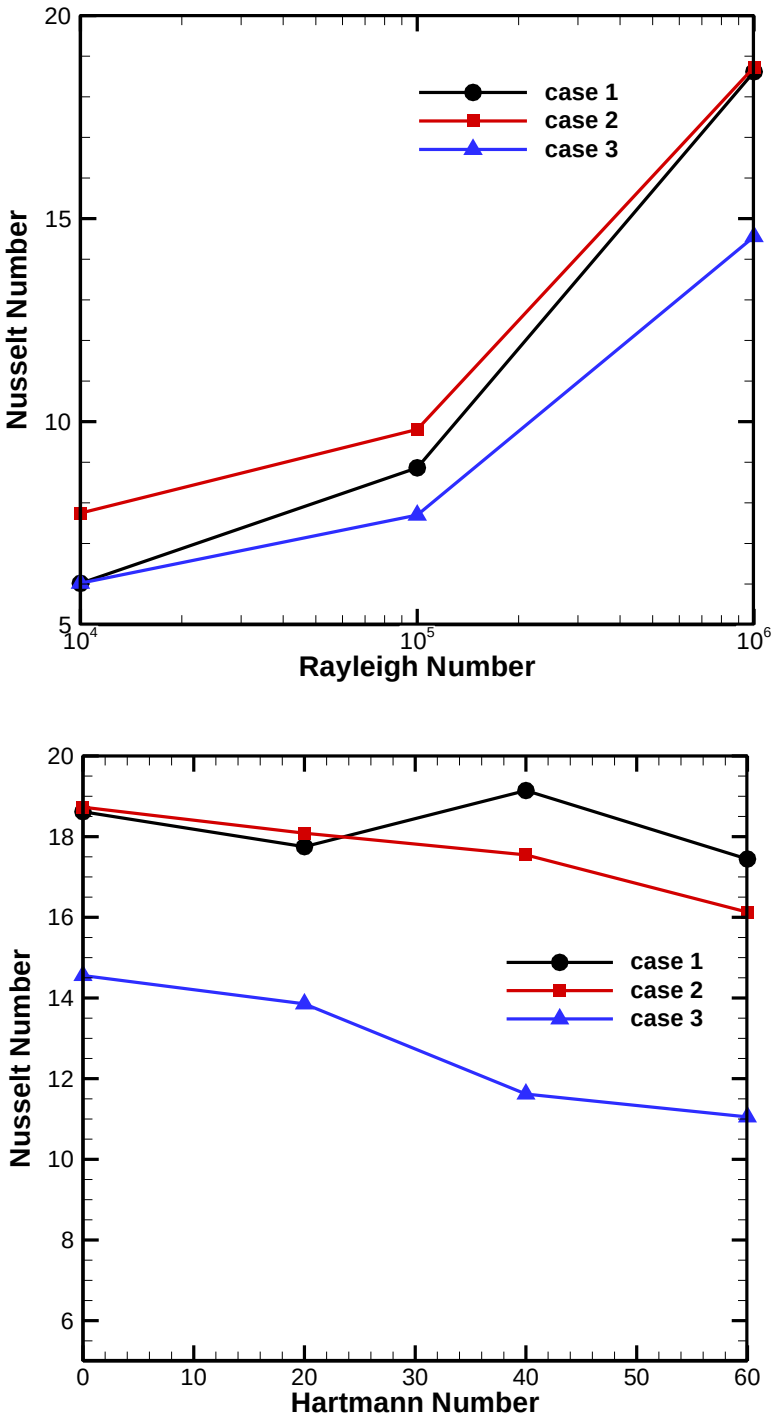

Figure (5. 25) The influence of Ra and Ha on Nu of the inner hot body

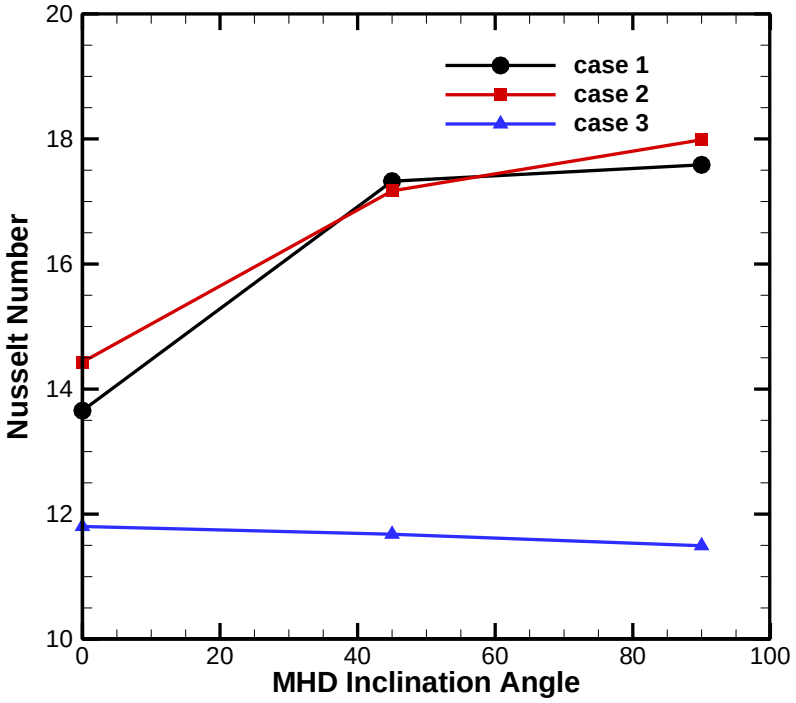

Figure (5. 26) The influence of MHD inclination angle for diferent cases of inner hot body location

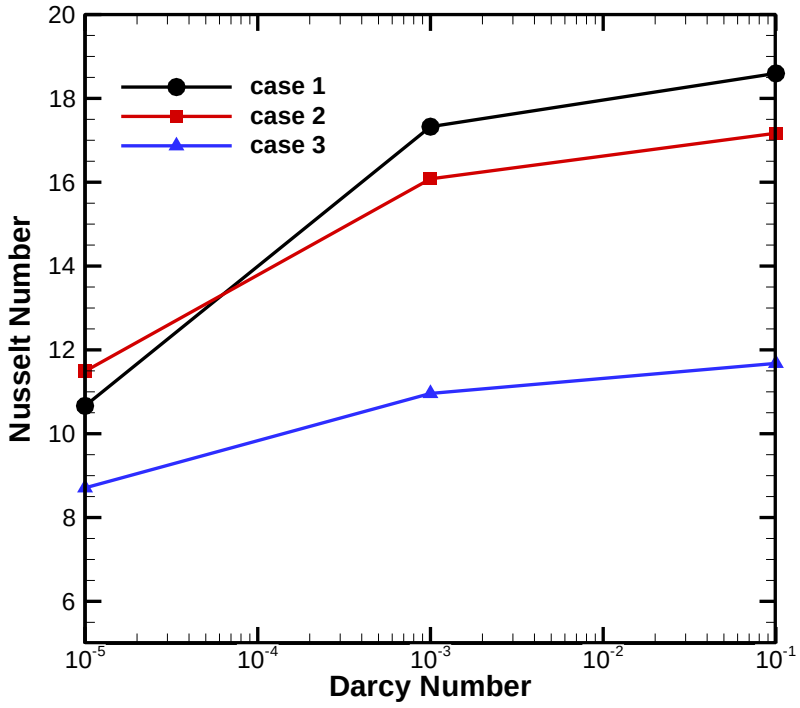

Figure (5. 27) The influence of Darcy number for diferent cases of inner hot body location

The undulation numbers on Nu are also shown in Figure (5.28) for three different locations of the internal hot bodies. It can be seen once again that Case

3, in which the hot body is located on top of the enclosure, has the lowest heat transfer rate. As for the other cases, case 1 with N=1, records the highest number of Nusselt followed by case 2. The increase in the number of undulations on Nu for case 2 is ignored until it reaches N=5 where a sudden fall of Nu is noticeable because this increase in the number of undulations leads to an increase in conduction heat transfer greater than the convection mode. For case 1, the increase in the number of undulations up to N=2, leads to a drop in Nu. The increase in the number of undulations for case 1 had a small impact on Nu that can be neglected. Finally, as indicated in Figure (5.29), regarding the impact of the thickness of the porous layer on Nu for three different locations of the internal hot body, it can be seen that increasing the thickness of the porous layer results in a reduction of the Nu in each case. However, case 3 had the lowest Nu while case 1 had the highest Nu.

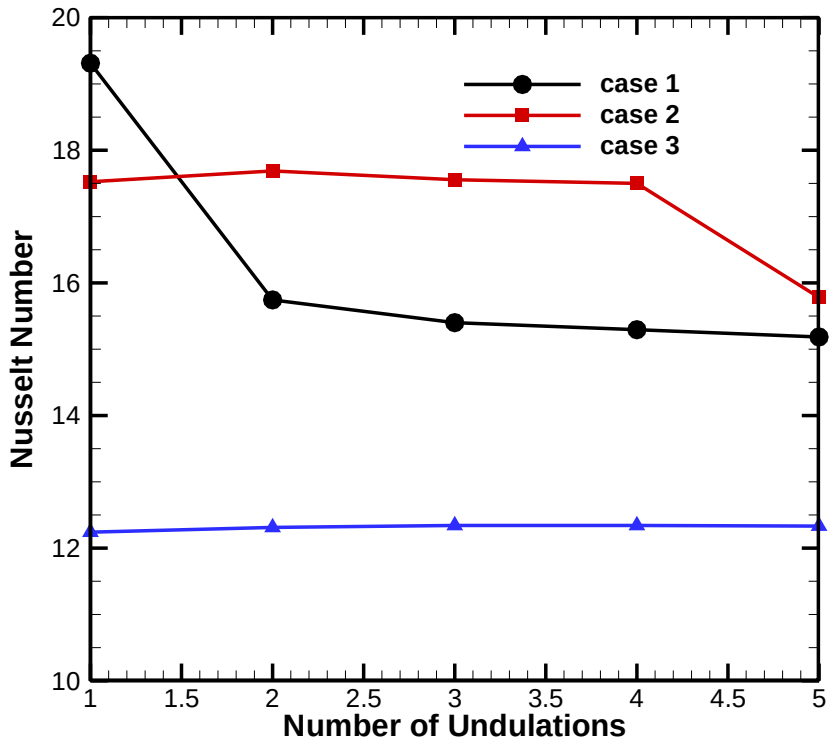

Figure (5. 28) The influence of number of undulations for different cases of inner hot body location

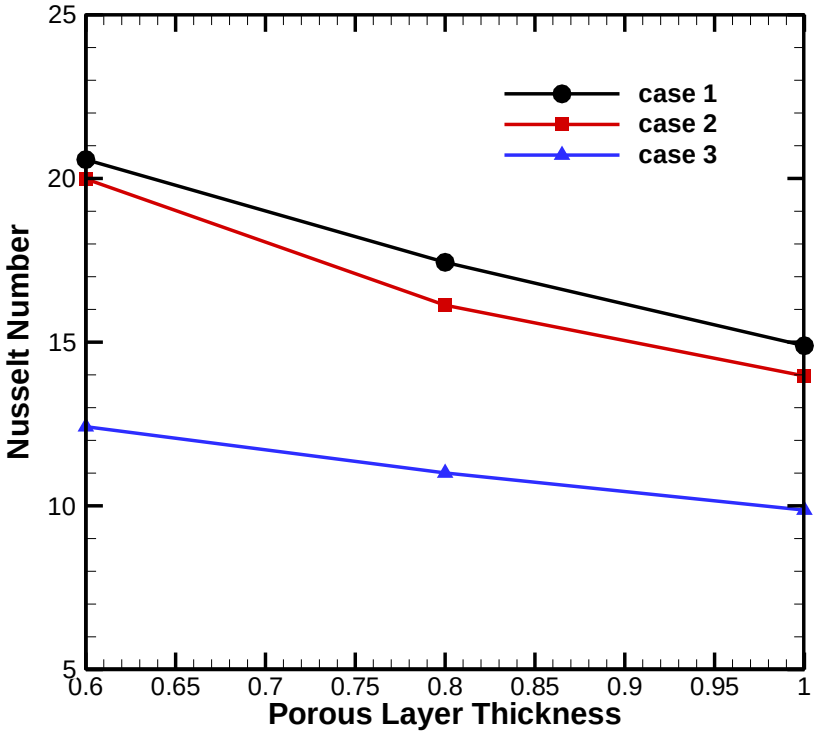

Figure (5. 29) The influence of porous layer thickness for different cases of inner hot body location

5.2.2. Inner Shapes Bodies Within the Novel Enclosure

The present section discuss the numerical results of natural convection heat transfer within I-shaped wavy-walled enclosure filled by nanofluid saturated with porous media (left layer) and the same nanofluid (right layer) under wide range of Rayleigh number ($10^4 \leq Ra \leq 10^6$), Darcy number ($10^{-5} \leq Da \leq 10^{-3}$), Hartmann number ($0 \leq Ha \leq 60$) considering three different positions of the hot inner body along with four different cases of the shapes of inner body (circle, square, rhombus and triangle) for three different number of the hot source inner body. The influence of these mentioned dimensionless parameters on heat transfer and fluid flow are presented and discussed in full-details.

5.2.2.1. The influence of dimensionless numbers on fluid flow and heat transfer

Since many dimensionless parameters under investigation, it has been started by illustrating the influence of Rayleigh, Darcy and Hartmann numbers along with

four different shapes of inner body such as (circle, square, rhombus and triangle) on fluid flow and heat transfer.

First of all, the influence of Rayleigh number and the inner body shape are presented in terms of streamlines and isotherms in Figure (5.30) and Figure (5.31), respectively.

With respect to Figure (5.30), at low Rayleigh number ($Ra = 10^4$), where the power intensity of natural convection is low and the conductive mode of heat transfer is the dominant mode, it can be seen that there are just two inner vortices formed closed to each shape of the inner body on the nanofluid region (right layer) while the streamlines on the nano-porous region (left layer) does not contain any circulation which reflect the lower strength of the fluid flow. This is due to the porous media which plays as additional resistance to the fluid flow in addition to the low Rayleigh number. Also, the inner body shape influences on the degree of the augmentation or reduction of the stream function. For example, the strength of fluid flow for $Case\ 4 > Case\ 3 > Case\ 2 > Case\ 1$ which makes the triangular shape (Case 4) recorded the better case in terms of the best fluid flow strength while the inner circular body gives the lowest strength of the fluid flow.

With increasing the Rayleigh number into $(Ra = 10^6)$, which reflect the changing of the heat transfer mode from the conduction mode into the thermogravitational (natural convection) mode leading to an increasing on the fluid flow strength for each case of the inner body shape. The physical reason behind this increasing is due to increasing buoyancy force in addition to the natural convection rate. For example, the strength for $Case\ 3 > Case\ 1 > Case\ 2 > Case\ 4$ which makes the triangular shape reveals the lowest case in terms of fluid flow strength while the rhombus shape give the best fluid flow strength. It is worthy to mention that increasing the Rayleigh number helps more nanofluid to penetrate from the right layer into the left layer due to increasing the permeability of the porous media which leads to the formation of the inner vortices in many regions within the enclosure at high Rayleigh number.

With respect to Figure (5.31), which reveals the isotherms under various dimensionless values of Rayleigh number considering four different cases of inner body, it can be seen that the isotherms lines at low Rayleigh number ($\mathrm{Ra} = 10^4$) are vertical which reflect the conduction heat transfer mode is dominant while at high Rayleigh number ($Ra = 10^6$), the shapes of isotherms lines obviously changed into the non-uniform curved lines which is an indication of the thermogravitional mode is dominated. It can be seen that the behavior of isotherms are similar regardless the inner body shape.

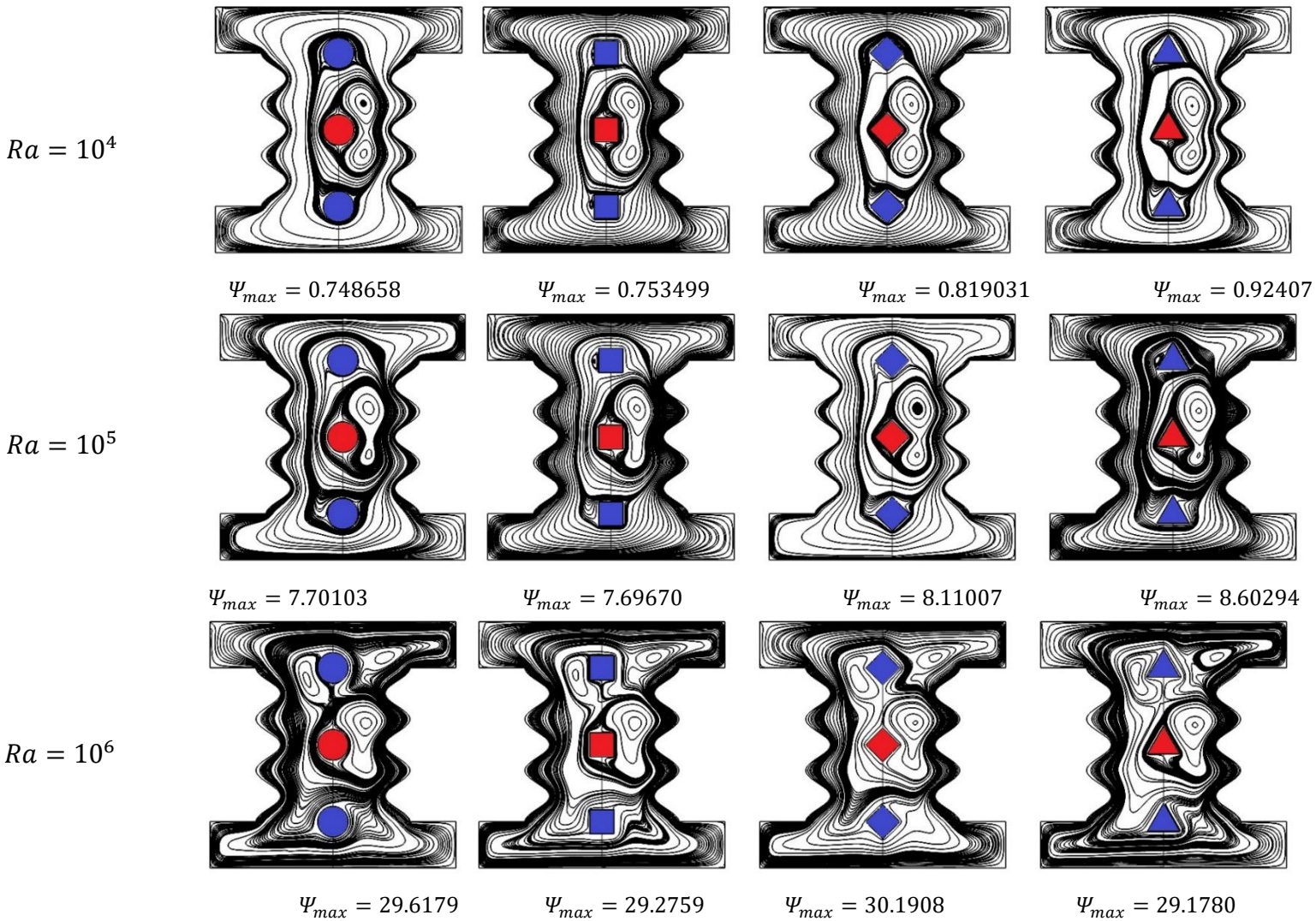

Figure (5. 30) Streamlines contours considering different inner hot shapes under various Rayleigh number at $Da = 0.001, \varphi = 0.02, Ha = 0$

$Ra = 10^4$

$Ra = 10^5$

$Ra = 10^6$

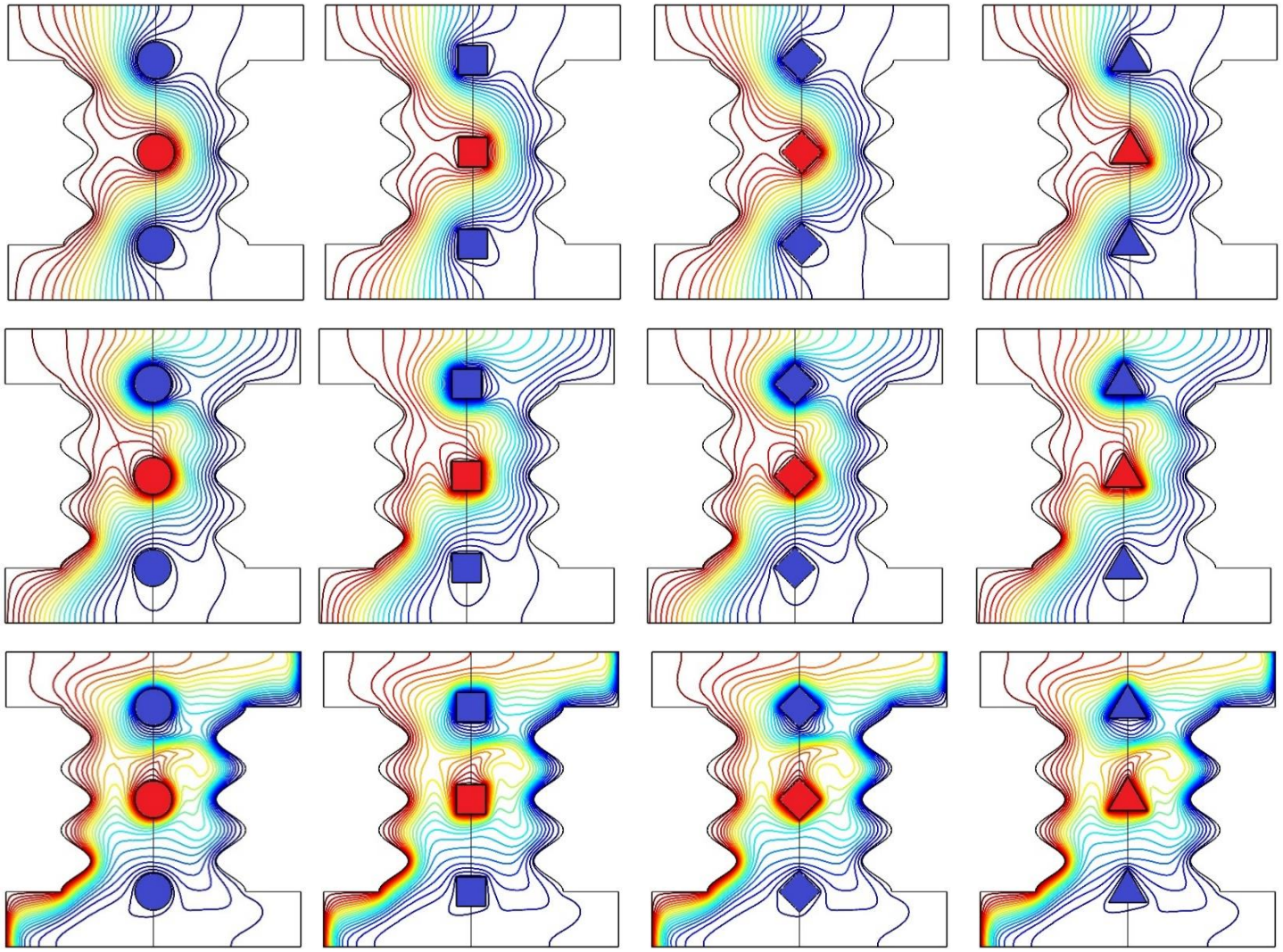

Figure (5. 31) Isotherms contours considering different inner hot shapes under various Rayleigh number at $Da = 0.001, \varphi = 0.02, Ha = 0$

The influence of Darcy number and the inner body shape is presented in terms of streamlines and isotherms in Figure (5.32) and Figure (5.33), respectively. Firstly, with respect to the Figure (5.32) which illustrates the influence of various Darcy number and different four cases of inner body shape on the fluid flow strength. By constriction our analysis on the left layer of the enclosure which contains (porous media saturated with nanofluid) and keep track of the influence of Darcy number along with the inner body shape, it can be noted that at low Darcy number ($Da = 10^{-5}$), there is no inner vortices formed while as the Darcy number increases into $Da = 10^{-1}$, more inner vortices formed which means that the fluid flow strength is increasing as Darcy number increases. The physical reason behind this, is that increasing the dimensionless value of Darcy number leads to an obvious increment in the permeability of the porous media which helps nanofluid to penetrate into the left layer leading to increases the convection heat transfer mode because the conductive mode is dominant at low Darcy number and this is obvious also from the shape of the streamlines in the left layer as there is no inner cells which reflect low fluid flow strength. Also, the shape of inner body had great impact on the fluid flow strength. For example, at low Darcy number ($Da = 10^{-5}$), the maximum stream function of the left layer for $Case\ 1 > Case\ 2 > Case\ 3 > Case\ 4$, while at high Darcy number ($Da = 10^{-5}$), the maximum stream function of the left layer for $Case\ 2 > Case\ 4 > Case\ 3 > Case\ 1$. Thus, at low Darcy number Case 1 which represents the inner circular shape had the highest fluid flow strength while the lowest fluid flow strength was when the inner shape is triangular. Actually, at low Darcy number the influence of inner body shape had great influence on the fluid flow characteristics. On the other hand, at high Darcy number Case 1 which is the inner circular shapes recorded the lowest case in the fluid flow strength while the square shape is better in the enhancing the fluid flow strength.

With respect to the Figure (5.32), which examines the isotherms under various Darcy number and different cases of inner body shape, it can be seen obviously that increasing Darcy number leads to change the isotherm lines from the vertical lines as

the conduction heat transfer is dominant at low Darcy number into curved-horizontal lines at high Darcy number.

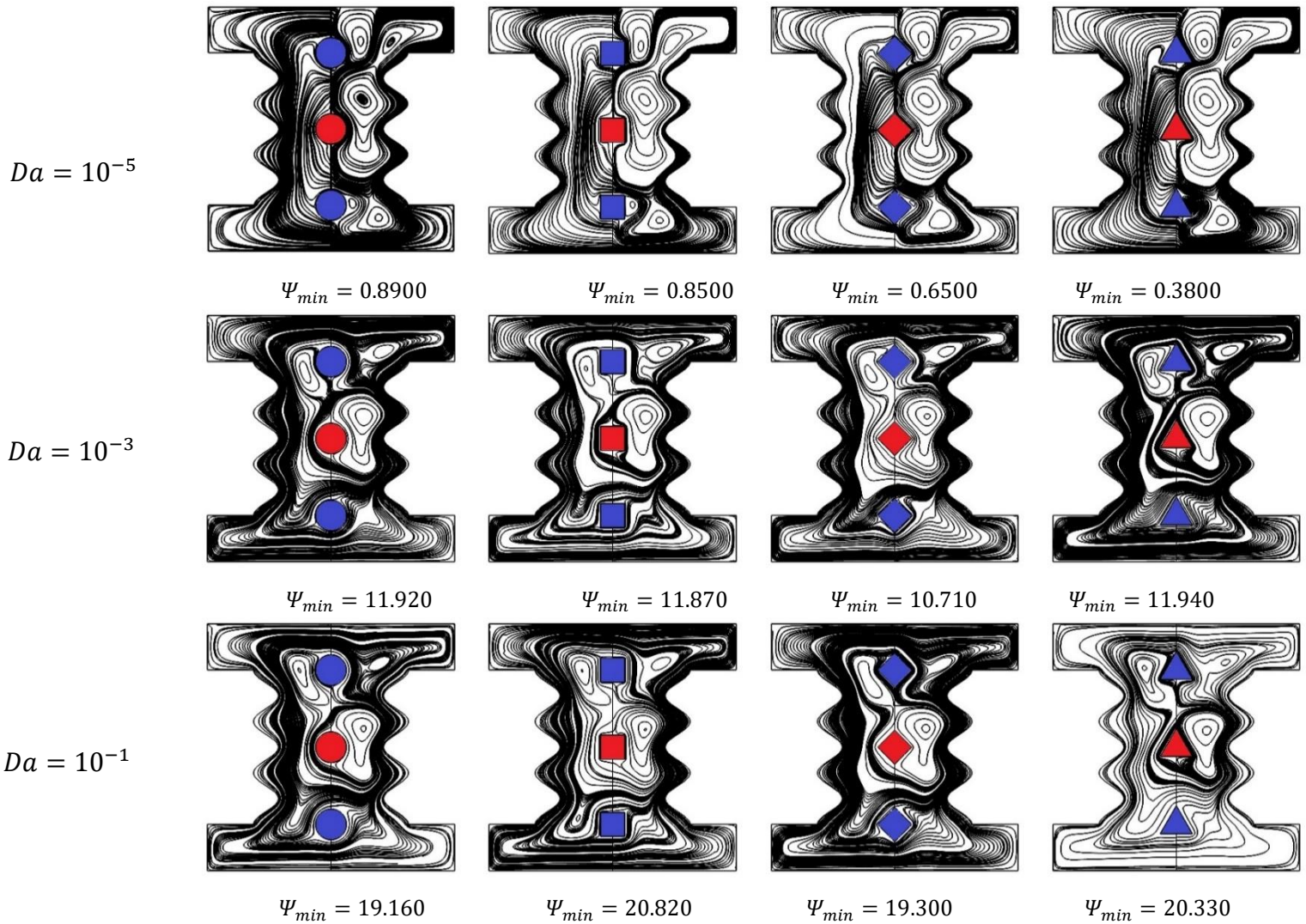

Figure (5. 32) Streamlines contours considering different inner hot shapes under various Darcy number at $Ra = 10^6, \varphi = 0.02, Ha = 0$

$Da = 10^{-5}$

$Da = 10^{-3}$

$Da = 10^{-1}$

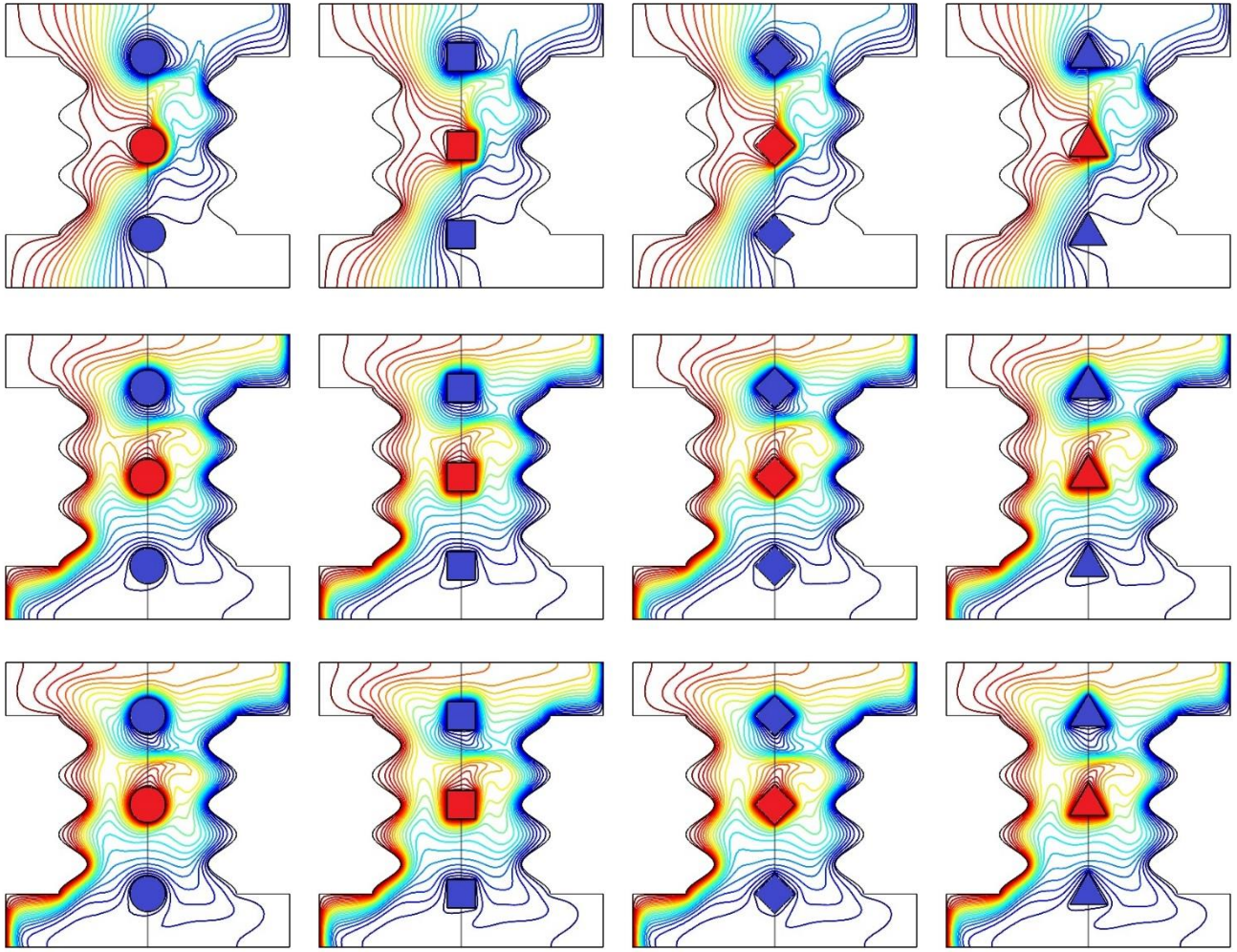

Figure (5. 33) Isotherms contours considering different inner hot shapes under various Darcy number at $Ra = 10^6, \varphi = 0.02, Ha = 0$

With respect to the magnetic field influence on fluid flow and heat transfer which is presented in Figure (5.34) and Figure (5.35). Firstly, the influence of Hartmann number considering different shapes of inner body had been presented in Figure (5.34). It can be seen that the Hartmann number influences strongly on the fluid flow contours because increasing Hartmann number leads to reduce the fluid flow strength. For example, for case 1, it can be seen that maximum stream function reduces from $\Psi_{max} = 29.6179$ at $Ha = 0$, into $\Psi_{max} = 13.2388$ at $Ha = 60$ which makes this behavior is quite reverse to the influence of Rayleigh number on the strength of the fluid flow. This behavior is similar for all of the other cases of inner body shapes but at different rate. For example, in the absence of magnetic field $(Ha = 0)$, it can be seen that the maximum stream function for different cases of inner body shape is $Case\ 3 > Case\ 1 > Case\ 2 > Case\ 4$ while increasing the Hartmann number into $(Ha = 60)$, leads for further decrement in the maximum stream function which makes it for $Case\ 2 > Case\ 4 > Case\ 1 > Case\ 3$. The physical reason behind this is that increasing the Hartmann number is an indication of increasing the electromagnetic force which its role is to reduce the natural convection buoyancy force and reduces the fluid flow strength. With respect to Figure (5.35) which shows that increasing Hartmann number slightly reduces on the isotherms.

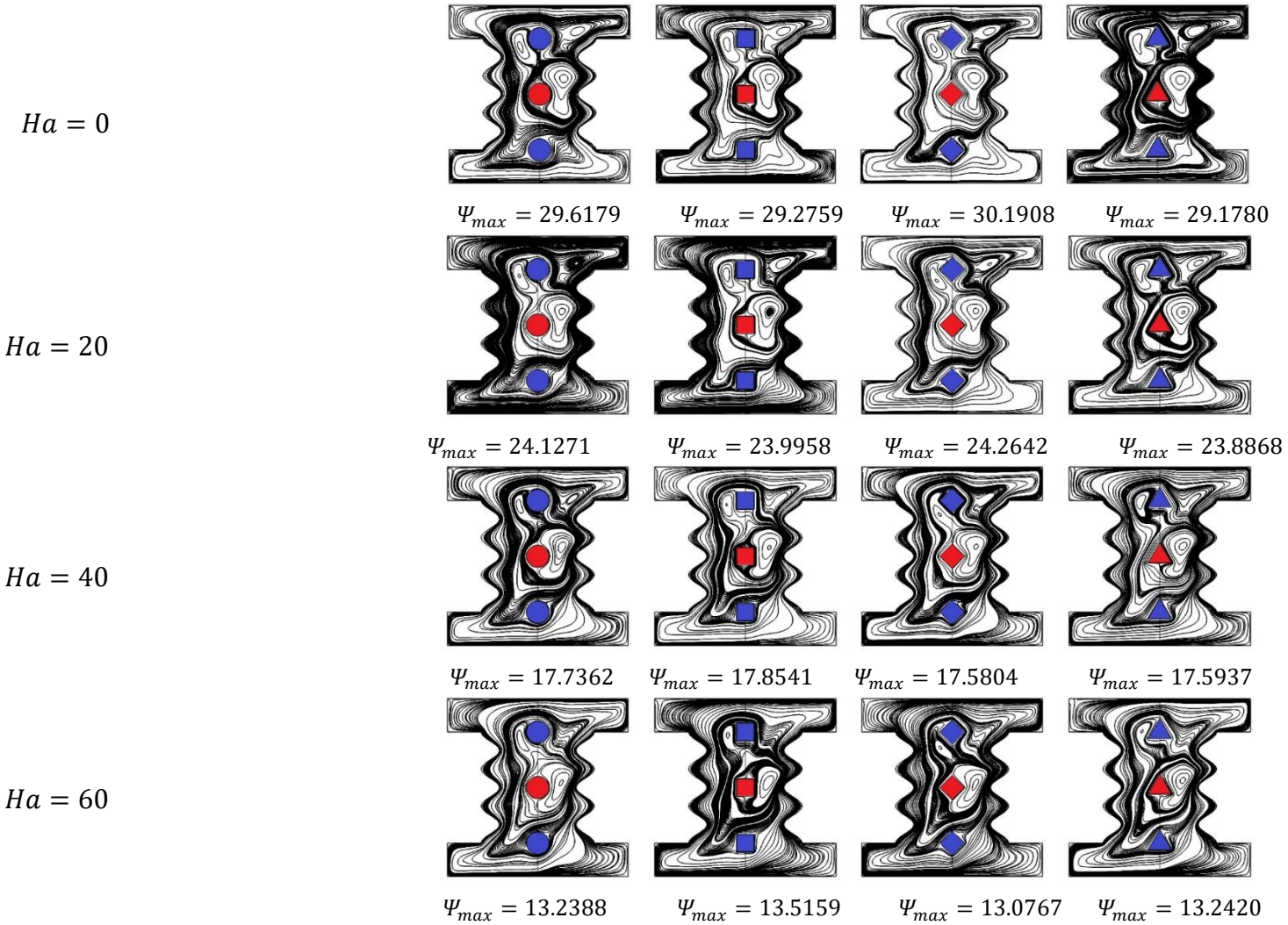

Figure (5. 34) Streamlines contours considering different inner hot shapes under various Hartmann number at $Ra = 10^6, \varphi = 0.02, Da = 0.001$

$Ha = 0$

$Ha = 20$

$Ha = 40$

$Ha = 60$

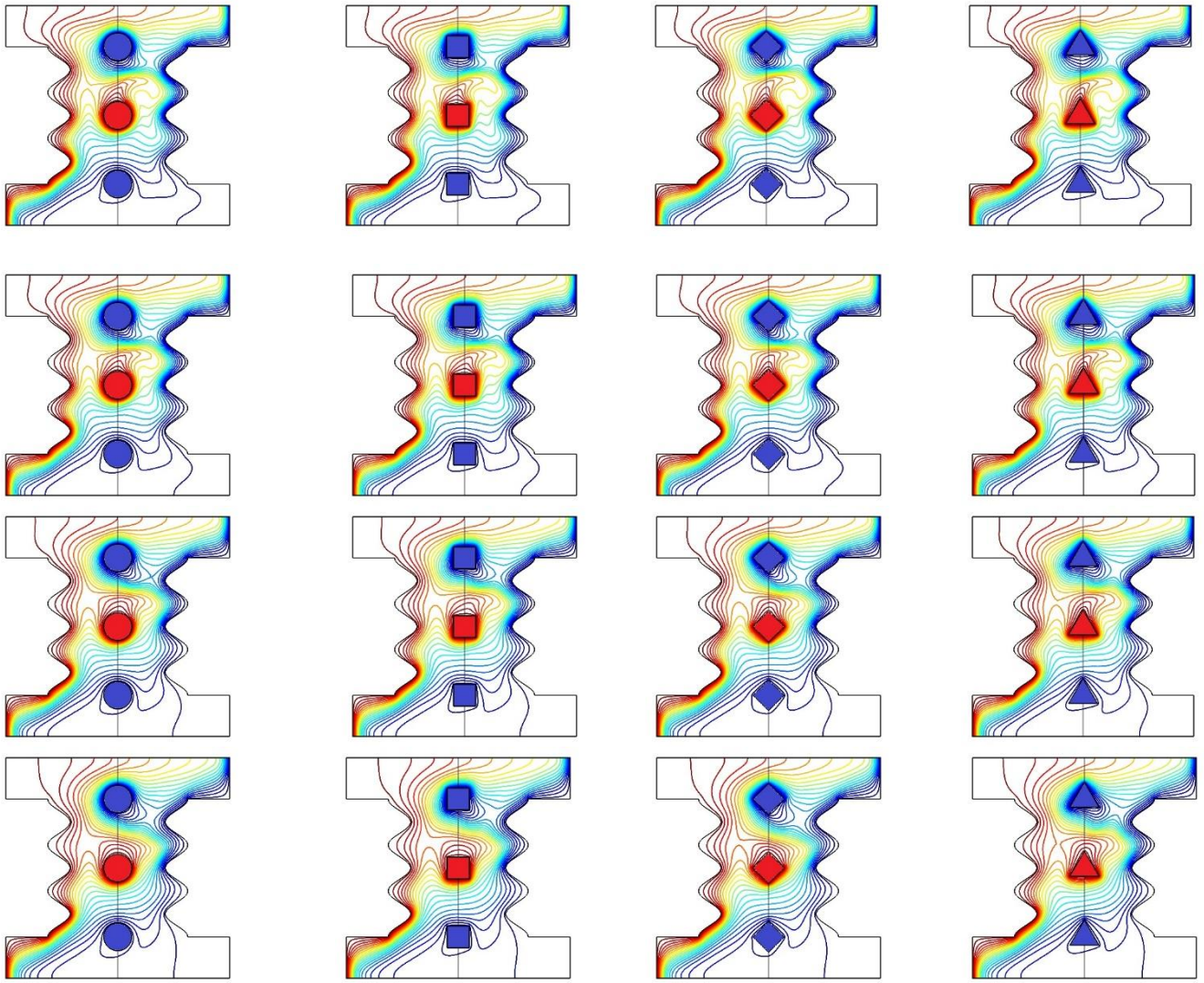

Figure (5. 35) Isotherms contours considering different inner hot shapes under various Hartmann number at $Ra = 10^6, \varphi = 0.02, Da = 0.001$

5.2.2.2. The influence of heaters number

The influence of number of inner hot body (heater) for each of the four selected cases of the inner body shape (circle, square, rhombus and triangular) on streamlines and isotherm are presented in Figure (5.36) and Figure (5.37), respectively.

With respect to Figure (5.36), it may be noted that regardless the inner body shape, increasing the number of heaters from $No = 1$ into $No = 2$, leads to increasing the fluid flow strength by increasing the maximum stream function. This is due to the increasing of the internal thermal energy increases as a result of increasing the number of heaters that the fluid absorb this energy leading to more impact with the molecules which attains higher fluid flow strength. Also, further increasing in the number of heaters for $No = 3$, leads to slight reduction the fluid flow strength. For example, regarding Case 1 the maximum stream function increases from $\Psi_{max} = 18.3070$ into $\Psi_{max} = 27.9309$ and then reduces into $\Psi_{max} = 25.0989$ when the number of inner hot body increases from $N = 1, 2\ and\ 3$, respectively. It is worthy to mention, that the heaters shape along with the number of heaters had great impact on the strength of fluid flow. For example, when the number of inner hot body is $No = 1$, the maximum stream function for $Case\ 4 > Case\ 2 > Case\ 1 > Case\ 3$ which make the fluid flow strength of Case 4 which represents the triangular shape had the highest fluid flow strength. The influence of heaters shape for further increasing of inner heaters number when $No = 3$ is approximately negligible where the maximum stream function is approximately around $\Psi_{max} = 25$.

With respect to the isotherms as shown in Figure (5.37) it can be seen that increasing the number of hot inner heaters leads to increase the hot temperature lines in the left layer (nanofluid saturated with the porous media) as the hot lines resulted from the inner hot bodies will combine with the hot line resulted from the left wall of the enclosure.

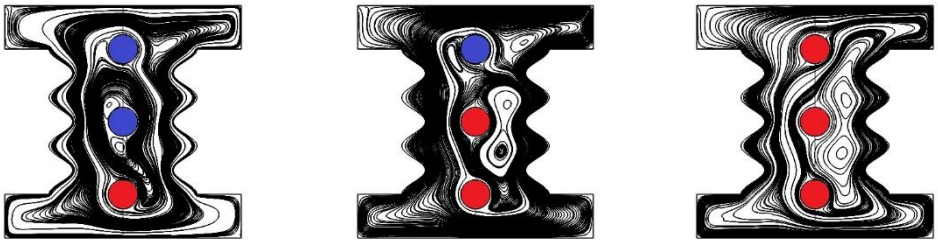

$\Psi_{max} = 17.0935$ $\Psi_{max} = 28.0352$ $\Psi_{max} = 25.0544$

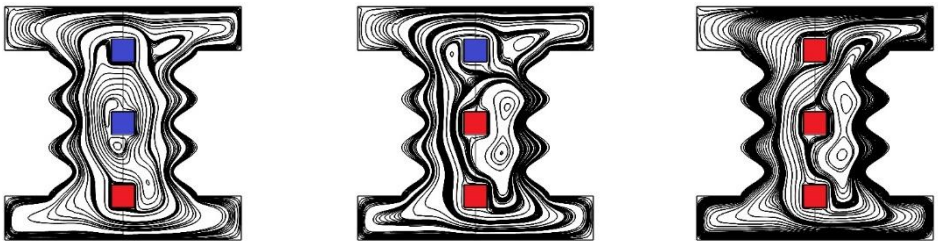

$\Psi_{max} = 18.3070$ $\Psi_{max} = 27.9309$ $\Psi_{max} = 25.0989$

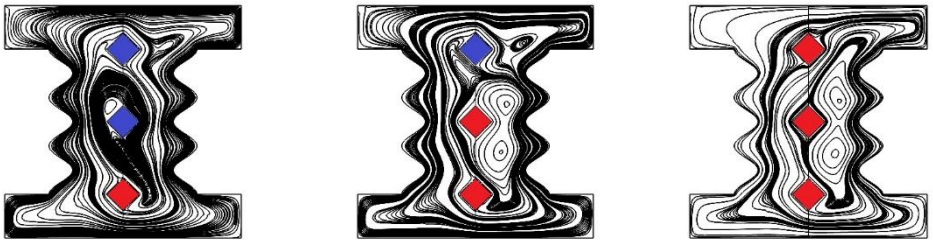

$\Psi_{max} = 16.4889$ $\Psi_{max} = 27.9001$ $\Psi_{max} = 25.2058$

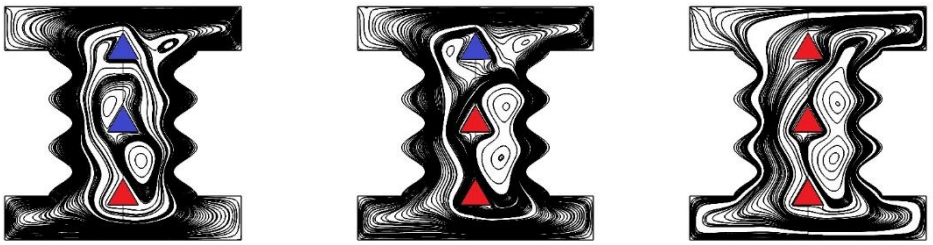

$\Psi_{max} = 26.5025$ $\Psi_{max} = 27.5546$ $\Psi_{max} = 25.7497$

Figure (5. 36) Streamlines contours considering different number of inner hot shapes at $Ra = 10^6, \varphi = 0.02, Da = 0.001, Ha = 20$

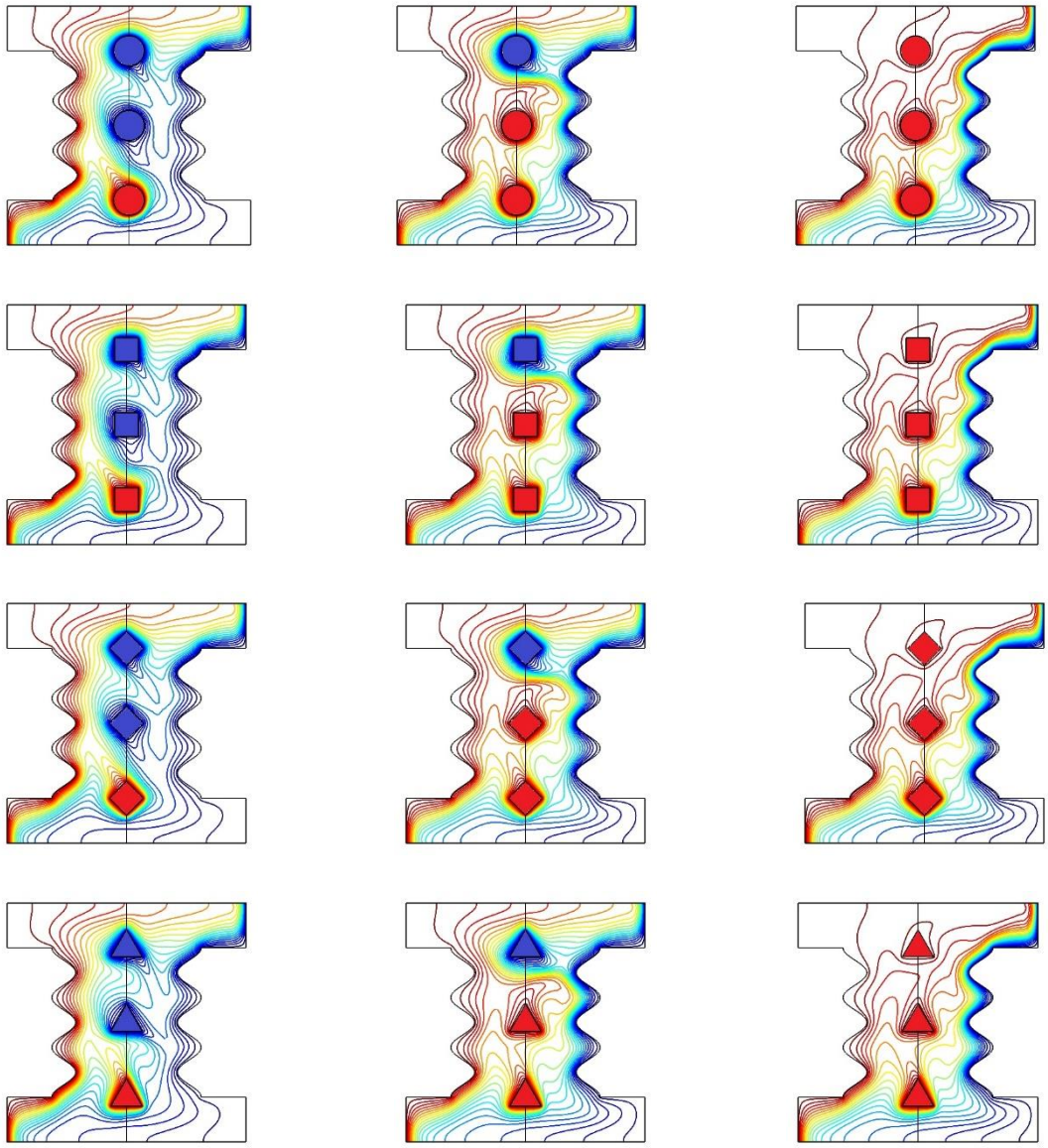

Figure (5. 37) Isotherms contours considering different number of inner hot shapes at $Ra = 10^6, \varphi = 0.02, Da = 0.001, Ha = 20$

5.2.2.3. The influence of position of the heater

The influence of the heater position on fluid flow and heat transfer are presented in this section in Figure (5.38) and Figure (5.39), respectively. Three different positions of the heater had been taken which are (i) at the bottom when the distance between the position of the heater and the base of the enclosure wall is $\delta = 0.3$, in the same manner, (ii) at the center of the enclosure at $\delta = 0.8$ and (iii) at the top of the enclosure at $\delta = 1.3$. Firstly, with respect to the streamlines which is presented in Figure (5.38). It can

be seen for Case 1 which indicate the circular shape of inner body by follow its position when it moved from bottom into the top, that the maximum stream function increases from $\Psi_{max} = 17.0935$ when it located at $\delta = 0.3$ into $\Psi_{max} = 24.1271$ when it located at $\delta = 0.8$. However, more upward movement leads to a reduction in the fluid flow strength into $\Psi_{max} = 16.1245$ at $\delta = 1.3$. This behavior is repeated to Case 2 and Case 3 except Case 4 because the fluid flow strength decreases as the inner hot triangular body moved upward. It worthy to mention that the influence of inner hot body shape is negligible on fluid flow strength when it is located at the center and top of the enclosure while the influence of inner body location when it located at the bottom of the enclosure is strong especially for the Case 4 which is the triangular shape. With respect to Figure (5.39) which shows the isotherms clearly influenced by the position of the inner body shape.

$\delta = 0.3$	$\delta = 0.8$	$\delta = 1.3$
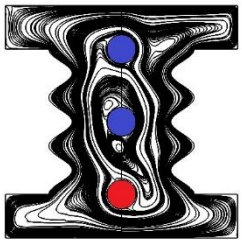	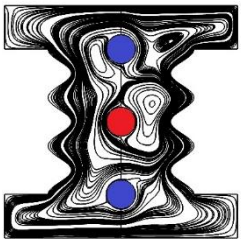	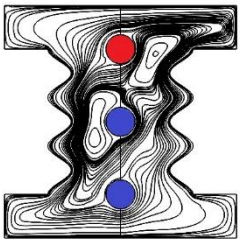
$\Psi_{max} = 17.0935$	$\Psi_{max} = 24.1271$	$\Psi_{max} = 16.1245$
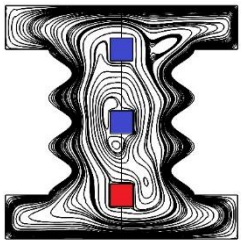	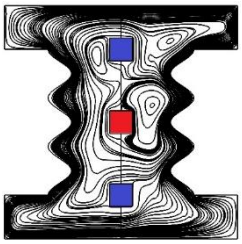	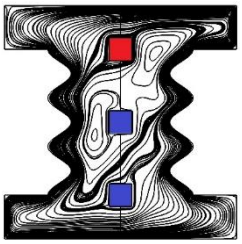
$\Psi_{max} = 18.3070$	$\Psi_{max} = 23.9958$	$\Psi_{max} = 16.1465$
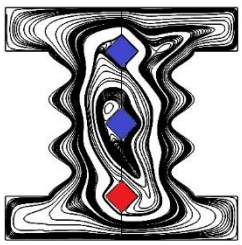	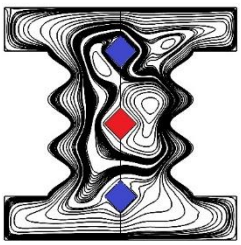	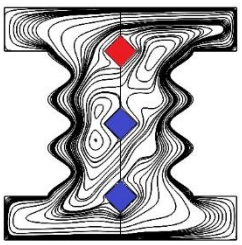
$\Psi_{max} = 16.4889$	$\Psi_{max} = 24.2642$	$\Psi_{max} = 16.0393$
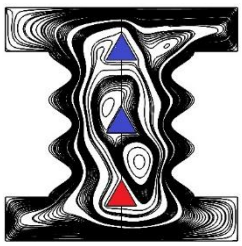	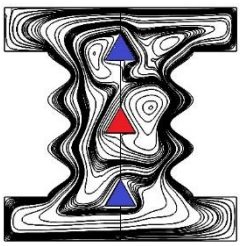	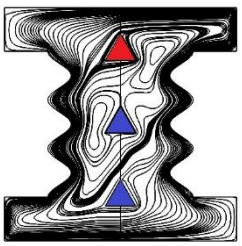
$\Psi_{max} = 26.5024$	$\Psi_{max} = 23.8868$	$\Psi_{max} = 16.0134$

Figure (5. 38) Streamlines contours considering different position of inner hot shapes at $Ra = 10^6, \varphi = 0.02, Da = 0.001, Ha = 20$

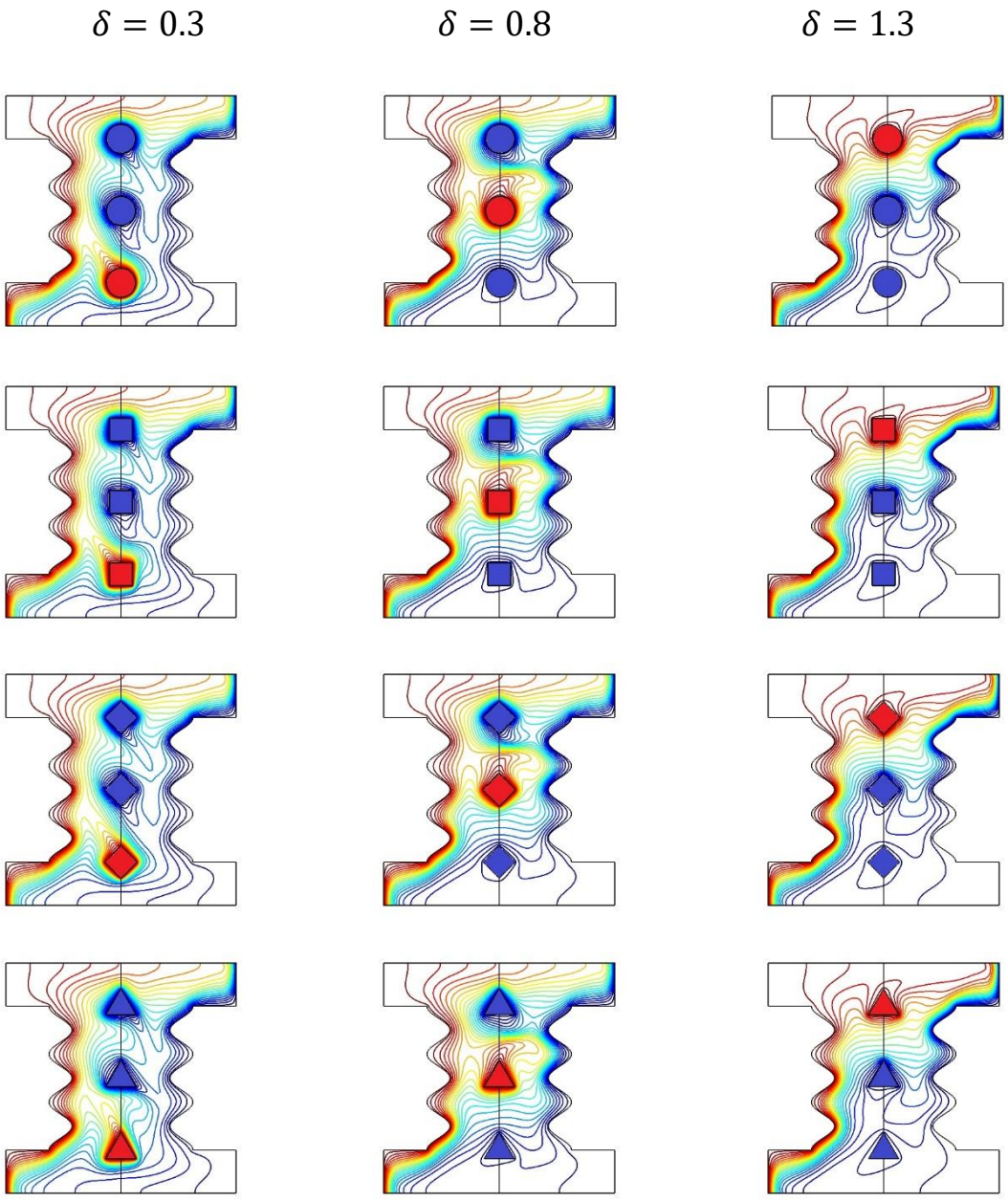

Figure (5. 39) Isotherms contours considering different position of inner hot shapes at $Ra = 10^6, \varphi = 0.02, Da = 0.001, Ha = 20$

5.2.2.4. Nusselt number results

The Nusselt number is the most important parameters in the augmentation of heat transfer rate. So, the influence of the mentioned parameters on Nusselt number will be discussed in full details to draw the major conclusions.

The influence of Rayleigh number considering different inner body shape on average Nusselt number had been displayed in Figure (5.40). It can be seen that increasing Rayleigh number leads to an increasing in the Nusselt number because of increasing the fluid flow strength and natural convection rate which increasing the rate impact between the fluid molecules which increasing the thermal energy transferred from the hot inner body into the enclosure area. This increasing of Rayleigh number changed the mode of heat transfer into the thermogravitional (natural convection) mode. It is also noted that the inner body shape plays an important role in the augmentation of Nusselt number which leads to improving the thermal rate of heat transfer. For example, Nusselt number for $Case\ 1 > Case\ 3 > Case\ 2 > Case\ 4$.

With respect to the influence of Darcy number as illustrated in Figure (5.41) which shows obviously that increasing Darcy number improves Nusselt number because of increasing Darcy number leads to augmentation of natural convection and buoyancy force which changed the mode of heat transfer from the conductive mode into the convection. Again, Nusselt number for $Case\ 1 > Case\ 3 > Case\ 2 > Case\ 4$.

Besides, increasing Hartmann number leads to express more resistance of the MHD force to the movement of the fluid flow which leads to a reduction of Nusselt number as shown in Figure (5.42) which makes its influence is quite reversible to the influence of Rayleigh and Darcy number. It may be noted that influence of Hartmann number on Nusselt number is highly affected by the inner body shape of each case. For example, the reduction in Nusselt number for $Case\ 1 > Case\ 3 > Case\ 2 >$

$Case$ 4 which makes Case 4 is the best solution to reduce the heat transfer rate in a comparison with the other cases.

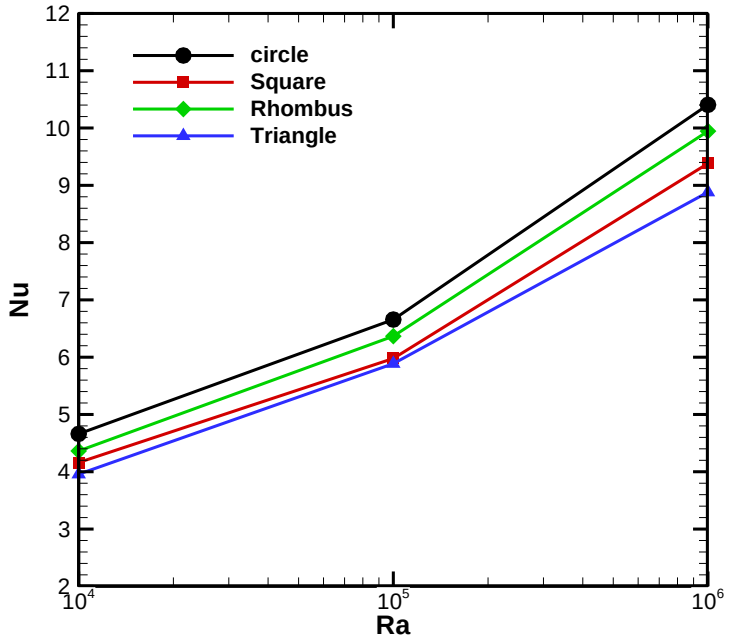

Figure (5. 40) Nusselt number with respect to Rayleigh number for different shapes of inner body at $\phi = 0.02, Da = 0.001, Ha = 0$

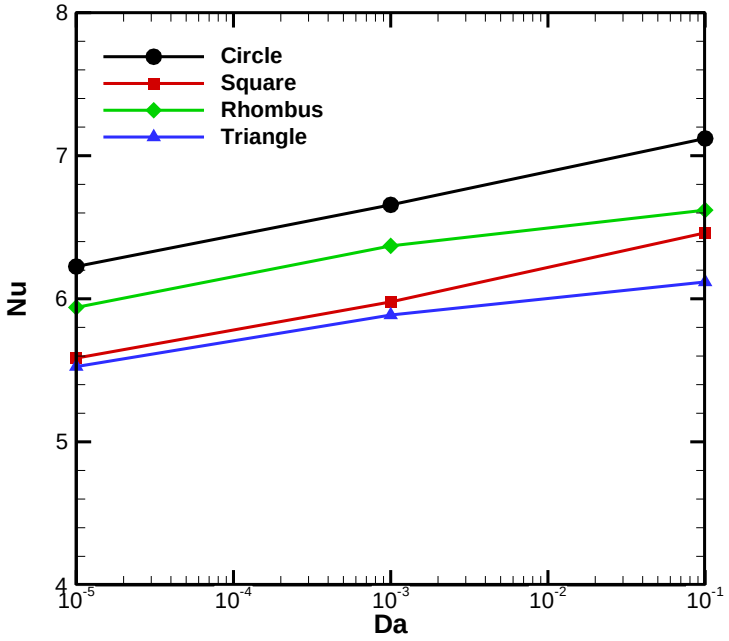

Figure (5. 41) Nu with respect to Da for different shapes of inner body at $\phi = 0.02, Ra = 10^5, Ha = 0$

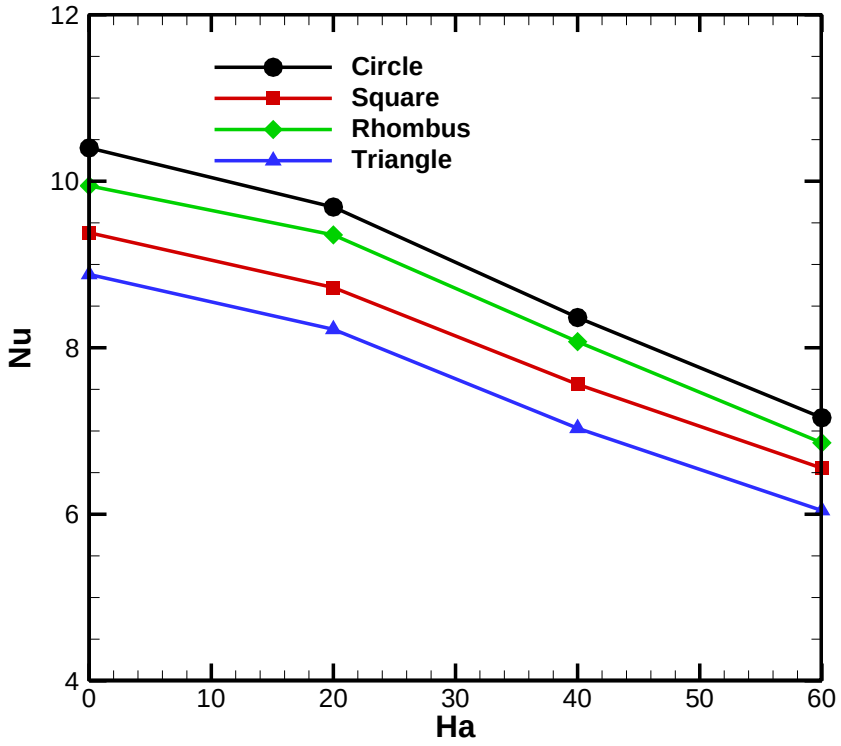

Figure (5. 42) Nusselt number with respect to Hartmann number for different shapes of inner body at $\phi = 0.02, Ra = 10^5, Da = 0.001$

Also, the influence of MHD angle on the Nusselt number is presented in Figure (5.43). Different behaviors of Nusselt number is obtained based upon the angle of magnetic field inclination angle. When $0° \leq \gamma \leq 30°$, it is observed that increasing the inclination angle of magnetic field leads to decreasing in the Nusselt number for all of the inner body shapes. When $\gamma \geq 30°$, it can be seen that the influence of angle of MHD is positive on the Nusselt number as the latter increases as the magnetic field angle increases for all of the inner body shape. It can be seen that Nusselt number for $Case\ 1 > Case\ 3 > Case\ 2 > Case\ 4$ for the entire magnetic field angle of inclination.

The influence of nanofluid loading is showed in Figure (5.44) for various inner body shapes. It can be seen that Nusselt number increases as the nanofluid loading

increases. It can be seen again that the inner body shape plays an important role in the enhancement of Nusselt number which Case 1 indicate the best case in the augmentation of heat transfer while the Case 4 record the lowest improving in Nusselt number.

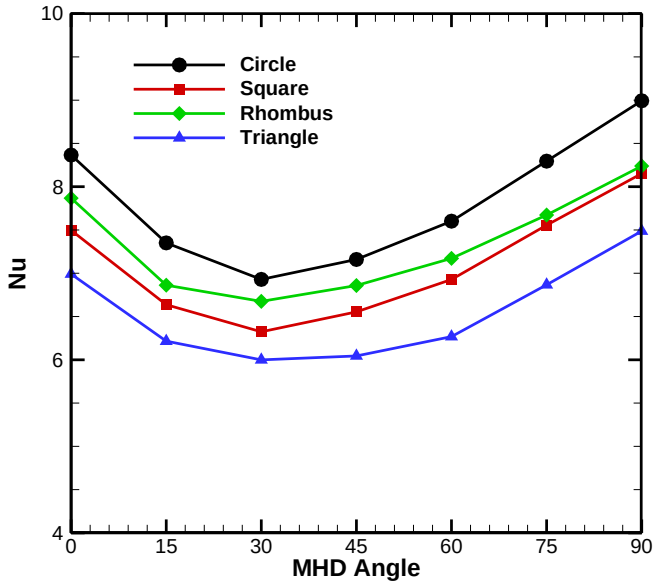

Figure (5. 43) Nu with respect to MHD Angle for different shapes of inner body at $\varphi = 0.02, Ra = 10^5,\ Da = 0.001, Ha = 60$

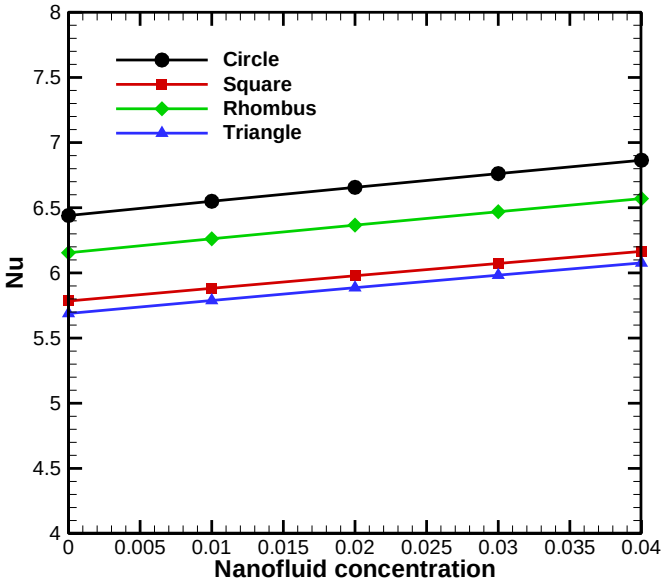

Figure (5. 44) Nu with respect to nanofluid loading for different shapes of inner body at $\varphi = 0.02, Ra = 10^5, Da = 0.001$

The impact of number of inner hot bodies on the Nusselt number is presented in Figure (5.45). It is observed that when the number of inner bodies are $No = 3$, leads to reduces the Nusselt number for all of the four cases of inner body shapes. It is noted that at low Rayleigh there is no change on Nusselt when the number of inner hot bodies for all cases are $No = 1, 2$. While the deviation (difference) in Nusselt number for $No = 1, 2$ increases as Rayleigh number increases.it is obtained that Case 1 reveals better augmentation of Nusselt number for all cases. Finally, with respect to the influence of the inner hot body location on Nusselt number is discussed in Figure (5.46) and Figure (5.47). It can be seen that when the inner hot body start moving upwards, there would be a reduction in Nusselt number for all of the shapes of inner bodies. Besides that, the Nusselt number for $Case\ 1 > Case\ 3 > Case\ 2 > Case\ 4$ in any position of inner bodies.

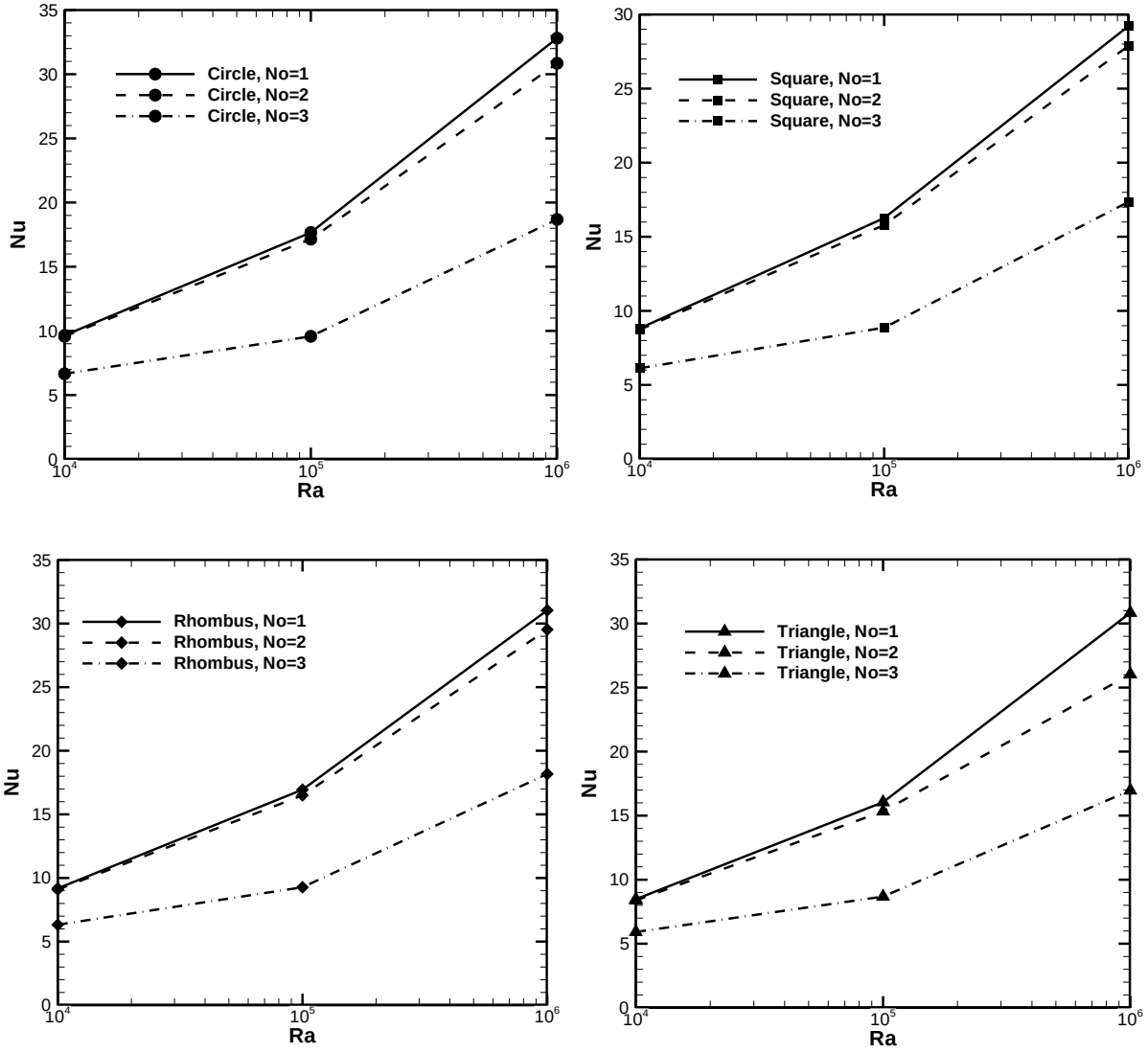

Figure (5. 45) Nu with respect to Rayleigh number for various number of inner hot bodies considering different shapes at $\varphi = 0.02, Da = 0.001, Ha = 20$

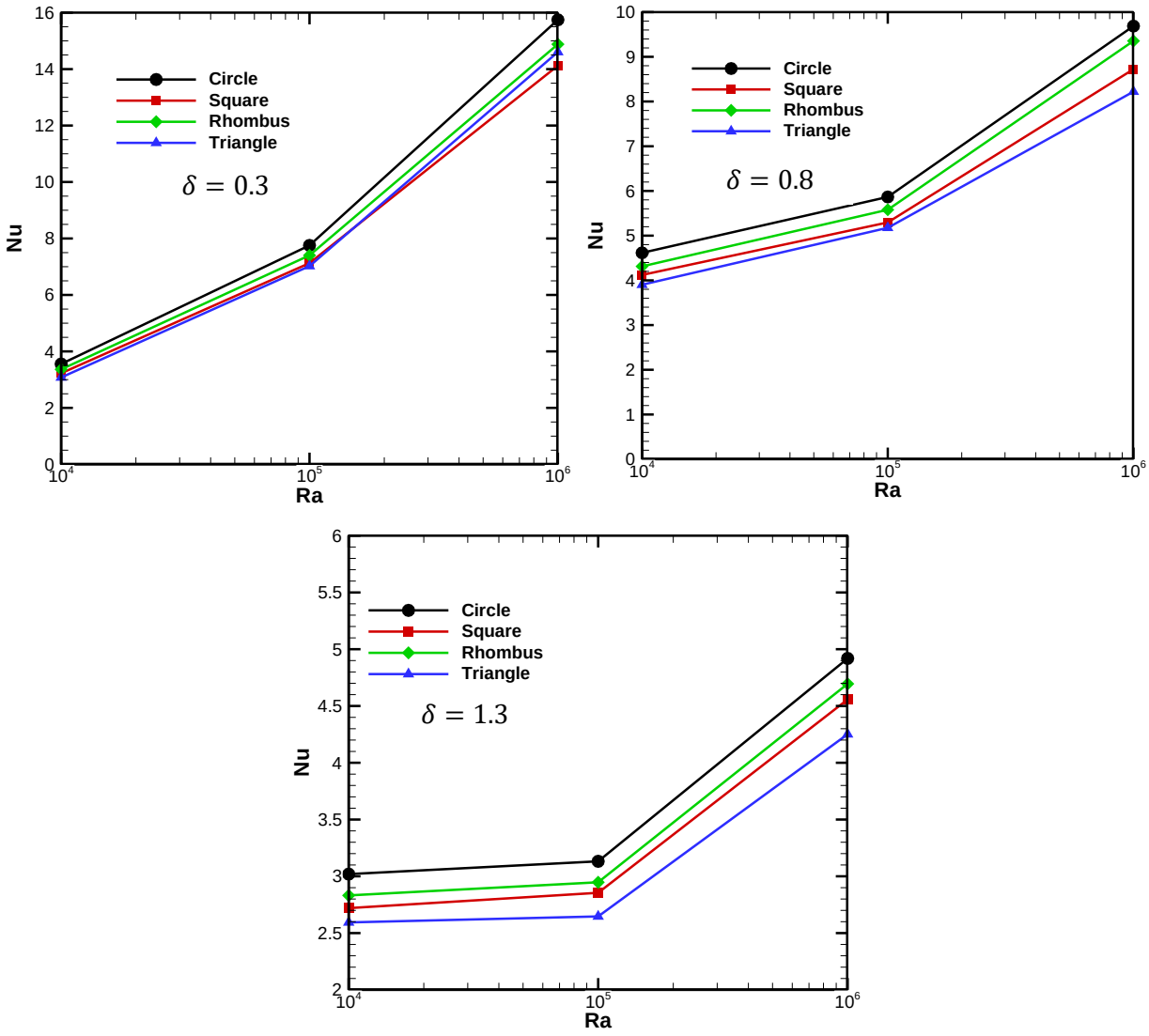

Figure (5. 46) Nusselt number with respect to Rayleigh number under various location of inner hot body considering different shapes at $\varphi = 0.02, Da = 0.001, Ha = 20$

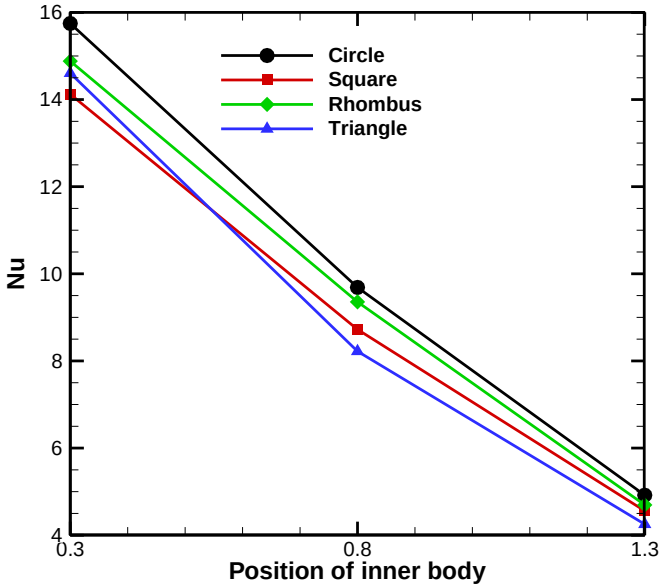

Figure (5. 47) Nusselt number with respect to various position of inner hot body considering different shapes at $\varphi = 0.02, Ra = 10^6, Da = 0.001, Ha = 20$

5.2.3. Trapezoidal Heater Attached to the Novel Enclosure

The present case is demonstrated the natural convection within the proposed enclosure considering trapezoidal heater from its bottom wall

5.2.3.1. The influence of dimensionless numbers

Firstly, the influence of Rayleigh number on streamlines (first row) and isotherms (second row) had been presented via Figure (5.48) at $Da = 0.001, Ha = 20, \gamma = 45°, \phi = 0.02, B = 0.6, E = 0.5, \delta = 0.8$. It can be seen that the streamlines contours are approximately similar in low and high Rayleigh numbers but the strength of the fluid flow is totally different. For example, it can be seen that at low Rayleigh number $[Ra = 10^4]$, the maximum stream function is $\Psi_{max} = 0.535162$ but it increases into $\Psi_{max} = 22.7814$ when Rayleigh number increases into $[Ra = 10^6]$. The physical reason behinds this is due to increasing of the buoyancy force and natural convection heat transfer as Rayleigh number increases. On the other side, it can be seen that the influence of Rayleigh number on isotherms contours is strong which completely change the isotherms lines distributions. For example, as Rayleigh number increases from $[Ra = 10^4]$ into $[Ra = 10^6]$, the isotherms changes into more curved lines which reflect the heat transfer is due to convection mode after it was due to conduction mode at low Rayleigh number.

Secondly, the influence of Darcy number on streamlines (first row) and isotherms (second row) had been presented via Figure (5.49) at $Ra = 10^6, Ha = 20, \gamma = 45°, \phi = 0.02, B = 0.6, E = 0.5, \delta = 0.8$. It can be seen that as Darcy number increases, the maximum stream function on the left layer which consists of nanofluid saturated with porous media increases which reflect the increasing of the fluid flow strength. For example, increasing Darcy numbers from $Da = 1e-5$ into $Da = 0.1$, attends to increase the fluid flow strength from $\Psi_{min} = 0.62000$ into

$\Psi_{min} = 16.2296$ due to increase the buoyancy force and natural convection rate. So, the increasing Darcy number leads to make the isotherms line mote curved which indicate the heat is transfer is due to convection mode not due to conduction mode at low Darcy number.

Lastly, the influence of Hartmann number on streamlines (first row) and isotherms (second row) had been presented via Figure (5.50) at $Ra = 10^6, Da = 0.001, \gamma = 45°, \phi = 0.02, B = 0.6, E = 0.5, \delta = 0.8$. It can be seen that the influence of Hartmann number is quietly inverse to the influence of both Rayleigh and Darcy numbers. The relation is that as Hartmann number increases, the fluid flow strength decreases. For example, increasing of Hartmann number from $Ha = 30$, into $Ha = 60$, leads to reduce the maximum stream function from $\Psi_{max} = 20.5028$ into $\Psi_{max} = 10.1917$. This is due to increasing of the magnetic force as Hartmann number increases which resists the fluid flow strength. It can be seen that as Hartmann number increases, more inner cells formed within the enclosure which indicate the reduction of the fluid flow strength. Also, the Hartmann number is highly effects on isotherms lines and change their shape.

5.2.3.2. The influence of magnetic field angle

The present section illustrates the influence of magnetic field applied in horizontal, tilted and vertical direction within the range $0° \leq \gamma \leq 90°$ at low and high Rayleigh numbers as indicate in Figure (5.51). It can be seen that, at low Rayleigh number $[Ra = 10^4]$, the maximum stream function increases from $\Psi_{max} = 0.472695, \Psi_{max} = 0.481297, \Psi_{max} = 0.582529, \Psi_{max} = 0.626590$ as the magnetic field angle increases from horizontal into normal direction i.e., $\gamma = 0°, 30°, 60°, 90°$. In this way, increasing of the magnetic field inclination angles increases the fluid flow strength. For example, the rate of fluid flow strength improves by 32.55% as the magnetic field angle increases from $\gamma = 0°$ into $\gamma = 90°$.

While with increasing of Rayleigh number into [$Ra = 10^6$], the magnetic field angle increasing leads to increase the fluid flow strength till it reaches critical angle value which is $\gamma = 60°$ after this value, the influence of angle of MHD is negligible. Before the critical value, the rate of improving in the stream function when the angle of MHD increases from $\gamma = 0°$ into $\gamma = 60°$ is about 15.57%. However, the influence of angle of inclination on isotherms contours as indicated in Figure (5.52) refers that the impact is very small.

5.2.3.3. The influence of the trapezoidal heater length

The influence of the length of the trapezoidal heater on the streamlines of the fluid flow (top images) and isotherms lines (bottom images) at $Ra = 10^5, Da = 0.001, Ha = 20, \gamma = 45°, \phi = 0.02, E = 0.5, \delta = 0.8$ had been presented via Figure (5.53). It can be seen that increasing the dimensionless length from $B = 0.4$ into $B = 0.6$, leads to increasing the maximum stream function from $\Psi_{max} = 5.13343$ into $\Psi_{max} = 5.16149$ which make the rate of improving the fluid flow strength by 0.67% which is slight small. More increasing of the dimensionless length beyond $B = 0.6$ leads to reduction in the fluid flow strength in spite it is very small reduction. It is worthy to mention that as the increasing the dimensionless length of the trapezoidal heater attends to form four inner cells closed to it which is the major reason beyond the reduction of the fluid flow strength as the length increases. The influence of the trapezoidal heater length on the isotherms is that more fluids heated in the bottom region.

5.2.3.4. The influence of inner body position

The present paragraph demonstrates the influence of position of inner heated circular cylinder under low and high Rayleigh numbers on the streamlines and isotherms as shown in Figure (5.54).

Firstly, with respect to low Rayleigh number [$Ra = 10^4$], when the heated circular cylinder is located closed to the trapezoidal heater i.e., in the bottom of the enclosure at $\delta = 0.3$, the fluid flow strength is at its lowest value as indicated by its maximum stream function value is $\Psi_{max} = 0.402447$. It can be seen that there is two inner cells formed on each side of the circular body. When the cylinder moved up till it reaches the center of the enclosure at $\delta = 0.8$, the maximum stream function increases into $\Psi_{max} = 0.535162$ which increases the fluid flow strength. After that more increasing of the circular cylinder position till it reaches $\delta = 1.3$ is not recommended as this action reduces the fluid flow strength but it still stronger more than its location at $\delta = 0.3$.

Secondly, with increasing of Rayleigh number, the fluid flow strength increases for all positions of the inner circular cylinders. Location of the cylinder closed to the trapezoidal heater at $\delta = 0.3$ recorded the highest fluid flow strength as the maximum stream function is $\Psi_{max} = 26.1282$. It can be seen that there is some of porous media penetrate into the right layers which helps in the increasing of the fluid flow strength in the right layer. Movement of the inner cylinder upwards till it reaches the center of the enclosure at $\delta = 0.8$, leads to reduce the fluid flow strength into $\Psi_{max} = 22.7814$. It can be noticed that there is some nanofluid penetrate into right layer. More increasing in the location of the inner cylinder till it reaches $\delta = 1.3$, leads to increases the fluid flow strength in a comparison with that at the center of the enclosure at $\delta = 0.8$ but it still lower than that in the bottom of the enclosure at $\delta = 0.3$.

With respect to the isotherms and how the position of the inner cylinder effect on it. It can be seen that location of the cylinder closed to the trapezoidal heater leads to combine the heated lines from the trapezoidal and cylindrical heater while as the distance between the cylindrical heater and the trapezoidal heater increases, leads to change the isotherms line counters significantly.

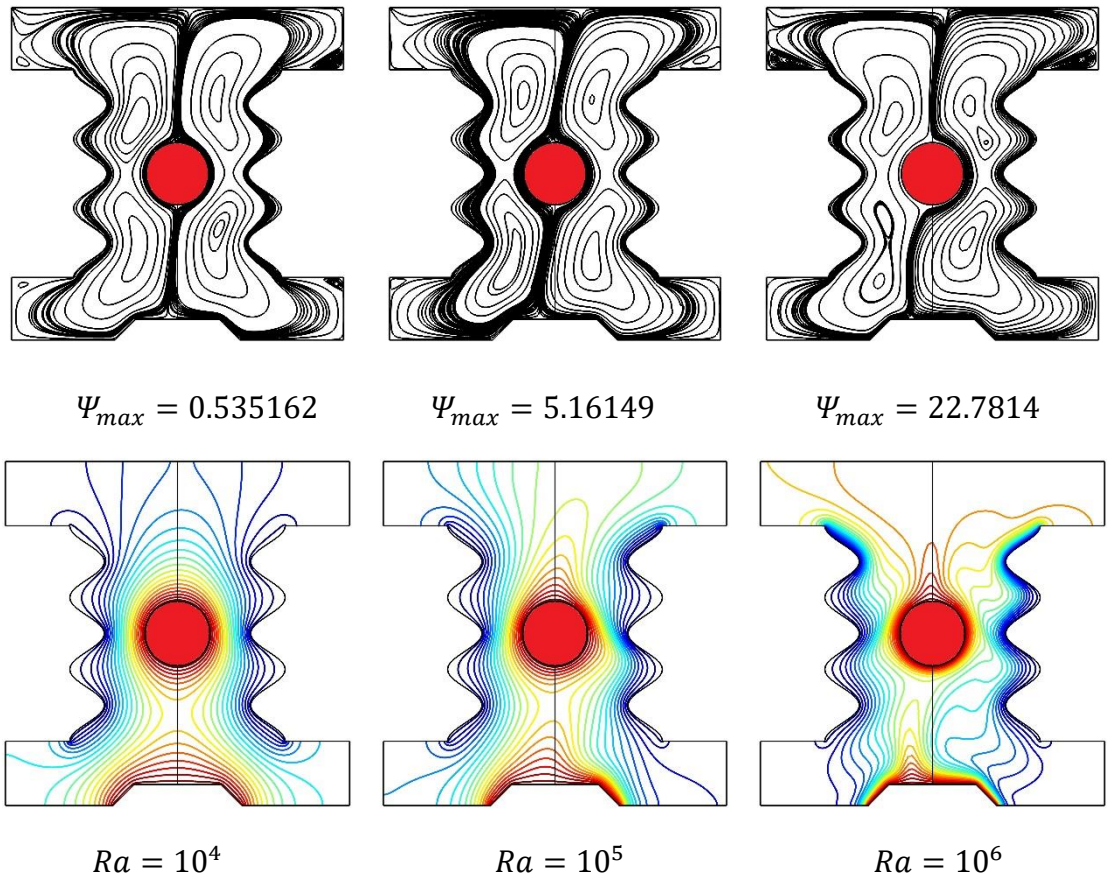

Figure (5. 48) Streamlines (top image) and isotherms (bottom image) contours under various Rayleigh numbers at $Da = 0.001, Ha = 20, \gamma = 45°, \phi = 0.02, B = 0.6, E = 0.5, \delta = 0.8$

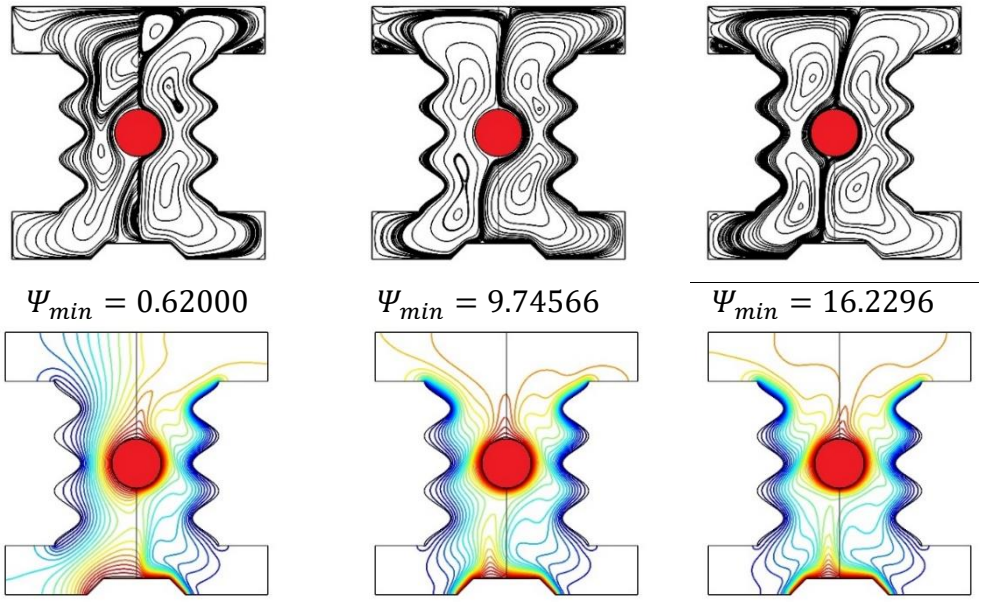

Figure (5. 49) Streamlines (top image) and isotherms (bottom image) contours under various Darcy numbers at $Ra = 10^6, Ha = 20, \gamma = 45°, \phi = 0.02, B = 0.6, E = 0.5, \delta = 0.8$

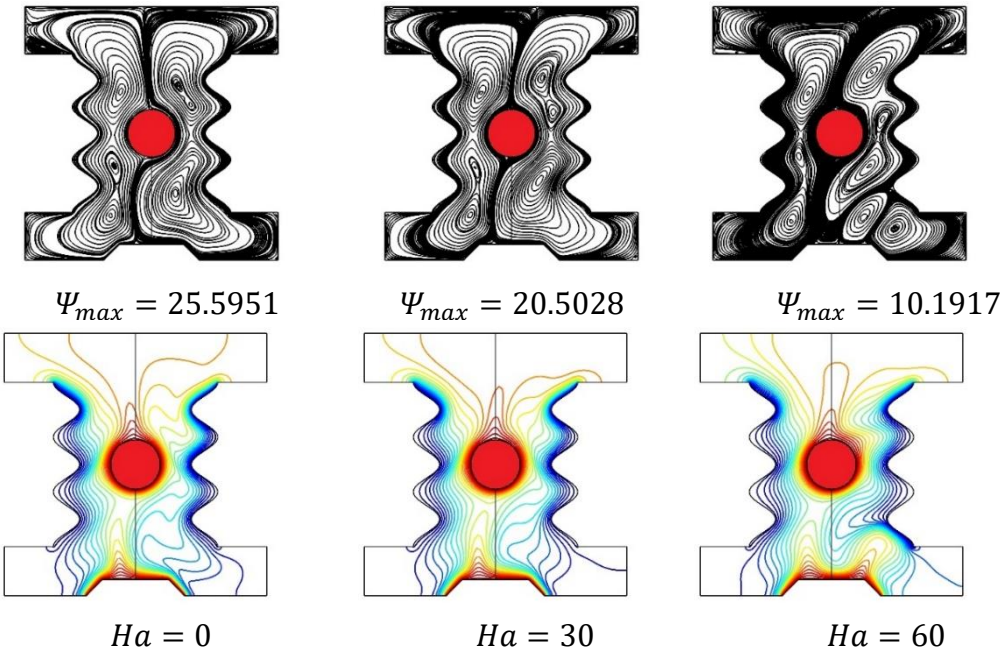

Figure (5. 50) Streamlines (top image) and isotherms (bottom image) contours under various Hartmann numbers at $Ra = 10^6, Da = 0.001, \gamma = 45°, \phi = 0.02, B = 0.6, E = 0.5, \delta = 0.8$

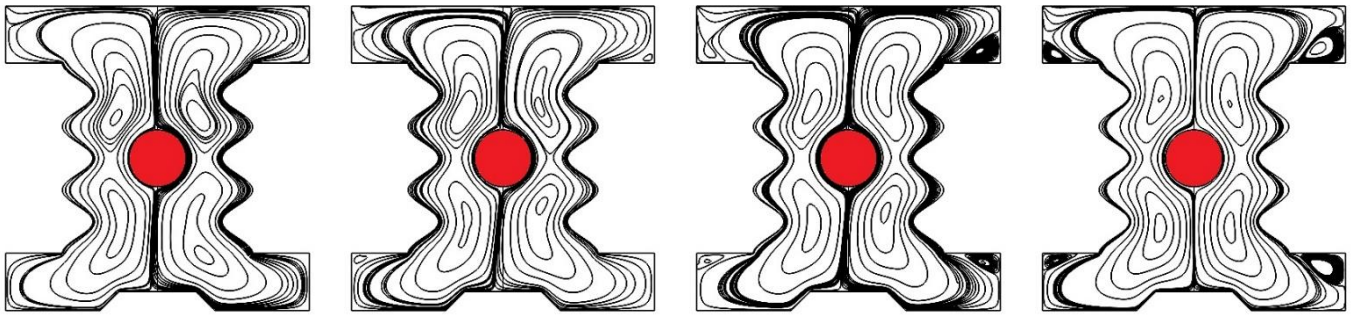

$\Psi_{max} = 0.472695$ $\Psi_{max} = 0.481297$ $\Psi_{max} = 0.582529$ $\Psi_{max} = 0.626590$

$\gamma = 0$ $\gamma = 30$ $\gamma = 60$ $\gamma = 90$

$[Ra = 10^4]$

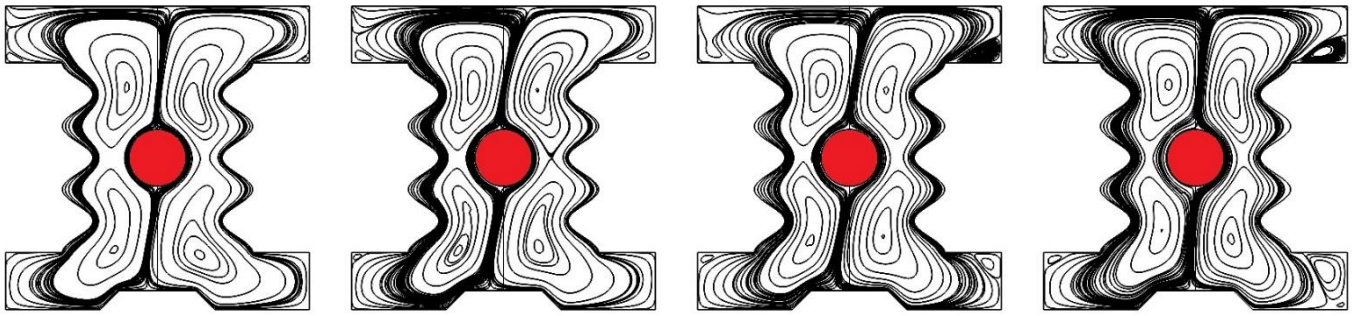

$\Psi_{max} = 5.12492$ $\Psi_{max} = 4.85360$ $\Psi_{max} = 5.59623$ $\Psi_{max} = 6.11313$

$\gamma = 0$ $\gamma = 30$ $\gamma = 60$ $\gamma = 90$

$[Ra = 10^5]$

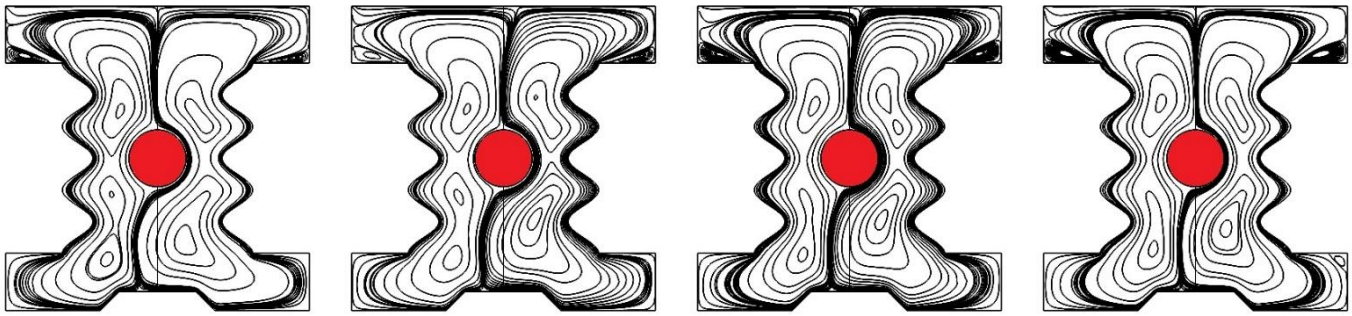

$\Psi_{max} = 20.3339$ $\Psi_{max} = 21.6852$ $\Psi_{max} = 23.4805$ $\Psi_{max} = 23.3087$

$\gamma = 0$ $\gamma = 30$ $\gamma = 60$ $\gamma = 90$

$[Ra = 10^6]$

Figure (5. 51) Streamlines contours under various magnetic field inclination angle at law and high Rayleigh numbers at $Da = 0.001, Ha = 20, \gamma = 45°, \phi = 0.02, B = 0.6, E = 0.5, \delta = 0.8$

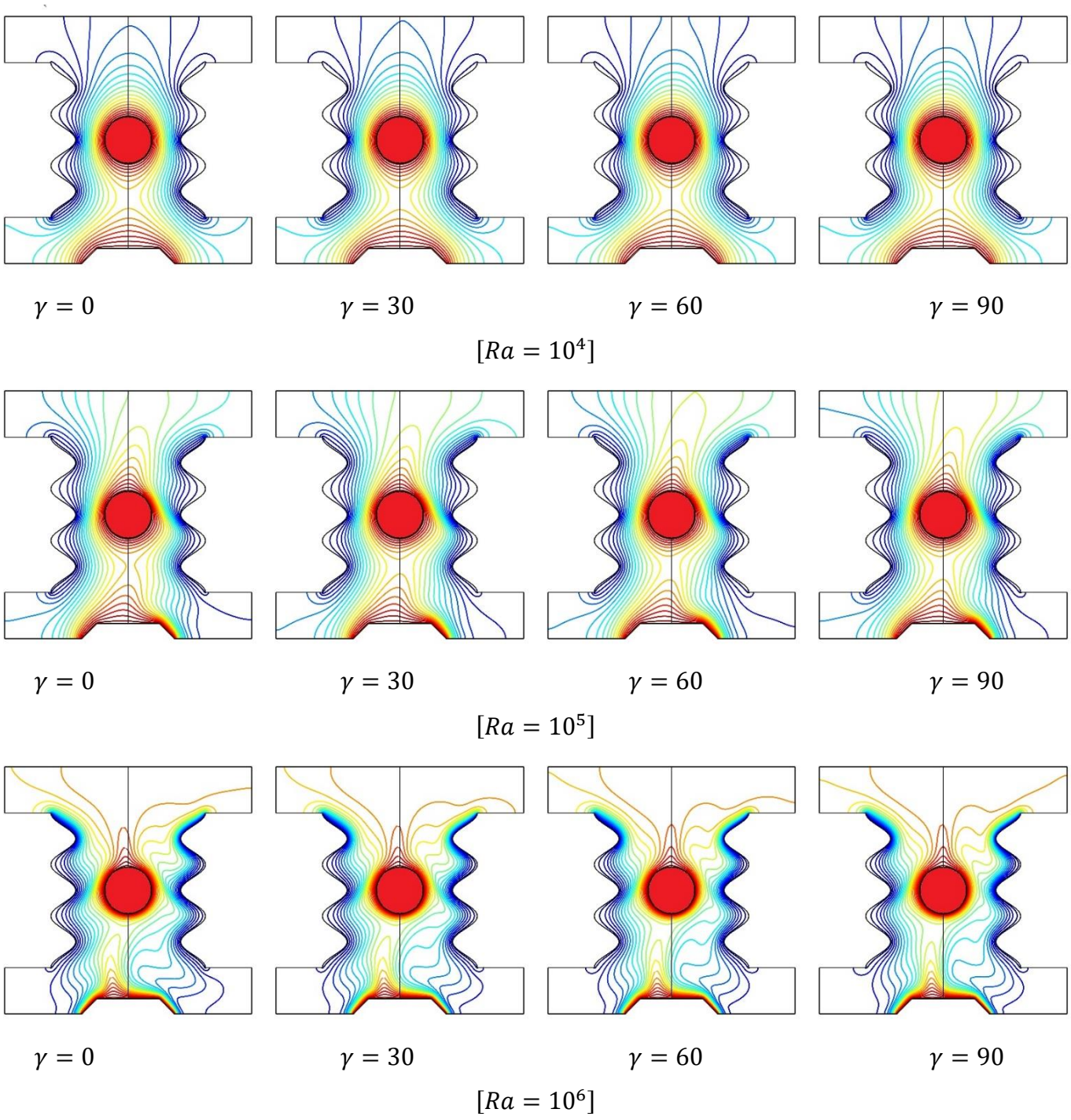

Figure (5. 52) Isotherms contours under various magnetic field inclination angle at law and high Rayleigh numbers at $Da = 0.001, Ha = 20, \gamma = 45°, \phi = 0.02, B = 0.6, E = 0.5, \delta = 0.8$

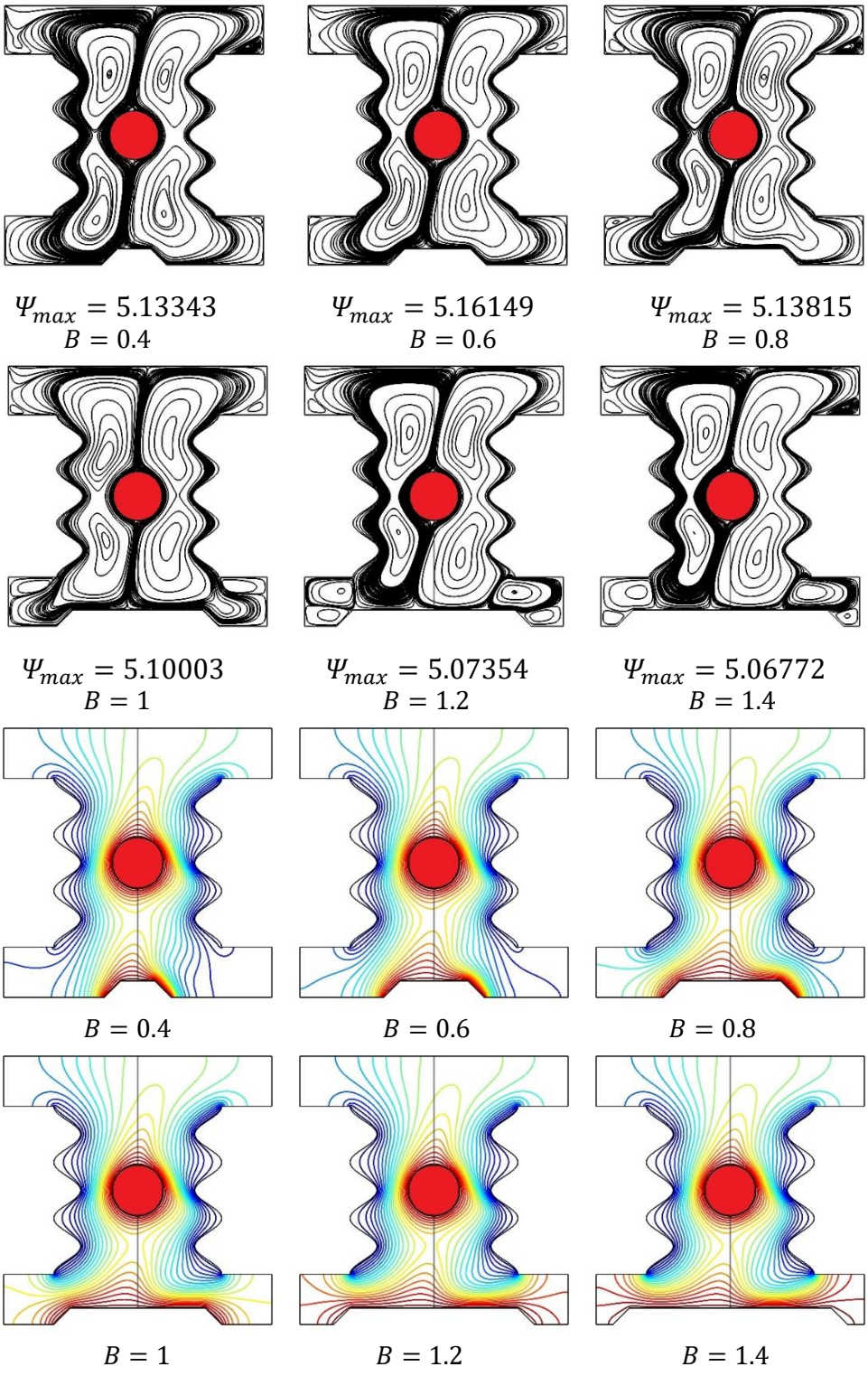

Figure (5. 53) Streamlines (top image) and Isotherms (bottom image) contours under different trapezoidal heater length at $Ra = 10^5, Da = 0.001, Ha = 20, \gamma = 45°, \phi = 0.02, E = 0.5, \delta = 0.8$

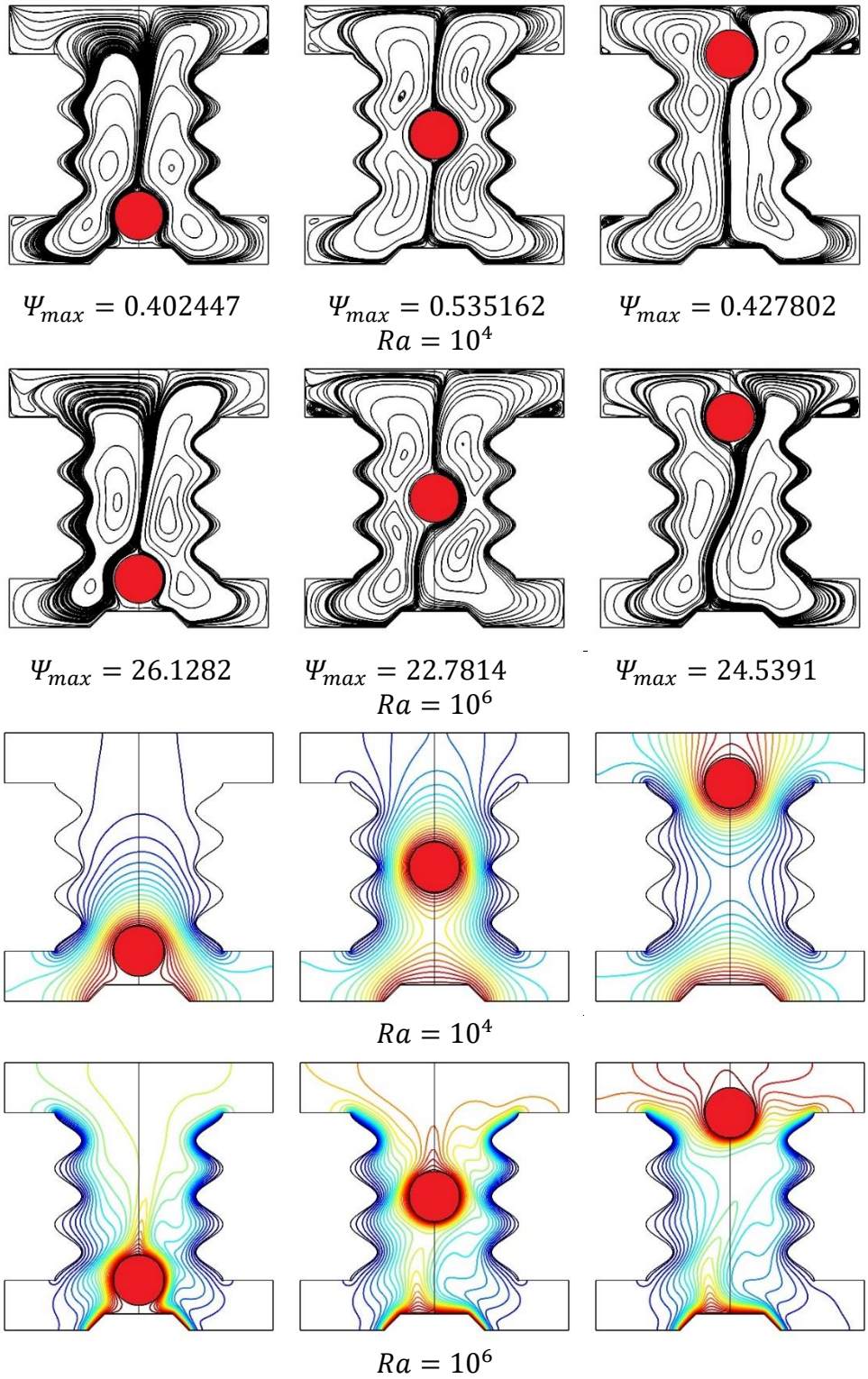

Figure (5. 54) Streamlines (top image) and Isotherms (bottom image) contours under various location of circular heater at $Ra = 10^6, Da = 0.001, Ha = 20\ \gamma = 45°, \phi = 0.02, E = 0.5, \delta = 0.8$

5.2.3.5. The influence of number of undulations under various MHD angle

Figures (5.55-5.56) demonstrate the influence of number of undulations along with magnetic field angle on the streamlines and isotherms, respectively at $Ra = 10^6, Da = 0.001, Ha = 20, \phi = 0.02, E = 0.5, \delta = 0.8.$

With respect to Figure (5.55) when the number of undulation is $N = 1$, it can be seen that increasing the inclination angle of magnetic field leads to increasing the fluid flow strength. This is when the magnetic field direction is on the same direction of fluid flows. For example, when the magnetic field is applied in the horizontal direction, the maximum stream function $\Psi_{max} = 10.3114$ while it increases into $\Psi_{max} = 16.0870$ when the angle of inclination is applied in the vertical direction which enhance the fluid flow strength by 56%. This behavior is repeated for all values of number of undulations but at lower strength of the fluid flows.

It can be seen that applied magnetic field horizontally does not change the fluid flow strength so much for all values of number of undulations $[1 \leq N \leq 5]$. While applied magnetic field in the vertical direction leads to reduces slightly the fluid flow strength with increasing the number of undulations. Also, there is different behavior when the magnetic field applied in the incline direction as the fluid flow strength sometimes increases and decreases. this is depends on the complexity of the enclosure shape which leads to form many vortices that changed due to the applied magnetic field direction and the number of undulations.

With respect to Figure (5.56), it can be seen that number of undulation parameter is more influencer on the temperature distribution more than the magnetic field angle.

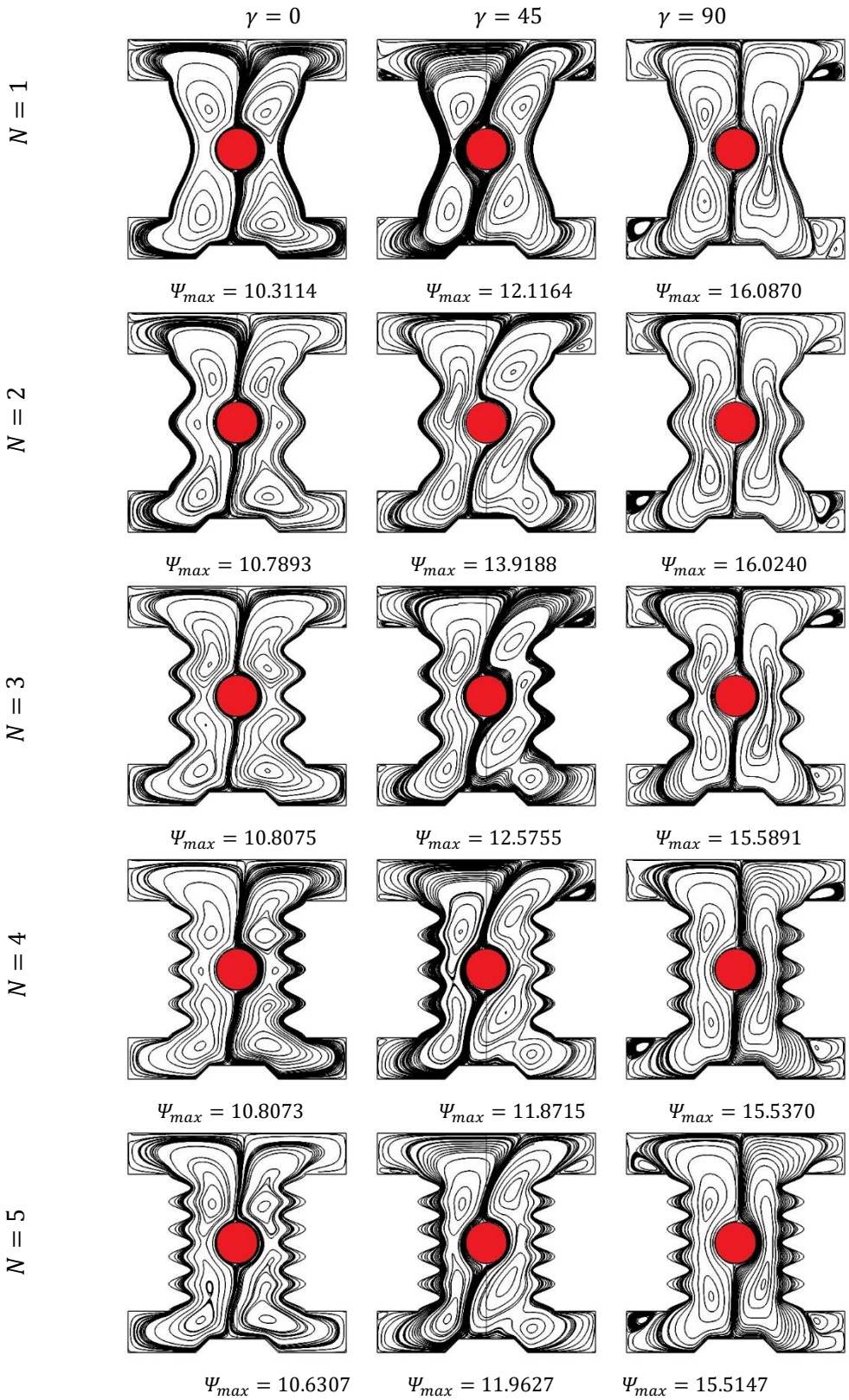

Figure (5. 55) Streamlines contours under number of undulations and different MHD inclination angle at $Ra = 10^6, Da = 0.001, Ha = 20, \phi = 0.02, E = 0.5, \delta = 0.8$

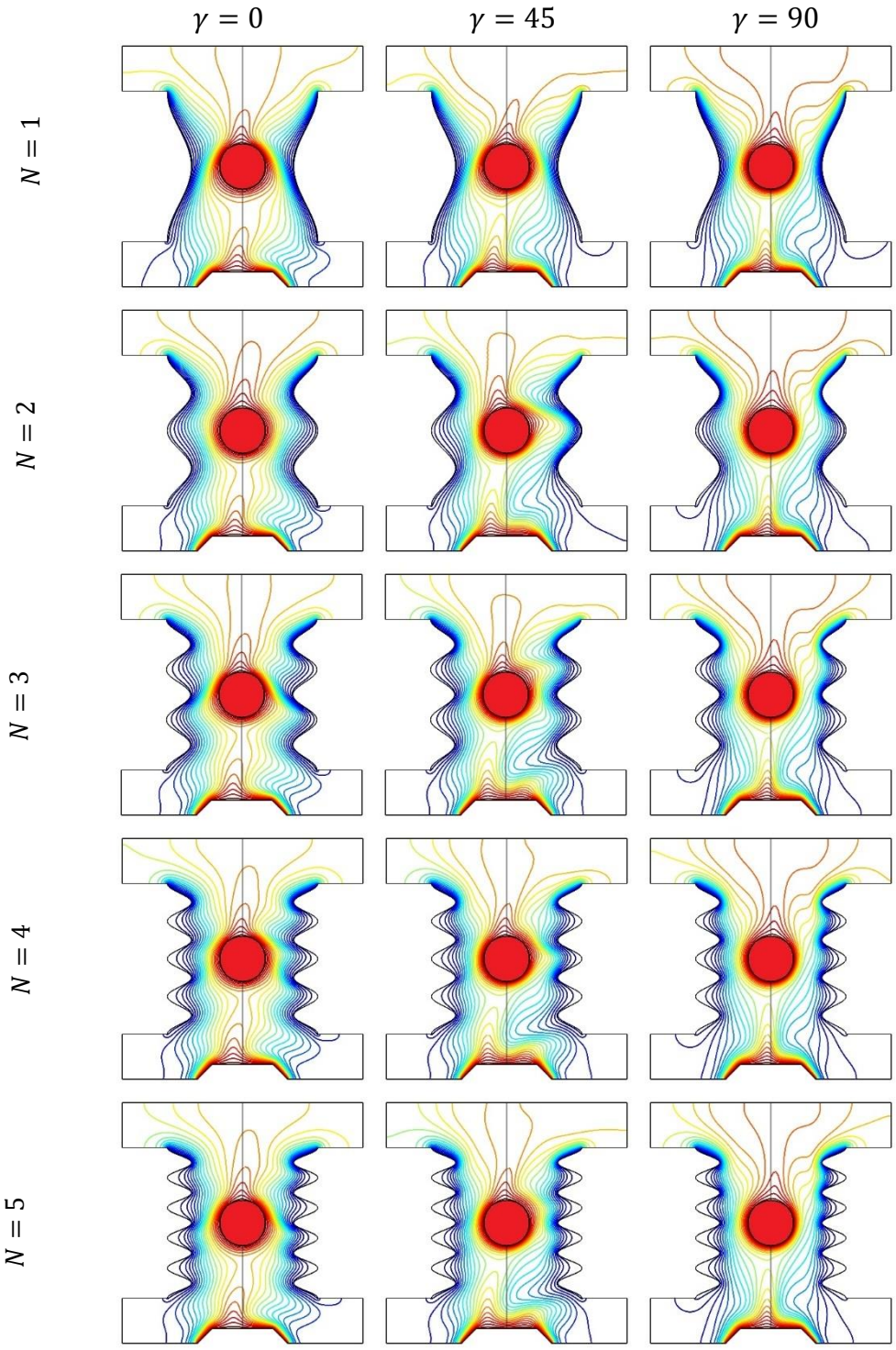

Figure (5. 56) Isotherms contours under number of undulations and different MHD inclination angle at $Ra = 10^6, Da = 0.001, Ha = 20, \phi = 0.02, E = 0.5, \delta = 0.8$

5.2.3.6. Nusselt Number Results

Firstly, the influence of inner circular position under various Rayleigh number, Darcy number, Hartmann number, MHD inclination angle had been presented via Figures (5.57-5.58). With respect to Figure (5.57) which demonstrates the variation of Nusselt number versus Rayleigh number considering three different positions of the inner cylinders. It can be seen that increasing of Rayleigh number increases Nusselt number which enhance the heat transfer rate. This behavior is takes place for each position of inner cylinder. However, it can be seen that for Rayleigh number values $[Ra = 10^4, 10^5]$ center location of the inner circular cylinder reveals better augmentation on heat transfer followed by top location while the bottom location gives the lowest heat transfer rate. At high value of Rayleigh number $[Ra = 10^6]$ the center location is still recommended in heat transfer augmentation followed by bottom location and the top. The influence of Darcy number under various location of inner cylinder on Nusselt number had been examined via Figure (5.58). It can be seen that the position of inner body in addition to the Darcy number are still effect on heat transfer enhancement. Again, the center position of the inner circular cylinder reveals the best augmentation in heat transfer while the top location gives the lowest rate in heat transfer. Considering the important impact of Hartmann number on Nusselt number which is presented via Figure (5.59) which emphasize that increasing Hartmann number leads to an obvious reduction in Nusselt number which it is inverse relation to the impact of Rayleigh and Darcy number. It can be seen that the position of the inner body is still effect on the bettering of the thermal rate of heat transfer. As it is noted that the moving of the inner circular body to the top of the enclosure gives the lowest enhancement in heat transfer while for the bettering of heat transfer, the center position of the inner body is recommended.

With respect to the influence of magnetic field angle which is showed in Figure (5.60) considering three different locations. It can be seen that again the center location reveals better heat transfer followed by the bottom position while the lowest case is where the cylinder kept at the top of the enclosure. However, the influence of magnetic field angle of Nusselt number value is so small in a comparison with the others mentioned parameters. To elaborate with the influence of magnetic field angle, its effect on Nusselt number under various Hartmann number had been illustrated in Figure (5.61) which clearly shows that as the Hartmann number increases, the magnetic field angle shows various effect on Nusselt number. For example, at $Ha = 20$, there is slight change of Nusselt number with magnetic field angle while as the Hartmann number increases into $Ha = 40$ and $Ha = 60$, there is ignoring impact of magnetic field angle on Nusselt number when the magnetic field applied in the horizontal direction and when increasing the angle of MHD into $\gamma = 30°$. However, applying the magnetic field in the inclined direction by increasing the magnetic field angle beyond $\gamma = 30°$ till reaching the vertical direction leads to increases gradually the rate of heat transfer. Besides, the influence of the trapezoidal heater location in the center region, right region (nanofluid layer) and the left region (nanofluid-porous media) on Nusselt number along the cylinder had been discussed in Figure (5.62) considering various magnetic field inclination angle. It can be seen that location of the trapezoidal heater in the center of the enclosure reveals the lowest augmentation in heat transfer while moving the trapezoidal heater in the right region (nanofluid layer) leads to the best case in heat transfer bettering this is due to increasing the kinetic energy of the internal molecules of the nanofluid which increase the thermal energy of the fluid as there is no porous media which may be work like resistance to the fluid movement. There is slight impact of magnetic field angle on the Nusselt number of circular cylinder.

Finally, the influence of magnetic field angle under various number of undulations had been revealed via Figure (5.63) which explains that when the magnetic field is applied in the horizontal direction ($\gamma = 0$), Nusselt number is in its best case when the number of undulation is $N = 3$. It is worthy to mention that as the magnetic field inclination angle increases, the Nusselt number increases for all of the number of undulations. However, Nusselt number will be at its maximum value when the magnetic field applied in the vertical direction.

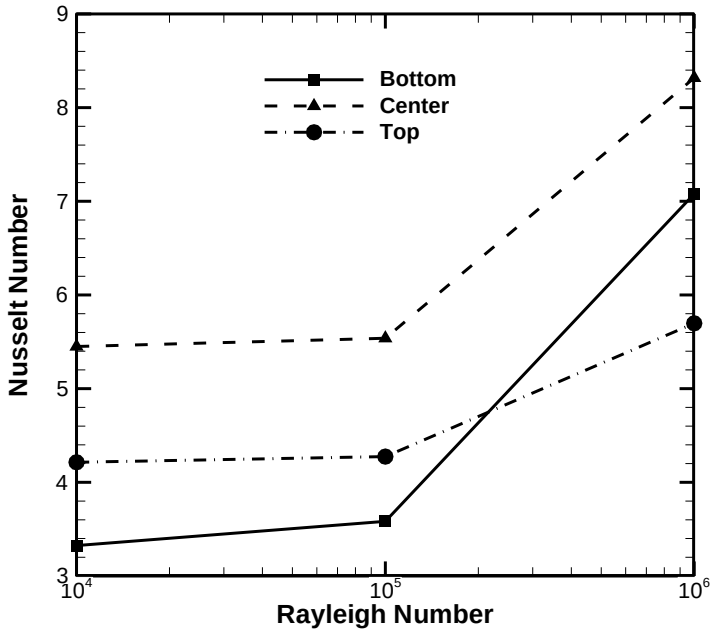

Figure (5. 57) Variation of Nusselt number along the circular cylinder various Rayleigh number considering different location of inner circular cylinder

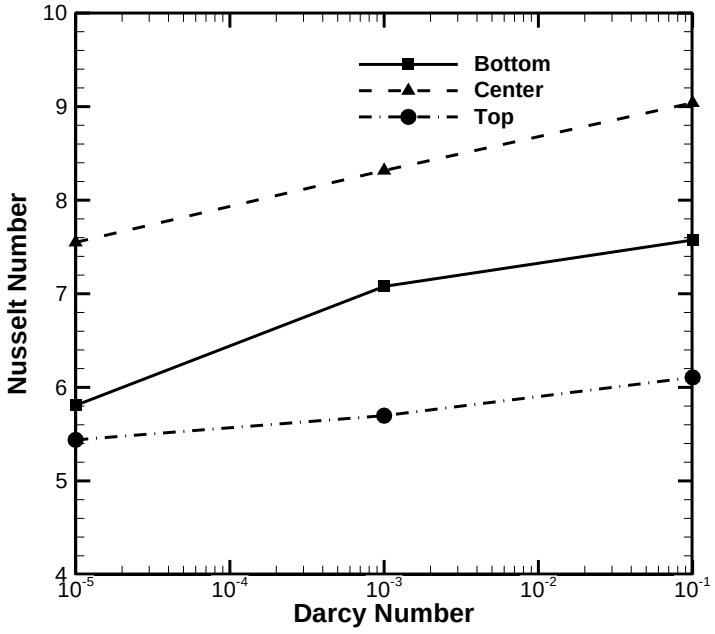

Figure (5. 58) Variation of Nusselt number along the circular cylinder various Darcy number considering different location of inner circular cylinder

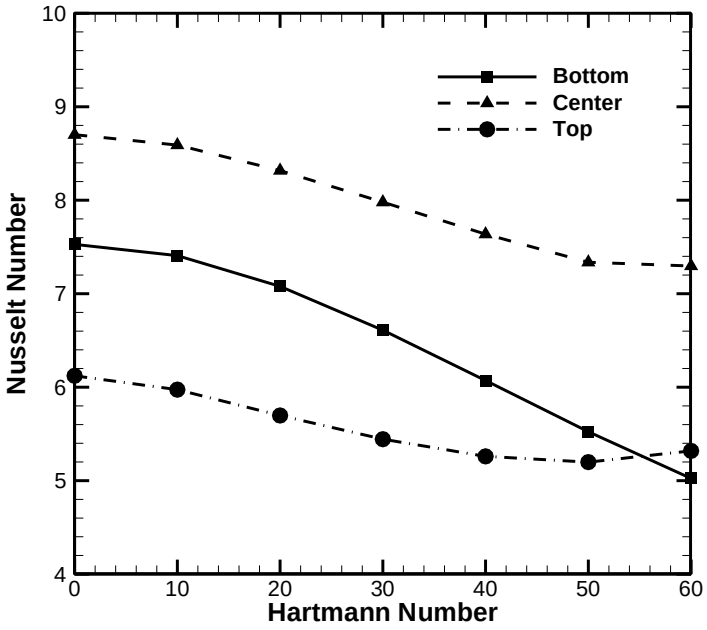

Figure (5. 59) Variation of Nusselt number along the circular cylinder various Hartmann number considering different location of inner circular cylinder

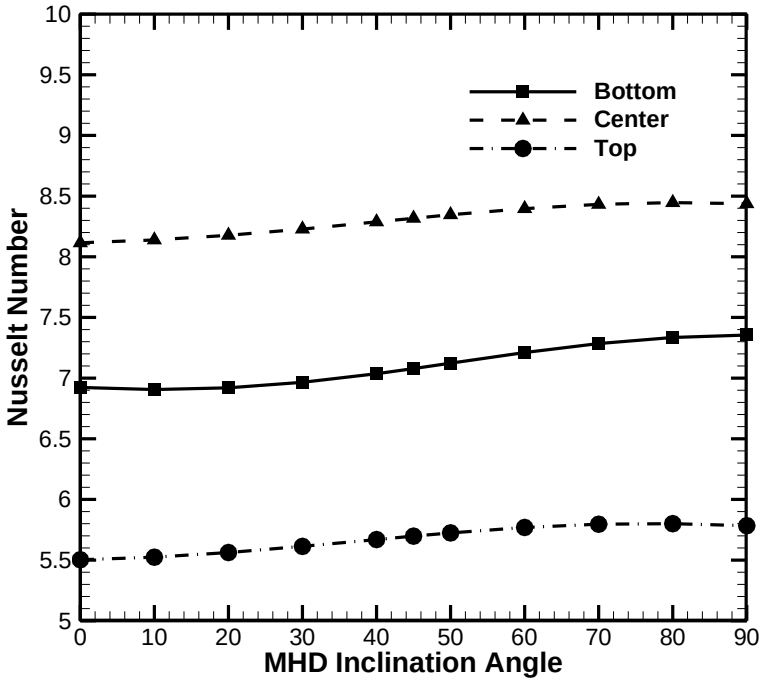

Figure (5. 60) Variation of Nusselt number along the circular cylinder various MHD inclination angle considering different location of inner circular cylinder

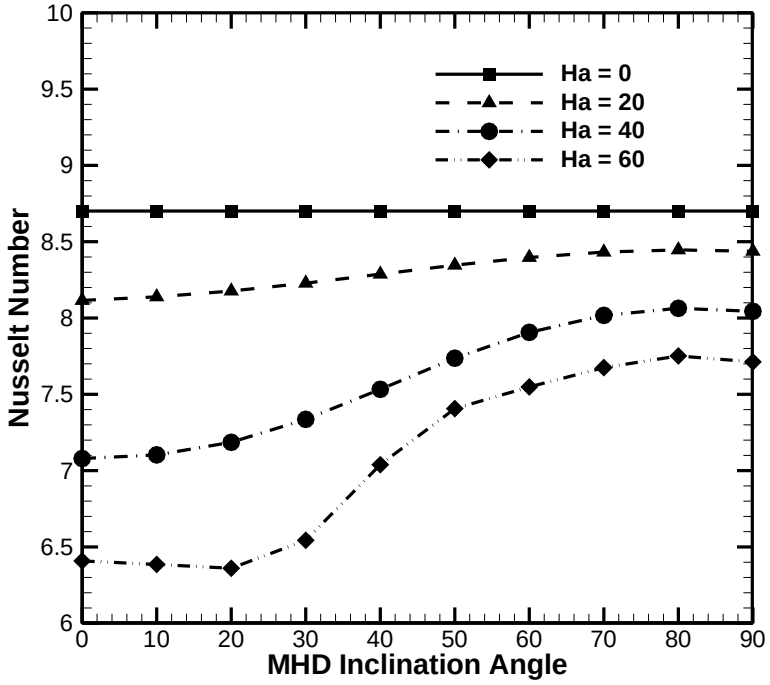

Figure (5. 61) Nu vs MHD inclination angle for various Hartmann number when the cylinder at the center at $Ra = 10^6$

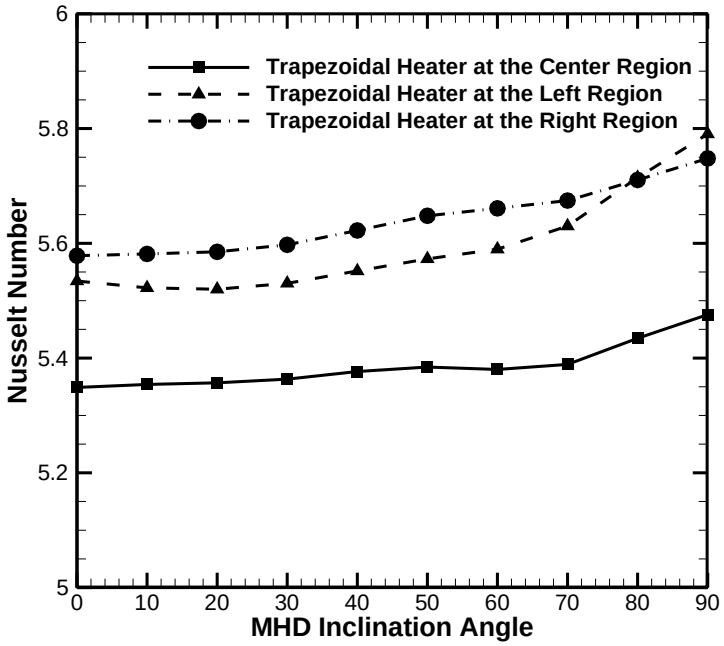

Figure (5. 62) Nusselt number along cylinder versus MHD inclination angle considering different position of the trapezoidal heater

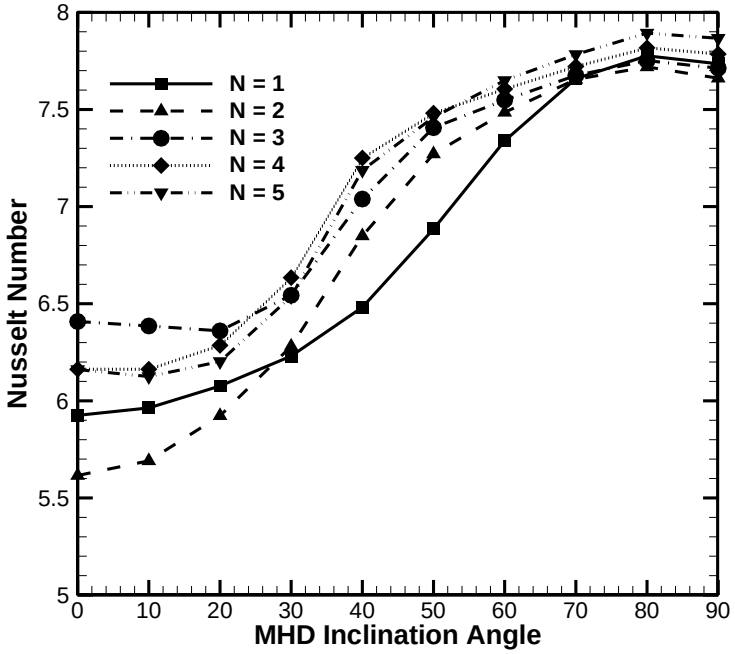

Figure (5. 63) Nusselt number along cylinder versus MHD inclination angle considering different number of undulations when the trapezoidal heater is located at the center region

5.2.4.Natural Convection within different patterns of wavy walls

In this section, the influence of various physical in addition to the geometrical dimensionless parameters on fluid flow strength and heat transfer will be discussed in full-details.

5.2.4.1. The influence of number of undulations

In this section the influence of number of undulations $(1 \leq N \leq 4)$ considering four different cases of wavy patterns on streamlines and isotherms with and without magnetic field had been presented in Figures (5.64-5.67).

Firstly, considering the absence of magnetic field to examine the influence of number of undulations along with the impact of wavy shape patterns on fluid flow strength and isotherms is presented via Figures (5.64-5.67). So, regarding the streamlines as shown in Figure 5.64, it, may be noted that when the number of undulations is $(N = 1)$, Case 3 reveals the highest strength in fluid flow as its maximum stream function $|\Psi_{max}| = 34.229$ while Case 2 reveals the lowest fluid flow strength as its maximum stream function $|\Psi_{max}| = 30.1766$ which make Case 3 better than Case 2 by 13.42%. It can be seen that increasing the number of undulations beyond $(N = 1)$ leads to make the influence of wavy patterns is negligible. However, increasing the number of undulations leads to decreasing the fluid flow strength for most of the cases as the area of the wall increases which makes the resistance of internal wavy surfaces increases and resist the movement of nanofluid as its kinetic energy decreases. On the other side, the influence of number of undulations and wavy patterns on isotherms are demonstrated via Figure 5.65. It can be seen that the hottest region is on the top area of the enclosure as it denser while the cold isotherms lines are on the lower side of the enclosure. Besides, it can

be seen that the wavy patterns completely change the distribution of isotherms lines in a comparison with the number of undulations.

Secondly, considering the existence of magnetic field to examine the influence of number of undulations along with the impact of wavy shape patterns on fluid flow strength and isotherms is presented via Figures (5.66-5.67). It can be seen for Figure (5.66) that the magnetic field at ($Ha = 60$), an obvious reduction for all of the cases of wavy patterns and number of undulations. For example, if a comparison had been made between the stream function with and without magnetic field i.e., at $Ha = 0$ and $Ha = 60$, respectively considering Case 1. It is an obvious the magnetic field reduces the stream function by 48.95%. So, it can be seen that the impact of magnetic field on the fluid flow strength is higher than the impact of wavy patterns and the number of undulations. It can be seen as illustrated in Figure (5.67) that the magnetic field change the distribution of isotherms obviously in a comparison in the case of absence of the magnetic field.

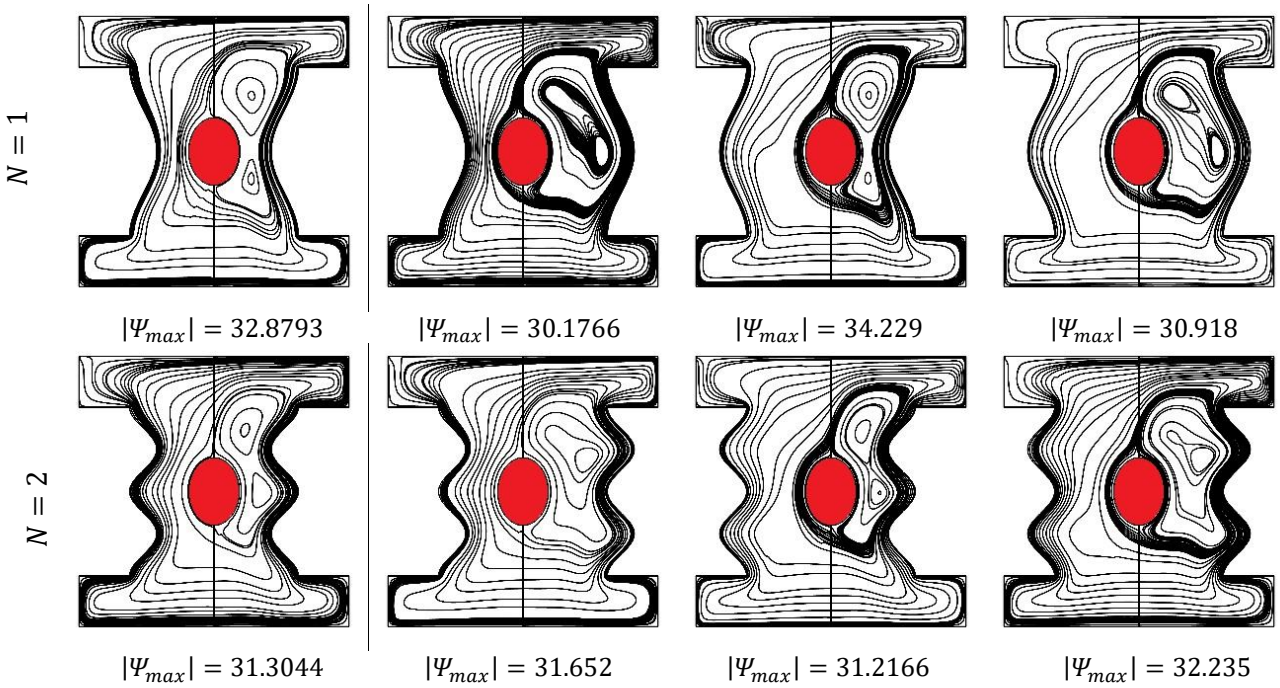

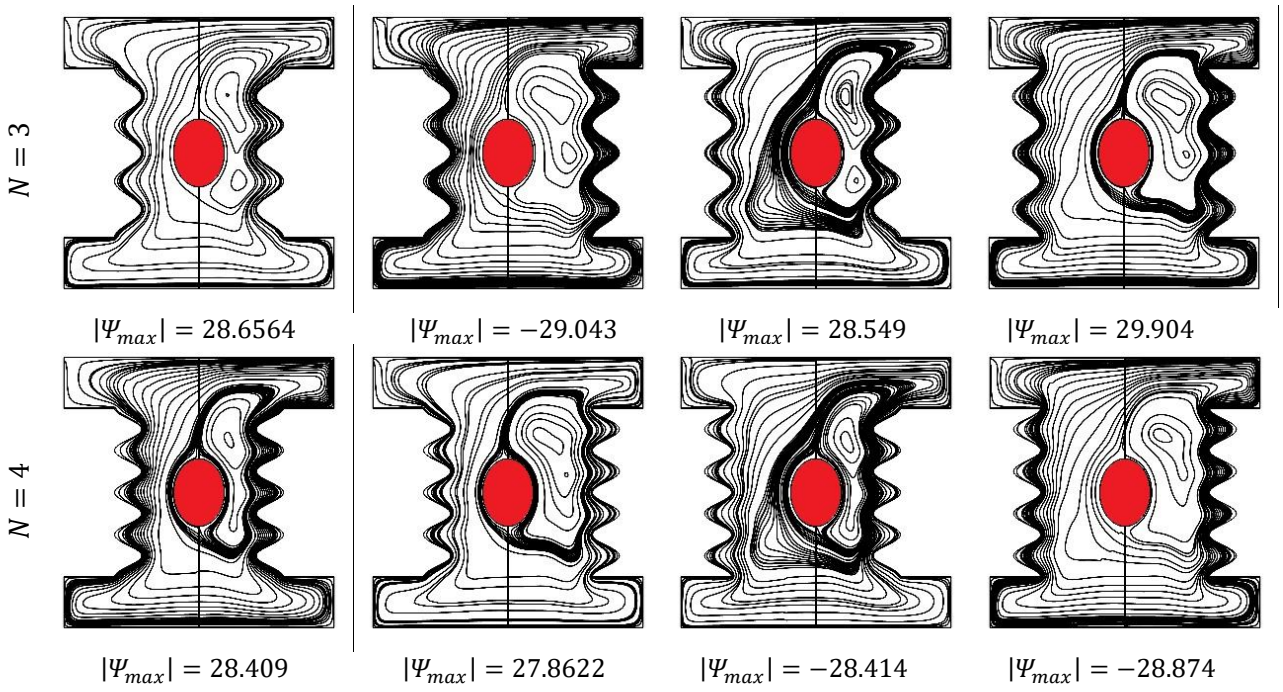

Figure (5. 64) Streamlines contours in the absence of magnetic field considering different cases of wavy patterns and different number of undulations at $Ra = 10^6, Ha = 0, Da = 0.001, \phi = 0.02, \gamma = 45°$

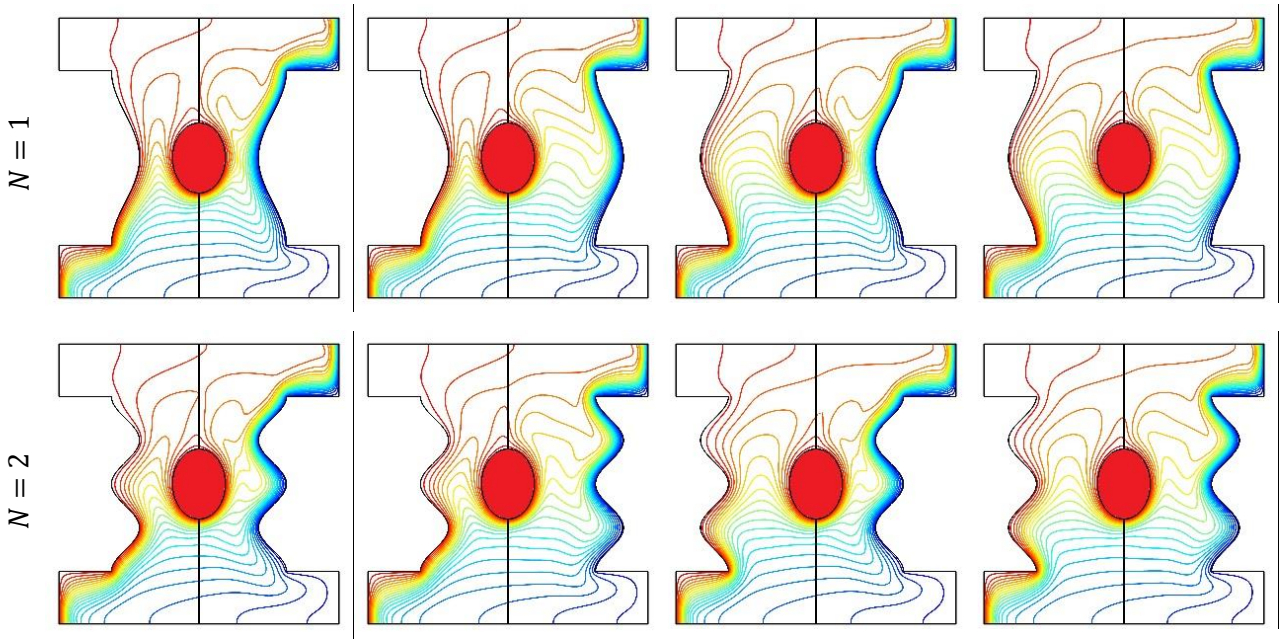

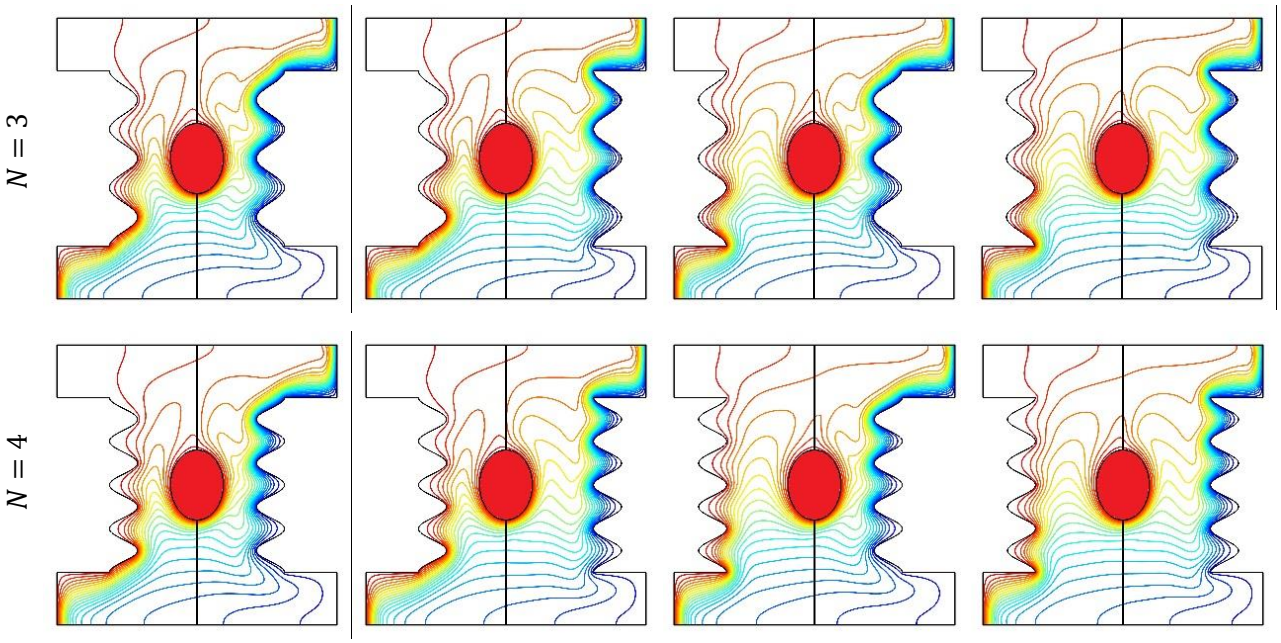

Figure (5. 65) Isotherms contours in the absence of magnetic field considering different cases of wavy patterns and different number of undulations at $Ra = 10^6, Ha = 0, Da = 0.001, \gamma = 45°, \phi = 0.02$

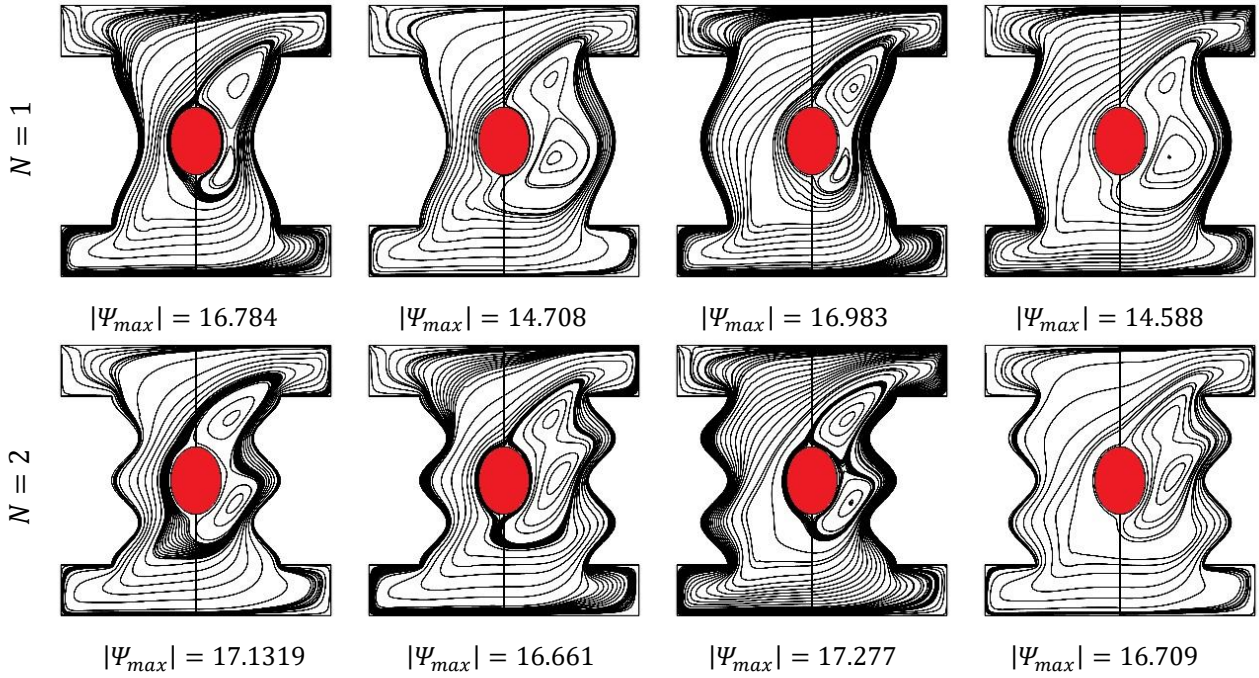

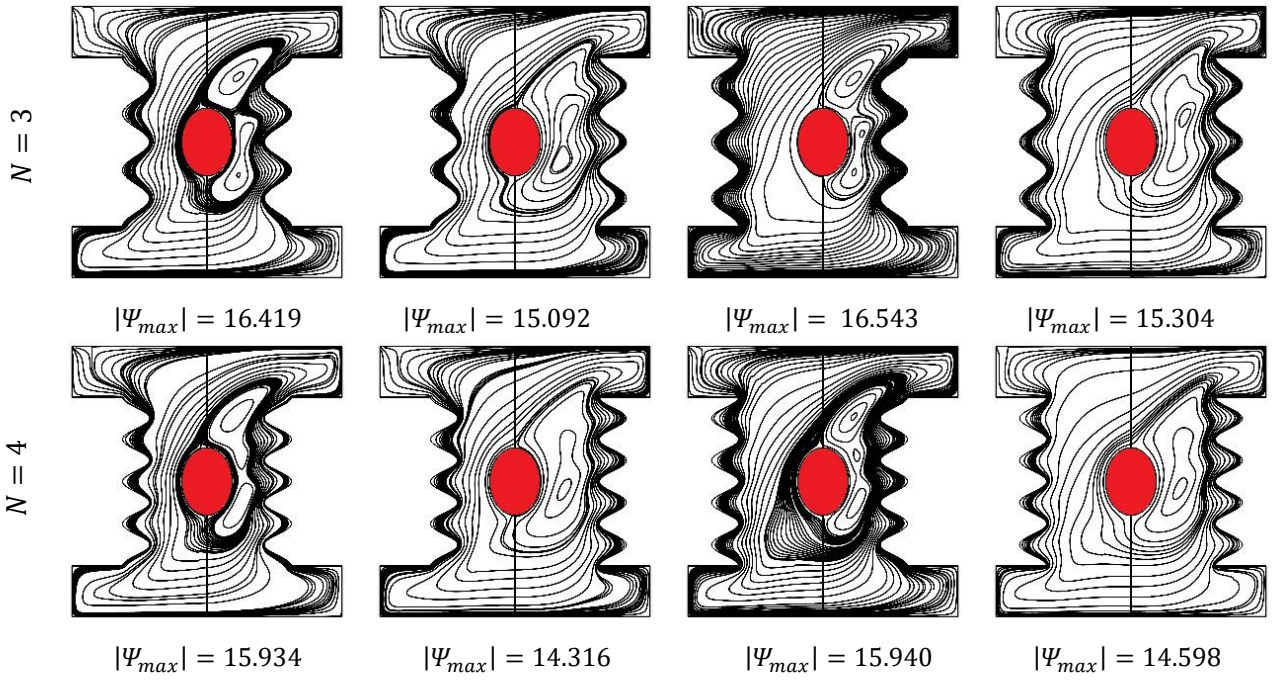

Figure (5. 66) Streamlines contours in the existence of the magnetic field considering different cases of wavy patterns and different number of undulations at $Ra = 10^6, Ha = 60, Da = 0.001, \gamma = 45°, \phi = 0.02$

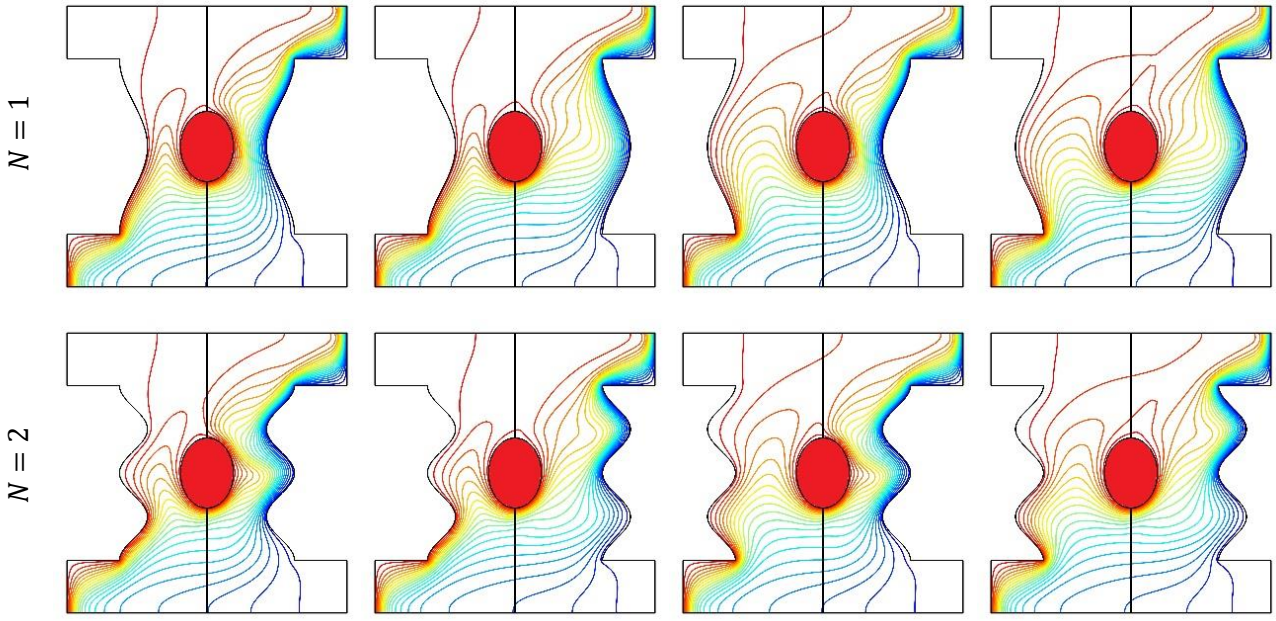

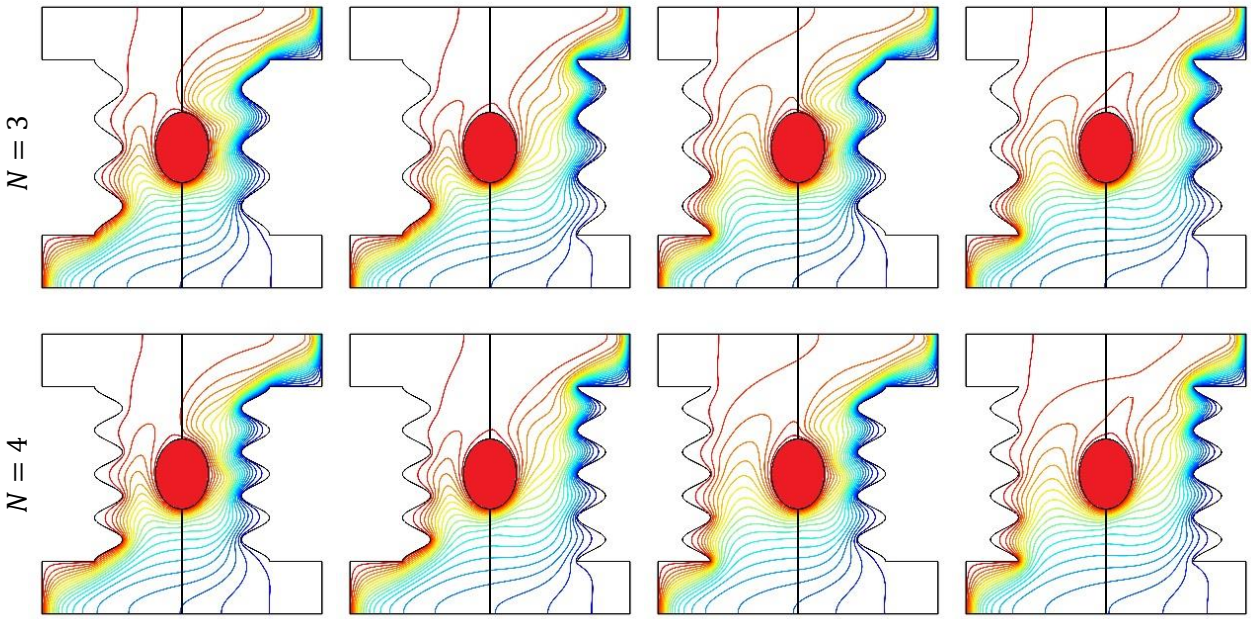

Figure (5. 67) Isotherm lines contours in the existence of the magnetic field considering different cases of wavy patterns and different number of undulations at $Ra = 10^6, Ha = 60, Da = 0.001, \gamma = 45°, \phi = 0.02$

5.2.4.2. The influence of distance between wavy walls

In this section, the influence of distance between the wavy walls considering four different cases of wavy patterns with and without magnetic field had been presented via Figures (5.68-5.71). The number of undulations is fixed to $(N = 1)$. The selected distance between wavy walls had been taken as $(B = 0.8 - 1.4)$. Considering the absence of magnetic field and regarding Figure (5.68), which shows the strong relation between the distance between wavy walls and the wavy patterns on the stream function which reveals the strength of the fluid flow. It can be seen that at $B = 0.8$, the stream function values would be for Case 2 > Case 3 > Case 4 > Case 1. Also, regardless the wavy shape patterns, the fluid flow would be at its minimum values when the distance parameter between two wavy walls is at $B = 0.8$. In this way i.e., at $= 0.8$, Case 1 reveals the lowest fluid flow strength with maximum stream function $|\Psi_{max}| = 23.270$. This is noted by two inner cells that

formed above and below the inner elliptical body because the distance between the elliptical body and wavy walls too small which break down the natural convection currents into two inner cells. Considering Case 1, it can be seen that increasing the distance parameter between two wavy walls into $B = 1.0$, leads to improve the fluid flow strength by 41.17 %. However, further increasing of the wavy walls distance had negligible impact on the fluid flow strength for all cases of wavy patterns. The impact of the distance between the wavy walls on isotherms had been presented in Figure (5.69) which clearly influences on their distribution.

The magnetic field taken into account to examine its effect on streamlines and isotherms had been shown via Figure (5.70) and Figure (5.71), respectively. The results when the magnetic field and the distance parameter between the wavy walls are crucial. With respect to Figure (5.70) there are many important points. Firstly, for all four cases of wavy walls, it can be seen that there is increasing in the fluid flow strength with increasing of the distance parameter between wavy walls but in a lower rate in a comparison with the case of the absence of magnetic field that had been illustrated in Figure (5.68). For example, taking Case 1 it can be seen that increasing the distance between wavy walls from ($B = 0.8$) into ($B = 1.4$) leads to improve the fluid flow strength by 16.07%. The impact of magnetic field and the distance between wavy walls are presented in Figure (5.71) which clearly change the distribution of isotherms in a comparison with the absence of magnetic field.

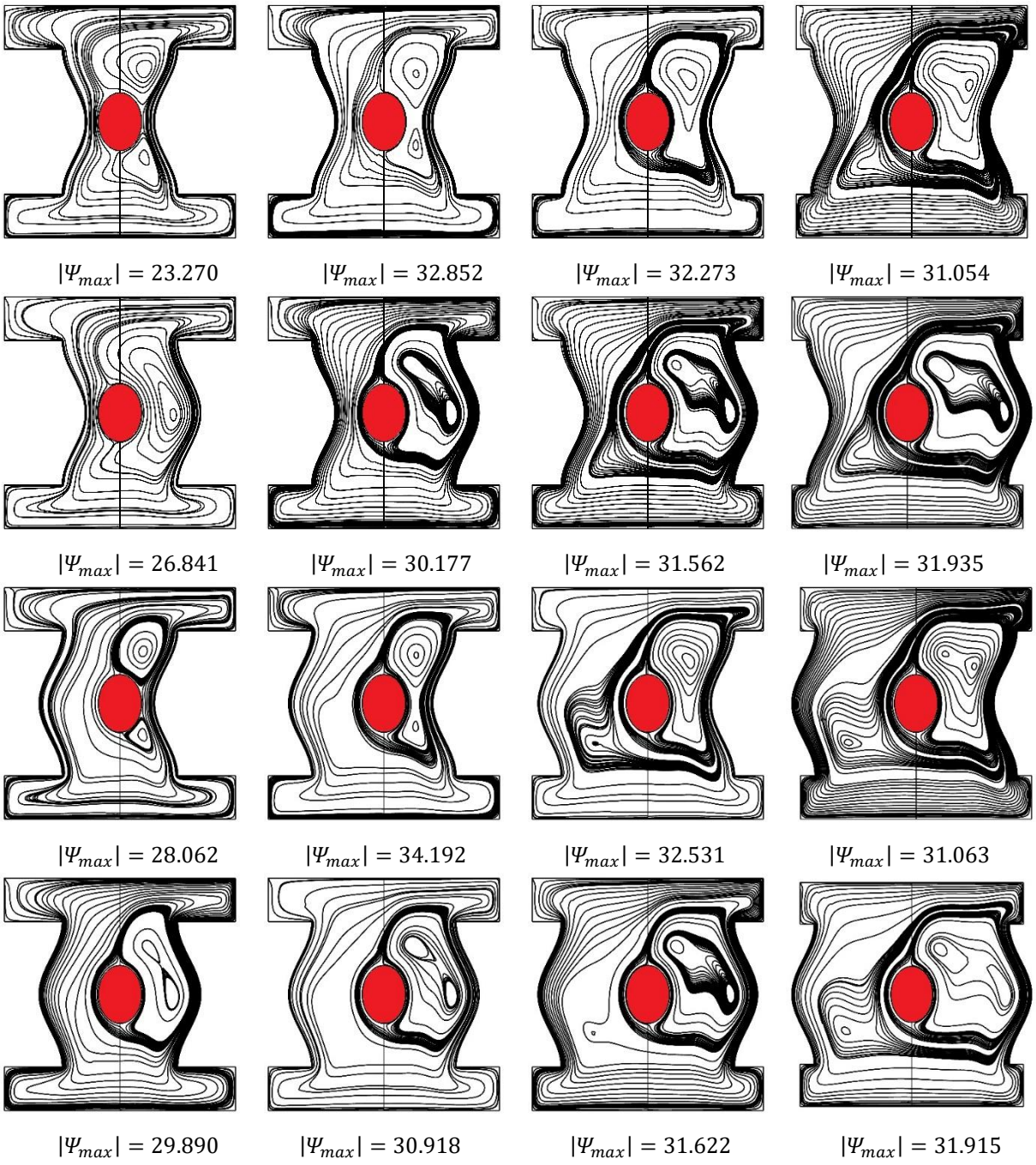

Figure (5. 68) Streamlines contours in the absence of the magnetic field considering different cases of wavy patterns and different distance between wavy patterns at $Ra = 10^6, Ha = 0, Da = 0.001, \gamma = 45°, \phi = 0.02$

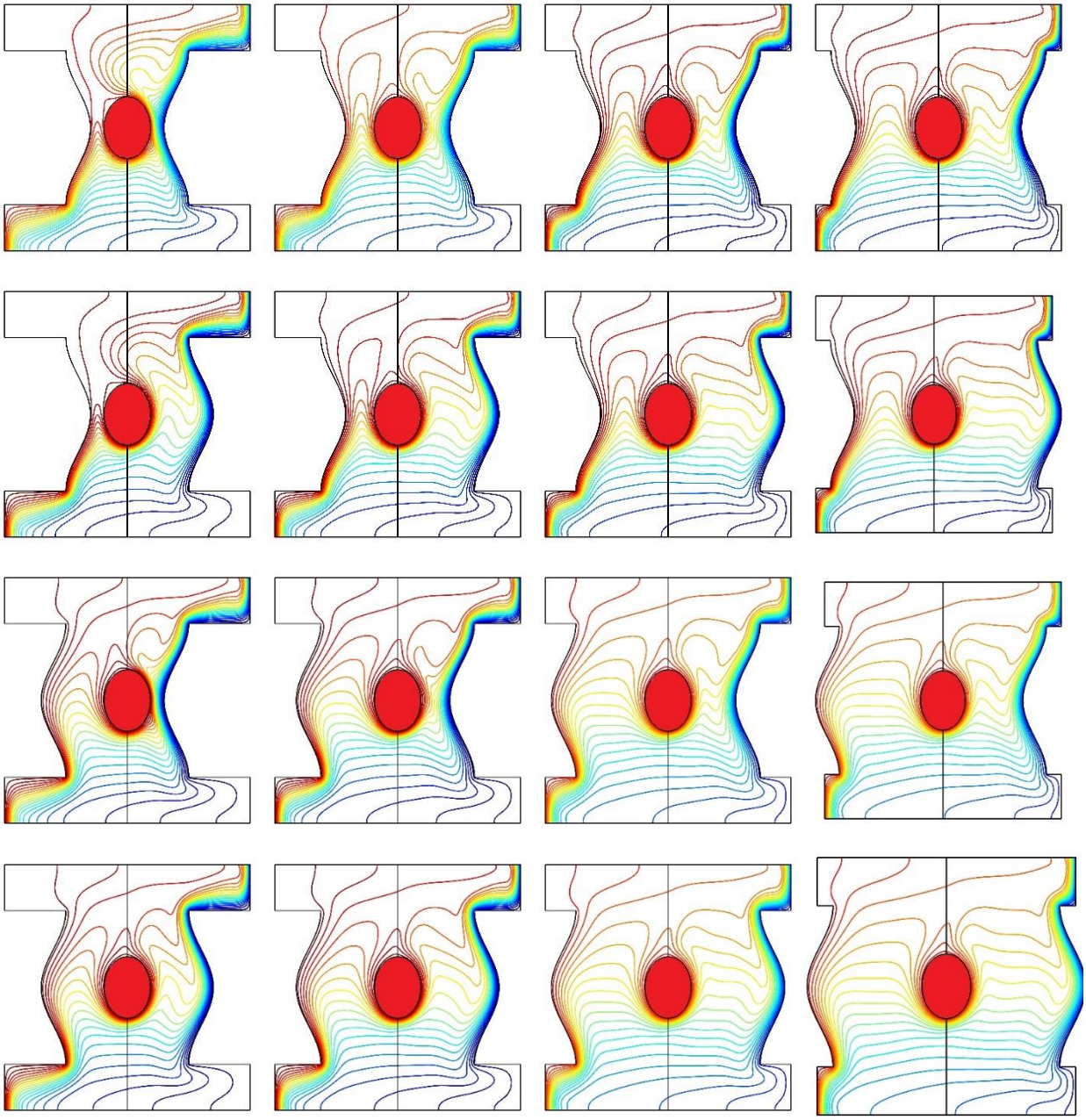

Figure (5. 69) Isotherm lines contours in the absence of the magnetic field considering different cases of wavy patterns and different distance between wavy patterns at $Ra = 10^6, Ha = 0, Da = 0.001, \gamma = 45°, \phi = 0.02$

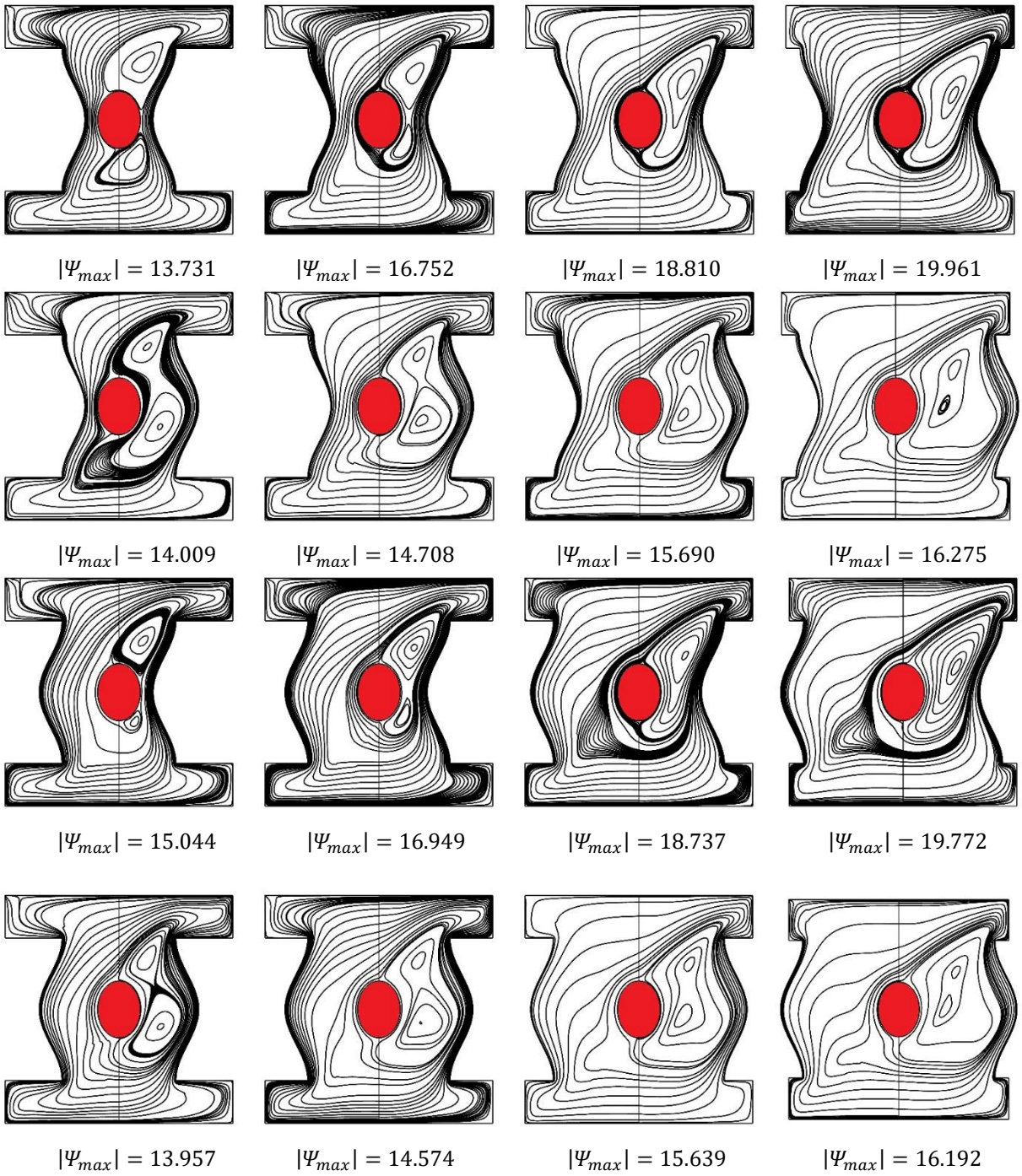

Figure (5. 70) Streamlines contours in the existence of the magnetic field considering different cases of wavy patterns and different distance between wavy patterns at $Ra = 10^6, Ha = 60, Da = 0.001, \gamma = 45°, \phi = 0.02$

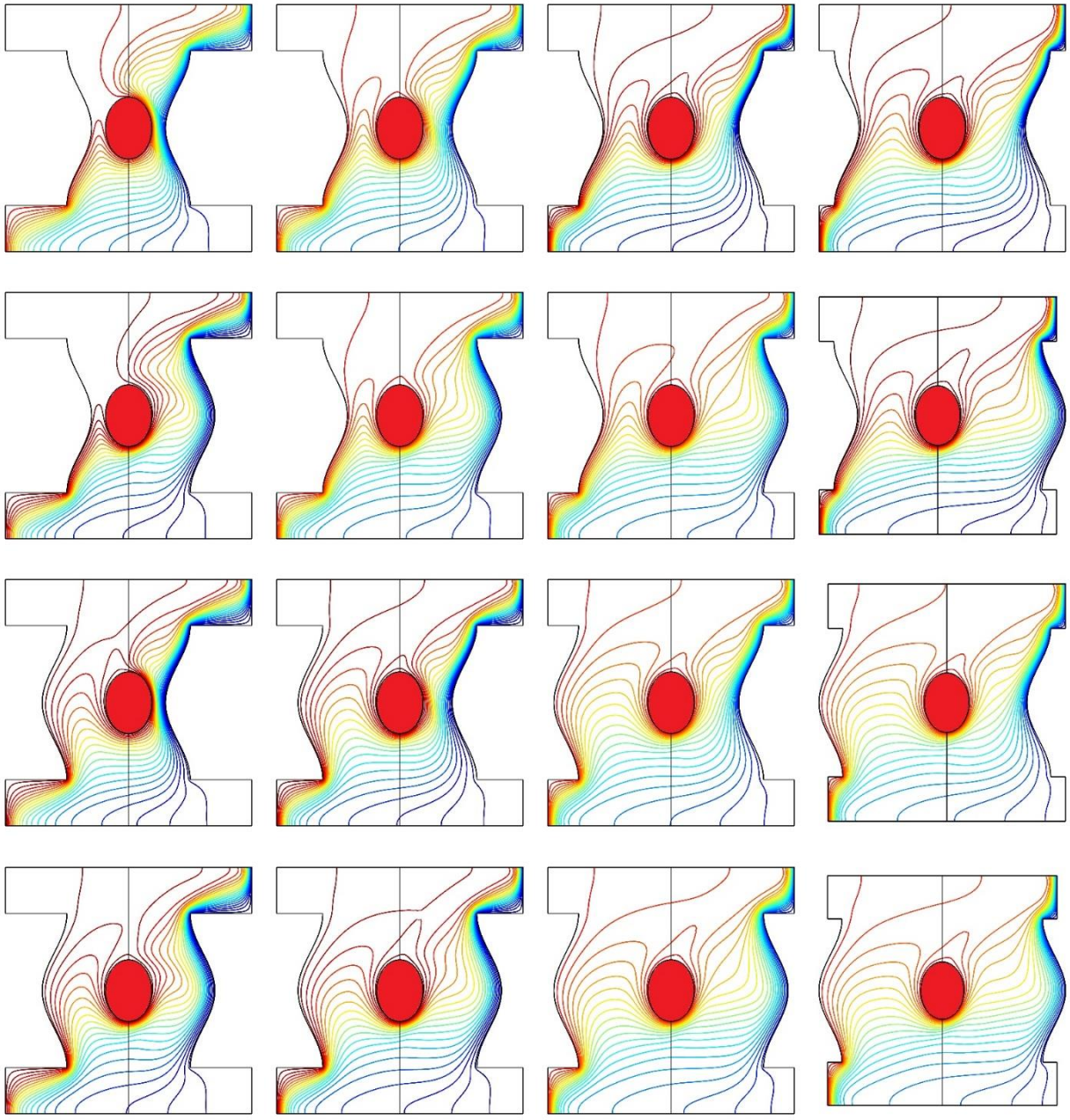

Figure (5. 71) Isotherm lines contours in the existence of the magnetic field considering different cases of wavy patterns and different distance between wavy patterns at $Ra = 10^6, Ha = 60, Da = 0.001, \gamma = 45°, \phi = 0.02$

5.2.4.3. The influence of inner elliptical body position

The influence of inner elliptical body position on fluid flow and heat transfer had been presented in terms of streamlines and isotherms in Figure (5.72) and Figure (5.73), respectively for four different cases of wavy walls patterns.

Firstly, With respect toFigure (5.72), it can be seen that for all wavy patterns that moving of the inner elliptical body from the center of the enclosure into the top region leads to an obvious reduction in the fluid flow strength while its movement into the lower region reveals better fluid flow strength. For example, considering Case 1 when the inner body located at the center ($\delta = 0.8$), the absolute maximum stream function $|\Psi_{max}| = 32.852$ while when it moves into the top at ($\delta = 1.3$), the absolute maximum stream function $|\Psi_{max}| = 19.304$ while when it moves to the lower region at ($\delta = 0.3$), the absolute maximum stream function $|\Psi_{max}| = 34.019$. The same behavior is noted for other wavy patterns. However, the magnitude of fluid flow strength is different from wavy patterns to another patterns along with the position of inner elliptical body. For example, at ($\delta = 0.8$), the fluid flow strength of Case 3 > Case 1 > Case 4 > Case 2 while at ($\delta = 0.3$), Case 4 > Case 2 > Case 3 > Case 1. On the other hand at ($\delta = 1.3$), Case 4 > Case 2 > Case 1 > Case 3. It is also noted that two inner cells had been created above and below the inner elliptical body when it positioned at the center while these inner cells had been broken into on one inner cell located above the inner body when it moved towards the lower region while the inner cell formed below the inner body when the latter moved towards the top region. Secondly, With respect to isotherms that had been presented in Figure (5.73), it can be seen that when the inner body located in the bottom region more hot isotherms lines distributed among the area of the enclosure while location of the inner body in the top region leads to a lot of cold isotherms lines fills the enclosure area.

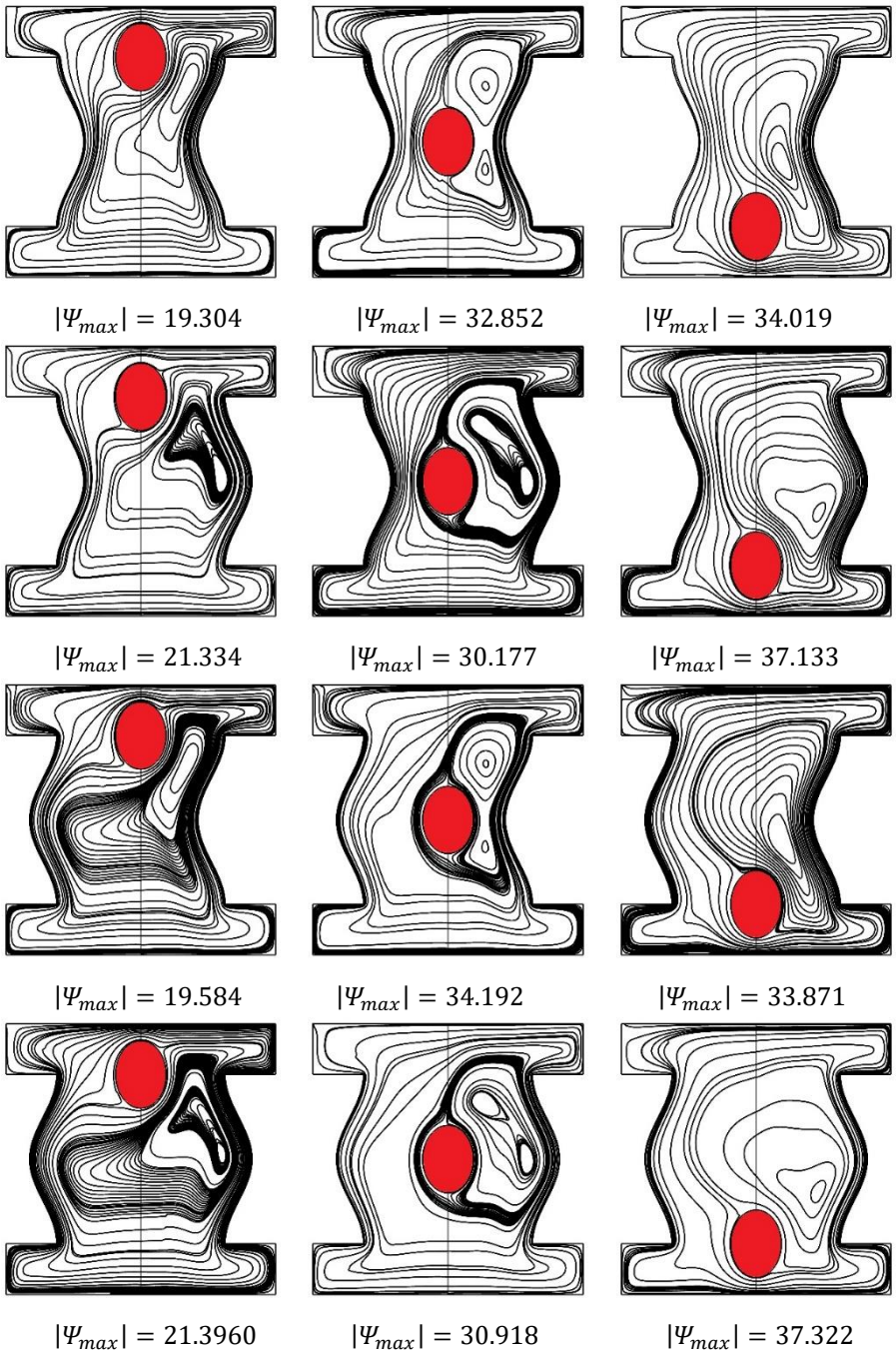

Figure (5. 72) Streamlines contours considering different cases of wavy patterns under different position of inner elliptical body at $Ra = 10^6, Ha = 0, Da = 0.001, \gamma = 45°, \phi = 0.02$

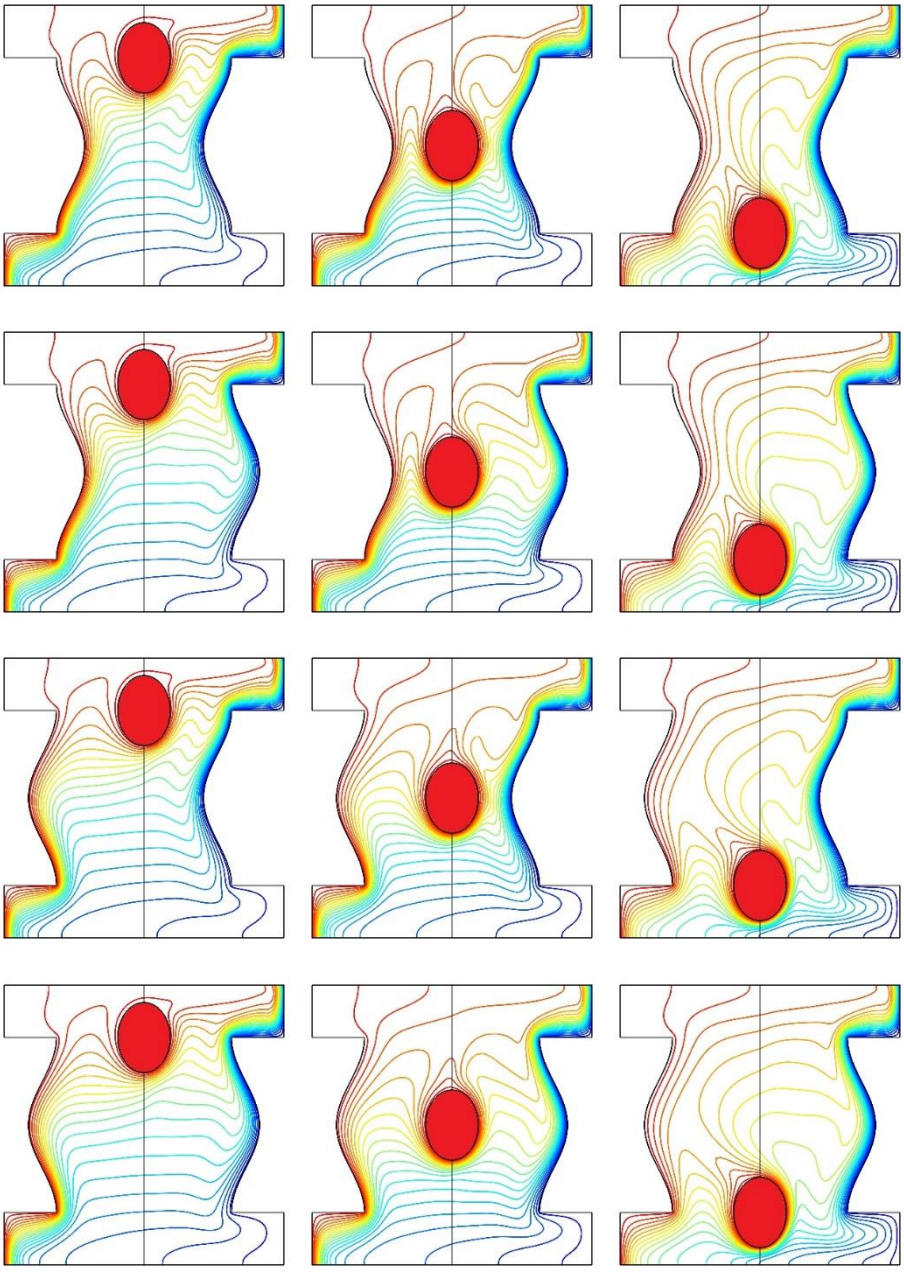

Figure (5. 73) Isotherm lines contours considering different cases of wavy patterns under different position of inner elliptical body at $Ra = 10^6, Ha = 0, Da = 0.001, \gamma = 45°, \phi = 0.02$

5.2.4.4. The influence of selected parameters on Nusselt number

The most important dimensionless parameter in heat transfer analysis which in the indicator of heat transfer bettering is Nusselt number. So, this section will explain this idea in-full details.

The influence of different wavy patterns along with the number of undulations in the absence of magnetic field i.e., at $(Ha = 0)$ had been shown in Figure (5.74). It can be seen that increasing the number of undulations reduces the Nusselt number which turn in reduction of heat transfer. It can be seen that when the number of undulations is $(N = 1)$, the Nusselt number of Case 3 > Case 1 > Case 4 > Case 2. This behavior of Nusselt number remains the same when the number of undulations increases into $(N = 2)$. However, increasing the number of undulations into $(N = 3)$, make Nusselt number of wavy shapes of Case 1 had the highest value in a comparison with that of Case 2 which had the lowest Nusselt number. While increasing the number of undulations into $(N = 4)$ leads to make Nusselt number of Case 3 had the highest value along with keeping Case 2 had the lowest Nusselt number. It can see that based upon the numerical observations that in the absence of magnetic field that the influence of number of undulations and the wavy patterns are high as illustrated in Figure (5.74). While considering the influence of magnetic field at Figure (5.75) which reveals that the impact of magnetic field is higher than the influence of wavy walls patterns. For example, when the number of undulations are $(N = 3, 4)$, there are similar contribution on Nusselt number for Case 1 and Case 2. As well as approximately similar value of Nusselt number for Case 3 and Case 4. Additionally, Nusselt number of Case 3 and Case 4 are higher than that of Case 1 and Case 2.

The influence of the distance between the wavy walls had been shown via Figure (5.76) and Figure (5.77) without and with magnetic field, respectively. Considering

Figure (5.76), it can be seen that increasing the distance between wavy walls for all four cases of the wavy patterns leads to enhance the heat transfer by increasing the dimensionless value of Nusselt number. For example, for Case 1 increasing the distance from $B = 0.8$ into $B = 1.4$ leads to increase Nusselt number by 31.67 %. On the other hands when the magnetic field effect taken into account as shown in Figure (5.77), it can be seen that still increasing the distance between the wavy patterns enhance Nusselt number but lower than that in the absence of magnetic field. It is worthy to mention that in the existence of the magnetic field, Case 4 had the lowest Nusselt number in a comparison with the other cases of wavy patterns.

The impact of the position of inner body is illustrated via Figure (5.78) and Figure (5.79) without and with the magnetic field, respectively. Three different position of inner elliptical body had been selected which are at the center ($\delta = 0.8$), at the top region ($\delta = 1.3$), at the bottom region ($\delta = 0.3$). It can be seen for Case 1 as shown in Figure (5.78) that when the inner elliptical body moves from the center into the top, Nusselt number decreases from $Nu = 14.8685$ into $Nu = 7.5926$ while movement the inner elliptical body from the center top into the bottom leads to enhance the heat transfer rate by increasing of Nusselt number about 67.70%. In this way, it can be seen that the similar trends is observed for all wavy patterns. Also, in Figure (5.79) which show the behavior of Nusselt number with the position of inner elliptical body inner the influence of magnetic field. It may be noted that the magnetic field make a notice difference and the influence of wavy shape patterns stronger in a comparison of that in the absence of magnetic field.

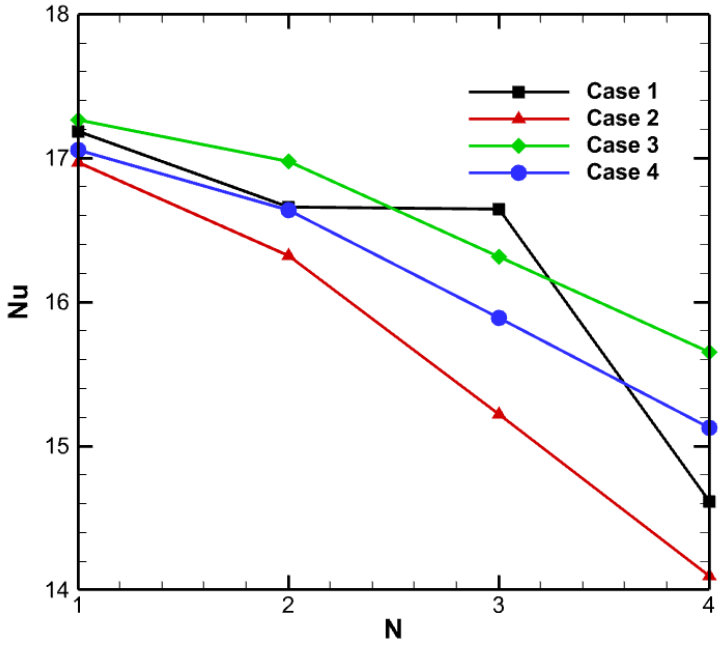

Figure (5. 74) Nusselt number variation with respect to number of undulations considering different cases of wavy patterns in the absence of magnetic field at $Ra = 10^6, Da = 0.001, Ha = 0, \gamma = 45°$

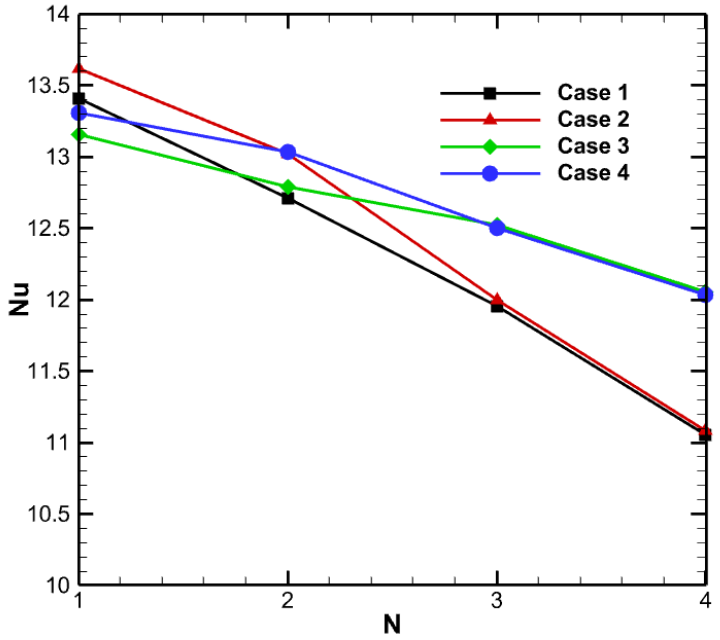

Figure (5. 75) Nusselt number variation with respect to number of undulations considering different cases of wavy patterns in the existence of magnetic field at $Ra = 10^6, Da = 0.001, Ha = 60, \gamma = 45°$

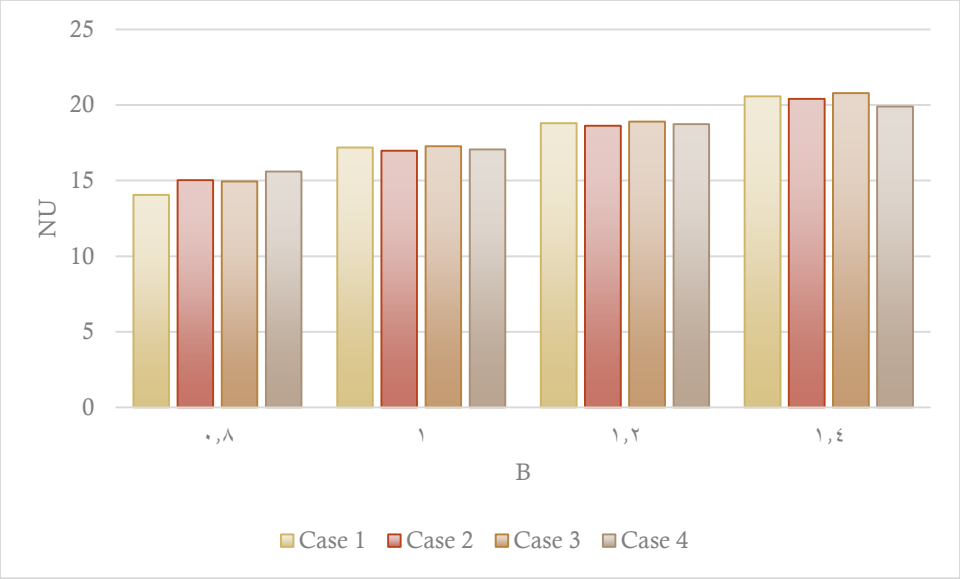

Figure (5. 76) Nusselt number variation with respect to distance between wavy walls considering different cases of wavy patterns in the absence of magnetic field at $Ra = 10^6, Da = 0.001, Ha = 0$

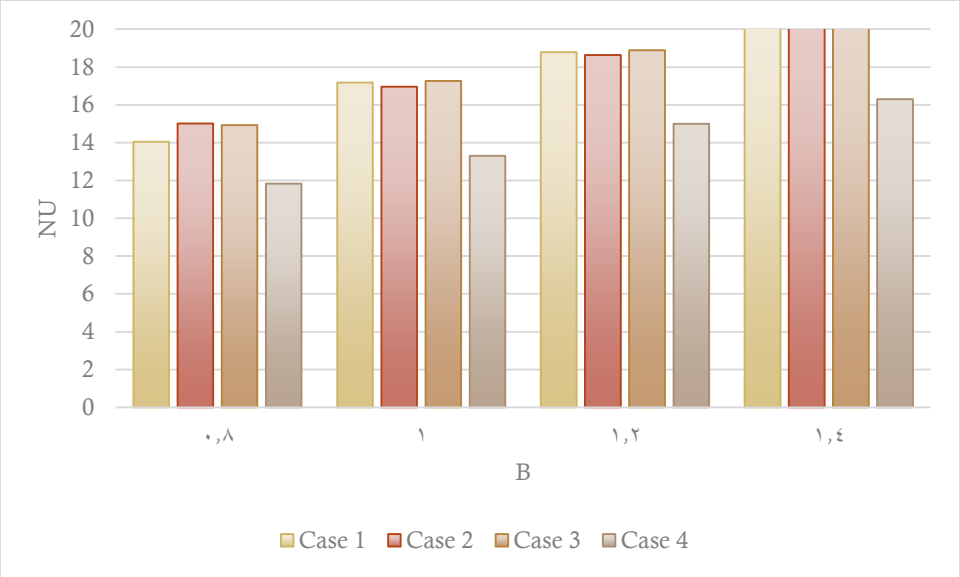

Figure (5. 77) Nusselt number variation with respect to distance between wavy walls considering different cases of wavy patterns in the existence of magnetic field at $Ra = 10^6, Da = 0.001, Ha = 60, \gamma = 45°$

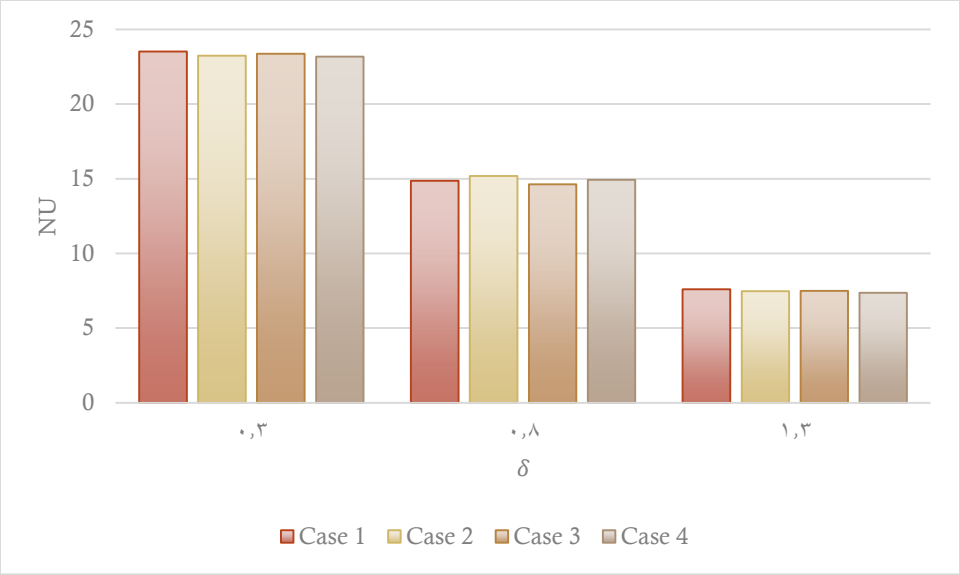

Figure (5. 78) Nusselt number variation with respect to vertical position of the elliptical inner body considering different cases of wavy patterns in the absence of magnetic field at $Ra = 10^6, Da = 0.001, Ha = 0$

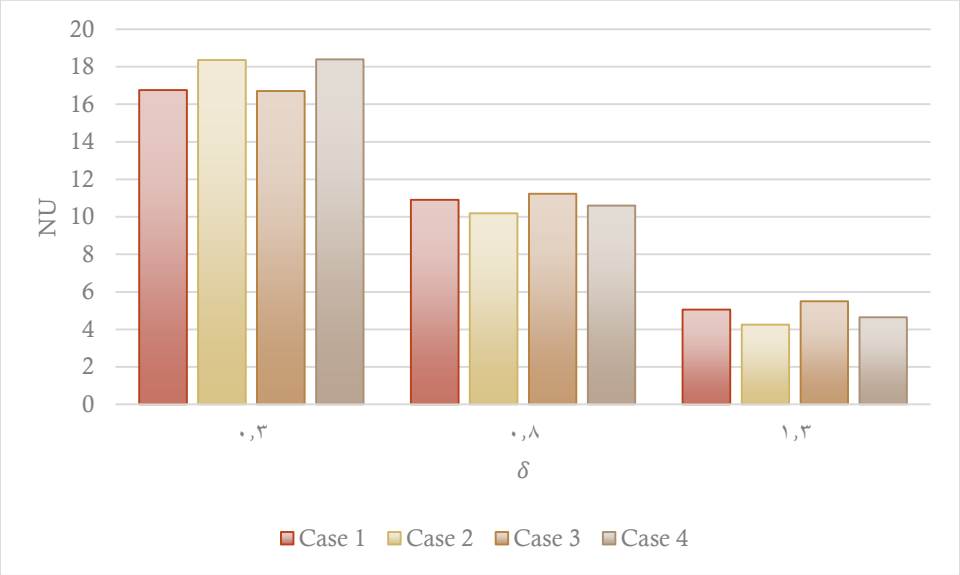

Figure (5. 79) Nusselt number variation with respect to vertical position of the elliptical inner body considering different cases of wavy patterns in the existence of magnetic field at $Ra = 10^6, Da = 0.001, Ha = 60, \gamma = 45°$

5.3. Experimental Results

The experimental results had been presented in this section considering the existence of different concentration of nanofluids with and without magnetic field.

5.3.1. Thermophysical Properties of Nanofluids

The nanofluid density that had been measured using Densitometer device at 27.5 °C with four different concentrations of nanofluid ($\phi = 0.00, \phi = 0.02, \phi = 0.04, \phi = 0.06$) is presented in Figure 5.80. The measured experimental data of the present work shows good agreement with the theoretical model. It may be noted that when $\phi = 0.00$ which represents the pure water, the density equals to $\rho = 996.4062$ kg/m^3 based upon the correlation that had been used in Eq. (4.7) while the measured density equals to $\rho = 997$ kg/m^3. With addition of nanoparticle, it can be seen that there is an obvious increment in the density. Additionally, it can seen that as inserted in Figure (5.80) that there is good agreement between the theoretical measurements of nanofluid density based upon Eq. (4.10) and the experimental measurements of nanofluid density based upon Densitometer device.

The measurements of thermal conductivity is demonstrated in Figure 5.81 with respect to three different temperature (30, 35 and 40 °C) under four different concentration of nanofluid (0, 0.02, 0.04 and 0.06). It can be seen that increasing the temperature of nanofluid and nanofluid concentration lead to an obvious increment in thermal conductivity of nanofluid. For example, it can be seen that when the temperature of nanofluid is 30 °C and changing the nanofluid concertation from $\phi = 0.02$ into $\phi = 0.04$ leads to increase the thermal conductivity of nanofluid from $k = 0.64$ into $k = 0.691$ based upon the experimental measurements. Additionally, when the nanofluid concentration is kept at $\phi = 0.06$ with increasing of the temperature from $T = 30°C$ into $T = 40°C$, the thermal conductivity of nanofluid from $k = 0.742$ into $k = 0.77$.

On the other hand, as presented in Figure 5.82, it can be seen that increasing of nanofluid concentration increases the dynamics viscosity of the nanofluid. There is good agreement between the measured experimental data with the results based upon Maxwell Model

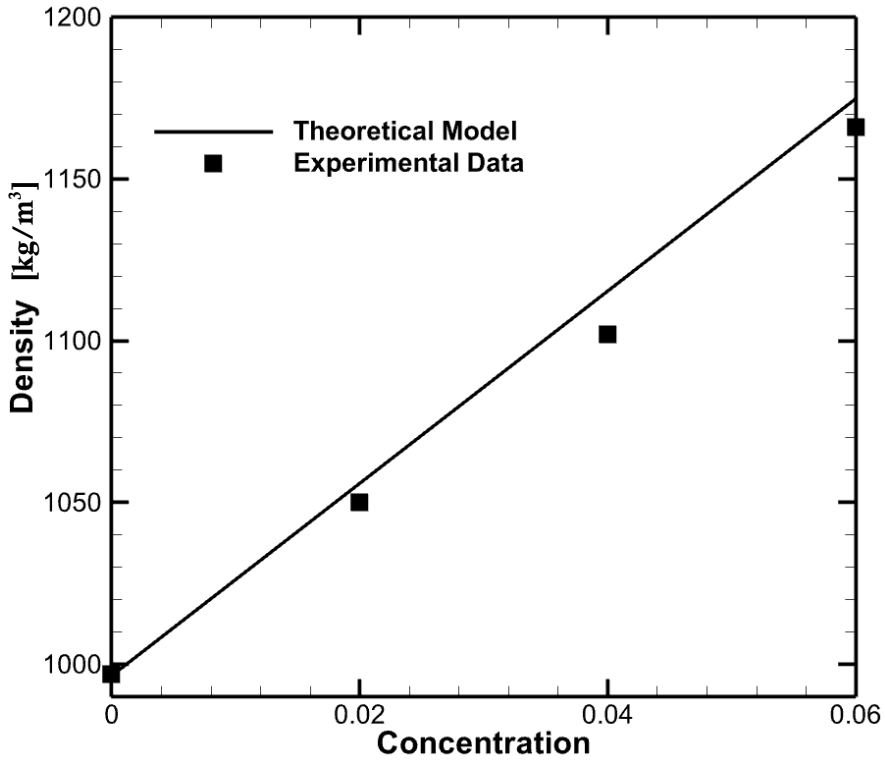

Figure (5. 80) comparison between experimental measured data and the theoretical data of nanofluid density

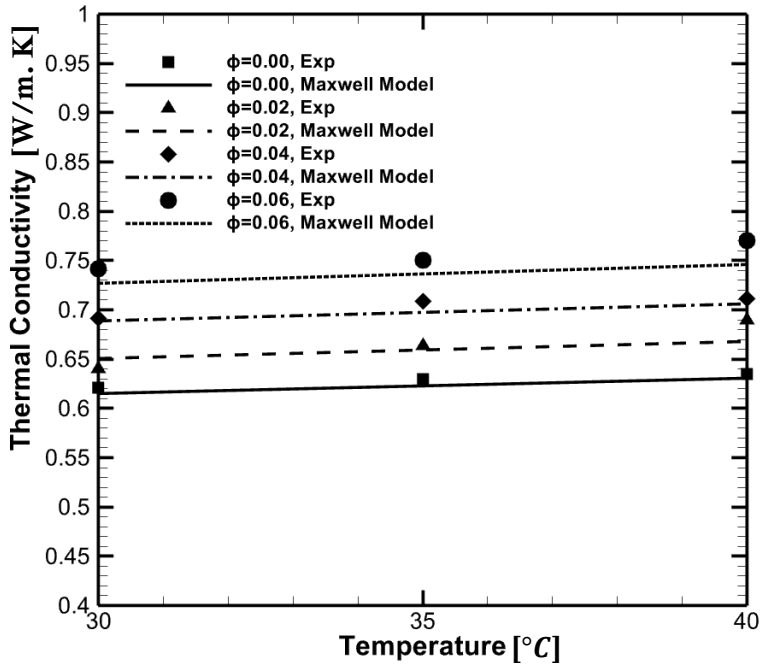

Figure (5. 81) comparison between experimental measured data and the theoretical data of nanofluid thermal conductivity

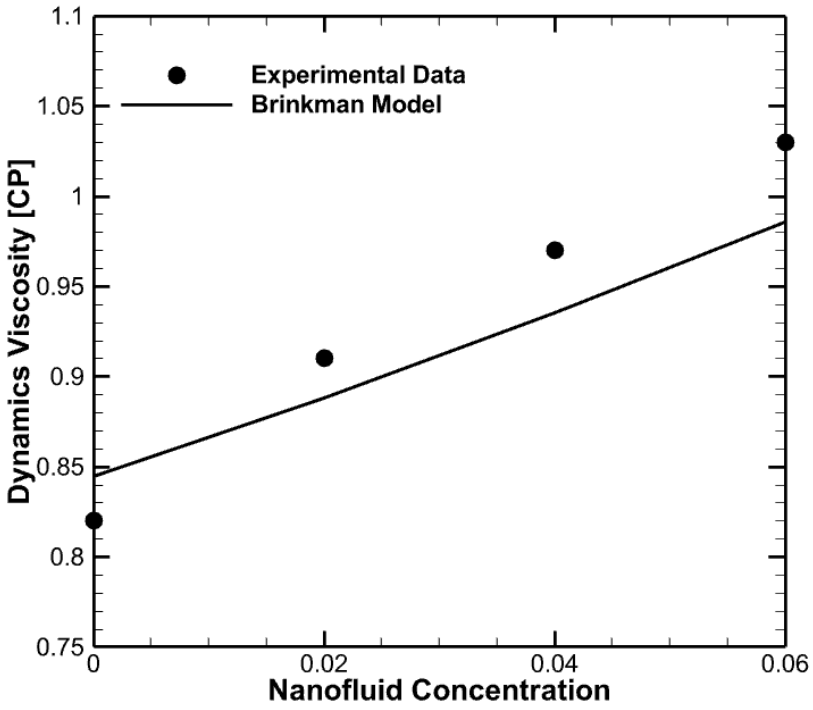

Figure (5. 82) comparison between experimental measured data and the theoretical data of nanofluid dynamics viscosity

5.3.2. Repeatability

Repeatability of heat transfer experiment is considered as a key parameter in the heat transfer and fluid flows research. It is a measure of getting the exact results when doing an experiment more than one times and under the same conditions. This gives a trust on the measurements instruments (thermocouples) as well as verify that the measured data are physically true and not just a chance. This will indicate the error for each thermocouple. Figure (5.83) shows the repeatability of temperature sensors along the hot right wavy wall at $T_h = 30\ ℃, T_c = 25\ ℃, \phi = 0$. It can be seen as indicated in Table (4.8) that the difference in the reading of each thermocouples within range of $-0.2\ ℃$ to $+\ 0.6℃$.

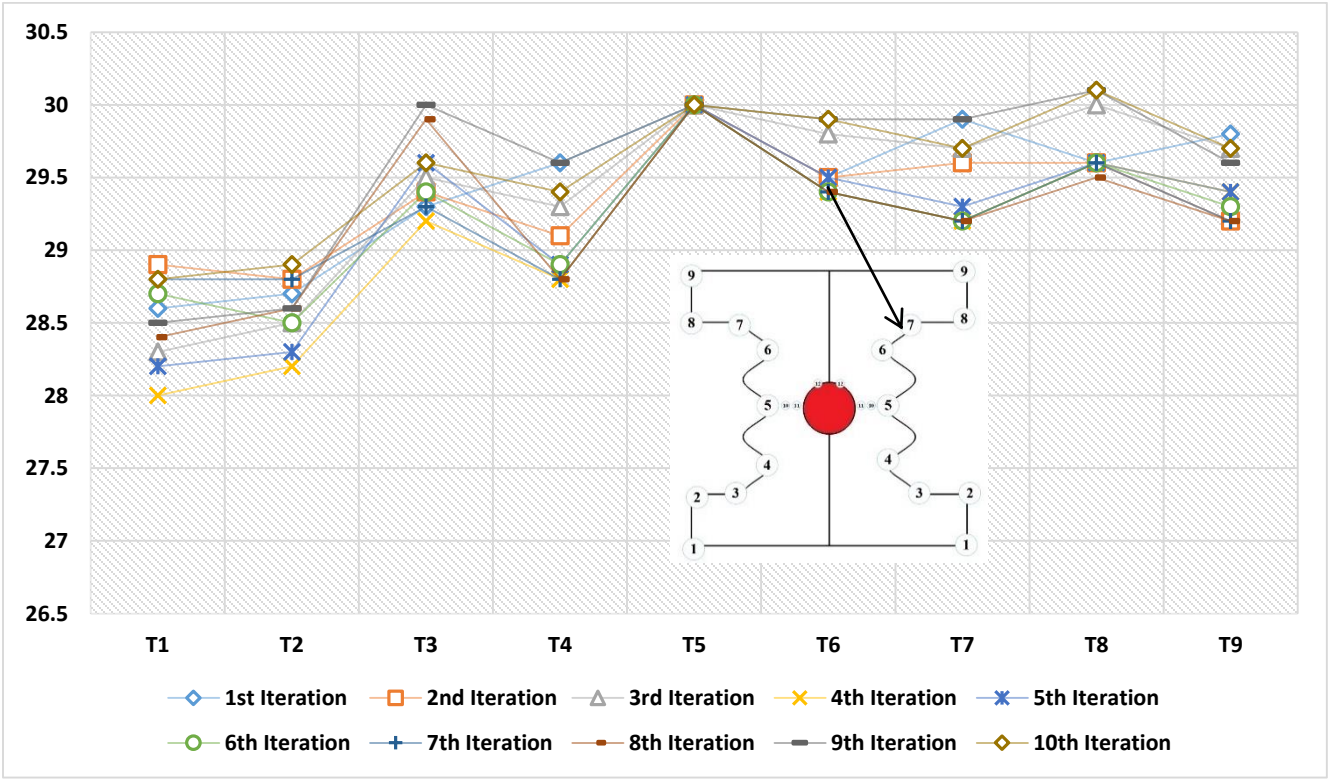

Figure (5. 83) Repeatability of the experimental measured data along the hot right wall on the nanoporous region of the experimental model under $T_h = 30\ ℃, T_c = 25\ ℃, \phi = 0$

5.3.3. Temperature at the mid-section of the enclosure

The temperature at the mid-section of the enclosure is presented in Figure (5.84) under three different experiments. The first experiment is done when the hot temperature on the right hot wall is 31℃. The second and the third experiments are kept when the hot wavy wall are kept at $33℃, 35℃$, respectively at $\phi = 0.02$. The inner hot body is kept at the same hot right wall temperature of each experiment. The left cold wall is kept at 25℃ for all of the three experiments. This makes the temperature difference for the first, second and third experiment equals to $\Delta T = 6℃, 8℃$ and 10℃, respectively. It can be seen that increasing the hot side wavy wall temperature leads to increase the temperature difference which increases the temperature level in the nanofluid-porous region and the nanofluid region.

When the hot wall temperature is set at $T_h = 31℃$ and following the heat flows through the nanofluid-region and till reaching the left wall, there will be temperature decrement from temperature $T_5 = 31℃$ to $T_{10} = 25℃$ due to the existence of the porous media filled the right layer which resist the movement of the nanofluid and work as insulator that damping the nanofluid and absorb its kinetic energy leading reducing its internal energy. After that, there is slight increment in the thermocouple's temperature from $T_{10} = 25℃$ till $T_{11} = 27℃$ as it affected by the inner hot body temperature which is kept at $T_{12} = 31℃$. When completing the following of heat transfer into the left nanofluid region, it can be seen that temperature decreases till it reaches the cold wall wavy temperature that equals to $T_5 = 25.4℃$. additionally, increasing the hot temperature of the wavy right wall attends more increasing in the temperatures measured by the thermocouples. This behavior is the same for further increasing at the hot and cold wavy temperatures as shown in Figure (5.85) when the hot walls temperature in three different experiments are $T_h = 36℃, 38℃$ and 40℃ when the cold wall temperature is $T_c = 30℃$.

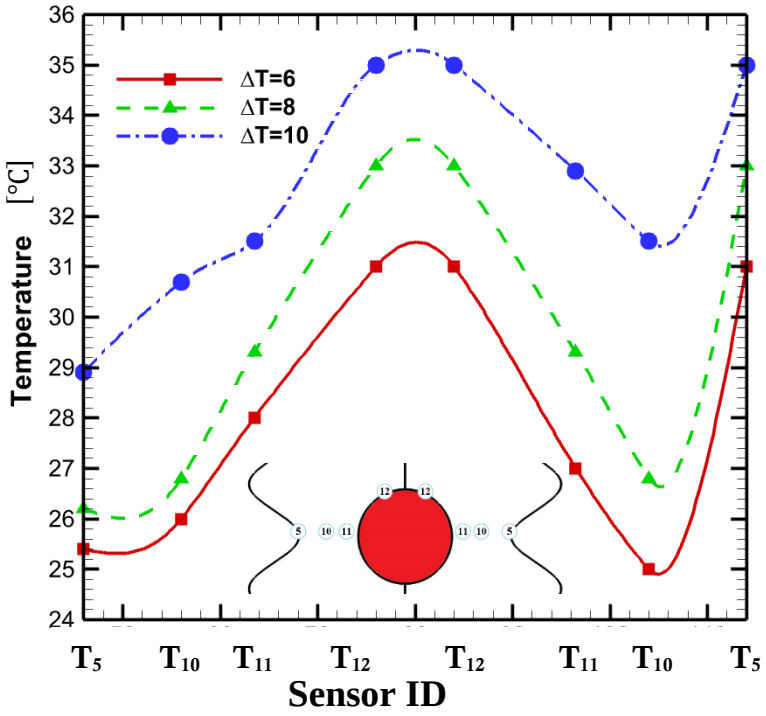

Figure (5. 84) Temperature experimental measured data at the mid-section of the Novel-I-Shaped enclosure T_h = 31, 33, 35 ºC, T_c = 25 ºC

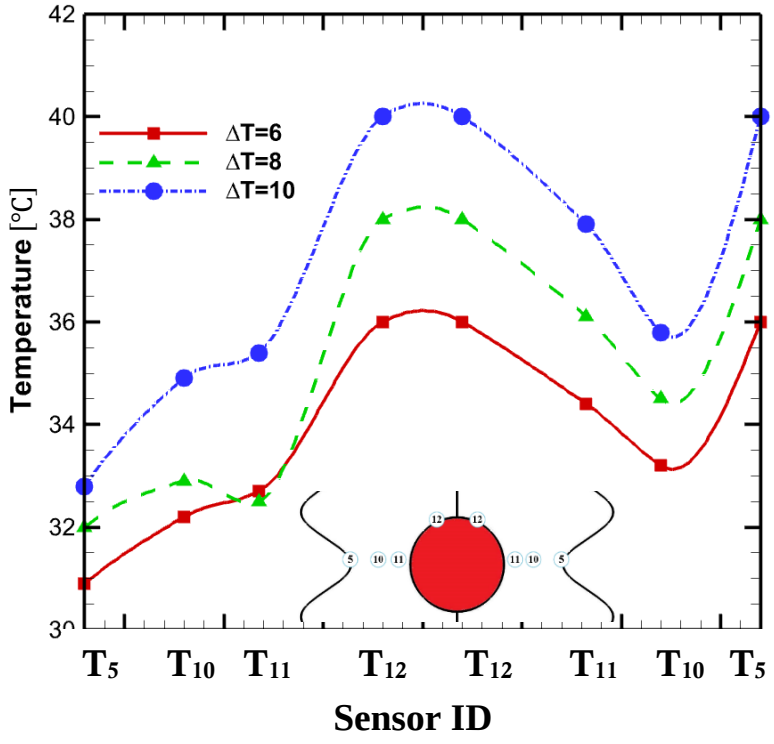

Figure (5. 85) Temperature experimental measured data at the mid-section of the Novel-I-Shaped enclosure T_h =36, 38, 40 ºC , T_c =30 ºC

5.3.4. Magnetic Field Role

The influence of the absence and the existence of the magnetic field with intensity of 20 mT is discussed in this section in full-details. Figure (5.86) demonstrates the temperature readings along the hot side wavy wall of the nanofluid-porous region. It can be seen that there is slight increasing in the temperature with the existence of the magnetic field. Additionally, Figure (5.87) illustrates the temperature reading measured by the thermocouples of the nanofluid region which also promote that the magnetic field increases the temperature.

This behavior of magnetic field still had the same impact on the temperature in the nanoporous right layer as shown in Figure (5. 88) and the left nanofluid layer as in Figure (5. 89) even when increasing the hot sidewall temperature $T_h = 36℃, 38℃$ and $40℃$ when the cold wall temperature is $T_c = 30℃$. Finally, the influence of the existence and the absence of MHD on the temperature profile along the mid-section is illustrated in Figure (5.90).

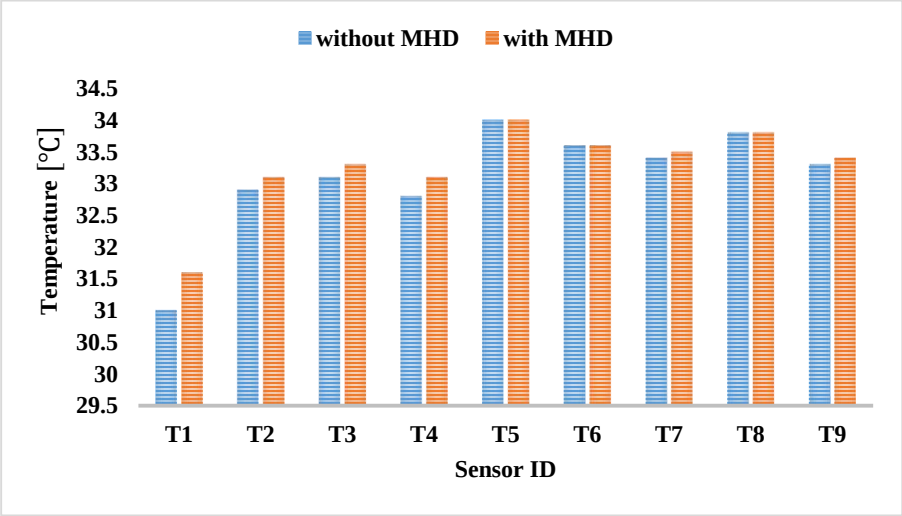

Figure (5. 86) Temperature measured data along the right hot wall in the nanoporous layer with and without the magnetic field under different temperature difference at $\phi = 0.02$

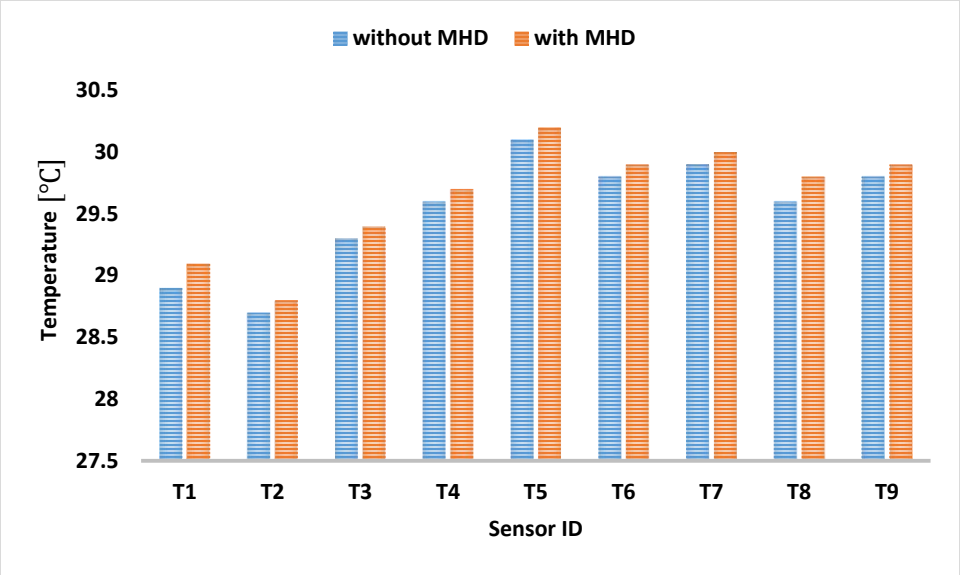

Figure (5. 87) Temperature measured data along the left cold wall in the nano layer with and without the magnetic field under different temperature difference $\phi = 0.02$

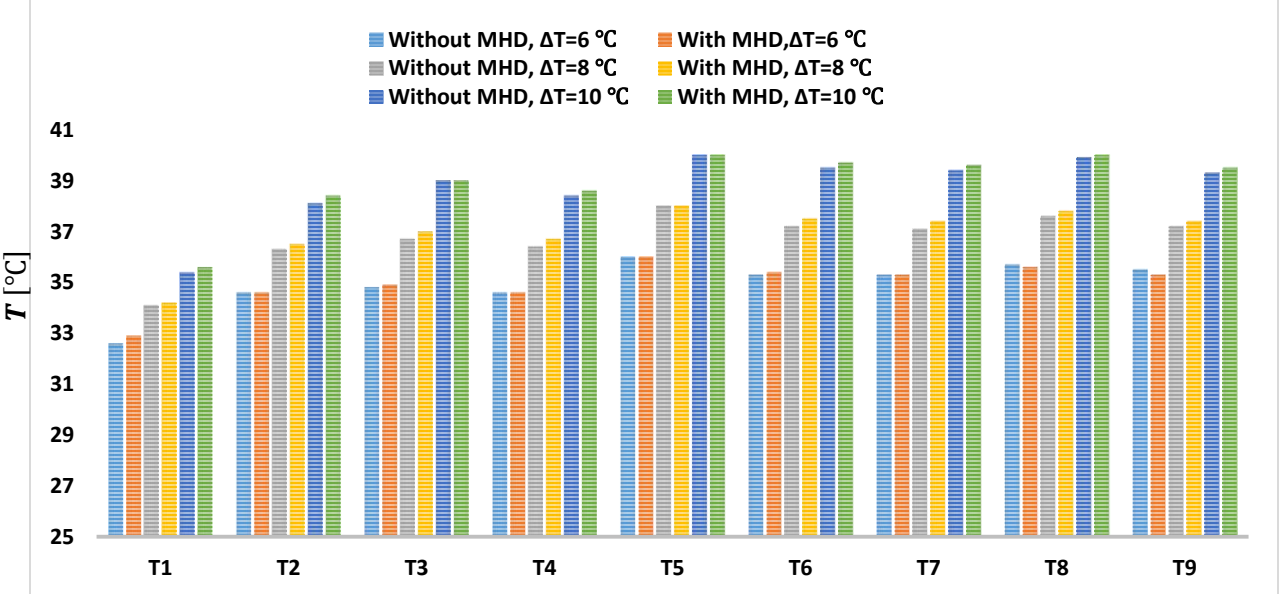

Figure (5. 88) Temperature measured data along the right hot wall in the nanoporous layer with and without the magnetic field under different temperature difference

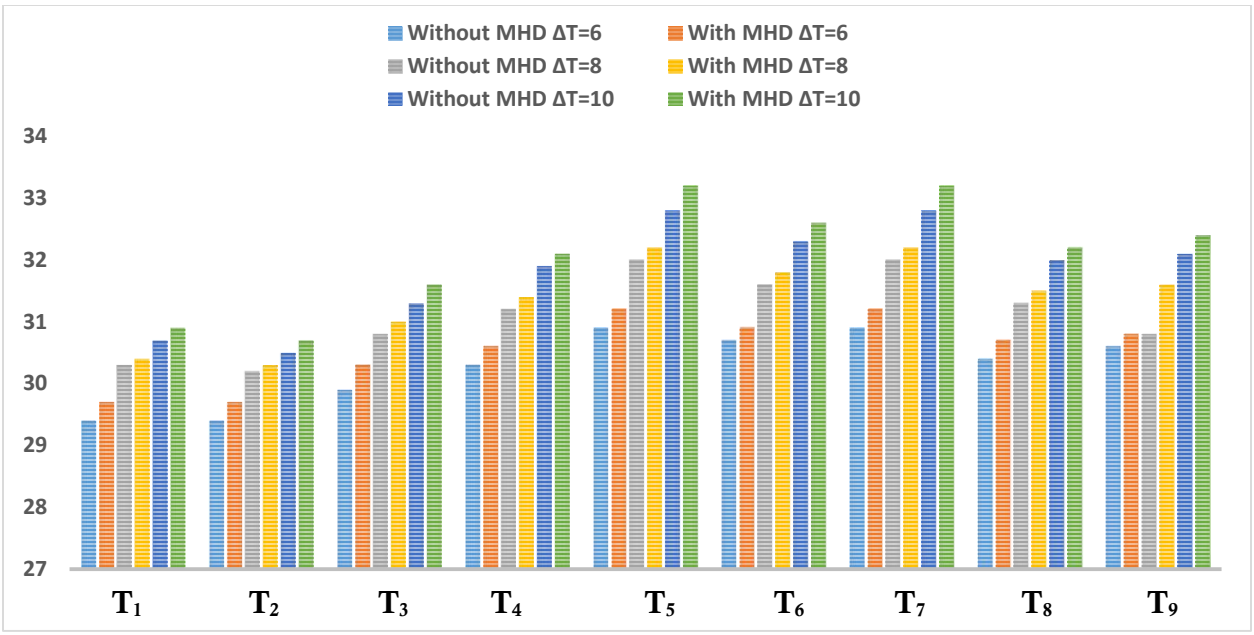

Figure (5. 89) Temperature measured data along the left cold wall in the nanofluid layer with and without the magnetic field under different temperature difference

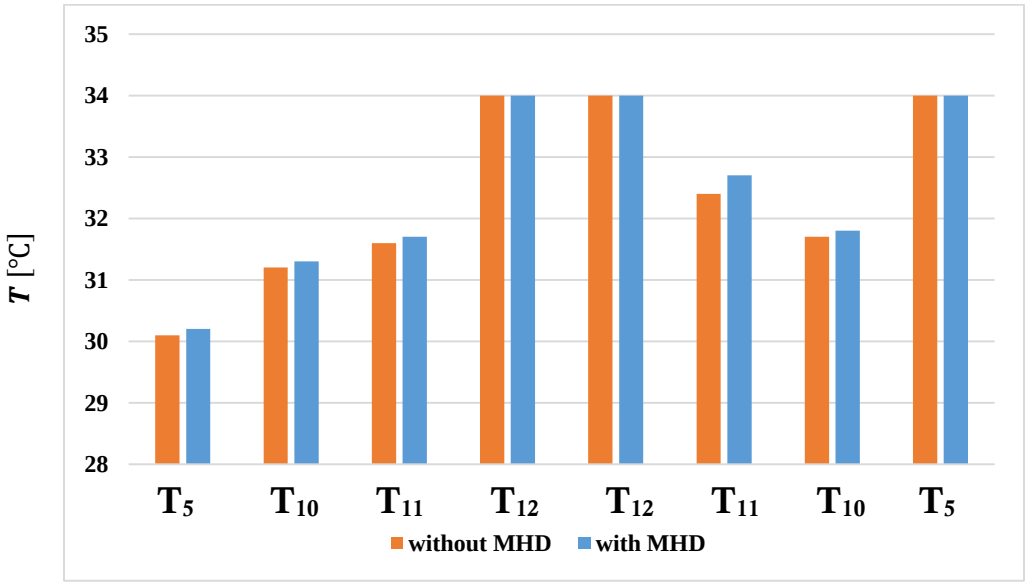

Figure (5. 90) Mid-section temperature considering the existence and the absence of magnetic field at $\phi = 0.02$

5.3.5. Comparison of experimental and CFD results

A comparison between the measured experimental data and numerical CFD results in terms of temeprature distribution is presented in Figure (5.91) and (5.92). It can be seen that there is good agreement which show that the whole numerical results through this work are accepted and the selected case study in the experimental measurements is physically right.

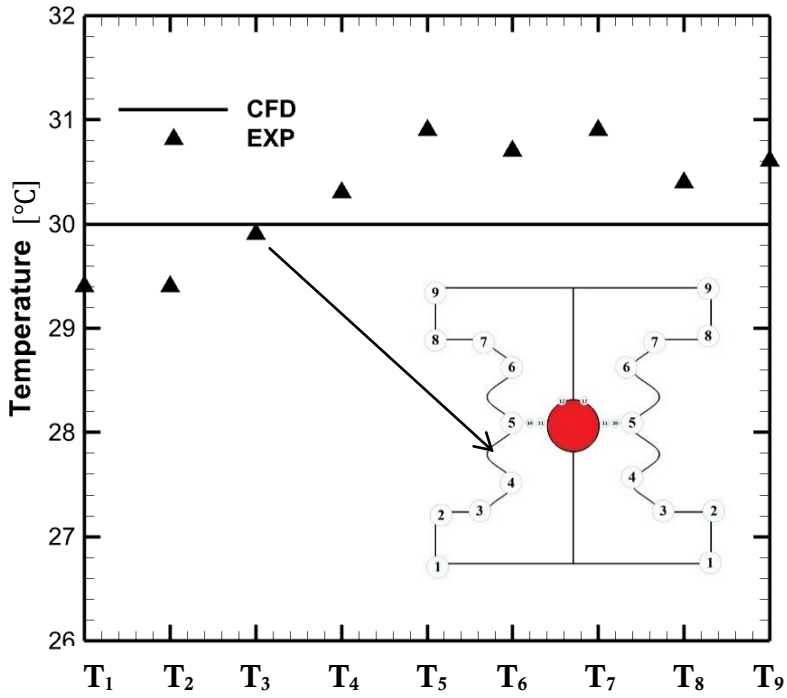

Figure (5. 91) Validation of the numerical and experimental results of temperature profile in the nanofluid layer along the left cold wall at $T_h = 36, T_c = 30$.

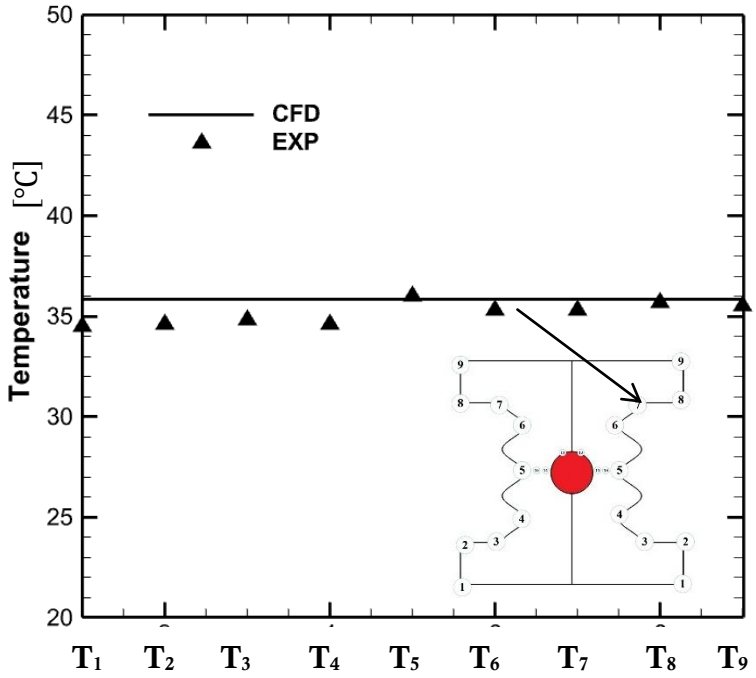

Figure (5. 92) Validation of the numerical and experimental results of temperature profile in the nanoporous layer along the right hot wall at T_h=36, T_c=30

Chapter Six
Conclusions and Recommendations

Chapter Six

Conclusions and Recommendations for Future Works

6.1. Conclusions

After completing the present work, it is important to write the paragraph of the conclusions part based upon the numerical and experimental results.

So, the major conclusions can be summarized based upon numerical and experimental work. Firstly, with respect to the numerical work, the major conclusion can be summarized as indicated below:

1. MHD considering different inner hot body location case

- Regarding the first proposed numerical CFD investigation which focusing on the influence of three different cases of inner hot body locations. There is no noticeable influence of the inner hot body locations for all of the selected three cases on the fluid flow strength at low Rayleigh number ($Ra = 10^3$) while in at high Rayleigh number ($Ra = 10^6$), the fluid flow strength increases for Case 1 by 84.16% in a comparison with Case 3. Additionally, it can be seen that Case three reveals the lowest heat transfer augmentation.
- Applied the magnetic field in the vertical direction leads to intensify the fluid flow strength of Case one by approximately three times that for case three.
- When the number of undulations is N=1, Case one reveals the best rate of heat transfer, followed by Case two. However, the number of undulations does not affect Case three.
- Increasing the thickness of the porous layer from $X_P = 0.6$ into $X_P = 1$ leads to attenuate the force of fluid flow by 39.13% and heat transfer rate by 38.17% considering Case one.

2. MHD considering different shape of inner bodies (circle, square, rhombus and triangle)

- For various values of Ra, Da, Ha, γ_{MHD}, ϕ, Case 1 which represent the circular shapes reveals the highest augmentation in Nusselt number followed by Case 3 (rhombus), Case 2 (square) and Case 4 (triangular) reveals the lowest improving in heat transfer rate.
- The magnetic field inclination angle reveals different behavior on heat transfer rate where it was concluded that increasing its value from 0° into 30° leads to reduces the Nusselt number. further increasing of magnetic field angle more than 30° leads to increasing of Nusselt number

3. MHD considering the existence of trapezoidal heater and inner body

- The position of the inner circular body is highly effect on thermal augmentation of heat transfer rate.
- As Hartmann number increases, the magnetic field inclination angle be more effect on the heat transfer behavior as it is noted that applied the magnetic field in the vertical direction at γ=90° enhance Nusselt number by 20% in a comparison with applied the magnetic field in the horizontal direction.

4. MHD considering different wavy shape patterns

- The influence of wavy shape patterns is higher when the number of undulations ($N = 1$).
- Case 3 is highest than Case 2 by 13.42% in terms of fluid flow strength.
- Increasing Hartmann number from $Ha = 0$ into $Ha = 60$ leads to an obvious reduction in the fluid flow by 48.95%.
- Case 4 along with locating the inner elliptical body in the bottom of the enclosure reveals the best strength in the fluid flow.
- For bettering the thermal rate of heat transfer, it is recommended to move the inner elliptical body downwards for all cases of wavy patterns.

- Increasing the number of undulations along with Hartmann number reduces the heat transfer rate.
- Nusselt number improved with increasing the parameter of the distance between the wavy walls

Secondly, regarding the major conclusions of the experimental results may be summarized in the following points;

- It can be seen that increasing the hot side wavy wall temperature leads to increase the temperature difference which increases the temperature level in the nanofluid-porous region and the nanofluid region.
- It can be seen that there is slight increasing in the temperature with the existence of the magnetic field.

6.2. Recommendation for future works

The natural convection within I-shaped wavy-walled enclosure is studied in this experimental CFD work in full details considering various dimensionless parameters. However, there is an extension for this study as indicated below;

- Entropy generation can be taken as a numerical study.
- The Inclined I-shaped enclosure could studied.
- A study of different heater shapes such as (circular, rectangular, wavy).
- Mixed convection due to rotating the inner body or even lid-driven enclosure.
- Studying of porous media saturated with hybrid nanofluids.
- Examination the influence of different nanoparticle types and its relation with the magnetic field

References

References

1. Mehrizi, A.A., M. Farhadi, K. Sedighi, and M.A. Delavar, *Effect of fin position and porosity on heat transfer improvement in a plate porous media heat exchanger*. Journal of the Taiwan Institute of Chemical Engineers, 2013. **44**(3): p. 420-431.
2. Abdesslem, J., S. Khalifa, N. Abdelaziz, and M. Abdallah, *Radiative properties effects on unsteady natural convection inside a saturated porous medium. Application for porous heat exchangers.* Energy, 2013. **61**: p. 224-233.
3. Al-Kayiem, H.H. and T.A. Yassen, *On the natural convection heat transfer in a rectangular passage solar air heater.* solar energy, 2015. **112**: p. 310-318.
4. Nadeem, S. and S. Saleem, *Analytical treatment of unsteady mixed convection MHD flow on a rotating cone in a rotating frame.* Journal of the Taiwan Institute of Chemical Engineers, 2013. **44**(4): p. 596-604.
5. Abdulkadhim, A., I.M. Abed, and N. Mahjoub Said, *Review of natural convection within various shapes of enclosures.* Arabian Journal for Science and Engineering, 2021. **46**(12): p. 11543-11586.
6. Abdulkadhim, A., I. mejbel Abed, and N. mahjoub Said, *An exhaustive review on natural convection within complex enclosures: Influence of various parameters.* Chinese Journal of Physics, 2021. **74**: p. 365-388.
7. Nield, D.A. and A. Bejan, *Convection in porous media*. Vol. 3. 2006: Springer.
8. Hadi Hussain, S. and A. Kadhim Hussein, *Natural convection heat transfer enhancement in a differentially heated parallelogrammic enclosure filled with copper-water nanofluid.* Journal of heat transfer, 2014. **136**(8): p. 082502.
9. Motlagh, S.Y. and H. Soltanipour, *Natural convection of Al2O3-water nanofluid in an inclined cavity using Buongiorno's two-phase model.* International Journal of Thermal Sciences, 2017. **111**: p. 310-320.
10. Turan, O., N. Chakraborty, and R.J. Poole, *Laminar natural convection of Bingham fluids in a square enclosure with differentially heated side walls.* Journal of Non-Newtonian Fluid Mechanics, 2010. **165**(15): p. 901-913.
11. Turan, O., A. Sachdeva, N. Chakraborty, and R.J. Poole, *Laminar natural convection of power-law fluids in a square enclosure with differentially heated side walls subjected to constant temperatures.* Journal of Non-Newtonian Fluid Mechanics, 2011. **166**(17): p. 1049-1063.
12. Pishkar, I., B. Ghasemi, A. Raisi, and S.M. Aminossadati, *Numerical study of unsteady natural convection heat transfer of Newtonian and non-Newtonian*

fluids in a square enclosure under oscillating heat flux. Journal of Thermal Analysis and Calorimetry, 2019. **138**(2): p. 1697-1710.
13. Biswal, P., A. Nag, and T. Basak, *Analysis of thermal management during natural convection within porous tilted square cavities via heatline and entropy generation.* International Journal of Mechanical Sciences, 2016. **115-116**: p. 596-615.
14. Roy, M., S. Roy, and T. Basak, *Finite element simulations on heatline trajectories for mixed convection in porous square enclosures: Effects of various moving walls.* European Journal of Mechanics - B/Fluids, 2016. **59**: p. 140-160.
15. Ho, C.J., W.K. Liu, Y.S. Chang, and C.C. Lin, *Natural convection heat transfer of alumina-water nanofluid in vertical square enclosures: An experimental study.* International Journal of Thermal Sciences, 2010. **49**(8): p. 1345-1353.
16. Lai, F.-H. and Y.-T. Yang, *Lattice Boltzmann simulation of natural convection heat transfer of Al2O3/water nanofluids in a square enclosure.* International Journal of Thermal Sciences, 2011. **50**(10): p. 1930-1941.
17. Corcione, M., *Empirical correlating equations for predicting the effective thermal conductivity and dynamic viscosity of nanofluids.* Energy Conversion and Management, 2011. **52**(1): p. 789-793.
18. Sheikhzadeh, G.A., M. Dastmalchi, and H. Khorasanizadeh, *Effects of nanoparticles transport mechanisms on Al2O3–water nanofluid natural convection in a square enclosure.* International Journal of Thermal Sciences, 2013. **66**: p. 51-62.
19. Ghasemi, B., S. Aminossadati, and A. Raisi, *Magnetic field effect on natural convection in a nanofluid-filled square enclosure.* International Journal of Thermal Sciences, 2011. **50**(9): p. 1748-1756.
20. Ahmed, S.E., A.K. Hussein, H.A. Mohammed, I.K. Adegun, X. Zhang, L. Kolsi, A. Hasanpour, and S. Sivasankaran, *Viscous dissipation and radiation effects on MHD natural convection in a square enclosure filled with a porous medium.* Nuclear Engineering and Design, 2014. **266**: p. 34-42.
21. Bourantas, G.C. and V.C. Loukopoulos, *MHD natural-convection flow in an inclined square enclosure filled with a micropolar-nanofluid.* International Journal of Heat and Mass Transfer, 2014. **79**: p. 930-944.
22. Hong, Y.K., S.W. Baek, and M.Y. Kim, *Inverse natural convection problem with radiation in rectangular enclosure.* Numerical Heat Transfer, Part A: Applications, 2010. **57**(5): p. 315-330.
23. Sivasankaran, S., Y. Do, and M. Sankar, *Effect of discrete heating on natural convection in a rectangular porous enclosure.* Transport in porous media, 2011. **86**(1): p. 261-281.

24. Alam, P., A. Kumar, S. Kapoor, and S.R. Ansari, *Numerical investigation of natural convection in a rectangular enclosure due to partial heating and cooling at vertical walls.* Communications in Nonlinear Science and Numerical Simulation, 2012. **17**(6): p. 2403-2414.
25. Hossain, M., S. Asghar, and R.S.R. Gorla, *Buoyancy-driven flow of a viscous incompressible fluid in an open-ended rectangular cavity with permeable horizontal surfaces.* International Journal of Numerical Methods for Heat & Fluid Flow, 2010.
26. Al-Badawi, Y.M. and H.M. Duwairi, *MHD natural convection with Joule and viscous heating effects in iso-flux porous medium-filled enclosures.* Applied Mathematics and Mechanics, 2010. **31**(9): p. 1105-1112.
27. Wu, F., W. Zhou, and X. Ma, *Natural convection in a porous rectangular enclosure with sinusoidal temperature distributions on both side walls using a thermal non-equilibrium model.* International Journal of Heat and Mass Transfer, 2015. **85**: p. 756-771.
28. Rahimi, M., A.A. Ranjbar, M.J. Hosseini, and M. Abdollahzadeh, *Natural convection of nanoparticle–water mixture near its density inversion in a rectangular enclosure.* International Communications in Heat and Mass Transfer, 2012. **39**(1): p. 131-137.
29. Ilyas, S.U., R. Pendyala, and M. Narahari, *An experimental study on the natural convection heat transfer in rectangular enclosure using functionalized alumina-thermal oil-based nanofluids.* Applied Thermal Engineering, 2017. **127**: p. 765-775.
30. Salari, M., E.H. Malekshah, and M.H. Malekshah, *Natural convection in a rectangular enclosure filled by two immiscible fluids of air and Al2O3-water nanofluid heated partially from side walls.* Alexandria Engineering Journal, 2018. **57**(3): p. 1401-1412.
31. Teamah, M.A., A.F. Elsafty, and E.Z. Massoud, *Numerical simulation of double-diffusive natural convective flow in an inclined rectangular enclosure in the presence of magnetic field and heat source.* International Journal of Thermal Sciences, 2012. **52**: p. 161-175.
32. Kaluri, R.S., R. Anandalakshmi, and T. Basak, *Bejan's heatline analysis of natural convection in right-angled triangular enclosures: Effects of aspect-ratio and thermal boundary conditions.* International Journal of Thermal Sciences, 2010. **49**(9): p. 1576-1592.
33. Bhardwaj, S. and A. Dalal, *Analysis of natural convection heat transfer and entropy generation inside porous right-angled triangular enclosure.* International Journal of Heat and Mass Transfer, 2013. **65**: p. 500-513.
34. Mansour, M.A. and S.E. Ahmed, *A numerical study on natural convection in porous media-filled an inclined triangular enclosure with heat sources using*

nanofluid in the presence of heat generation effect. Engineering Science and Technology, an International Journal, 2015. **18**(3): p. 485-495.

35. Ghasemi, B. and S.M. Aminossadati, *Brownian motion of nanoparticles in a triangular enclosure with natural convection.* International Journal of Thermal Sciences, 2010. **49**(6): p. 931-940.
36. Aminossadati, S.M. and B. Ghasemi, *Enhanced natural convection in an isosceles triangular enclosure filled with a nanofluid.* Computers & Mathematics with Applications, 2011. **61**(7): p. 1739-1753.
37. Mahmoudi, A.H., I. Pop, and M. Shahi, *Effect of magnetic field on natural convection in a triangular enclosure filled with nanofluid.* International Journal of Thermal Sciences, 2012. **59**: p. 126-140.
38. Rashad, A., A.J. Chamkha, M.A. Ismael, and T. Salah, *Magnetohydrodynamics natural convection in a triangular cavity filled with a Cu-Al2O3/water hybrid nanofluid with localized heating from below and internal heat generation.* Journal of Heat Transfer, 2018. **140**(7).
39. Basak, T., S. Roy, A. Matta, and I. Pop, *Analysis of heatlines for natural convection within porous trapezoidal enclosures: Effect of uniform and non-uniform heating of bottom wall.* International Journal of Heat and Mass Transfer, 2010. **53**(25): p. 5947-5961.
40. Basak, T., D. Ramakrishna, S. Roy, A. Matta, and I. Pop, *A comprehensive heatline based approach for natural convection flows in trapezoidal enclosures: Effect of various walls heating.* International Journal of Thermal Sciences, 2011. **50**(8): p. 1385-1404.
41. Natarajan, S.K., K.S. Reddy, and T.K. Mallick, *Heat loss characteristics of trapezoidal cavity receiver for solar linear concentrating system.* Applied Energy, 2012. **93**: p. 523-531.
42. Ul Haq, R., S. Naveed Kazmi, and T. Mekkaoui, *Thermal management of water based SWCNTs enclosed in a partially heated trapezoidal cavity via FEM.* International Journal of Heat and Mass Transfer, 2017. **112**: p. 972-982.
43. Gowda, B.M.K., M.S. Rajagopal, Aswatha, and K.N. Seetharamu, *Heat transfer in a side heated trapezoidal cavity with openings.* Engineering Science and Technology, an International Journal, 2019. **22**(1): p. 153-167.
44. Saleh, H., R. Roslan, and I. Hashim, *Natural convection heat transfer in a nanofluid-filled trapezoidal enclosure.* International Journal of Heat and Mass Transfer, 2011. **54**(1): p. 194-201.
45. Alsabery, A.I., A.J. Chamkha, S.H. Hussain, H. Saleh, and I. Hashim, *Heatline visualization of natural convection in a trapezoidal cavity partly filled with nanofluid porous layer and partly with non-Newtonian fluid layer.* Advanced Powder Technology, 2015. **26**(4): p. 1230-1244.

46. Sheremet, M.A., T. Groşan, and I. Pop, *Steady-state free convection in right-angle porous trapezoidal cavity filled by a nanofluid: Buongiorno's mathematical model.* European Journal of Mechanics - B/Fluids, 2015. **53**: p. 241-250.
47. Saleh, H., R. Roslan, and I. Hashim, *Natural convection in a porous trapezoidal enclosure with an inclined magnetic field.* Computers & Fluids, 2011. **47**(1): p. 155-164.
48. García de María, J.M., A. Baïri, and V.A.F. Costa, *Empirical correlations at high Ra for steady-state free convection in 2D air-filled parallelogrammic enclosures with isothermal discrete heat sources.* International Journal of Heat and Mass Transfer, 2010. **53**(19): p. 3831-3838.
49. Baïri, A., *Correlations for transient natural convection in parallelogrammic enclosures with isothermal hot wall.* Applied Thermal Engineering, 2013. **51**(1): p. 833-838.
50. Hussein, A.K., *Computational analysis of natural convection in a parallelogrammic cavity with a hot concentric circular cylinder moving at different vertical locations.* International Communications in Heat and Mass Transfer, 2013. **46**: p. 126-133.
51. Baïri, A., E. Zarco-Pernia, and J.M. García de María, *A review on natural convection in enclosures for engineering applications. The particular case of the parallelogrammic diode cavity.* Applied Thermal Engineering, 2014. **63**(1): p. 304-322.
52. Hussein, A.K. and A.W. Mustafa, *Natural convection in fully open parallelogrammic cavity filled with Cu–water nanofluid and heated locally from its bottom wall.* Thermal Science and Engineering Progress, 2017. **1**: p. 66-77.
53. Anandalakshmi, R. and T. Basak, *Analysis of energy management via entropy generation approach during natural convection in porous rhombic enclosures.* Chemical Engineering Science, 2012. **79**: p. 75-93.
54. Choi, C., S. Jeong, M.Y. Ha, and H.S. Yoon, *Effect of a circular cylinder's location on natural convection in a rhombus enclosure.* International Journal of Heat and Mass Transfer, 2014. **77**: p. 60-73.
55. Hosseinjani, A.A. and M. Nikfar, *Numerical analysis of unsteady natural convection from two heated cylinders inside a rhombus enclosure filled with Cu-water nanofluid.* International Communications in Heat and Mass Transfer, 2020. **113**: p. 104510.
56. Lee, M. and Y.-J. Kim, *Effect of non-uniform magnetic fields on the characteristics of ferrofluid flow in a square enclosure.* Journal of Magnetism and Magnetic Materials, 2020. **506**: p. 166697.

57. Mahfouz, F.M., *Buoyancy driven flow within an inclined elliptic enclosure.* International Journal of Thermal Sciences, 2011. **50**(10): p. 1887-1899.
58. Ghasemi, E., S. Soleimani, and H. Bararnia, *Natural convection between a circular enclosure and an elliptic cylinder using Control Volume based Finite Element Method.* International Communications in Heat and Mass Transfer, 2012. **39**(8): p. 1035-1044.
59. Hu, Y.-P., Y.-R. Li, X.-F. Yuan, and C.-M. Wu, *Natural convection of cold water near its density maximum in an elliptical enclosure containing a coaxial cylinder.* International Journal of Heat and Mass Transfer, 2013. **60**: p. 170-179.
60. Ravnik, J. and L. Škerget, *A numerical study of nanofluid natural convection in a cubic enclosure with a circular and an ellipsoidal cylinder.* International Journal of Heat and Mass Transfer, 2015. **89**: p. 596-605.
61. Cho, H.W., Y.G. Park, and M.Y. Ha, *The natural convection in a square enclosure with two hot inner cylinders, Part I: The effect of one elliptical cylinder with various aspect ratios in a vertical array.* International Journal of Heat and Mass Transfer, 2018. **125**: p. 815-827.
62. Sheikholeslami, M., T. Hayat, and A. Alsaedi, *On simulation of nanofluid radiation and natural convection in an enclosure with elliptical cylinders.* International Journal of Heat and Mass Transfer, 2017. **115**: p. 981-991.
63. Hashemi, H., Z. Namazian, S.M.H. Zadeh, and S.A.M. Mehryan, *MHD natural convection of a micropolar nanofluid flowing inside a radiative porous medium under LTNE condition with an elliptical heat source.* Journal of Molecular Liquids, 2018. **271**: p. 914-925.
64. Aghakhani, S., A.H. Pordanjani, M. Afrand, M. Sharifpur, and J.P. Meyer, *Natural convective heat transfer and entropy generation of alumina/water nanofluid in a tilted enclosure with an elliptic constant temperature: Applying magnetic field and radiation effects.* International Journal of Mechanical Sciences, 2020. **174**: p. 105470.
65. Oztop, H.F., E. Abu-Nada, Y. Varol, and A. Chamkha, *Natural convection in wavy enclosures with volumetric heat sources.* International Journal of Thermal Sciences, 2011. **50**(4): p. 502-514.
66. Esmaeilpour, M. and M. Abdollahzadeh, *Free convection and entropy generation of nanofluid inside an enclosure with different patterns of vertical wavy walls.* International Journal of Thermal Sciences, 2012. **52**: p. 127-136.
67. Cho, C.-C., C.-L. Chen, and C.o.-K. Chen, *Natural convection heat transfer and entropy generation in wavy-wall enclosure containing water-based nanofluid.* International Journal of Heat and Mass Transfer, 2013. **61**: p. 749-758.

68. Tang, W., M. Hatami, J. Zhou, and D. Jing, *Natural convection heat transfer in a nanofluid-filled cavity with double sinusoidal wavy walls of various phase deviations.* International Journal of Heat and Mass Transfer, 2017. **115**: p. 430-440.
69. Bhardwaj, S., A. Dalal, and S. Pati, *Influence of wavy wall and non-uniform heating on natural convection heat transfer and entropy generation inside porous complex enclosure.* Energy, 2015. **79**: p. 467-481.
70. Gibanov, N.S., M.A. Sheremet, and I. Pop, *Natural convection of micropolar fluid in a wavy differentially heated cavity.* Journal of Molecular Liquids, 2016. **221**: p. 518-525.
71. Sheremet, M.A., H.F. Oztop, and I. Pop, *MHD natural convection in an inclined wavy cavity with corner heater filled with a nanofluid.* Journal of Magnetism and Magnetic Materials, 2016. **416**: p. 37-47.
72. Sheremet, M.A., D.S. Cimpean, and I. Pop, *Free convection in a partially heated wavy porous cavity filled with a nanofluid under the effects of Brownian diffusion and thermophoresis.* Applied Thermal Engineering, 2017. **113**: p. 413-418.
73. Sheremet, M.A., I. Pop, and A. Ishak, *Time-dependent natural convection of micropolar fluid in a wavy triangular cavity.* International Journal of Heat and Mass Transfer, 2017. **105**: p. 610-622.
74. Hatami, M. and H. Safari, *Effect of inside heated cylinder on the natural convection heat transfer of nanofluids in a wavy-wall enclosure.* International Journal of Heat and Mass Transfer, 2016. **103**: p. 1053-1057.
75. Hatami, M., *Nanoparticles migration around the heated cylinder during the RSM optimization of a wavy-wall enclosure.* Advanced Powder Technology, 2017. **28**(3): p. 890-899.
76. Bararnia, H., S. Soleimani, and D.D. Ganji, *Lattice Boltzmann simulation of natural convection around a horizontal elliptic cylinder inside a square enclosure.* International Communications in Heat and Mass Transfer, 2011. **38**(10): p. 1436-1442.
77. Sheikholeslami, M., H. Keramati, A. Shafee, Z. Li, O.A. Alawad, and I. Tlili, *Nanofluid MHD forced convection heat transfer around the elliptic obstacle inside a permeable lid drive 3D enclosure considering lattice Boltzmann method.* Physica A: Statistical Mechanics and its Applications, 2019. **523**: p. 87-104.
78. Dogonchi, A.S., M. Sadeghi, M. Ghodrat, A.J. Chamkha, Y. Elmasry, and R. Alsulami, *Natural convection and entropy generation of a nanoliquid in a crown wavy cavity: effect of thermo-physical parameters and cavity shape.* Case Studies in Thermal Engineering, 2021. **27**: p. 101208.

79. Abdelmalek, Z., T. Tayebi, A.S. Dogonchi, A.J. Chamkha, D.D. Ganji, and I. Tlili, *Role of various configurations of a wavy circular heater on convective heat transfer within an enclosure filled with nanofluid.* International Communications in Heat and Mass Transfer, 2020. **113**: p. 104525.
80. Sheremet, M.A., H. Oztop, I. Pop, and K. Al-Salem, *MHD free convection in a wavy open porous tall cavity filled with nanofluids under an effect of corner heater.* International Journal of Heat and Mass Transfer, 2016. **103**: p. 955-964.
81. Biswas, N., A.J. Chamkha, and N.K. Manna, *Energy-saving method of heat transfer enhancement during magneto-thermal convection in typical thermal cavities adopting aspiration.* SN Applied Sciences, 2020. **2**(11): p. 1-25.
82. Kashani, S., A.A. Ranjbar, M. Mastiani, and H. Mirzaei, *Entropy generation and natural convection of nanoparticle-water mixture (nanofluid) near water density inversion in an enclosure with various patterns of vertical wavy walls.* Applied Mathematics and Computation, 2014. **226**: p. 180-193.
83. Dixit, D.D. and A. Pattamatta, *Natural convection heat transfer in a cavity filled with electrically conducting nano-particle suspension in the presence of magnetic field.* Physics of Fluids, 2019. **31**(2): p. 023302.
84. Kargarsharifabad, H., *Experimental and numerical study of natural convection of Cu-water nanofluid in a cubic enclosure under constant and alternating magnetic fields.* International Communications in Heat and Mass Transfer, 2020. **119**: p. 104957.
85. Mahdi, R.A., H. Mohammed, K. Munisamy, and N. Saeid, *Review of convection heat transfer and fluid flow in porous media with nanofluid.* Renewable and Sustainable Energy Reviews, 2015. **41**: p. 715-734.
86. Das, S.K., S.U. Choi, W. Yu, and T. Pradeep, *Nanofluids: science and technology*. 2007: John Wiley & Sons.
87. Sharma, K., P. Sarma, W. Azmi, R. Mamat, and K. Kadirgama, *Correlations to predict friction and forced convection heat transfer coefficients of water based nanofluids for turbulent flow in a tube.* International Journal of Microscale and Nanoscale Thermal and Fluid Transport Phenomena, 2012. **3**(4): p. 1-25.
88. Holman, J.P., *Experimental methods for engineers.* 2012.
89. Al-Zamily, A. and M.R. Amin. *Natural convection and entropy generation in a cavity filled with two horizontal layers of nanofluid and porous medium in presence of a magnetic field*. in *ASME International Mechanical Engineering Congress and Exposition*. 2015. American Society of Mechanical Engineers.
90. Hussain, S.H. and M.S. Rahomey, *Comparison of natural convection around a circular cylinder with different geometries of cylinders inside a square*

enclosure filled with Ag-nanofluid superposed porous-nanofluid layers. Journal of Heat Transfer, 2019. **141**(2).

91. Malekpour, A., N. Karimi, and A. Mehdizadeh, *Magnetohydrodynamics, natural convection, and entropy generation of CuO–water nanofluid in an I-shape enclosure—a numerical study.* Journal of Thermal Science and Engineering Applications, 2018. **10**(6).
92. Ma, Y., R. Mohebbi, M. Rashidi, Z. Yang, and M. Sheremet, *Nanoliquid thermal convection in I-shaped multiple-pipe heat exchanger under magnetic field influence.* Physica A: Statistical Mechanics and its Applications, 2020. **550**: p. 124028.
93. Khanafer, K., K. Vafai, and M. Lightstone, *Buoyancy-driven heat transfer enhancement in a two-dimensional enclosure utilizing nanofluids.* International Journal of Heat and Mass Transfer, 2003. **46**(19): p. 3639-3653.
94. Fusegi, T., J.M. Hyun, K. Kuwahara, and B. Farouk, *A numerical study of three-dimensional natural convection in a differentially heated cubical enclosure.* International Journal of Heat and Mass Transfer, 1991. **34**(6): p. 1543-1557.
95. de Vahl Davis, G., *Natural convection of air in a square cavity: a bench mark numerical solution.* International Journal for numerical methods in fluids, 1983. **3**(3): p. 249-264.
96. Barakos, G., E. Mitsoulis, and D. Assimacopoulos, *Natural convection flow in a square cavity revisited: laminar and turbulent models with wall functions.* International journal for numerical methods in fluids, 1994. **18**(7): p. 695-719.

Appendices

Appendix A: Algorithm of the Numerical Simulation

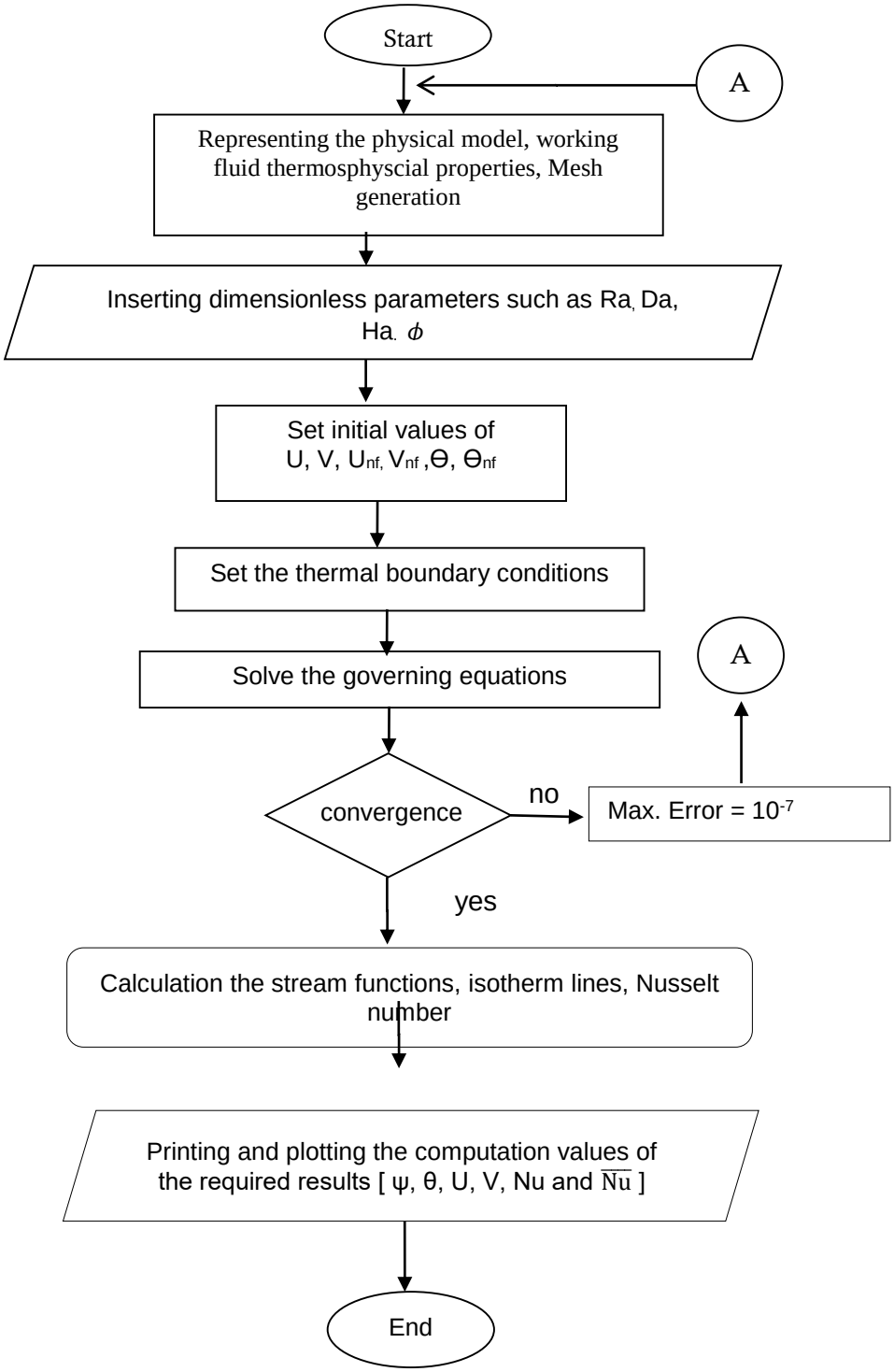

Appendix B: XRD Diffractometer: Nanofluid Results

Date: 05/18/2022 Time: 12:27:15 م File: nanoalo1-2 User: مكتب التقني

Name and formula

Reference code: 00-047-1308

Compound name: Aluminum Oxide
PDF index name: Aluminum Oxide

Empirical formula: Al_2O_3
Chemical formula: Al_2O_3

Crystallographic parameters

Crystal system: Unknown

RIR: -

Subfiles and Quality

Subfiles: Alloy, metal or intermetalic
Corrosion
Inorganic
Quality: Doubtful (O)

Comments

Creation Date: 01/01/1970
Modification Date: 01/01/1970

References

Primary reference: Wefers, K., Bell, G., *Alcoa Research Laboratories, Technical Paper No. 19*

Peak list

No.	h	k	l	d [A]	2Theta[deg]	I [%]
1				2.70000	33.153	20.0
2				2.41000	37.281	60.0
3				2.28000	39.492	60.0
4				2.18000	41.385	20.0
5				2.09000	43.254	10.0
6				1.98000	45.790	100.0
7				1.95000	46.535	60.0
8				1.54000	60.026	20.0
9				1.39000	67.307	100.0
10				1.14000	85.017	30.0
11				1.04000	95.578	10.0

Stick Pattern

1 Of 2

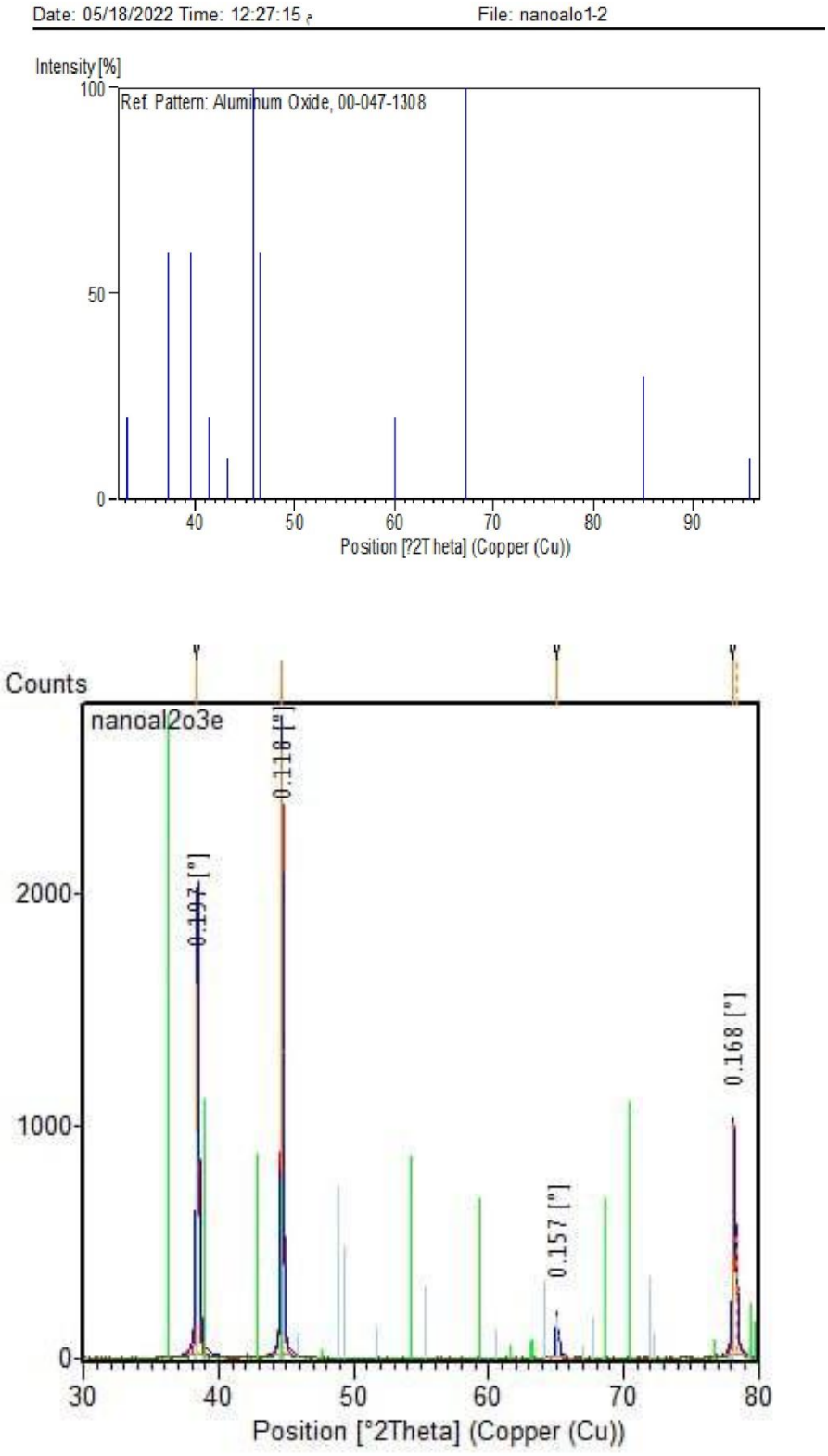

Figure B. *XRD Diffractometer results*

Appendix C: Publication of the PhD Thesis

Arabian Journal for Science and Engineering
https://doi.org/10.1007/s13369-021-05952-6

REVIEW--MECHANICAL ENGINEERING

Review of Natural Convection Within Various Shapes of Enclosures

Ammar Abdulkadhim[1,2] · Isam Mejbel Abed[1] · Nejla Mahjoub Said[3,4]

Received: 10 February 2021 / Accepted: 27 June 2021

Abstract
The previous studies related to the thermal-driven flow within enclosures had been summarized in the present work. Various geometries of enclosures like square, rectangular and triangular had been summarized. Besides, enclosures filled with different fluids had been taken into consideration like traditional and nanofluids as well as porous medium, Newtonian and non-Newtonian fluids and multilayer systems. The governing equations of heat transfer and fluid flows had been presented for different cases. Different numerical models like homogeneous, inhomogeneous and thermal non-equilibrium model, Darcy, Darcy extended–Forchheimer model, etc., had been summarized. The influence of various dimensionless parameters like Rayleigh, Darcy, Bejan and Hartmann number, nanofluid loading, diverse thermal cases of the applied boundary conditions, angle of inclination, the number for undulations, the existence of inner body and many others parameters acting and influencing hardly up on both of the entropy generation and the heat transfer was illustrated. The present review illustrates the physical mechanism behind the buoyancy thermally driven flow in terms of figures of contours as well as the Nusselt numbers profiles.

Keywords Natural convection · Enclosure · Heat transfer · Various shapes

List of Symbols

C_p	Specified heat at a steady pressure (kJ/kg.K)
g	Acceleration of gravity (m/s^2)
k	Thermal conductivity (W/m.K)
P	Pressure without dimension
p	Pressure (Pa)
Pr	Prandtl number (ν_f/α_f)
R	Radiation parameter
Ra	Rayleigh number ($g\beta_f L^3\Delta T/\nu_f\alpha_f$)
Ha	Hartmann number
T	Temperature (K)
T_c	The cold surface's temperature (K)
ϵ	Porosity
L	Length and height of enclosure
Y_O	Distance between original and wavy wall
Ω	Vorticity
d_p	Nanoparticle diameter
K_r	Thermal conductivity ratio
δ	Position of the inner body moved vertically
ζ	Position of the inner body moved diagonally
B	Length of heat source
D	Position of heat source
Q	Internal heat generation/absorption coefficient
ΔT	Temperature difference
T^*	The temperature without dimension ($T-Tc/T_h-T_c$)
μ	Dynamic viscosity (kg/ms)
ρ	Density (kg/m^3)
T_h	The hot surface's temperature (K)
u	The component of velocity in x-axis (m/s)
y	Cartesian coordinate in vertical axis (m)
V	The component of dimensionless velocity in y-axis
v	The component of velocity in y-axis (m/s)
X	Dimensionless coordinate in horizontal axis
x	Cartesian coordinates in horizontal direction (m)
Y	Dimensionless coordinate in vertical direction
A	Aspect ratio

✉ Nejla Mahjoub Said
mahjoub_nejla@yahoo.fr

[1] Mechanical Engineering Department, University of Babylon, Babylon Province, Iraq

[2] Air Conditioning and Refrigeration Techniques Engineering Department, Al-Mustaqbal University College, Babylon Province, Iraq

[3] Department of Physics, College of Science, King Khalid University, Abha 61413, Saudi Arabia

[4] LGM, Preparatory Institute for Engineering Studies, University of Monastir,, Monastir, Tunisia

Published online: 02 August 2021

Chinese Journal of Physics 74 (2021) 365–388

Contents lists available at ScienceDirect

Chinese Journal of Physics

journal homepage: www.sciencedirect.com/journal/chinese-journal-of-physics

An exhaustive review on natural convection within complex enclosures: Influence of various parameters

Ammar Abdulkadhim [a,b], Isam mejbel Abed [a], Nejla mahjoub Said [c,d,*]

[a] Mechanical Engineering Department, University of Babylon, Babylon Province, Iraq
[b] Air conditioning and Refrigeration Techniques Engineering Department, Al-Mustaqbal University College, Babylon Province, Iraq
[c] Department of Physics, College of Science, King Khalid University, Abha 61413, Saudi Arabia
[d] LGM, Preparatory Institute for Engineering Studies, University of Monastir, Tunisia

ARTICLE INFO

Keywords:
Natural convection
Enclosure
Heat transfer
Energy
Various geometry

ABSTRACT

The present work exhaustively examines natural convection in complex enclosure forms such as trapezoidal, rhombic (parallelogrammic), elliptical and wavy geometries, taking into account various numerical methods that have been used in previous studies over the last ten years. Many dimensionless parameters such as a wide range of dimensionless numbers like Rayleigh, Darcy, and Hartmann were treated. The influence of the volume fraction of nanofluids, the thickness of the porous layer, and the number of undulations are studied. The existence of an inner body with different shapes (square, rectangle, triangle, rhombic, elliptical and wavy) was also mentioned. The impact of the position of the inner body and its size were also examined. The results of the previous works are presented in term of streamlines, isotherms, local and mean Nusselt number. It can be seen that there was a real limitation to the existence of the inner body in trapezoidal enclosures. There is also a limitation of the action of the wavy form as an inner body.

1. Introduction

Convection is one of the fundamental modes in the subject of heat transfer and it is important to analysis this type of heat transfer due to its applications in engineering. When convection produced due to applied mechanical equipment such as fans or blower, it refers to forced convection. While when it happens due to temperature gradient in the absence of any mechanical meaning, it known as natural convection. This make the energy consumption of natural convection is less than that of the forced convection leading to the energy saving which is the major goals in the engineering applications. Researchers, scientists and designers, always looking for new technologies for the community, have developed new thermal heat transfer devices that aim to increase the rate of heat transfer by using different geometries, different types of nanofluids, MHD insertion, boundary conditions, existence inside the body, etc. Many physical phenomena have had important engineering applications, one of them being the natural convection that occurs inside the enclosures. The wide range of applications includes packed beds, Building and ventilation systems, Geological applications, cooling of electronic equipment, solar collectors, heat exchangers, design of nuclear energy and refrigeration systems [1, 2, 3, 4, 5, 6, 7, 8]. The shapes of the enclosures are divided into two categories, simple geometries such as square, rectangle and triangle. The second category includes complex enclosure shapes such as trapezoids, parallelograms (rhombus), ellipses and waves. The first category has been much more studied than the second [9, 10, 11, 12, 13, 14, 15, 16, 17, 18] . Most studies have focused on the fluid flow strength and heat

* Corresponding author.
E-mail address: nalmahjoub@kku.edu.sa (N. Said).

https://doi.org/10.1016/j.cjph.2021.10.012
Received 30 March 2021; Received in revised form 12 October 2021; Accepted 19 October 2021
Available online 23 October 2021

Journal of Thermal Analysis and Calorimetry
https://doi.org/10.1007/s10973-021-11072-y

Magnetohydrodynamics thermogravitational convective in a novel I-shaped wavy-walled enclosure considering various inner hot pipe locations

Ammar Abdulkadhim[1,2] · Isam Mejbel Abed[1] · Nejla Mahjoub Said[3,4]

Received: 29 March 2021 / Accepted: 8 September 2021

Abstract
The present work numerically examines natural convection within an I-shaped wavy-walled enclosure with multi-pipes of heat exchangers filled with multi-layers of nanofluid and porous medium saturated with the same nanofluid. The finite element scheme is used to solve governing equations of mass, momentum along with the energy in dimensionless form. The influence of various dimensionless parameters such as Rayleigh number $\left(10^4 \le Ra \le 10^6\right)$, Darcy number $\left(10^{-5} \le Da \le 0.1\right)$, Hartmann number $(0 \le Ha \le 60)$, number of undulations $(1 \le N \le 5)$, nanofluid volume fraction $(0.00 \le \phi \le 0.06)$, porous layer thickness $0.6 \le X_P \le 1$ and MHD inclination angle $(0° \le \gamma \le 90°)$ is studied to explain their effect on fluid flow and heat transfer that presented in terms of streamlines, isotherms and average Nusselt number. Three different thermal cases of the location of the internal hot pipe are treated. Our results are in a good agreement with previous works. The finding of this study proved that for better heat transfer, it was recommended to use number of undulation $N = 1$ and that the location of the inner pipe is at the bottom of the enclosure (case 1). Moreover, it was obtained that the increase of Rayleigh number (Ra), Darcy number (*Da*), inclination angle of MHD and the reduction of the porous layer thickness as well as the reduction of Hartmann number (Ha) leads to an increase in heat transfer. Also, the results indicate that enhancement percentage of Nusselt number is 57.77% for Case 1 in a comparison with Case 3 when the number of undulation is $N = 1$. Finally, applying the magnetic field in the vertical direction (at $\gamma = 90°$) enhances Nusselt number for Case 1 by 53% in a comparison with Case 3.

Keywords Wavy enclosure · Natural convection · Nanofluid · Porous medium · MHD

Introduction

The thermal mechanism of heat transfer by natural convection in various enclosures geometries such as square, rectangular, triangular, trapezoidal, rhombus and elliptical enclosures plays an essential and critical role in reducing thermal energy losses and optimizing energy production [1–13]. The reason for this high number of publications is due to its wide range of applications such as heat exchangers, HVAC systems, solar collectors and nuclear components, of which they are only a few illustrative examples. There is another enclosure geometry, called wavy, which is considered a little more complex in comparison with the shapes mentioned above. The wavy shapes of the enclosure walls have played an important role in saving energy and improving heat exchange within thermal systems. But there is another problem which is related to traditional working fluids such as water, oil, ethylene glycol. The major problem is related to the thermophysical properties of these conventional fluids which have low thermal conductivity, which is a real limitation in improving and increasing the rate of heat transfer. This problem has motivated many researchers to find a solution to this problem, which is now a new science of engineering and physics known as nanofluid. It is simply a matter of adding tiny, solid nanoparticles such as Cu, Zn,

✉ Nejla Mahjoub Said
mahjoub_nejla@yahoo.fr

[1] Mechanical Engineering Department, University of Babylon, Babylon, Babylon Province, Iraq

[2] Air Conditioning and Refrigeration Techniques Engineering Department, Al-Mustaqbal University College, Babylon, Babylon Province, Iraq

[3] Department of Physics, College of Science, King Khalid University, Abha 61413, Saudi Arabia

[4] LGM, Preparatory Institute for Engineering Studies, University of Monastir, Monastir, Tunisia

Published online: 29 September 2021

Journal of Thermal Analysis and Calorimetry
https://doi.org/10.1007/s10973-022-11509-y

MHD thermogravitational heat transfer within complex enclosure considering the influence of different wavy patterns

Ammar Abdulkadhim[1,2] · Isam Mejbel Abed[1] · Nejla Mahjoub Said[3,4]

Received: 4 January 2022 / Accepted: 13 July 2022

Abstract
The present work examines utilizing CFD simulation of the natural convection within complex enclosure with four different cases of wavy patterns considering the existence of inner heated elliptical body. The influence of inclined magnetic field had been taken into consideration. The space between the inner body and the enclosure had been filled by two layers. The first right layer was filled by nanofluid while the second left layer had been filled by porous medium with the same nanofluid. The influence of various parameters such as number of undulations, the distance between the wavy walls, and the inner elliptical body position for four different cases of wavy walls patterns with and without magnetic field on fluid flow and heat transfer had been drawn in terms of streamlines, isotherms and Nusselt number. The results indicate that in the absence of magnetic field the Case 3 has the highest stream function with a dimensionless value of $|\Psi_{max}| = 34.229$ which make Case 3 is recommended wavy patterns for bettering the fluid flow strength when the number of undulations kept at ($N = 1$) and the distance between the wavy walls kept at ($B = 0.8$). It is important to note that at ($B = 0.8$), Case 1 has the lowest strength of the fluid flow while it enhanced by 41.17% when ($B = 1.0$). On the other hand, increasing the distance between wavy walls from ($B = 0.8$) into ($B = 1.4$) enhances Nusselt number by 31.67%. The influence of inner body position had the highest impact of heat transfer rate in a comparison with the other as it helps in improvement of Nusselt number by 67.70% when it moves toward to bottom of the enclosure. Generally, the magnetic field reduces both of the fluid flow intensity and heat transfer for all of the shape of wavy patterns.

Keywords Natural convection · Nanofluid · Porous medium · MHD · Wavy · Elliptical

Introduction

The study of buoyancy driven flow which formally known as natural convection within enclosures considering different geometrical shapes had been studied a lot due to their outstanding applications related to energy consumption and conversion such as food processing [1] sustainable building [2], solar air heaters [3], different shapes of solar collectors [4–7], materials processing [8], chemical reactions [9], cooling systems of nuclear chemical reactor [10–12], heat exchangers [13, 14], etc. Many of previous works were presented to study the phenomenon of natural convection within different shape of enclosures such as square [15–17], rectangular [18–20], triangular [21], trapezoidal [22–24], rhombus [25], circular [26], parallelogrammic [27], elliptical [28, 29], wavy [30] utilizing different numerical method such as finite difference, finite element and finite volume formulation. Based upon the previous publications, there is abundant in the studies regarding the simple shapes while there is gap regarding the more complex shapes such as wavy-shaped enclosure.

Some of the studies of natural convection within simple shapes of enclosures had been presented by numerous researchers. The convection within square enclosure had been investigated by Goodarzi et al. [31, 32]. Also, MHD effect on natural convection within square enclosure had

✉ Nejla Mahjoub Said
nejla.mahjoub@fsm.rnu.tn; nalmahjoub@kku.edu.sa

[1] Mechanical Engineering Department, University of Babylon, Hillah, Babylon Province, Iraq

[2] Air Conditioning and Refrigeration Techniques Engineering Department, Al-Mustaqbal University College, Hillah, Babylon Province, Iraq

[3] Department of Physics, College of Science, King Khalid University, Abha 61413, Saudi Arabia

[4] LGM, Preparatory Institute for Engineering Studies, University of Monastir, 5000 Monastir, Tunisia

Published online: 21 August 2022

WAVES IN RANDOM AND COMPLEX MEDIA
https://doi.org/10.1080/17455030.2022.2110331

Taylor & Francis
Taylor & Francis Group

Check for updates

Insight view on the CFD simulation of magneto-hydrodynamics natural convection in wavy enclosure with trapezoidal heater and circular cylinder

Ammar Abdulkadhim[a,b], Isam Mejbel Abed[a] and Nejla Mahjoub Said [c,d]

[a]Mechanical Engineering Department, University of Babylon, Hillah, Iraq; [b]Air conditioning and Refrigeration Techniques Engineering Department, Al-Mustaqbal University College, Hillah, Iraq; [c]Department of Physics, College of Science, King Khalid University, Abha, Saudi Arabia; [d]LGM, Preparatory Institute for Engineering Studies, University of Monastir, Monastir, Tunisia

ABSTRACT

The present work examines numerically using a finite element scheme the magnetic field on natural convection within I-shaped wavy-walled enclosure filled by a nanofluid and porous medium. The porous medium had been modeled by the Darcy–Brinkman model while a single phase model treats the nanofluid. The thermal equilibrium model had been applied between the nanofluid and porous medium under steady-state conditions. The enclosure contains a trapezoidal heater attached to its bottom wall with an internal heated circular cylinder immersed in the enclosure. The two wavy walls are kept at a cold temperature, while the rest walls are insulated. The influence of the Rayleigh number $10^4 \leq Ra \leq 10^6$, Darcy number $10^{-5} \leq Da \leq 0.1$, Hartmann number $0 \leq Ha \leq 60$, nanofluid loading $0 \leq \phi \leq 0.05$, magnetic field inclination angle $0^\circ \leq \gamma \leq 90^\circ$, trapezoidal heater length $0.4 \leq B \leq 1.4$, location of the trapezoidal heater $0.2 \leq E \leq 0.8$, and position of the circular cylinder $0.3 \leq \delta \leq 1.3$ on fluid flow and heat transfer have been discussed deeply. It is obtained that the Nusselt number increases as the Rayleigh number, Darcy number, magnetic field angle increase, and the Hartmann number decreases. Also, for better heat transfer it is obtained that the center location gives the highest value at $\delta = 0.8$. Also, the location of the trapezoidal heater in the right region at $E = 0.8$ reveals the best location in terms of heat transfer improvement.

ARTICLE HISTORY
Received 9 January 2022
Accepted 1 August 2022

KEYWORDS
Natural convection; wavy; I-shaped enclosure; porous medium; magnetic field; energy

1. Introduction

Various researchers utilized passive methods to bettering the heat transfer rate in addition to the thermal performance of a wide range of industrial applications related to the buoyancy-driven flow. Some of these applications are solar collectors and heat exchangers [1–4]. However, the working fluids of these applications, such as water, oil, and other conventional fluids, have serious problems related to their low thermal conductivity limiting the improvement in the rate of heat transfer so the addition of metallic or non-metallic particles in the nanoscale promotes bettering the heat transfer [5–7]. Besides corrugating

CONTACT Nejla Mahjoub Said nalmahjoub@kku.edu.sa, mahjoub_nejla@yahoo.fr

Brazilian Journal of Chemical Engineering
https://doi.org/10.1007/s43153-022-00251-5

ORIGINAL PAPER

Computational investigation of magnetohydrodynamics convective heat transfer in I-shaped wavy enclosure considering various shapes of inner bodies filled with nanofluid–porous layers

Ammar Abdulkadhim[1,2] · Isam Mejbel Abed[1] · Nejla Mahjoub Said[3,4]

Received: 21 January 2022 / Revised: 26 April 2022 / Accepted: 28 May 2022

Abstract
The present work examines numerically the inclined magnetic field on thermogravitional heat transfer in a novel I-shaped enclosure filled partially with nanofluid in the left layers and filled by partially by porous medium saturated by the same nanofluid using finite element method. Three different shapes of inner bodies had been embedded in the enclosure. The enclosure is partially wavy from its vertical walls with four different cases of multi-inner bodies of various shapes such as case 1, 2, 3 and 4 represent circular, square, rhombus and triangular in order to examine their impact on heat transfer and fluid flow. Also, the influence of nanofluid loading, Rayleigh number $\left(10^4 \le Ra \le 10^6\right)$, Darcy number $\left(10^{-5} \le Da \le 0.1\right)$, Hartmann number $(0 \le Ha \le 60)$, MHD angle $(0° \le \gamma \le 90°)$ along with the number $(1 \le No \le 3)$ and position $(0.3 \le Y \le 1.3)$ of inner hot bodies had been examined in terms of streamlines, isotherms and Nusselt number. The results indicate that the number of inner body and its position along with its shape influence on the heat transfer rate. It is obtained that Nusselt number for $Case1 > Case3 > Case2 > Case4$. Also, movement the inner hot body from bottom to the top leads to an obvious reduction in the Nusselt number. The increasing of magnetic field angle from $\gamma = 0°$ into $\gamma = 30°$ leads to decreases the heat transfer rate while more increasing of magnetic field angle augments the rate of heat transfer. Finally, increasing the number of inner hot bodies leads to reduce the total Nusselt number. Thus, for better heat transfer augmentation it is recommended to locate the inner hot body at $Y = 0.3$ and $No = 1$.

Keywords Magnetic field · Natural convection · Nanofluid · Porous medium · Wavy enclosure

Abbreviations

C_p	Specific heat at constant pressure (KJ/kg K)
g	Gravitational acceleration (m/s^2)
k	Thermal conductivity (W/m K)
R	Radius differences of inner and outer cylinder cavity (m)
R_o	Base circle (m)
P	Dimensionless pressure
p	Pressure (Pa)
Pr	Prandtl number (ν_f/α_f)
Ra	Rayleigh number ($g\beta_f L^3 \Delta T/\nu_f \alpha_f$)
T	Temperature (K)
T_c	Temperature of the cold surface (K)
T_h	Temperature of the hot surface (K)
No	Number of inner hot bodies
Nu	Local Nusselt number on the hot inner cylinder
AR	Aspect ratio
U	Dimensionless velocity component in x-direction
u	Velocity component in x-direction (m/s)
V	Dimensionless velocity component in y-direction
v	Velocity component in y-direction (m/s)
X	Dimensionless coordinate in horizontal direction
x	Cartesian coordinates in horizontal direction (m)
Y	Dimensionless coordinate in vertical direction
y	Cartesian coordinate in vertical direction (m)
Gr	Grashof number

✉ Nejla Mahjoub Said
nejla.mahjoub@fsm.rnu.tn; nalmahjoub@kku.edu.sa

[1] Mechanical Engineering Department, University of Babylon, Hillah, Babylon, Iraq

[2] Air Conditioning and Refrigeration Techniques Engineering Department, Al-Mustaqbal University College, Hillah, Babylon, Iraq

[3] Department of Physics, College of Science, King Khalid University, Abha 61413, Saudi Arabia

[4] LGM, Preparatory Institute for Engineering Studies, University of Monastir, 5000 Monastir, Tunisia

Published online: 02 August 2022

، يؤدي تطبيق المجال المغناطيسي في الاتجاه الرأسي إلى تكثيف قوة تدفق السوائل في الحالة الأولى بحوالي ثلاثة أضعاف ذلك للحالة الثالثة.

فيما يتعلق العمل العددي الثاني، لقيم مختلفة من Ra و Da و Ha و γ . تم التوصل الى ان الحالة ١ التي تمثل الأشكال الدائرية أعلى زيادة في رقم Nusselt متبوعًا بالحالة ٣ (المعين) والحالة ٢ (المربع) والحالة ٤ (مثلث) كشفت عن أدنى تحسين في معدل نقل الحرارة. بالإضافة إلى ذلك ، بالنسبة للعمل العددي الثالث مع زيادة رقم هارتمان ، تكون زاوية ميل المجال المغناطيسي أكثر تأثيرًا على سلوك نقل الحرارة حيث لوحظ أن المجال المغناطيسي المطبق في الاتجاه الرأسي عند γ = 90 درجة يعزز رقم نسلت بنسبة ٢٠٪ في مقارنة مع المجال المغناطيسي المطبق في الاتجاه الأفقي. اخيراً، بالنسبة لحالة الأنماط المتموجة المختلفة ، فقد تم إثبات أن الحالة ٤ جنبًا إلى جنب مع تحديد موقع الجسم البيضوي الداخلي في الجزء السفلي من العلبة تكشف عن أفضل قوة في تدفق السوائل. من الناحية التجريبية ، يمكن ملاحظة أن هناك زيادة طفيفة في درجة الحرارة مع وجود المجال المغناطيسي. بالإضافة إلى ذلك ، ثبت أن زيادة درجة حرارة الجدار المتموج الجانبي الساخن يؤدي إلى زيادة فرق درجة الحرارة مما يزيد من مستوى درجة الحرارة في منطقة الموائع النانوي - المسامي ومنطقة المائع النانوي.

من الناحية التجريبية ، يمكن ملاحظة أن هناك زيادة طفيفة في درجة الحرارة مع وجود المجال المغناطيسي. بالإضافة إلى ذلك ، فقد ثبت أن زيادة درجة حرارة الجدار المتموج الجانبي الساخن يؤدي إلى زيادة فرق درجة الحرارة مما يزيد من مستوى درجة الحرارة في منطقة الموائع النانوية المسامية ومنطقة الموائع النانوية. أخيرًا ، هناك توافق ممتاز بين النتائج التجريبية والرقمية للعمل الحالي بالإضافة إلى وجود توافق جيد جدًا في اتجاهات وقيم النتائج العددية للعمل الحالي مع تلك التي حصل عليها باحثون مهمون.

الخلاصة
تبحث الدراسة الحالية الحمل الحراري الطبيعي المغناطيسي في حيز بشكل I و متموج مملوء جزئياً بمائع نانوي - مسامي تحت ظروف حرارية متنوعة .الحيز مملوء جزئيا بمائع الالومينا النانوي بينما الطبقة الاخرى مملوءة بوسط مسامي مشبع بنفس المائع النانوي مع اعتبار نموذج التوازن الحراري بينا المائع النانوي و الوسط المسامي. تم تضمين تاثير رقم رالي($10^4 \leq Ra \leq 10^6$) رقم دارسي($10^{-5} \leq Da \leq 0.1$) رقم هارتمان($0 \leq Ha \leq 60$) تركيز المادة النانوية($0.00 \leq \phi \leq 0.06$) زاوية الفيض المغناطيسي ($0° \leq \gamma_{MHD} \leq 90°$)طول السخان شبه المنحرف($0.4 \leq B \leq 1.4$) موقع السخان شبه المنحرف($0.2 \leq E \leq 0.8$) موقع الاسطوانة الدائرية ($0.2 \leq \delta \leq 0.8$)على قوة الجريان و معدل انتقال الحرارة.

الجزء الاول من الدراسة هي العمل العددي بتقنية CFD المبني على اساس نموذج التدفق المتجانس لنمذجة المائع النانوي و نموذج دارسي - برنكمان لمعالجة الوسط المسامي من خلال استخدام برنامج COMSOL

تم عرض اربعة حالات مختلفة عدديا. العمل الاول هو فحص تاثير الفيض المغناطيسي ضمن الحيز باعتبار عدة اجسام اسطوانية مع ثلاث حالات مختلفة للتوزيع الحراري فيها. العمل الثاني هو امتداد للدراسة الاولى مع الاخذ بنظر الاعتبار تاثير شكل الاجسام الداخلية (الدائرة، المربع، المعين، المثلث) داخل الحيز. العمل الثالث هو نظرة ثاقبة على تاثير السخان شكل شبه منحرف جنبا الى جنب مع الجسم الدائري على الحمل الحر مع الاخذ بنظر الاعتبار موقع وطول السخان نوع شبه المنحرف .اخيرا، تم اجراء دراسة تفصيلية لشكل الجدران المتموجة باعتبار أربع انماط مختلفة مع وجود جسم بيضوي

الجزء الثاني هو العمل التجريبي الذي يتضمن تصنيع حيز شكل I متموج مع وجود جسم اسطواني ايضا. الطبقة اليسرى مملوءة بمائع نانوي بينما الطبقة اليمنى مملوءة بوسط مسامي مشبع بنفس المائع النانوي. تم قياس الخواص الثرموفيزياوية عملياً. تم تثبيت قلبين من المجال المغناطيسي بشدة ٢٠ ملي تسلا

اظهرت النتائج ان فيما يتعلق بالعمل العددي الاول انه عند رقم رايلي المنخفض ($Ra = 10^4$) لا يوجد تأثير ملحوظ لمواقع الأنابيب الساخنة الداخلية لجميع الحالات الثلاث المحددة على قوة تدفق السوائل بينما في رقم Rayleigh المرتفع ($Ra = 10^6$) ، تزداد قوة تدفق السائل لـ الحالة ١ بنسبة ٨٤,١٦٪ مقارنة بالحالة ٣. بالإضافة إلى ذلك ، يمكن ملاحظة أن الحالة الثالثة تكشف عن أدنى زيادة في نقل الحرارة. بالإضافة إلى ذلك

وزارة التعليم العالي والبحث العلمي
جامعة بابل
كلية الهندسة
قسم الهندسة الميكانيكية

الحمل الحراري الطبيعي المغناطيسي في حيز بشكل I ومتموج الجدران مملوء جزئيا بمائع نانوي ـ مسامي

أطروحة
مقدمة الى كلية الهندسة جامعة بابل كجزء من متطلبات نيل درجة دكتوراه فلسفة في الهندسة / الهندسة الميكانيكية/ قدرة

من قبل

عمار عبد الكاظم فتحي سعيد

بإشراف

الأستاذ الدكتور عصام مجبل عبد الأستاذ الدكتور نجلاء محجوب سعيد

1444هـ 2022 م